LEGIBILITY NOTICE

A major purpose of the Technical Information Center is to provide the broadest dissemination possible of information contained in DOE's Research and Development Reports to business, industry, the academic community, and federal, state and local governments.

Although a small portion of this report is not reproducible, it is being made available to expedite the availability of information on the research discussed herein.

ORNL/TM-11294
Distribution Category UC-403

ORNL/TM--11294

DE90 000982

Energy Division

CALIBRATION OF A GROUNDWATER FLOW AND CONTAMINANT TRANSPORT COMPUTER MODEL: PROGRESS TOWARD MODEL VALIDATION

R. R. Lee
R. H. Ketelle
J. M. Bownds
T. A. Rizk*

Date published—September 1989

*North Carolina State University

Prepared by the
OAK RIDGE NATIONAL LABORATORY
Oak Ridge, Tennessee 37831
operated by
MARTIN MARIETTA ENERGY SYSTEMS, INC.
for the
U.S. DEPARTMENT OF ENERGY
under Contract No. DE-AC05-84OR21400

TABLE OF CONTENTS

TABLE OF CONTENTS (Continued)

LIST OF FIGURES

LIST OF FIGURES (Continued)

LIST OF FIGURES (Continued)

LIST OF FIGURES (Continued)

LIST OF TABLES

Calibration of a Groundwater Flow and Contaminant Transport Computer Model: Progress Toward Model Validation

R. R. Lee R. H. Ketelle J. M. Bownds
Energy Division

T. A. Rizk
North Carolina State University

ABSTRACT

A groundwater flow and contaminant transport model calibration was performed to evaluate the ability of a typical, verified computer code to simulate groundwater tracer migration in the shallow aquifer of the Conasauga Group. Previously, standard practice site data interpretation and groundwater modeling resulted in inaccurate simulations of contaminant transport direction and rate compared with tracer migration behavior. The site's complex geology, the presence of flow in both fractured and weathered zones, and the transient character of flow in the shallow aquifer combined to render inaccurate assumptions of steady-state, homogeneous groundwater flow.

The improvement of previous modeling results required iterative phases of conceptual model development, hypothesis testing, site field investigations, and modeling. The activities focused on generating a model grid that was compatible with site hydrogeologic conditions and on establishing boundary conditions based on site data. An annual average water table configuration derived from site data and fixed head boundary conditions was used as input for flow modeling. The contaminant transport model was combined with the data-driven flow model to obtain a preliminary contaminant plume. Calibration of the transport code was achieved by comparison with site tracer migration and concentration data.

This study documents the influence of fractures and the transient character of flow and transport in the shallow aquifer. Although compatible with porous medium theory, site data demonstrate that the tracer migration pathway would not be anticipated using conventional porous medium analysis. However, by incorporating a systematic approach to site characterization and conceptual model formulation coupled with rational interpretations of site data, a conventional porous medium model can reasonably simulate the level of resolution provided by monitoring a groundwater tracer test. Simulation accuracy over a period of weeks is constrained by the ability to conceptualize and predict the complex interactions of fracture occurrence, changing local hydraulic head configuration, and annual and event precipitation. Simulations over a period of months smooth the effects of short-term fluctuations in these factors for more accurate comparison with tracer migration behavior.

1. INTRODUCTION

Disposal of hazardous and radioactive waste in fractured, heterogeneous geologic media presents challenges in evaluating the ability of conventional applications of groundwater flow and contaminant transport computer models to accurately simulate natural conditions. At the U.S. Department of Energy (DOE) Oak Ridge Reservation (ORR) and elsewhere, the effects of these geologic complications on the aquifer system are difficult to demonstrate and verify; therefore, they are often omitted or minimally incorporated into conventional porous medium modeling. Results of these models, however, provide a partial basis for contaminant pathways analyses at waste disposal sites that affect decisions regarding waste disposal strategies, disposal unit designs, and approaches to site monitoring as part of performance assessment. In remedial studies, model results affect decisions regarding the feasibility of alternative corrective actions and monitoring network designs to demonstrate regulatory compliance. This study describes efforts to incorporate natural site conditions in groundwater flow and transport modeling to achieve model calibration. A calibrated model can then be applied to accurate predictions of transport behavior to achieve model validation.

On the ORR to date, computer model simulation of natural site conditions has not been rigorously demonstrated by comparing model results with the migration behavior of a groundwater tracer. Beginning in FY 1988, an attempt at such a comparison was made using a groundwater flow and transport computer model validation experiment. The experiment used data from geologic and hydrogeologic site characterization and the behavior of groundwater tracer migration under ambient conditions in a near-field location (determined on the basis of tracer migration) to predict tracer arrival time, location, and concentration in a computer-defined far-field location. Lessons learned in the FY 1988 activity were used in FY 1989 to calibrate the computer simulations to tracer migration. Because tracer had already migrated to the far-field location, predictions of tracer arrival were not performed, and this study is not considered a model validation study in the sense of predicting tracer behavior in the absence of a priori field data. Rather, the study focused on documenting the factors that control contaminant transport migration, on simulating tracer migration behavior, and on defining the modeling requirements to achieve the level of resolution provided by tracer migration. In this regard, the study may be considered empirical modeling, or calibration. As the report demonstrates, however, the study serves as a validation by confirming the legitimacy of ideas based on field data analysis through computer model simulations.

This report presents the results of FY 1989 activities to simulate the migration of a groundwater tracer under ambient conditions on the ORR. The report summarizes relevant highlights of the FY 1988 effort to perform a groundwater flow and contaminant transport computer model validation (for background purposes), as well as the methods and approaches employed in FY 1989, and the FY 1989 results and recommendations. The report is intended to be comprehensive. In addition to appending site data, the report provides a chronology of events in the FY 1989 study, which includes initial conceptual model development, hypothesis testing, test results, modifications to the conceptual model, and steps taken in computer simulations of site flow and transport. The authors provide this level of detail because they consider that the evolutionary process of conceptual model development and refinement is inseparable from, and may supersede, simulation results.

Because much of the work associated with these activities occurred simultaneously, some redundancy and forward referencing in the presentation is unavoidable; this is minimized, however, to the extent practicable.

2. SITE DESCRIPTION

The study site (Fig. 1, in back pocket) is located in West Bear Creek Valley on the ORR within a larger surrounding site under consideration for tumulus disposal of low-level radioactive waste as part of the Low Level Waste Disposal Development and Demonstration (LLWDDD) Program (Fig. 2, in back pocket). It is important to recognize the small scale of the study area relative to the overall West Bear Creek Valley site. The site area comprises ~2880 m^2 (0.7 acre); total tracer migration distance to date (16 months) is ~49 m (160 ft). The rectangle around the majority of wells in Fig. 1 describes the approximate location of the computer model grid boundary, which is illustrated in many figures to follow.

The study site is on the western side of a gently sloping topographic high and is bordered on the west by a small perennial stream. The site is underlain by complexly interbedded silty limestone and shale lithologies of the Maryville Formation of the Cambrian Conasauga Group. Although site geologic structure exhibits minor local variations, geologic strike is consistent with the regional norm (about N 60 E degrees), and bedrock dips uniformly at about 45° southeast. Bedrock fractures are ubiquitous. Those fractures that cross bedding seldom extend beyond individual bedrock lithologies (about 1 to 5 cm in length), while bedding plane fractures may extend laterally for much greater distances. Based on detailed stratigraphic studies of rock core, Lee and Ketelle (1989) describe mesoscale structural deformation features that consist of zones of intense fracturing, fault gouge, and drag folds. These features extend from 1 to 3 m vertically and from tens to hundreds of meters laterally; they occur erratically and may terminate or change character abruptly. Their occurrence is generally more common in limestone-rich lithologies.

Soil is thin (~0.3 m) to essentially absent at the site. Weathered bedrock (saprolite) extends from just beneath the surface to depths of ~3 to 10 m (10 to 30 ft). Saprolite thickness is related directly to elevation; greater thicknesses occur on the topographic high in the eastern portion of the site. Although the degree of weathering decreases with depth, the interface with unweathered bedrock is abrupt and generally is defined as the depth of machine auger refusal. Mean water table depth generally is coincident with the bedrock weathering interface, with seasonal water elevation fluctuations of ~0.3 to 1.5 m (1 to 5 ft) depending on ground surface elevation. Annual water table fluctuations are larger at higher topographic elevations.

3. PREVIOUS INVESTIGATIONS

The phase 1 study was completed in FY 1988. Phase 1 included the performance of hydrogeologic site characterization, the initiation of a groundwater dye (Rhodamine-WT) tracer test in the shallow aquifer, and flow and transport modeling. Lee and Ketelle (1988) summarize those activities in the following paragraphs.

The tracer test began April 20, 1988, and was performed under ambient conditions (natural site gradient). Following removal of ~10 L of water from the tracer injection well (GW-484 in Fig. 1), 10 L of a 40% Rhodamine-WT dye solution was introduced to the upper 0.3 m (1 ft) of the water table surface to simulate complete failure of a waste disposal unit and immediate introduction of leachate to the water table surface. Monitoring began immediately after tracer injection with eight automatic sampling devices located in strategic near-field locations in the downgradient path of tracer migration predicted by site aquifer testing. As detection of tracer began, sampling devices were moved and additional detection wells were constructed in the uppermost portions of the aquifer to monitor tracer migration. Quantitative tracer analysis at 1-ppb resolution was performed using fluorimetric techniques. Monitoring continues.

The initial flow and transport models did not accurately simulate natural site conditions or tracer migration. Results of site hydrologic testing and preliminary modeling in phase 1 predicted that tracer would migrate in a direction coincident with the maximum hydraulic gradient (in an ~210° azimuth) with moderate lateral dispersion and at a rate of ~1 m/day. Instead, tracer migrated in a 245° azimuth (parallel to geologic strike), in a plume less than 3 m wide, and at an early (1 week) rate as high as 5 m/d. Subsequent migration (6 months) occurred at rates of less than 0.5 m/d.

Among the conclusions from the FY 1988 study were that (1) the effects of regional geologic structure and local bedrock heterogeneities on flow and transport were not considered in site modeling; (2) the scale of site hydrogeologic testing was incapable of resolving the effects of local bedrock heterogeneities on flow; and (3) the reduced tracer migration rate was thought to be related to water table decline associated with seasonal drought.

Other groundwater tracer tests have been performed in the Conasauga Group on the ORR. Davis et al. (1984) summarized tracer test results at the Engineering Test Facility (ETF) in Melton Valley to obtain estimates of hydraulic properties. They reported tracer detection in all the radial well field wells, with the highest concentrations in locations oriented along the strike-parallel joint set. Based on the arrival time of the peak tracer concentration, a linear velocity value of 0.17 m/d (0.56 ft/d) was calculated. In tracer tests performed in SWASA 4 and SWASA 6, Webster and Bradley (1988) reported the largest tracer concentrations in wells oriented parallel to the hydraulic gradient (and normal to strike). An intermittent tracer pulse was correlated with precipitation. Finally, Webster (1976) summarized tracer tests in the solid waste burial grounds that were performed to compare the effects of the hydraulic gradient vs geologic strike on the groundwater flow direction. He concluded that in the uppermost aquifer, the hydraulic gradient was the principal factor controlling groundwater movement.

The Tennessee Valley Authority (TVA) is performing an ongoing study to compare the predictive accuracy of a contaminant transport model with the behavior of a groundwater tracer in heterogeneous media (Waldrop et al. 1988). That study is being

performed in heterogeneous, unconsolidated geologic media with generally high hydraulic conductivities, in contrast to the heterogeneous but lithified and fractured geologic media on the ORR with overall much lower hydraulic conductivities. Initial results of the TVA study indicated that the overall irregular plume shape and fingering at the leading edge of the tracer plume were related to zones of locally high hydraulic conductivity. This observation and annual fluctuations in the water table were attributed to a greater rate of advection than initially predicted.

Using stochastic techniques, Rafalko and Hawley (1989) associated uncertainties in model-predicted breakthrough curves in heterogeneous media to uncertainties in the spatial variation hydraulic conductivity. They found that model-predicted breakthrough curves in early time (years) were more sensitive to flow-field heterogeneities than were later time curves (tens of years), which were more representative of the average flow field. The inability to describe spatial variations in hydraulic conductivity was found to contribute greatly to uncertainties in model results and should be considered a minimum uncertainty given uncertainties in other parameters such as boundary condition selection and mass input rates.

4. STUDY METHODS

Commonly, interpretations of hydrogeologic data are provided for use as computer model input parameters after completion of data analysis. In contrast, the approach in this study was to initiate modeling activities at the beginning of task performance. The task was designed to provide for the interaction and updating of geologic, hydrogeologic, and computer modeling results through an iterative feedback system throughout task performance. The overall approach incorporated a comprehensive conceptual model for flow and transport into preliminary modeling and used modeling results and field data analyses to guide later activities related to conceptual model refinement. In this way, modeling was an integral part of the task that provided a method for testing hypotheses and for directing and focusing field activities. Thus, refinements to the conceptual model, data analyses, and numerical model simulations evolved in parallel throughout task performance.

Performance of the task proceeded incrementally beginning with conceptual model development, data acquisition, and mathematical formulation of those data for numerical problem solution. A preliminary geologic-based finite element model grid was designed for use in preliminary flow model calibration to site hydraulic head data. Because one of the objectives of the task was to evaluate the ability of field data to satisfy model input parameter requirements, the use of assumed values for parameter assignment was minimized or eliminated. Parameter values were constrained within a narrow range of those derived from the site data interpretations. Results of parameter optimization studies were used as an additional means of guiding field activities to maximize the ability of field data to satisfy model input requirements and to evaluate the compatibility of site aquifer characteristics with the conceptual model. The selected contaminant transport code was combined with the data-driven flow model to obtain a preliminary computer-generated contaminant plume. Calibration of the transport model was achieved by comparison with site tracer-concentration data.

As used above and throughout the remainder of this report, the term "geologic-based model grid" refers to the consideration and application of hydrogeologic conditions in overall computer model grid construction. It does not refer to the numerical representation of those conditions in model grid preparation.

4.1 PRELIMINARY CONCEPTUAL MODEL

Based on conclusions from the FY 1988 phase 1 activities, a conceptual model was developed that considered the effects of local and regional geology on flow and transport. Because tracer was observed to migrate in a narrow plume similar to the thickness of bedrock lithologic heterogeneities and in a direction parallel to geologic strike, these local and regional geologic influences were incorporated in FY 1989 modeling through numerical model grid construction and the assignment of grid element parameter values. A more detailed discussion of the process of incorporating the conceptual model into the numerical model grid is presented in Sect. 7.

The preliminary conceptual model consisted of two basic components. The first component assumed that under ambient conditions, undetermined local and regional geologic structure and resultant aquifer anisotropy controlled the general direction of flow

and transport in the shallow aquifer, in contrast to isotropic porous medium flow analysis that assumes flow is in the direction of maximum hydraulic gradient. The second component assumed that the extremely narrow width of the tracer plume was controlled by heterogeneous bedrock lithologies on the order of 1 m thick that possess different hydraulic conductivities. The absence of tracer in unweathered bedrock was caused by either the measured upward head gradient at the site or an overall hydraulic conductivity contrast between weathered and unweathered bedrock. The dramatically reduced tracer migration rate after the beginning of the test was assumed to be related to a declining water table and reduced head gradient associated with diminished precipitation.

Given the data acquired during the FY 1988 phase 1 study, the conceptual model provided a reasonable explanation for observed tracer migration behavior. The model could be incorporated in computer simulations, and working hypotheses could be developed for key elements of the model and tested in the field. As preliminary model simulations were performed and field data were acquired and analyzed, refinements to the conceptual model were made. A discussion of those refinements is presented in Sect. 8.

5. FY 1989 FIELD DATA ACQUISITION AND ANALYSIS

This section describes FY 1989 field data acquisition and analysis to document the hydrogeologic factors that control tracer migration. It discusses the scope and objectives of data acquisition, the types of additional characterization tests performed for hypothesis testing, the groundwater elevation and tracer migration monitoring program used to document the water table configuration and tracer migration, and the analyses of those data.

5.1 SCOPE

The approach to field data acquisition was to test hypotheses developed from the FY 1988 task by performing additional hydrologic testing and continued tracer monitoring and to obtain data for groundwater flow and contaminant transport modeling dictated by results of preliminary modeling. This approach remained consistent with the approach to overall task performance by incorporating modeling results throughout all task performance stages.

Hydrogeologic field testing was directed generally toward evaluating the legitimacy of working hypotheses developed to explain key elements of the conceptual model. Specific hypotheses tested include the following: (1) the heterogeneous bedrock units are laterally continuous across the site; (2) a hydraulic conductivity contrast exists between those bedrock units (specifically silty limestone and shale), within both weathered and unweathered bedrock; (3) an overall hydraulic conductivity contrast exists between weathered and unweathered bedrock; and (4) tracer is not migrating in unweathered bedrock beneath the depth of the tracer detection wells. Tracer concentration, water table elevation, and precipitation data were analyzed to test the hypothesis that the transient tracer migration rate was related to a reduced hydraulic gradient profile associated with drought conditions.

5.2 GEOLOGIC AND HYDROGEOLOGIC DATA ACQUISITION AND ANALYSIS

This section describes the acquisition and analysis of data acquired in FY 1989 in terms of their effect on the tracer migration behavior. It evaluates the validity of key components of the preliminary conceptual model, that is, that the hydrologic characteristics of the dipping bedrock lithologies strongly affect tracer migration.

5.2.1 Geologic and Hydrogeologic Test Description

A rock core drilling and hydrologic testing program was developed to investigate the lateral continuity of heterogeneous bedrock lithologies and to perform hydrologic testing of discrete stratigraphic intervals in both weathered and unweathered bedrock. The testing program was designed to evaluate the hypotheses listed above, which were developed from the preliminary conceptual model. Site testing was performed adjacent to the tracer plume to minimize disturbances to tracer migration behavior. Some tests were performed on correlative stratigraphic intervals to investigate the lateral continuity of hydraulic conductivity. Based on lithologic and fracture characteristics of the rock core, an attempt was made to select intervals for testing that would exhibit both low and high values of hydraulic conductivity. Core holes GW-499Q and GW-499X (Fig. 3) were drilled to

perform the tests. Fifteen falling-head tests were performed in weathered bedrock (8 in the vadose zone and 7 below the water table), and 12 straddle packer tests were performed in unweathered bedrock. Of the 27 tests performed, data from 2 tests were unsuitable for analysis. Ground heaving and bore wall blowouts observed during five of the vadose zone falling-head tests performed in GW-499X rendered those test results unreliable, and they were excluded from analysis. Estimated hydraulic conductivity values of the falling-head and straddle-packer test data are presented in Table 1.

To conduct falling-head tests in weathered bedrock, wash rotary drilling was performed using a tri-cone roller drill bit. This technique caused minimal disturbance to the bore wall, which helped maintain bore hole integrity and allowed the suspended fine particles to be lifted from the hole. Drilling proceeded in ~0.6- to 0.76-m (2- to 2.5-ft) increments. After drilling each increment, the drill string was removed from the hole and a falling-head test was performed by isolating the most recently drilled interval with an inflatable packer. After flooding the hole, water level decline was measured with a downhole pressure transducer and recorded in the field on a portable computer. The process was repeated to the top of competent bedrock to a depth of 10 m (31 ft). Following hydraulic testing in weathered bedrock, the hole was advanced into unweathered rock (by core drilling techniques) to a depth of 18 m (60 ft). Six straddle-packer tests were performed in the unweathered portion of the hole using a 1.1 m (3.66 ft) interpacker spacing, the shortest test interval possible using a straddle-packer test string.

To test the lateral continuity of hydraulic conductivity in discreet stratigraphic intervals and to determine if tracer was migrating down dip in unweathered bedrock, core hole GW-499Q was drilled on the southern periphery of the tracer area. The location of GW-499Q was selected by rock core and geophysical log correlation to minimize disturbance to the tracer area and to intercept the apparent stratigraphic horizon of tracer migration in the shallow unweathered bedrock. Six straddle-packer tests were performed with the same interpacker spacing described above. Four hydrologic tests were performed in GW-499Q in lithologically correlative intervals tested previously in GW-499X. Two of those correlative tests were performed in unweathered bedrock; the other two tests compared hydrologic characteristics of weathered bedrock in GW-499Q with unweathered bedrock below the water table in GW-499X.

5.2.2 Additional Piezometer Installation

To determine if tracer was migrating vertically beneath the tracer plume in unweathered bedrock, piezometer GW-499W also was drilled 3 m (10 ft) into unweathered bedrock. At the time of its construction, the location of GW-499W (slightly beyond the leading edge of the tracer plume) allowed for piezometer construction in the shallow unweathered bedrock, which minimized disturbances to the tracer flow field.

Locations for 14 additional shallow piezometers (GW-499R to GW-499W and GW-499Y to GW-499AF) and 5 stream elevations (CR-1 to CR-5) outside the immediate tracer area were selected based on the results of preliminary site groundwater flow modeling. Hydraulic head data from these locations were used to verify head values assigned to the model grid boundaries by a quintic spline based on measured head values from within the grid boundary. The locations of the additional off-site hydraulic head data points are shown in Fig. 3 (in back pocket).

Table 1. Estimated hydraulic conductivity data from falling head and straddle packer testing

Test number	Test interval (ft below g.s.)	Hydraulic conductivity estimate (cm/s)
GW-499Q-1[1]	16.70 – 20.36	5.67×10^{-6}
GW-499Q-2[2]	20.00 – 23.66	2.23×10^{-5}
GW-499Q-3	29.20 – 32.86	3.19×10^{-5}
GW-499Q-4[3]	32.00 – 35.66	7.17×10^{-5}
GW-499Q-5	37.60 – 41.26	8.71×10^{-5}
GW-499Q-6[4]	39.80 – 43.46	1.24×10^{-5}
GW-499X-1*	2.80 – 5.30	1.23×10^{-5}
GW-499X-2*	6.10 – 8.30	1.94×10^{-6}
GW-499X-3*	5.10 – 8.30	7.03×10^{-4}
GW-499X-4*	7.70 – 10.50	NA
GW-499X-5*	7.20 – 10.50	9.0×10^{-4}
GW-499X-6	9.00 – 12.50	8.56×10^{-6}
GW-499X-7	12.00 – 14.50	6.65×10^{-5}
GW-499X-8	14.00 – 16.50	2.07×10^{-5}
GW-499X-9	16.00 – 18.50	3.86×10^{-5}
GW-499X-10	18.00 – 20.50	3.83×10^{-5}
GW-499X-11	20.00 – 22.50	5.05×10^{-5}
GW-499X-12	22.00 – 24.50	1.11×10^{-4}
GW-499X-13[1]	24.00 – 26.50	4.55×10^{-5}
GW-499X-14[2]	26.00 – 28.50	2.77×10^{-5}
GW-499X-15	28.50 – 31.00	4.90×10^{-5}
GW-499X-16	33.70 – 37.36	NA
GW-499X-17	37.40 – 41.06	3.21×10^{-4}
GW-499X-18[3]	41.00 – 44.66	5.18×10^{-5}
GW-499X-19	45.00 – 48.66	9.02×10^{-5}
GW-499X-20[4]	50.00 – 53.66	3.51×10^{-5}
GW-499X-21	53.70 – 57.36	1.01×10^{-5}

Tests GW-499X-1 through GW-499X-8 are vadose zone tests.
Tests GW-499X-1 through GW-499X-15 are falling-head tests performed in saprolite; all other tests are straddle packer tests in unweathered bedrock.
Corresponding superscript numbers identify tests performed in correlative stratigraphic intervals.
*Ground surface heaving and bore wall blowouts observed during testing render these test results unreliable.
NA–Data unsuitable for analysis.

5.2.3 Geologic and Hydrogeologic Test Analysis

Rock core from GW-499Q and GW-499X was examined and compared with site core from GW-404 and GW-471, which were drilled in FY 1988. The bulk of the bedrock consists of planar and wavy-laminated, coalesced lenses of silty limestone and shale interbeds. Beds of relatively homogeneous intraclastic limestone and shale from 0.15- to 1-m (0.5- to 3-ft) thickness occur irregularly. Interbedded lithologies are laterally continuous across the site, and their location in the subsurface can be estimated with a high degree of precision. Zones of mesoscale (1-m scale) structural deformation identified near the tracer test site and elsewhere in the surrounding West Bear Creek Valley site do not underlie the pathway of tracer migration. Bedrock fractures are indistinguishable from the ubiquitous fractures noted throughout core from the surrounding Bear Creek Valley site.

As noted in Table 1, data from only 21 of the 27 hydrologic tests performed in core holes GW-499Q and GW-499X are suitable for analysis. These tests were performed to evaluate the lateral continuity of hydraulic conductivity within lithologies and to compare hydraulic conductivity values between weathered and unweathered bedrock. Review of the estimated hydraulic conductivity values in Table 1 indicates similar values for all tests performed. The mean values of the bedrock and saprolite tests are 6.72×10^{-5} cm/s and 4.56×10^{-5} cm/s (respectively), and the standard deviations of bedrock and saprolite tests are 8.52×10^{-5} cm/s and 2.68×10^{-5} cm/s (respectively). These numbers reflect the wide range in data values. No significant hydraulic conductivity contrast between saprolite and bedrock is apparent from these data. The 2.16×10^{-5} cm/s difference between the two sets of tests is within the limits of the hydraulic conductivity value estimation error. The standard deviation difference of 5.84×10^{-5} cm/s may slightly exceed the error associated with the methods for deriving the value and suggests that hydraulic conductivity is more variable in unweathered bedrock.

Four tests were performed in lithologically correlative strata, two in correlative limestone beds (superscript numbers 1 and 2 in Table 1) and two in correlative shale beds (superscript numbers 3 and 4). Of those four tests, one shows a hydraulic conductivity difference of more than one order of magnitude; the other three tests are very similar to one another and to the mean value of all tests performed. These results do not confirm a relationship between hydraulic conductivity and lithology but suggest that hydraulic conductivity is not laterally continuous within lithologies across the site. The results demonstrate, however, that the hydraulic conductivity of limestone-dominated lithologies is not significantly different from that of shale.

Comparison of FY 1989 hydrologic test results with those obtained in FY 1988 using a longer 3.66-m (12-ft) interpacker spacing indicates that the scale of testing has little to no effect on the interpreted values of hydraulic conductivity. The average hydraulic conductivity value for those tests is 5.44×10^{-5} cm/s, which suggests that individual bedrock lithologies exhibit the same range of hydraulic conductivity values as several lithologies combined. It also suggests that in the principal shallow aquifer (to depths perhaps as great as 100 ft), water-producing zones exceed 12 ft in thickness, making the ability to test the hypothesis impossible.

5.3 TRACER MIGRATION AND WATER ELEVATION DATA ACQUISITION AND ANALYSIS

This section describes the relationship between the water table configuration on the direction and rate of tracer migration consistent with working hypotheses developed from the preliminary conceptual model. In addition, it examines both aquifer and tracer migration response to precipitation.

5.3.1 Tracer and Water Table Elevation Data Acquisition

Water samples and water table elevation data were collected to analyze the hypothesis that the transient rate of tracer migration was related to a changing hydraulic gradient. Beginning in late December 1988, after the onset of precipitation and the accompanying rise in the water table, biweekly water level data and water samples were collected from the site. In general, water level data from all shallow wells were collected as close to the biweekly schedule as practicable. While sampling of the Rhodamine-WT dye was performed biweekly, not all wells were sampled at each sampling interval. The rationale was to perform sufficient sampling to delineate the leading edge of the tracer plume and to monitor changes in tracer concentration over time in the main body of the plume. A reduced sampling frequency was performed to verify the lateral and vertical boundaries of the plume. A greatly reduced water level and sampling program was implemented after many of the shallow wells went dry in the summer months.

Appendix A contains well hydrographs from April 1988 through June 1989. These data are still being obtained and will be included in the anticipated FY 1990 follow-on study results. Appendix B contains graphs of the change in tracer concentration over time; these illustrate differences in tracer arrival throughout the detection well field.

5.3.2 Analysis of the Rate of Tracer Migration

Tracer concentration data (Figs. 4 and 5) document the transient rate of tracer migration throughout the test. These data are illustrated as the log of the rate of change in tracer concentration as a function of time over the tracer travel distance to June 1989 (Fig. 6). Figure 6 suggests that the initially rapid rate of tracer migration is related to the presence of a narrow conduit of comparatively high hydraulic conductivity that is oriented parallel to geologic strike. The interpretation is supported by the erratic tracer migration rate and the extremely narrow overall plume shape. These data suggest that the conduit is hydrologically continuous for ~11 to 15 m (36 ft). The continued presence of extremely high tracer concentrations at and near the injection well suggests the conduit may represent bedding plane and/or strike set fractures that allow only small amounts of tracer to migrate from the injection source because of low fracture porosity. Prominent tracer fingers at the leading edge of the plume and an apparent bifurcation of the tracer plume through apparent preferred flow pathways midway along the tracer migration path suggest that additional conduits are present in the flow field.

Analysis of tracer migration and hydraulic head data indicates that the rate of migration is weakly dependent on the gradient. Figure 7 illustrates representative hydraulic gradient profiles from water elevation data that include the gradient immediately prior to tracer injection. Figure 8 illustrates the log of incremental tracer migration velocity for the 100- and 1000-ppb isopleths derived from contours of tracer concentration data. Caution

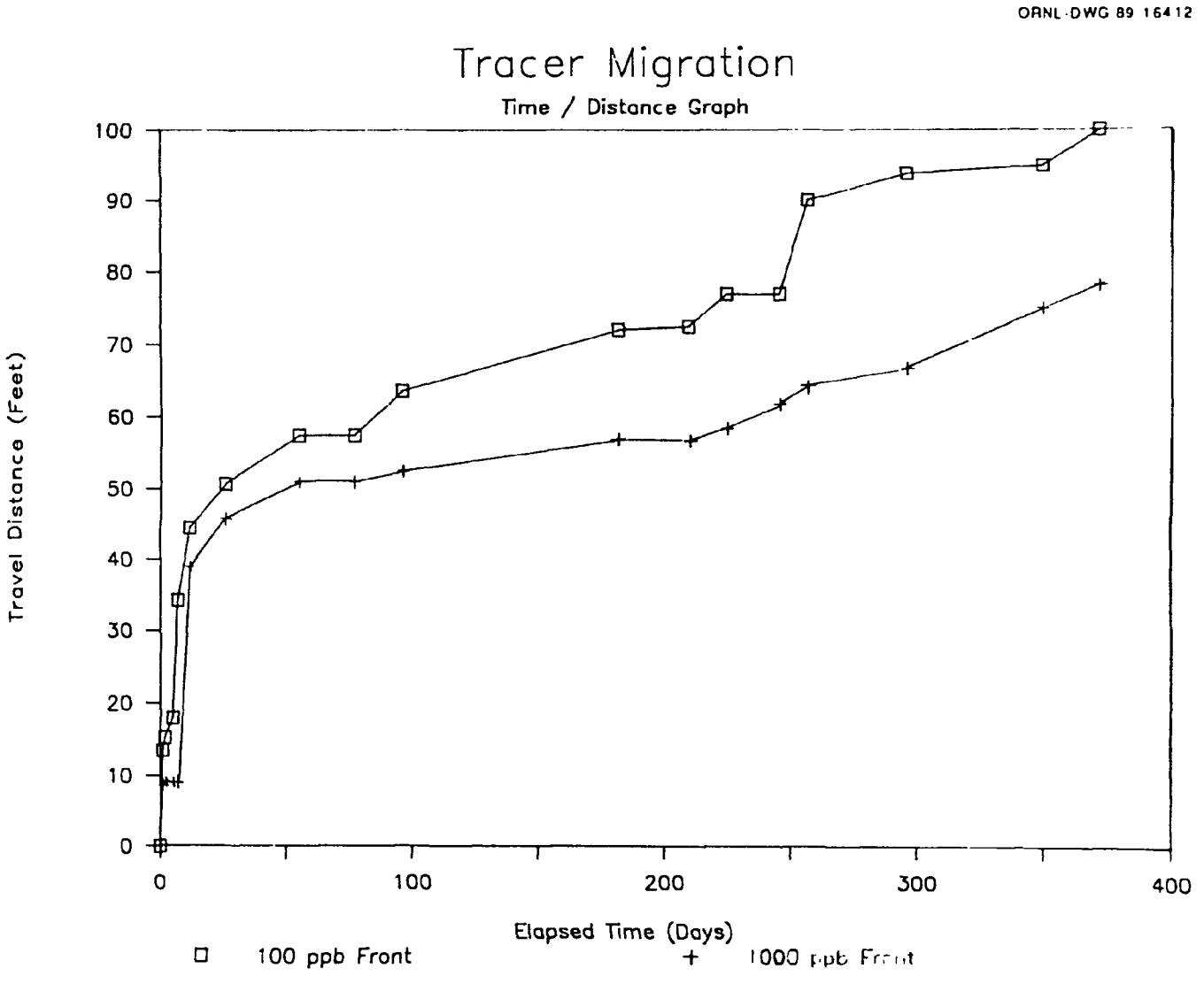

Fig. 4. Rate of tracer migration since time of injection.

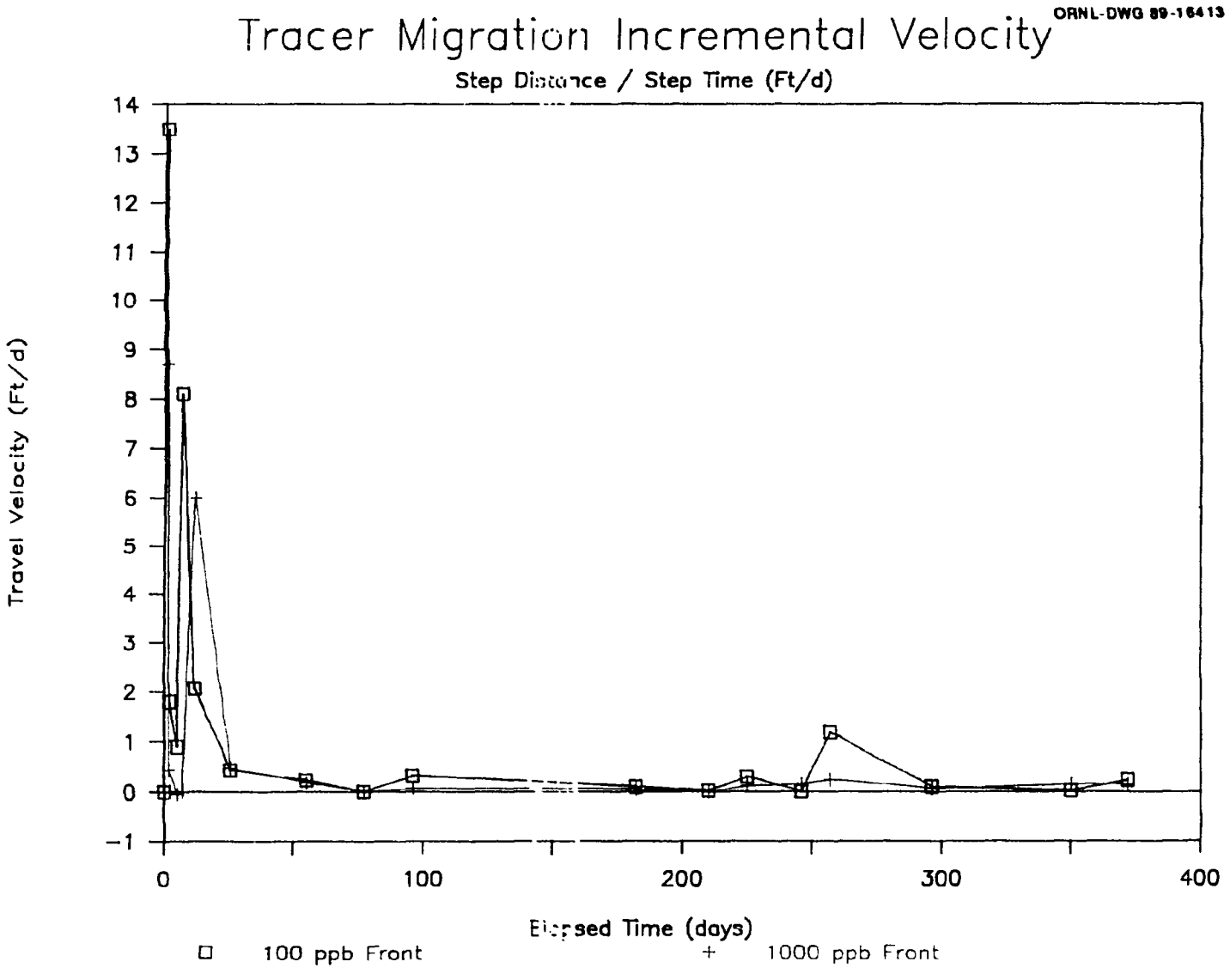

Fig. 5. Incremental velocity of tracer migration since time of injection.

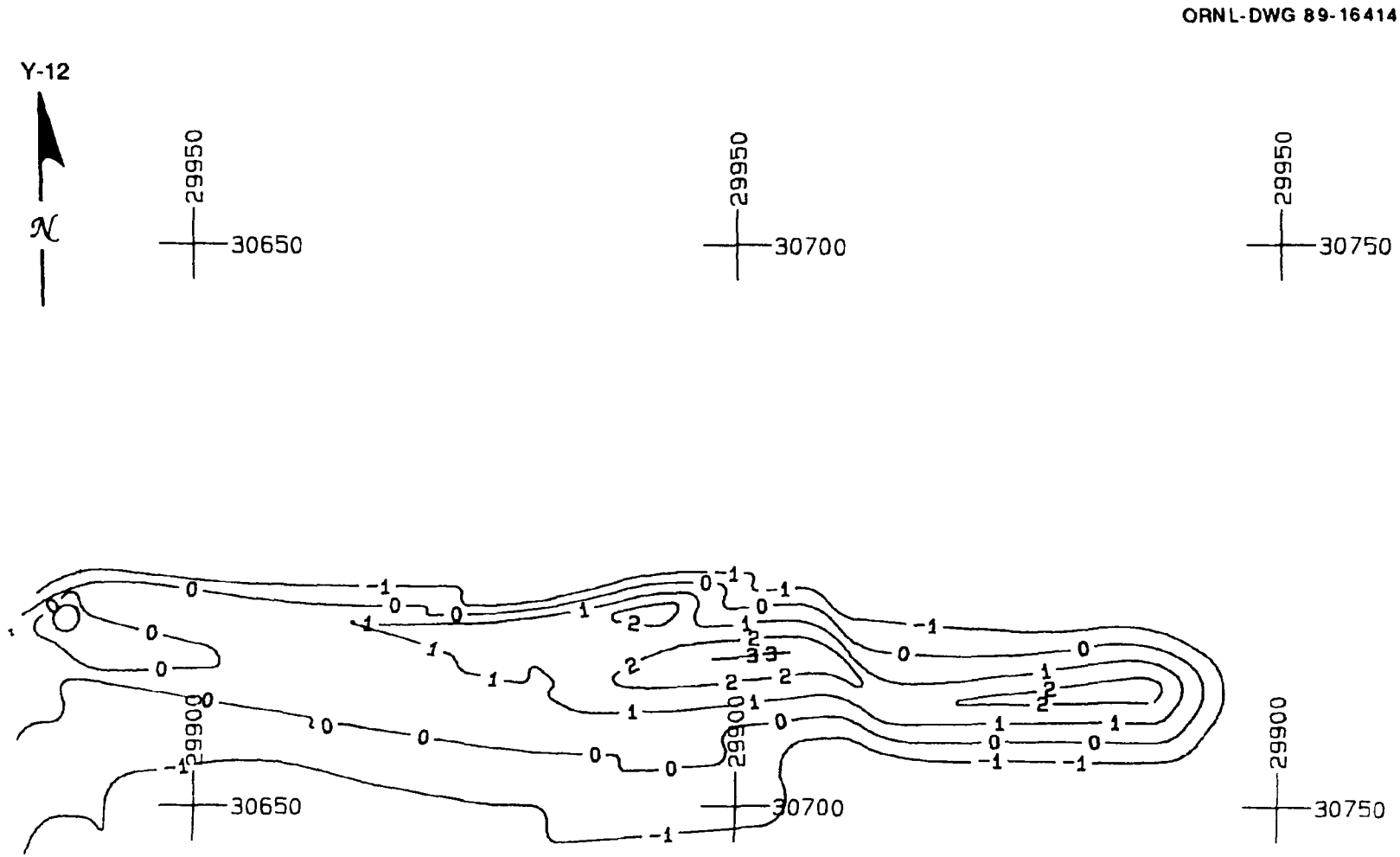

Fig. 6. Computer-generated contour map of log rate of change in tracer concentration over total plume pathway to June 1989. Contour interval log tracer concentration (ppb). Injection well located within 2 ppb contour at right of figure.

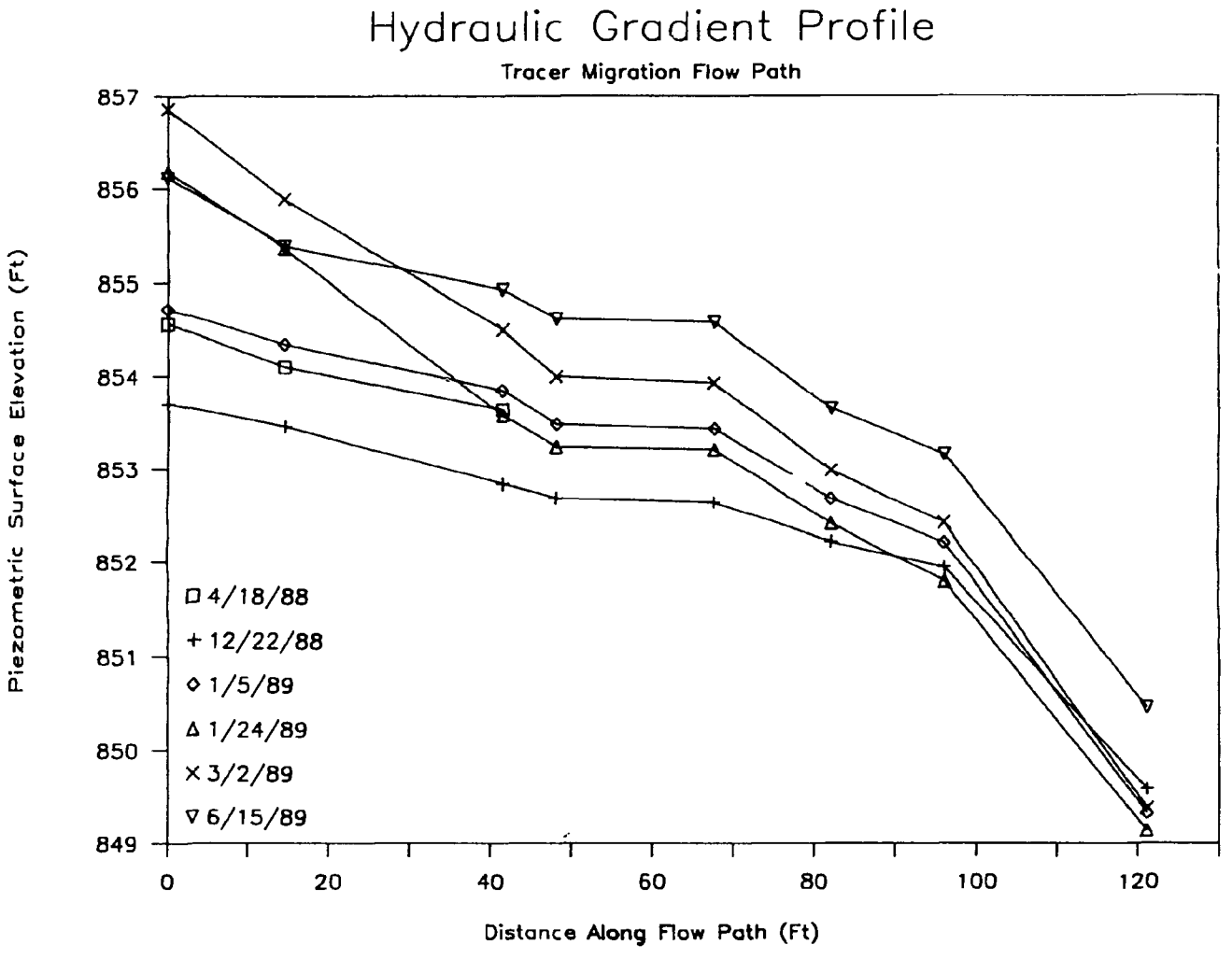

Fig. 7. Hydraulic gradient at representative locations in the well field. Square symbol represents gradient data 2 days prior to tracer injection.

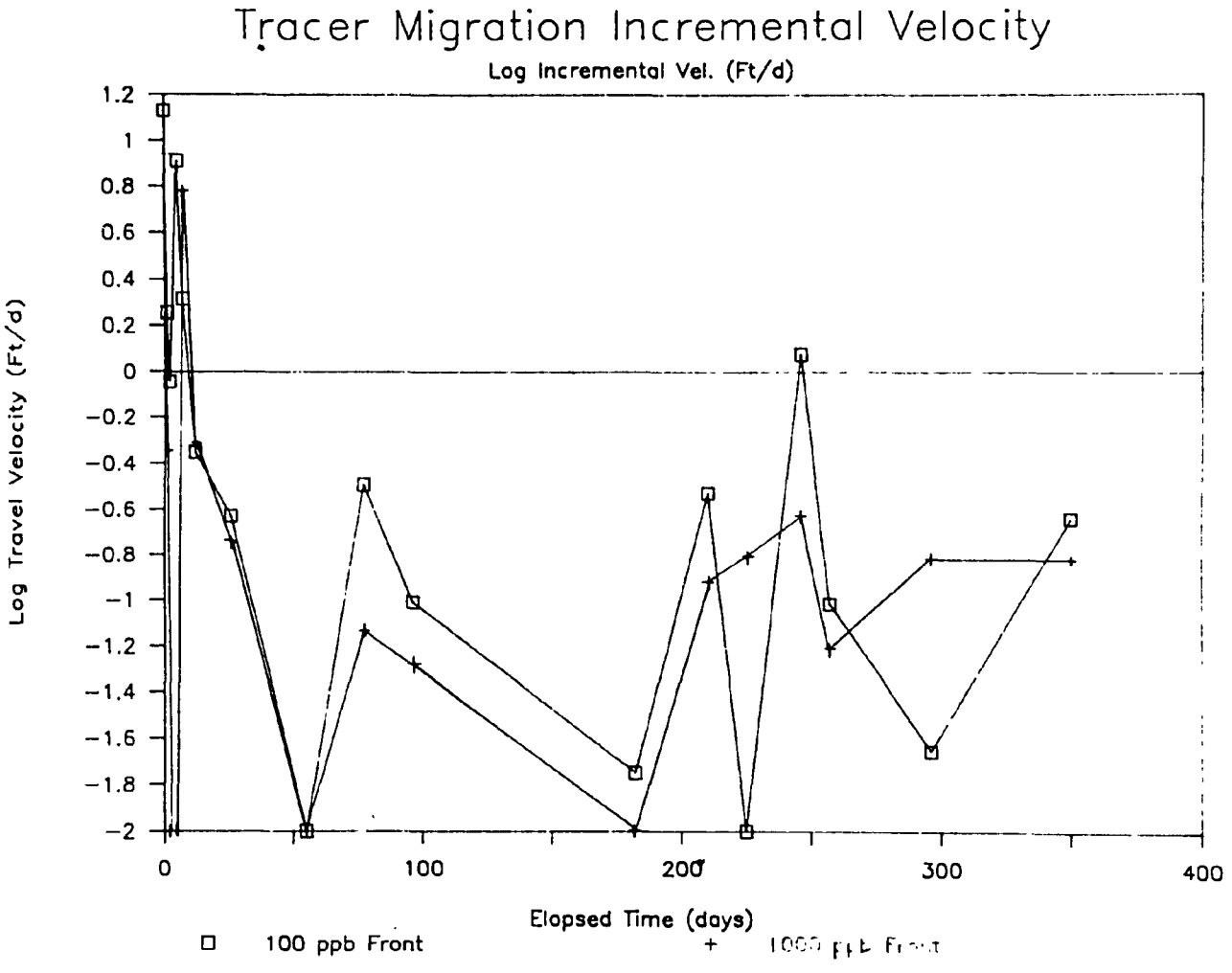

Fig. 8. Tracer migration incremental velocity for 100 and 1000 ppb tracer fronts.

must be used in possibly overinterpreting comparisons of these data because the contour-derived velocity figure may contain contour artifacts; however, in general, the tracer migration rate is not obviously related to the gradient. While a generally steeper slope in the near field (~40 ft from the injection well) and a generally flat slope in midfield (from ~40 to 70 ft) coincide with rapid and slower tracer migration rates, respectively, the much steeper gradient slopes in the far field do not coincide with rapid migration rates. These data are interpreted to support the concept of the presence of elevated hydraulic conductivity conduits. The tracer migration rate is interpreted to be weakly dependent on the hydraulic gradient and strongly dependent upon the presence or absence of bedrock features (connected fractures?) that alter local permeability.

The possibility that the initial rapid tracer migration rate in the near field was induced by a concentration gradient caused by the slug dye injection is not supported by tracer concentration data (Appendix B). Examination of those data for the dye injection well (GW-484) indicates that extremely high concentrations of dye remain in the well to provide a continued concentration gradient source. Data for near-field wells exhibiting high concentrations (GW-481B, GW-486, GW-487, and GW-493) indicate that maximum tracer concentration was reached very soon after initial detection and changed little thereafter despite the continued presence of a high concentration source in the injection well. In addition, the density similarity of the Rhodamine-WT dye to that of water is thought to essentially eliminate the possibility of a density-induced gradient.

5.3.3 Analysis of the Direction of Tracer Migration

Water table contour maps (Figs. 9, 10 and 11) reveal the irregular shape of the water table surface. Comparison of these figures with a representative tracer concentration contour map (Fig. 12) indicates that the pathway of maximum tracer concentration and the tracer fingers at the leading edge of the plume are coincident with narrow elevated hydraulic head zones. Rather than migrating in the direction of maximum gradient to a lower head position as predicted in conventional porous medium analysis, the center of mass of the tracer plume and the leading fingers remain on the axes of strike-parallel water table divides. The presence of these water table highs supports the suggestion that the tracer migration pathway is related to local and regional geologic structural features. The elevated head zones are interpreted to represent elevated hydraulic conductivity and head along strike-parallel zones of fracturing, and tracer is interpreted to be migrating along these pathways because these elevated conditions provide available flow for tracer transport.

5.3.4 Analysis of Tracer Position in the Aquifer

To document the presence or absence of tracer in unweathered bedrock beneath the depth of the majority of tracer detection wells, GW-499Q and GW-499W were drilled to intersect and sample the stratigraphic horizon of apparent tracer migration just beneath the bedrock weathering interface. Shallow bedrock piezometer cluster wells near and downgradient from the injection well were also sampled. Core hole GW-499Q was left as an open hole to a total depth of 51.5 ft, and a piezometer was constructed in the lower portion of GW-499W (4.5- to 9.5-ft depth) to isolate the tracer migration strata in unweathered bedrock. Tracer concentration data indicate that tracer is not present in GW-499Q or any of the bedrock cluster detection wells beneath the tracer plume and has not

Fig. 9. Computer-generated water table contour map based on December 22, 1988 data. Contour interval 0.5 ft. Irregular contours at left of figure are an artifact of the well boundary. Scale 1" = 60'.

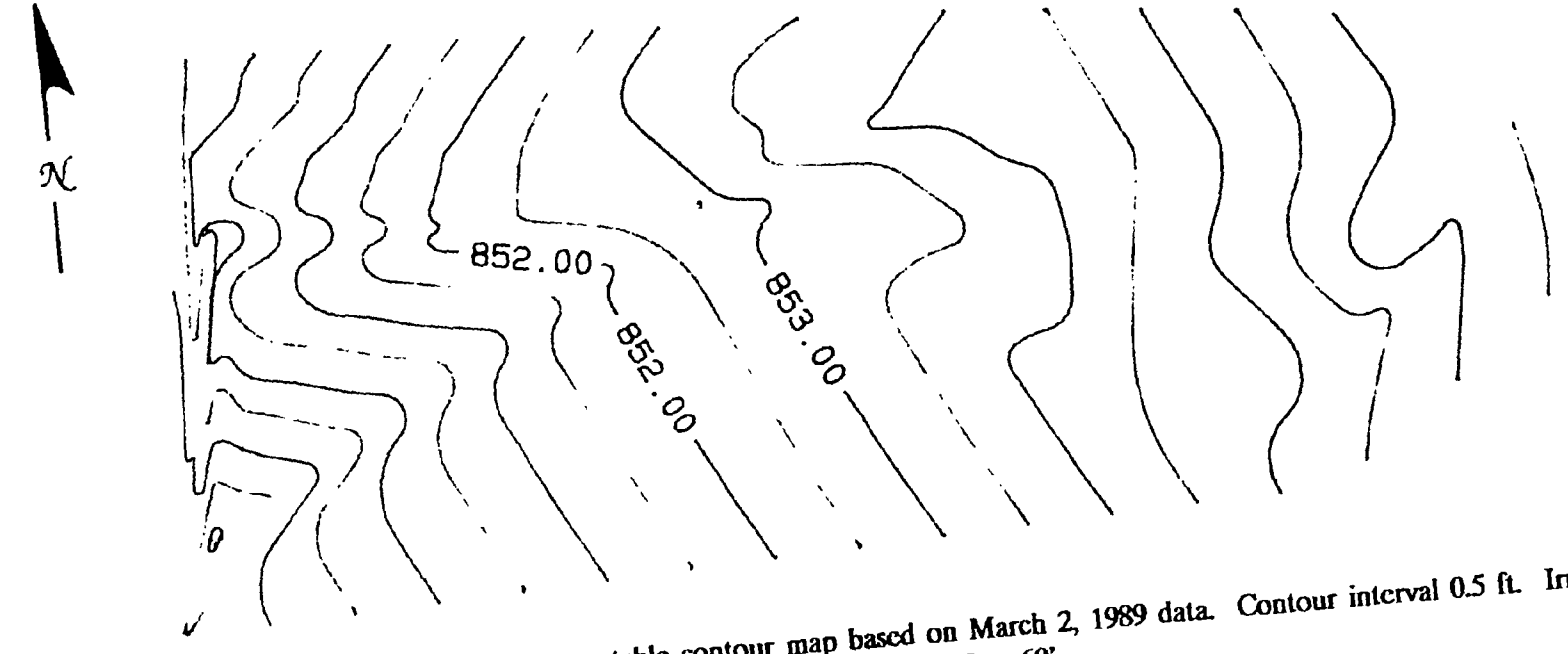

Fig. 10. Computer-generated water table contour map based on March 2, 1989 data. Contour interval 0.5 ft. Irregular contours at left of figure are an artifact of the well boundary. Scale 1" = 60'.

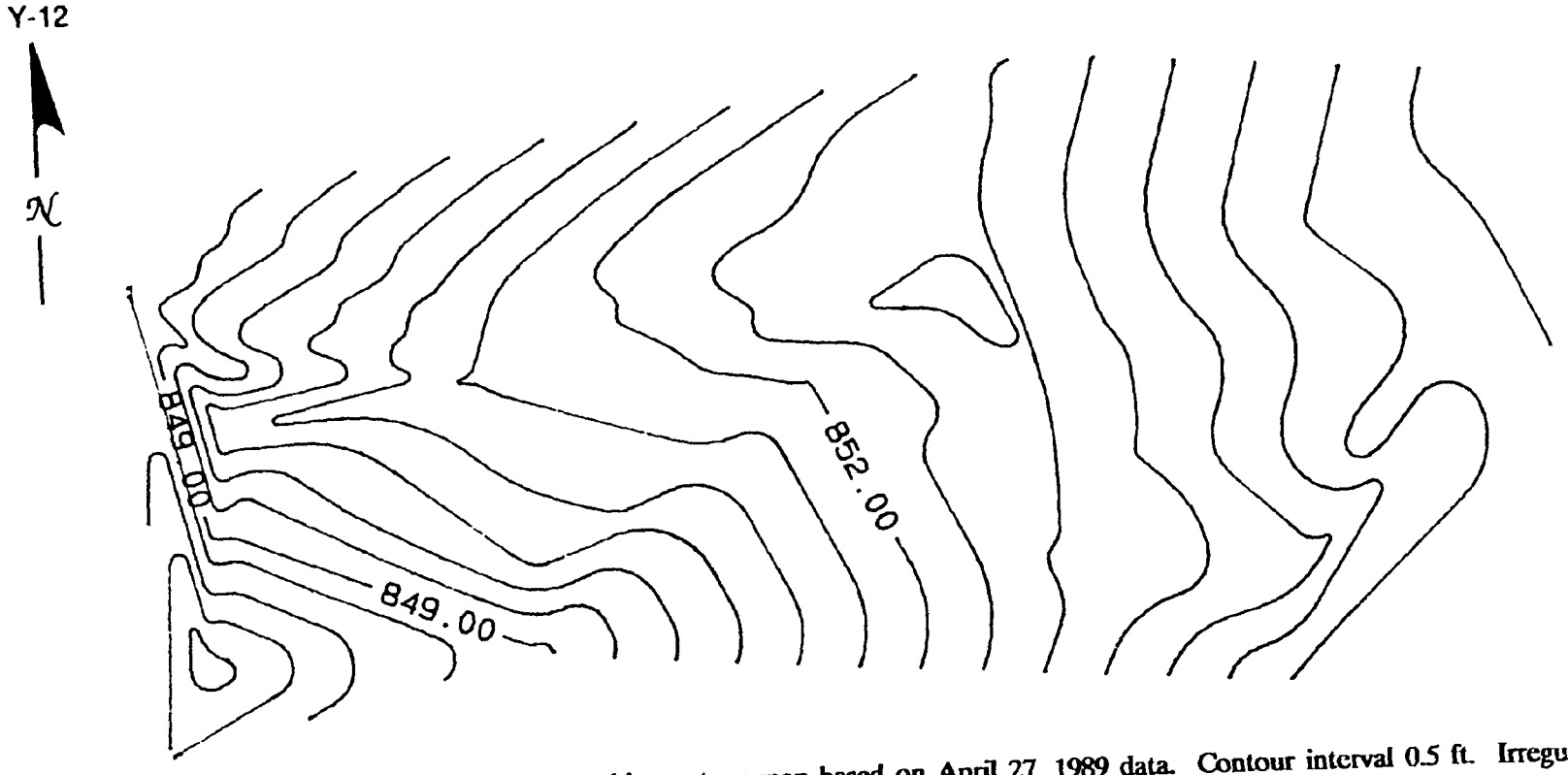

Fig. 11. Computer-generated water table contour map based on April 27, 1989 data. Contour interval 0.5 ft. Irregular contours at left of figure are an artifact of the well boundary. Scale 1" = 60'.

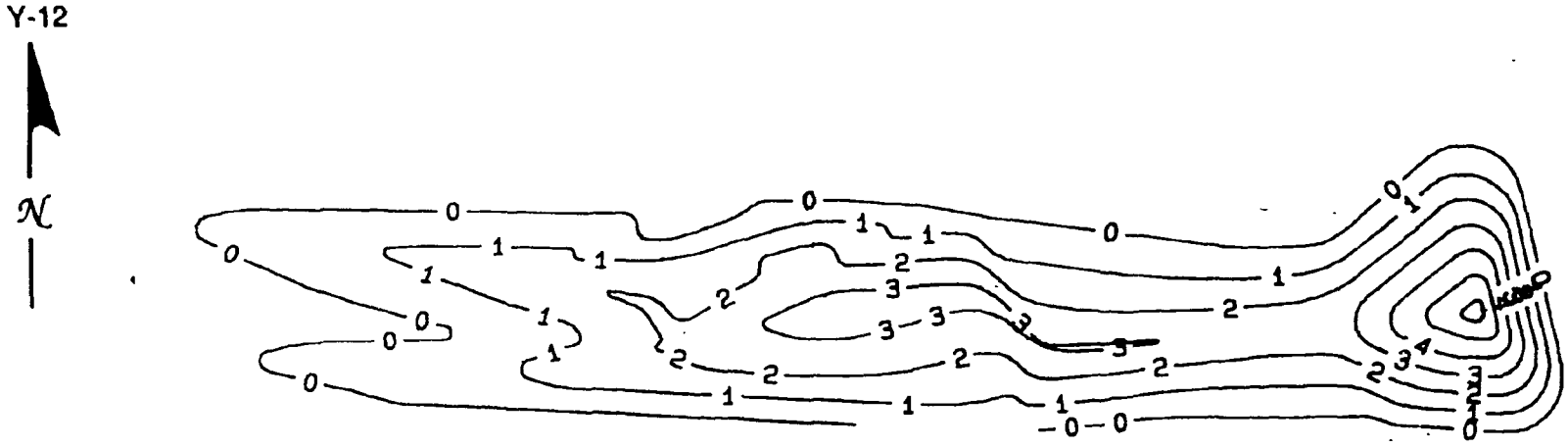

Fig. 12. Computer-generated contour map of log tracer concentration day 96 after injection. Contour interval log tracer concentration (ppb). Injection well within closed contours at right. Scale 1" = 24'.

migrated beneath the water table position in which it was injected. Low concentrations detected in GW-499W are attributed to suspected incomplete isolation of unweathered rock during piezometer construction or a reduction in the measured upward hydraulic head gradient at lower elevations near the creek. These data indicate that tracer is not migrating in unweathered bedrock beneath the depth of detection wells but is confined to the uppermost portions of the aquifer in saprolite. Because the analysis of hydrologic test data indicates a lack of significant conductivity contrast between bedrock and saprolite, the position of the tracer in the uppermost portions of the aquifer is thought to be related to the measured upward head gradient at the site.

The interpretation of an upward head gradient is supported by cross-sectional contouring of hydraulic head in cluster wells in the upper end of the well field (Figs. 13 and 14). While caution also must be used in possibly overinterpreting these figures, several features are germane to the discussion. First, consistent with Figs. 9, 10, and 11, the shallowest aquifer consists of alternating zones of higher and lower head. The tracer migration pathway is within the elevated head zone potential on the left side of Fig. 13; tracer has not migrated into the adjacent lower head zone to the right (southeast). Second, the overall shape of the isopleths essentially parallel to bedding dip suggests that lithology and/or strike-parallel fractures affect hydraulic head.

5.3.5 The Effect of Precipitation on the Water Table and Tracer Migration

Figures 15a and 15b compare study site water elevation data and precipitation data from the Bear Creek Valley Burial Grounds. The water elevation data were obtained from a 3-tiered cluster well in the upper portion of the well field for which data were collected by downhole pressure transducers and a data logger at 8- or 12-h intervals. For the period for which sufficient data are available and illustrated, the comparison shows the essentially immediate aquifer response to precipitation events. While some minor delay is evident in the deep well response compared with the shallow and intermediate-depth wells, the aquifer response at all depths is essentially immediate. The comparison also documents that in all cases, aquifer recharge is essentially immediate while discharge is a gradual water table decline.

Precipitation data from the Bear Creek Burial Grounds and incremental tracer velocity data for the 100- and 1000-ppb tracer concentration isopleths were compared to evaluate the effects of the annual precipitation cycle and precipitation events on the tracer migration rate. The comparison (Figs. 16a and 16b) indicates that within the limits of data density, a general relationship exists. Depending on the time of year, tracer migration in the shallow aquifer responds almost immediately to rainfall events of ~20 mm and greater. Intuitively, one would anticipate precipitation to cause reduced tracer concentrations; however, small increases in tracer concentration can be correlated with rainfall events at wells throughout the well field. This provides a predictable relationship between increases in concentration and precipitation. A more rigorous analysis of the effects of annual and short-term precipitation on the flow rate can be performed with the available data that would document the transient nature of the shallow aquifer and provide temporal boundary data for computer simulations.

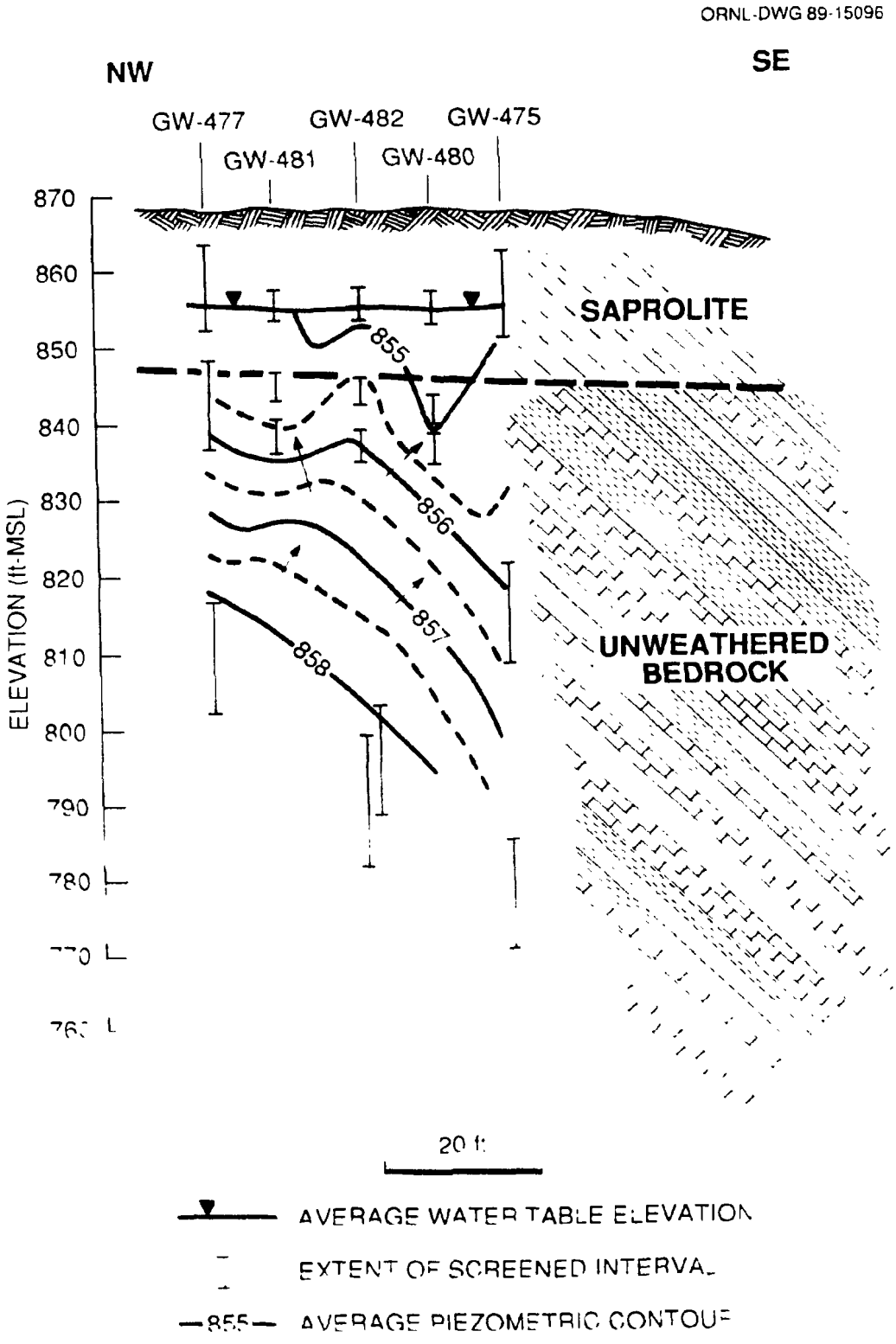

Fig. 13. Strike normal, computer-generated piezometric contour cross section of the eastern portion of the site. Arrows represent direction of maximum vertical hydraulic head gradient. No vertical exaggeration.

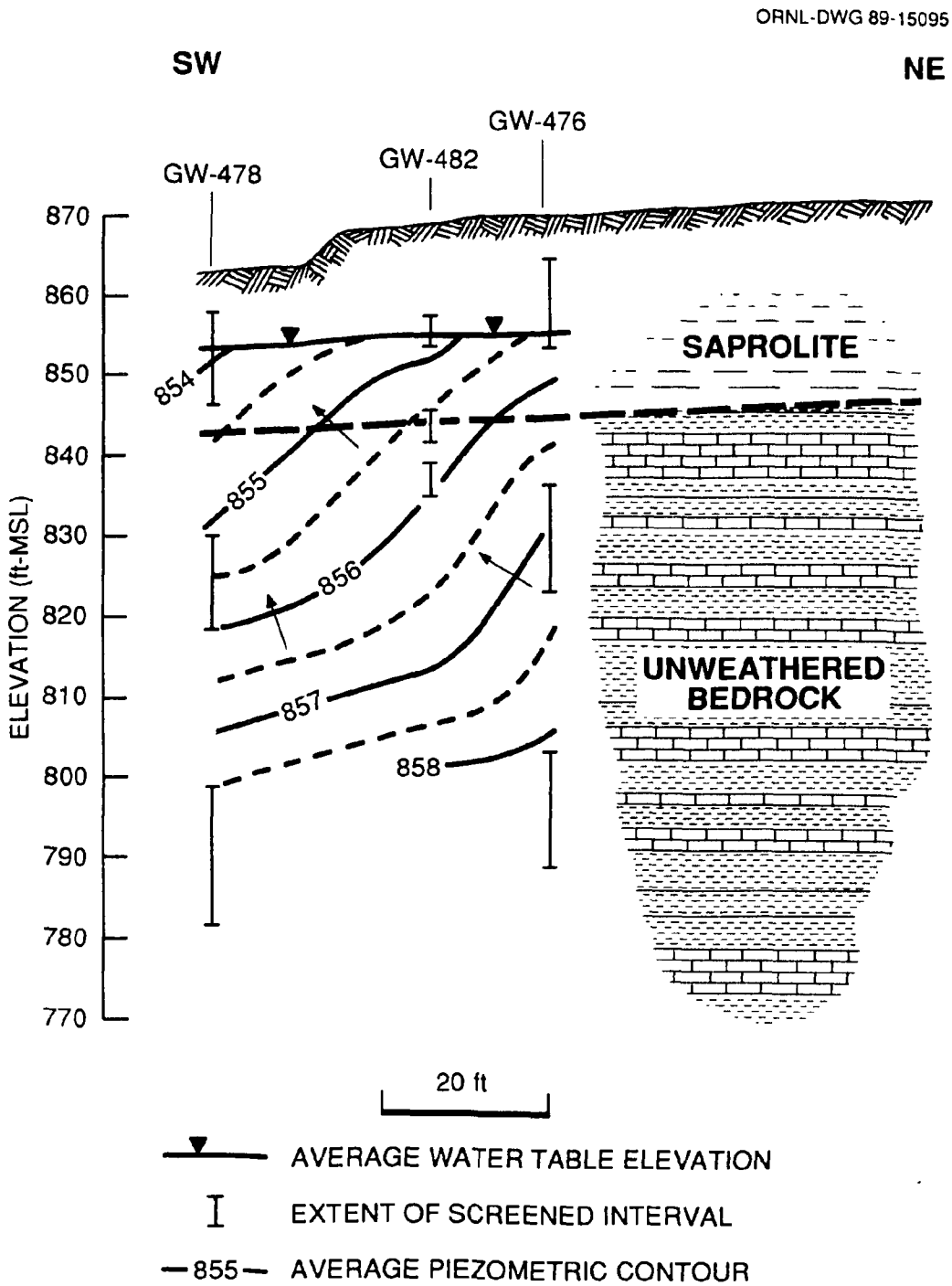

Fig. 14. Strike parallel, computer-generated piezometric contour cross section of the eastern portion of the site. Arrows represent direction of maximum vertical hydraulic head gradient. No vertical exaggeration.

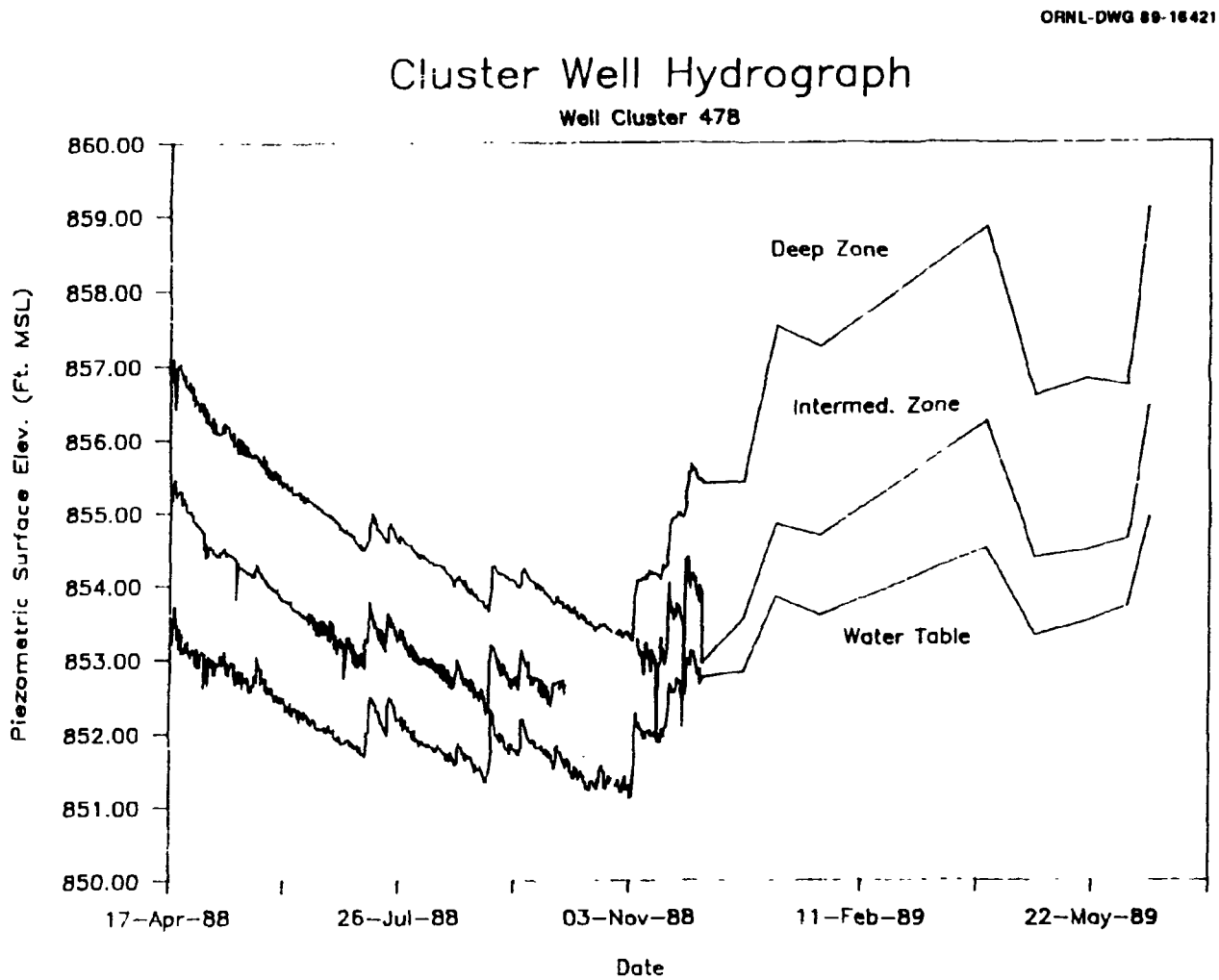

Fig. 15a. Cluster well hydrograph, well GW-478.

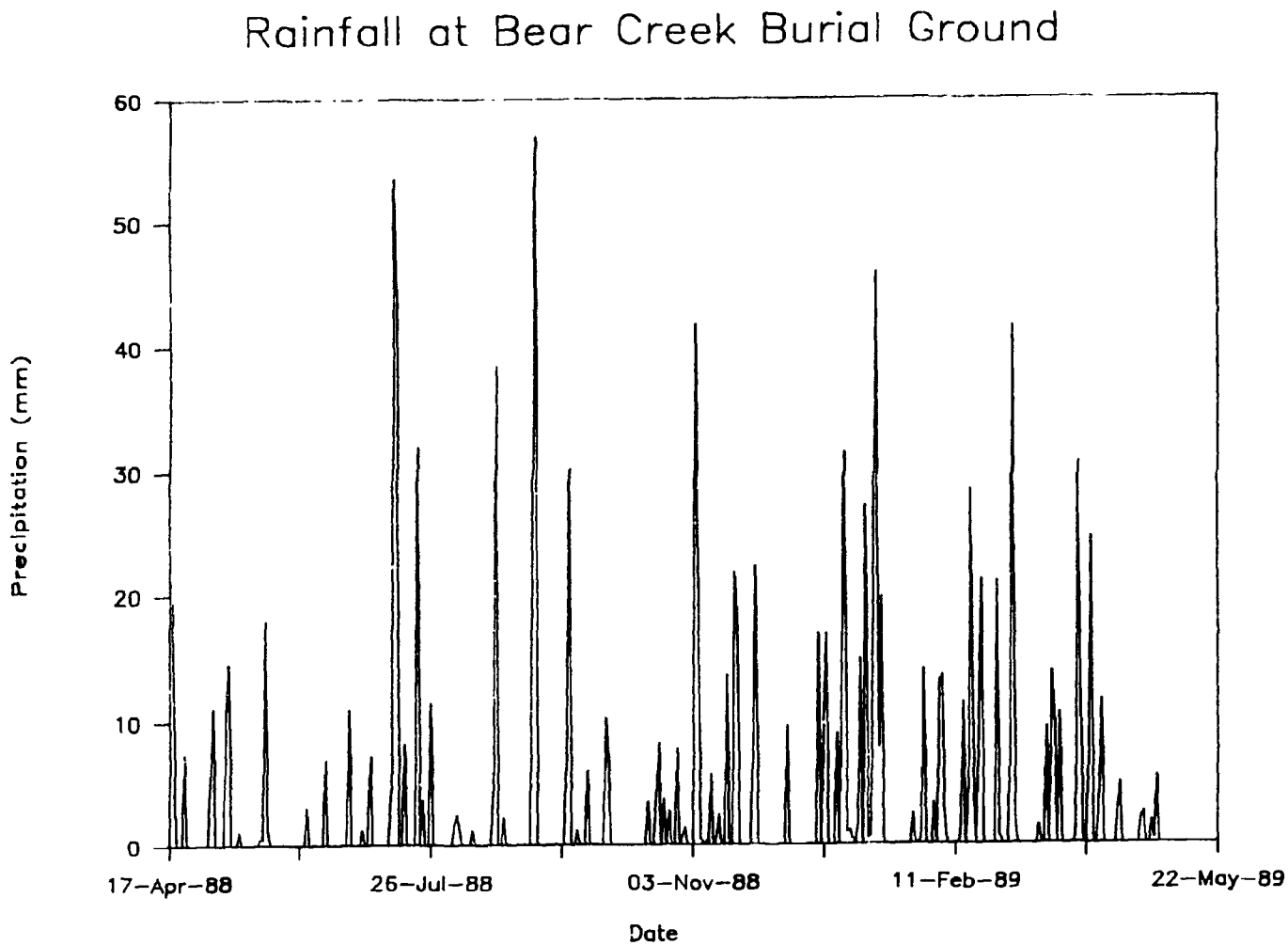

Fig. 15b. Precipitation data from the Bear Creek Burial Grounds.

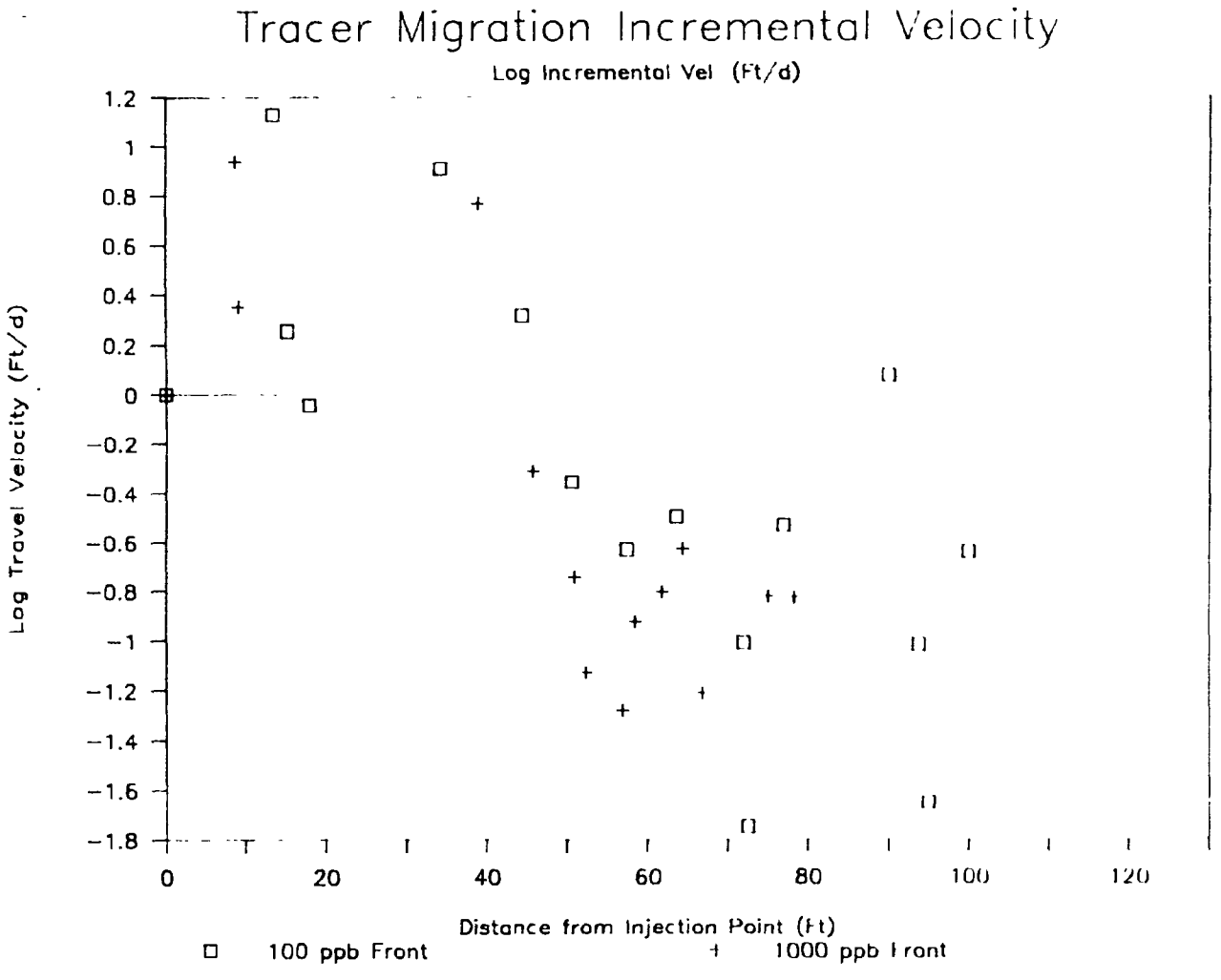

Fig. 16a. Log incremental tracer migration velocity for the 100 and 1000 ppb tracer fronts.

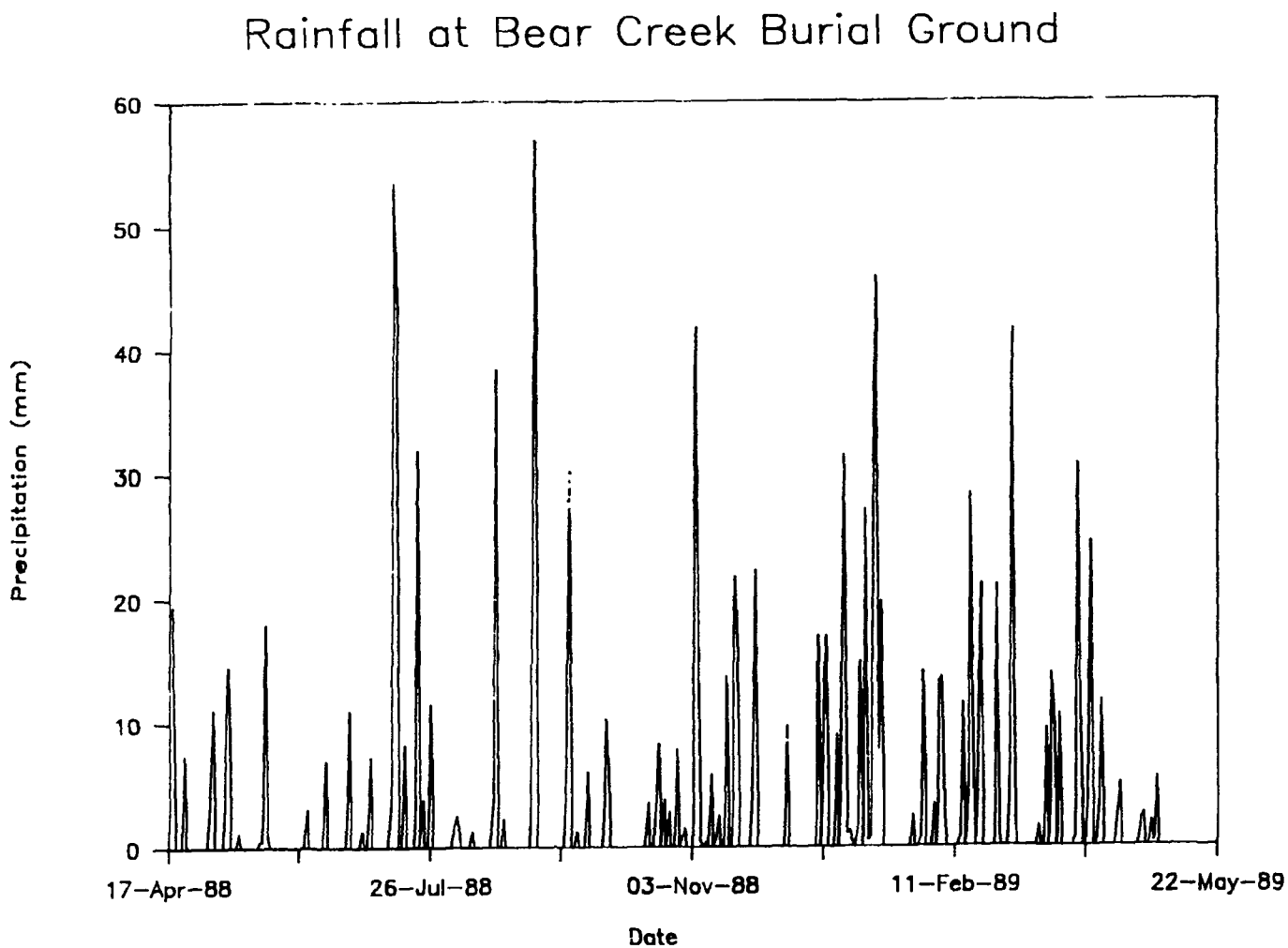

Fig. 16b. Precipitation data from the Bear Creek Burial Grounds.

5.3.6 The Overall Site Water Table Configuration

Analysis of water table data indicates ~0.3- to 1.5-m (1- to 5-ft) annual fluctuation in the water table, with the greatest fluctuation occurring at higher elevations on the eastern portion of the site. Water table contours, including those outside the immediate tracer site, indicate that the topographic divide east of the model validation site is not a groundwater divide (Fig. 17). This suggests that head potential for the tracer test is derived from a location farther to the east and/or from greater depths, and the water table at the test site is not a subdued replica of surface topography. Because of greater distances for discharge to local surface drainages, this observation may alter conceptual models regarding groundwater residence time in the shallow aquifer.

5.4 DATA SYNTHESIS AND CONCEPTUAL MODEL REVISION

Hypotheses developed in FY 1988 based on observed tracer migration behavior are as follows: (1) the heterogeneous bedrock units are laterally continuous across the site, (2) a hydraulic conductivity contrast exists between silty limestone and shale interbeds within both weathered and unweathered bedrock, (3) an overall hydraulic conductivity contrast exists between weathered and unweathered bedrock, and (4) tracer is not migrating in unweathered bedrock beneath the depth of the tracer detection wells. The direction of tracer migration and its narrow width (2 to 3 m) was believed to be controlled by the hydrologic characteristics of the dipping heterogeneous bedrock lithologies, and the transient tracer migration rate was thought to be related to a fluctuating hydraulic head gradient profile caused by drought conditions.

The presence of a hydraulic conductivity contrast between heterogeneous bedrock lithologies or between weathered and unweathered bedrock is not supported by analysis of site hydrologic test data. Hydraulic conductivity values appear to vary randomly between $\sim 1 \times 10^{-4}$ and 5×10^{-6} cm/s for any selected test interval or depth. Rather than being controlled by the orientation of heterogeneous lithologies, the direction of tracer migration and the narrow plume width are related to elevated hydraulic head and hydraulic conductivity along strike-parallel fracturing zones. The tracer migration rate is related the presence of these zones and to precipitation exceeding 20 mm, not to the hydraulic gradient profile.

Based on these findings and results of flow and transport modeling to be described in Sect. 7, a revised conceptual model has evolved that is a modification of the preliminary conceptual model. The revised conceptual model describes bedrock material property heterogeneity with respect to hydraulic conductivity as randomly distributed within the range of values measured at the site. Flow occurs primarily through fractures oriented parallel to geologic strike (consistent with aquifer anisotropy) and secondarily through fractures that cross bedding. Randomly distributed, discontinuous, strike-parallel zones of elevated hydraulic conductivity act as preferred pathways for flow and transport.

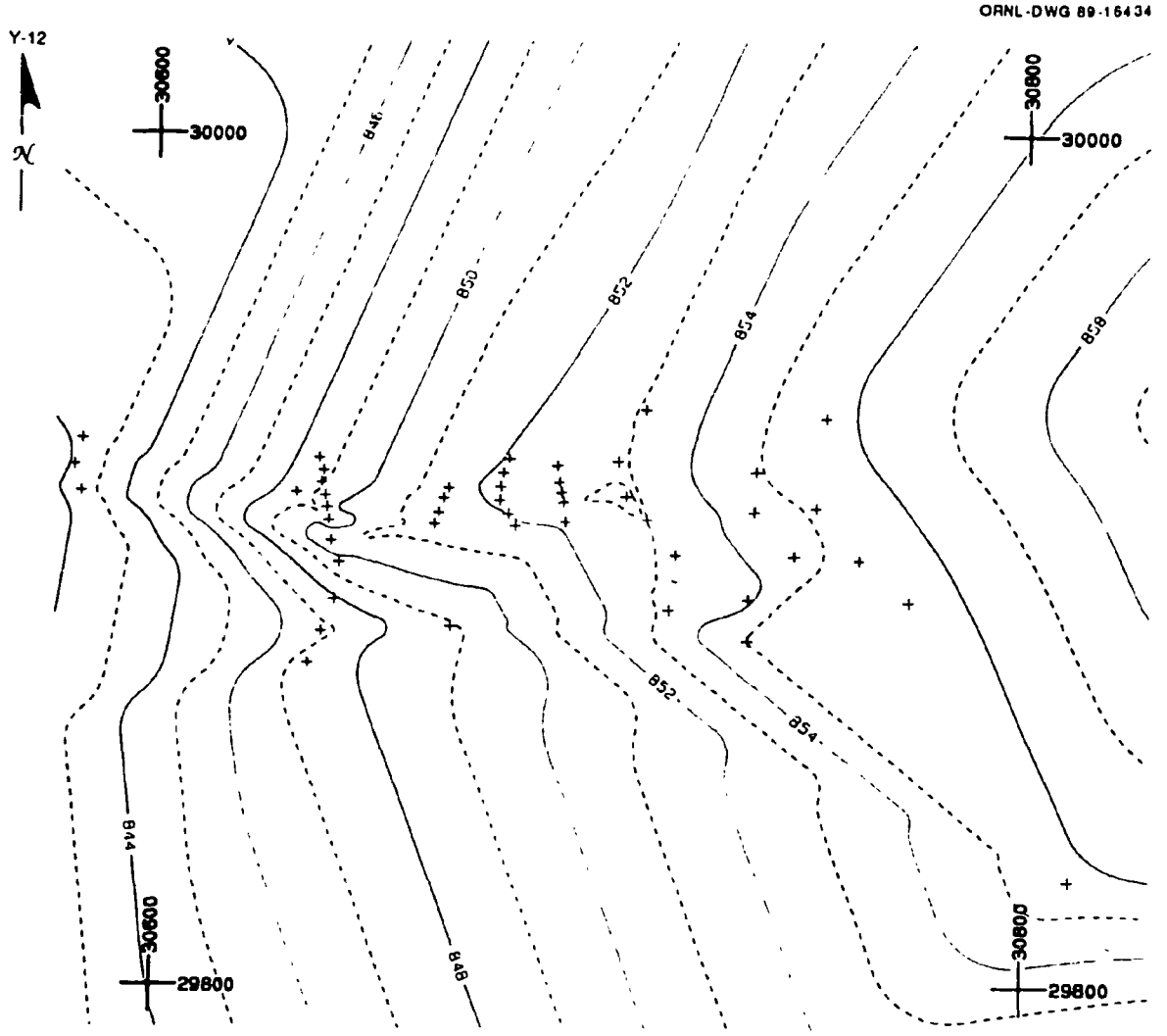

Fig. 17. Computer-generated, tracer test site piezometric surface contour map using on and off-site well and creek data from April 14, 1989. Contour interval 1 ft. Data locations represented by + symbol;

6. MODELING

6.1 GRID DEVELOPMENT

The geologic-based conceptual model for flow and transport that was developed following the FY 1988 phase 1 study was incorporated into preliminary modeling in FY 1989 by the construction of the computer model grid. This section describes the process of model grid development and modifications to the grid as the task progressed and the conceptual model was refined.

Rock core and geophysical log data from FY 1988 phase 1 site core holes were correlated and examined in detail to identify the character of bedrock heterogeneities. These data were projected to the weathered/unweathered bedrock interface (the depth of observed tracer migration). Alternating higher and lower hydraulic conductivity values were assigned to adjacent bedrock materials in an orientation normal to geologic strike. The result was a plan view series of lines parallel to geologic strike that represent boundaries between heterogeneous bedrock materials at the bedrock weathering interface.

Review of drilling logs also indicated that in any line of closely spaced detection wells drilled normal to geologic strike, depths to unweathered bedrock commonly varied by as much as 0.6 m (2 ft). To determine the nature of these apparent large variations in depth to unweathered bedrock, site rock core and geophysical log data were compared with detection well locations. The comparison revealed that shallower depths to bedrock occurred in shale lithologies and deeper depths corresponded to limestone lithologies. The model grid, then, not only corresponded to materials of different hydraulic conductivity but also to materials exhibiting greater and lesser degrees of weathering. Rather than a relatively planar surface, the weathering interface exhibits a corrugated appearance with as much as 0.6 m (2 ft) of vertical relief. One consideration of the preliminary conceptual model was that the tracer plume could be following a weathered limestone channel.

Figure 18 is a simplified block diagram of the geologic basis for the preliminary model grid preparation. The grid is a gently sloping plane tha represents the intersection of the dipping and heterogeneous bedrock lithologies at the bedrock weathering interface (the depth of tracer detection). This depth coincides closely with the water table. The grid consisted of a series of cells of alternating higher (representing limestone) and lower (representing shale and silty shale) hydraulic conductivity with the long axes parallel to geologic strike.

6.1.1 Grid Modification

As described earlier, continued use of the preliminary grid was not supported by analyses of all FY 1989 data. Rock core and tracer migration data indicated that orientation of the model grid parallel to geologic strike (the direction of aquifer anisotropy) was justified. Hydrologic test data indicated that with the exception of elevated hydraulic conductivity conduits, the distribution of hydraulic conductivity values occurred randomly, and the use of alternating layers of higher and lower hydraulic conductivity was not justified. To include the FY 1989 hydrologic test data, the hydraulic conductivity data frequency distribution function was sampled, and values were randomly assigned to all the elements of the grid. Initially, a conduit of 1×10^1 higher hydraulic conductivity was superimposed on the grid parallel to geologic strike from the tracer injection point for a distance of

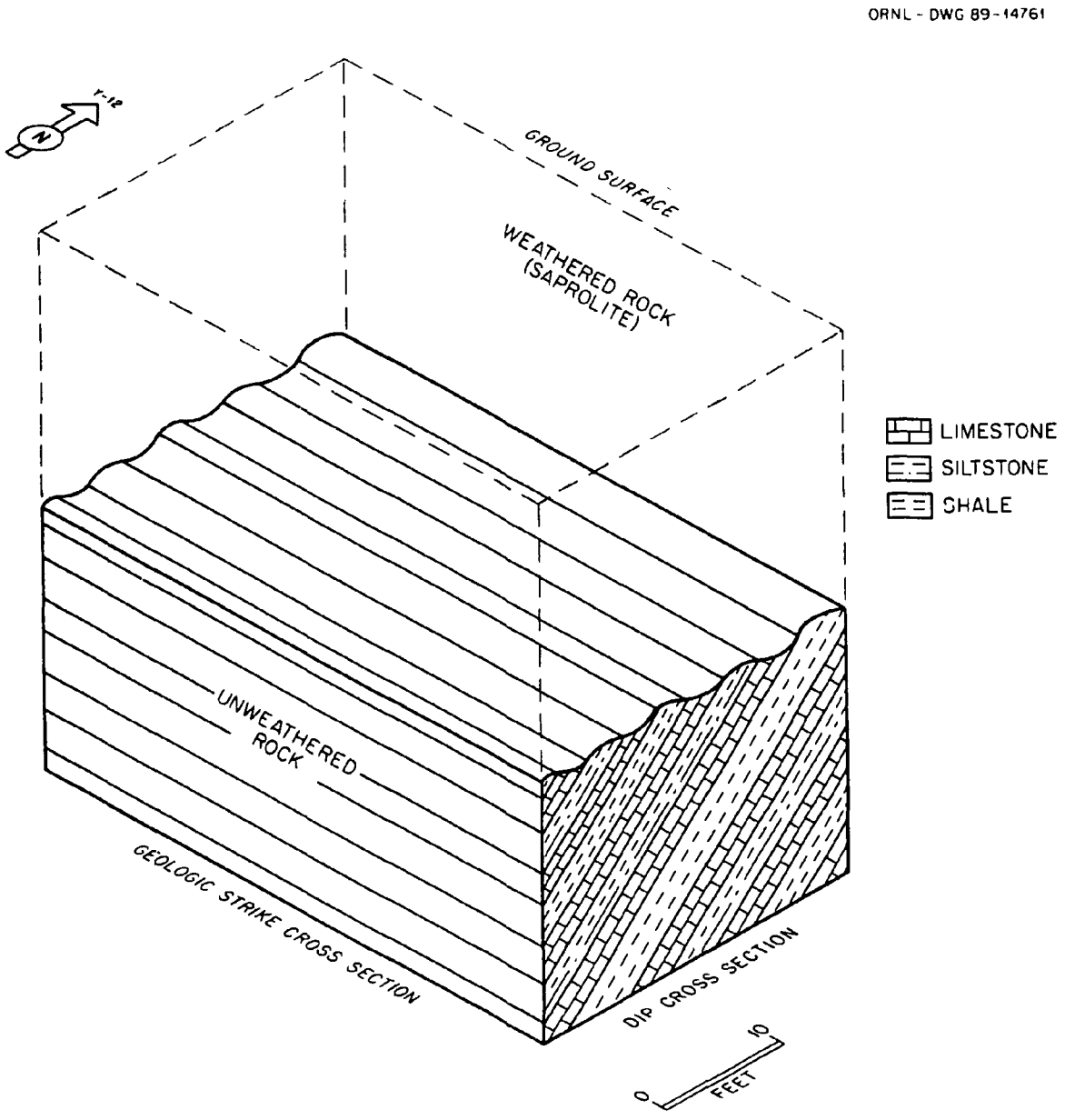

Fig. 18. Simplified conceptual block diagram of site geologic conditions.

~11 m (Fig. 19). After further analysis of tracer concentration and water table elevation data, two additional conduits were superimposed at locations dictated by those data (Fig. 20).

The final model grid consisted of a series of 1 × 3.6 m rectangular elements, with their long axes oriented parallel to geologic strike. Although all site test data do not support differences in hydrologic characteristics at the 1-m scale, this level of detail is required in the grid to resolve details in the tracer plume shape. Test simulations using larger dimension grid elements grossly resembled the tracer plume but failed to resolve details in tracer concentration.

6.2 MODELING ASSUMPTIONS

The approach to modeling was to begin at the most uncomplicated level and to increase complexity as dictated by preliminary results. The mathematical/computer modeling of tracer migration was performed by making the following basic assumptions:

1. Tracer migration can be simulated two dimensionally in a water table aquifer of nearly constant thickness.
2. Tracer concentration depends on hydrodynamic dispersion and advective transport.
3. No chemical reactions occur between the dye tracer (Rhodamine-WT) and any other agent that might alter tracer concentration.
4. Neither the groundwater nor the tracer undergoes changes in fluid properties (i.e., density or viscosity), and variations in conditions that might alter velocity (such as temperature) are negligible.
5. Darcy's Law is valid such that average linear velocity is determined by the hydraulic gradient and the principal directions and magnitudes of major hydraulic conductivities.
6. The principal media parameters, porosity and hydraulic conductivity, are temporally constant, and although the geologic media may be heterogeneous, the porosity is assumed constant throughout.
7. Although conceptual models may infer fractures to strongly affect flow, the system can be modeled as an equivalent porous medium.
8. Assuming a plan view model, vertical variations in hydraulic head are negligible.
9. The aquifer longitudinal and horizontal dispersivity are constant throughout the domain.

6.3 MATHEMATICAL FORMULATION

This section describes the mathematical basis for problem formulation and solution both in conjunction with and independent of field data acquisition and analysis. It includes and distinguishes between data derived and constrained model input parameters.

6.3.1 Domain

As described earlier, the direction and transient tracer migration rate was believed to be related to the hydrologic characteristics of the dipping and heterogeneous bedrock lithologies and a fluctuating hydraulic head gradient, respectively. To simulate the flow field and derive values for the velocity vector, the preliminary domain represented a

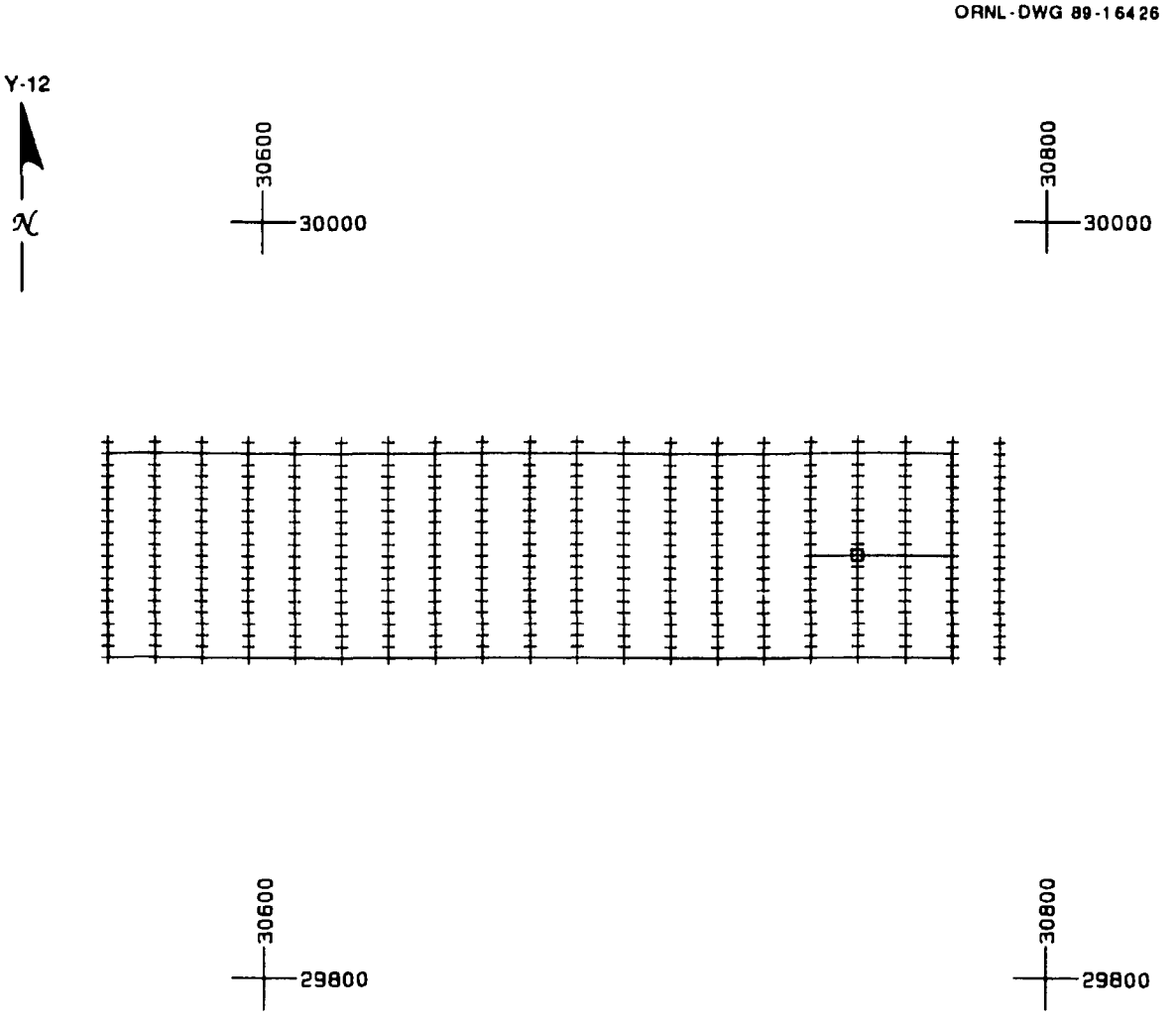

Fig. 19. Transport model grid domain with 1 superimposed conduit of elevated conductivity. Boundary coincides with rectangle in Fig. 1. Creek represented by line at left.

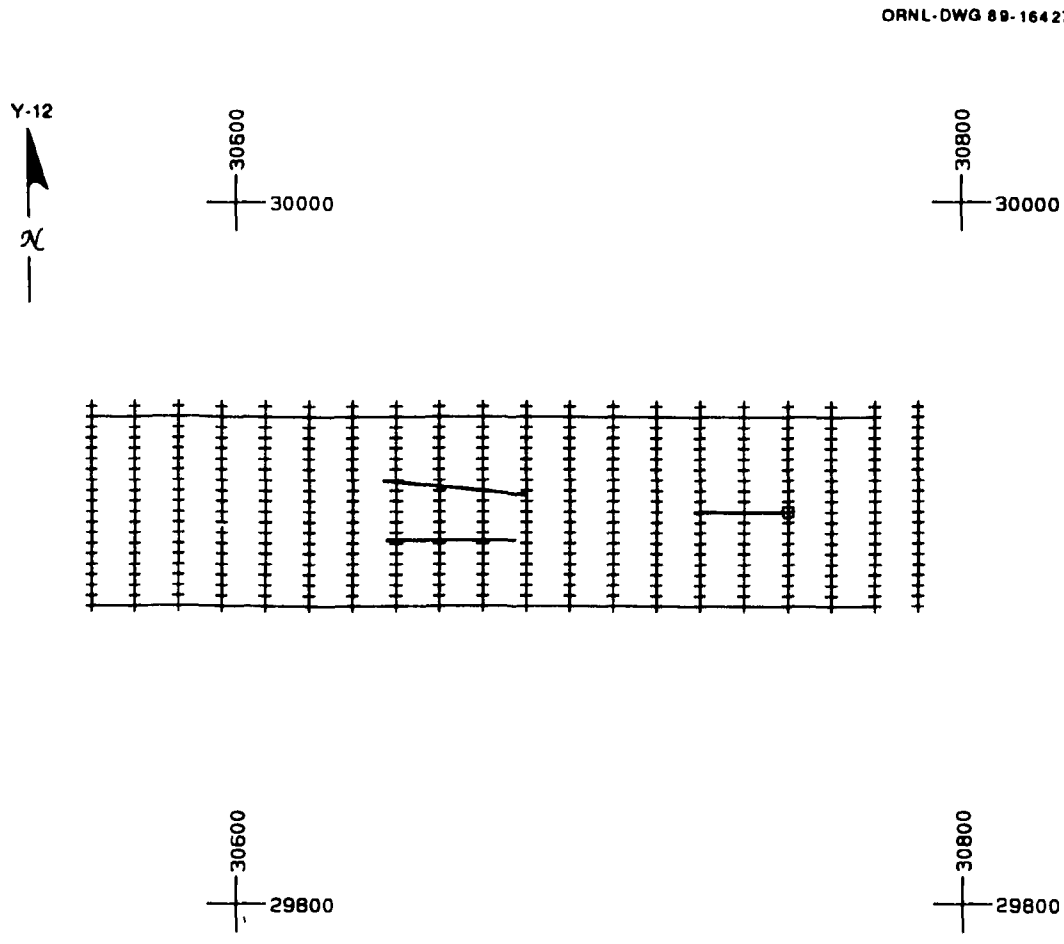

Fig. 20. Transport model grid domain with 3 superimposed conduits of elevated conductivity. Boundary coincides with rectangle in Fig. 1. Creek represented by line at left.

strike-parallel rectangle wherein concentration contours could be computed throughout the depth of the aquifer, consistent with the preliminary conceptual model and grid described previously. Figure 21 illustrates the grid with respect to the site well field, and Fig. 22 illustrates the grid cell boundaries, selected to coincide as closely with field data locations as possible. Flow-field simulation was achieved by solving the hydraulic head equation and the simulated velocity field using Darcy's Law.

6.3.2 The Hydraulic Head Equation

The equation for hydraulic head h (x,y,t) is derived in Freeze and Cherry (1979), and under the assumptions of homogeneity is seen to be

$$\frac{\partial}{\partial x}\left(T_x \frac{\partial h}{\partial x}\right) + \frac{\partial}{\partial y}\left(T_y \frac{\partial h}{\partial y}\right) = S \frac{\partial h}{\partial t} .$$

where $T_x = K_x b$.

$T_y = K_y b$.

$S = S_s b$.

The quantities K_x and K_y are hydraulic conductivities that were assumed piecewise constant throughout the domain. S_s is specific storage, and aquifer thickness (b) is assumed constant. The assignment of the actual values was assumed to be dependent on the subregions that described the orientation of geologic strike and lithologic heterogeneity, consistent with the preliminary conceptual model.

Equation (1) may be solved subject to boundary conditions that provide any linear combination of flux and hydraulic head on the boundary of the rectangular domain. Because the model assumes a steady state head distribution over a period of one year, the right-hand side of Eq. (1) is taken as zero. Also, because it was feasible to measure approximate hydraulic head values in regions roughly surrounding the rectangular site (Fig. 1), it was possible to use interpolating spline techniques for determining boundary values. The simulated head distribution was obtained by solving the homogeneous equation

$$\frac{\partial}{\partial x}\left(T_x \frac{\partial h}{\partial x}\right) + \frac{\partial}{\partial y}\left(T_y \frac{\partial h}{\partial y}\right) = 0, \qquad (1)$$

where $T_x = K_x b$.

$T_y = K_y b$.

subject to Dirichlet boundary data (constant head),

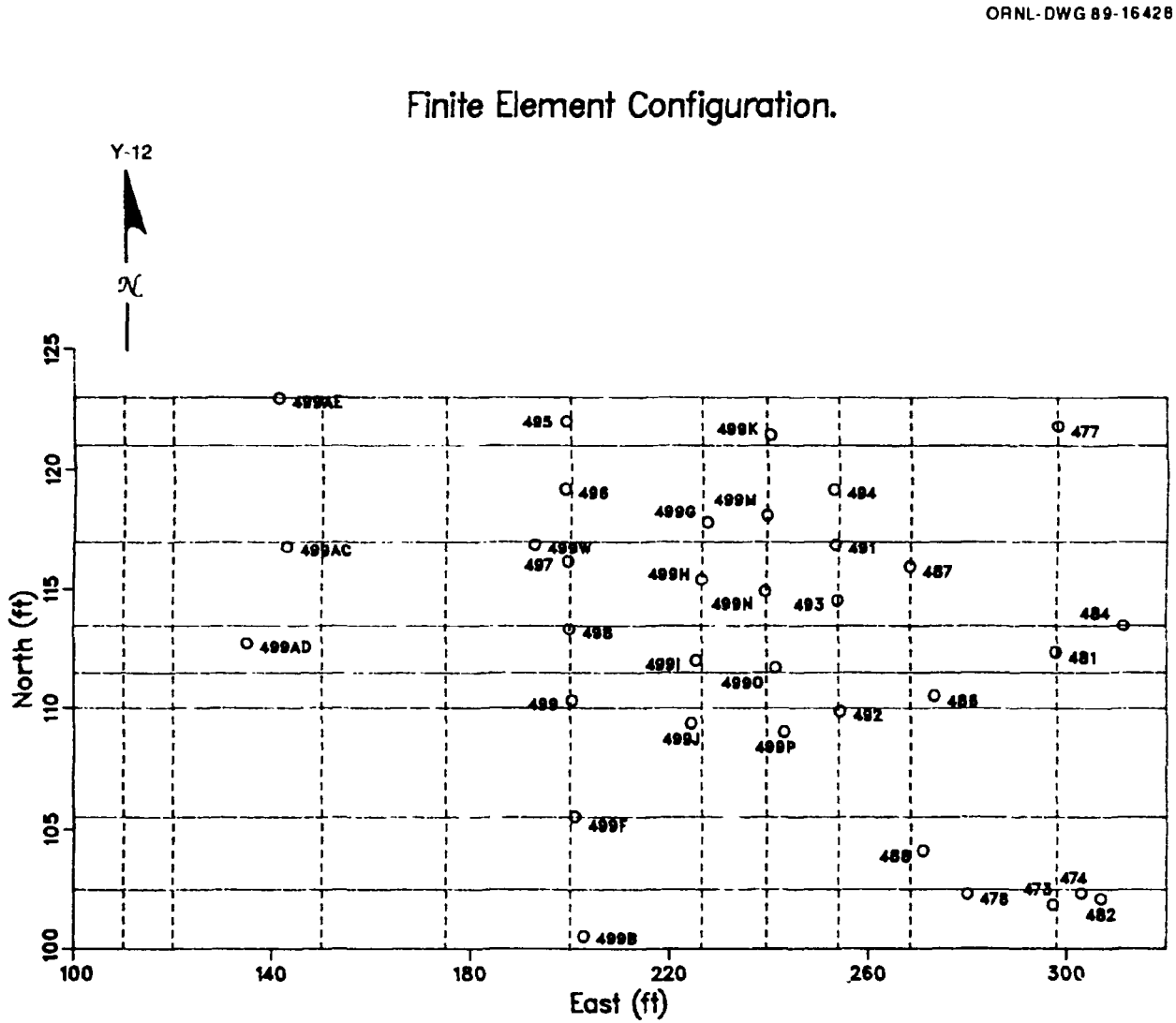

Fig. 21. Flow modeling grid domain with respect to tracer test well field based on preliminary conceptual model.

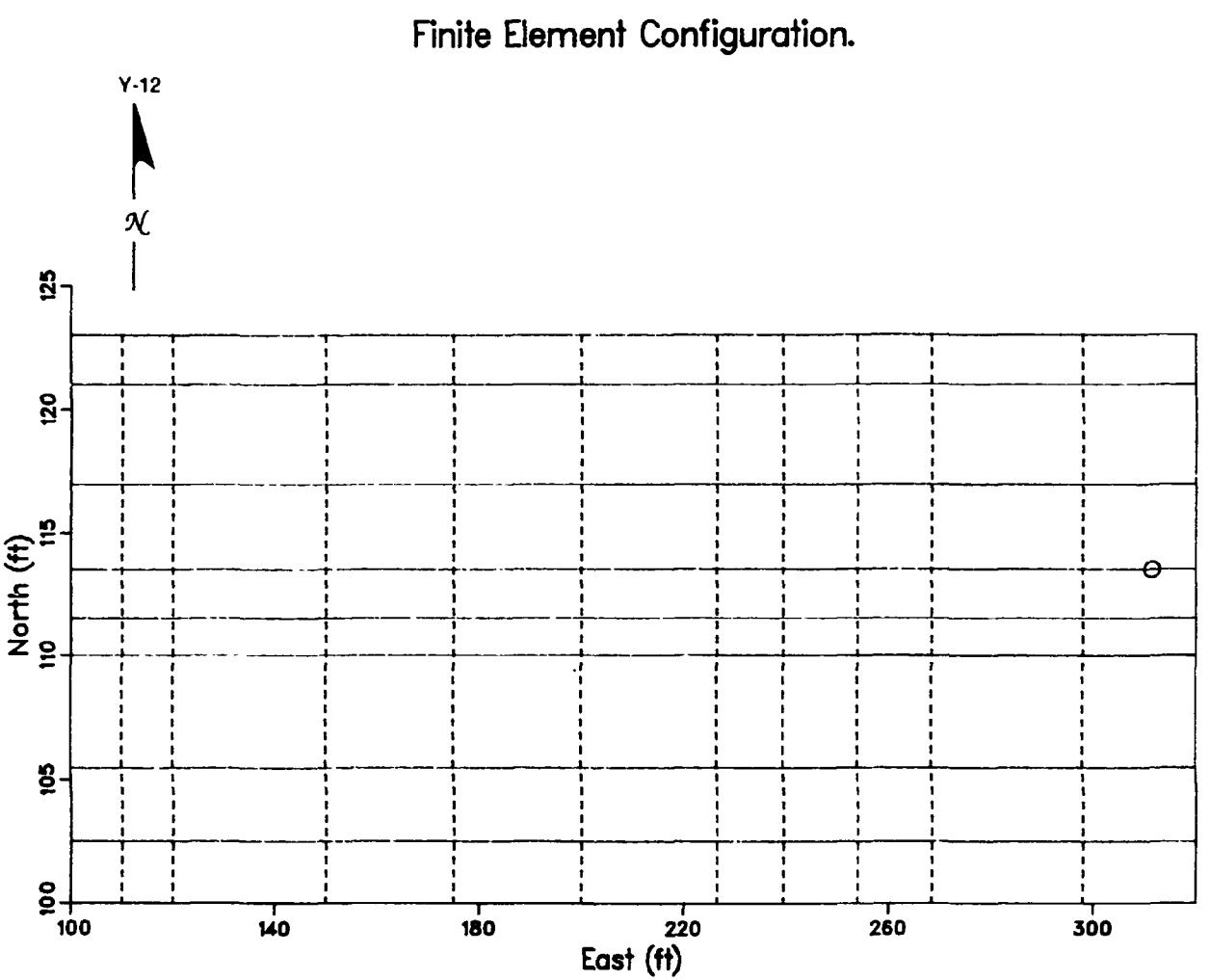

Fig. 22. Flow modeling grid cells based on preliminary conceptual model and field data locations.

$$h(x,y) = h_0(x,y) \Big|_{\partial h} \tag{2}$$

6.3.3 Determination of Boundary Conditions for Equation (1)

Hydraulic head values at the wells and creek locations in Fig. 3 for the interval of April 1988 to January 1989 revealed that the distribution for January 5, 1989, was representative of the entire year (Fig. 23). To establish reasonable interpolative values on the boundary of the domain, application of a continuously differentiable quintic spline for irregularly spaced data (Akima 1978) was implemented. One of the desirable features is that it provides a low-degree extrapolation for boundary points outside the convex hull produced by the triangular connections of all the points. The contour plot in Fig. 22 shows the spline-produced piezometric surface. Interpolated head values were obtained for the discrete boundary points as needed for the grid in the subsequently discussed numerical solution.

The option of describing known values for flux on the boundary (Neumann Data) was rejected because the data provided no reliable estimate for the flux. This was true even at the apparent discharge boundary represented by the creek at the western boundary of the site.

The boundary conditions thus described may, of course, be changed as time evolves, with the effect that the hydraulic head distribution will be described "piecewise." Because the steady distribution (January 5, 1989 data) appeared to produce an acceptable plume simulation, time evolution was not included. If temporal effects were to be included, periodic updates for transient boundary conditions such as storm events, seasonal precipitation, and evapotranspiration were required.

6.3.4 The Darcy Velocity Field; Seepage Velocity

To determine the groundwater velocity field, Darcy's Law and the presumed known values of the hydraulic head h (x,y,t) at any point in the rectangular domain are used. Specifically, the steady-state velocity field is given by

$$\vec{v} = -K\vec{\nabla}h, \tag{3}$$

where the conductivity matrix K is assumed to have zero off-diagonal elements. Hence, it is simply assumed that

$$K = \begin{pmatrix} k_x & 0 \\ 0 & k_y \end{pmatrix}.$$

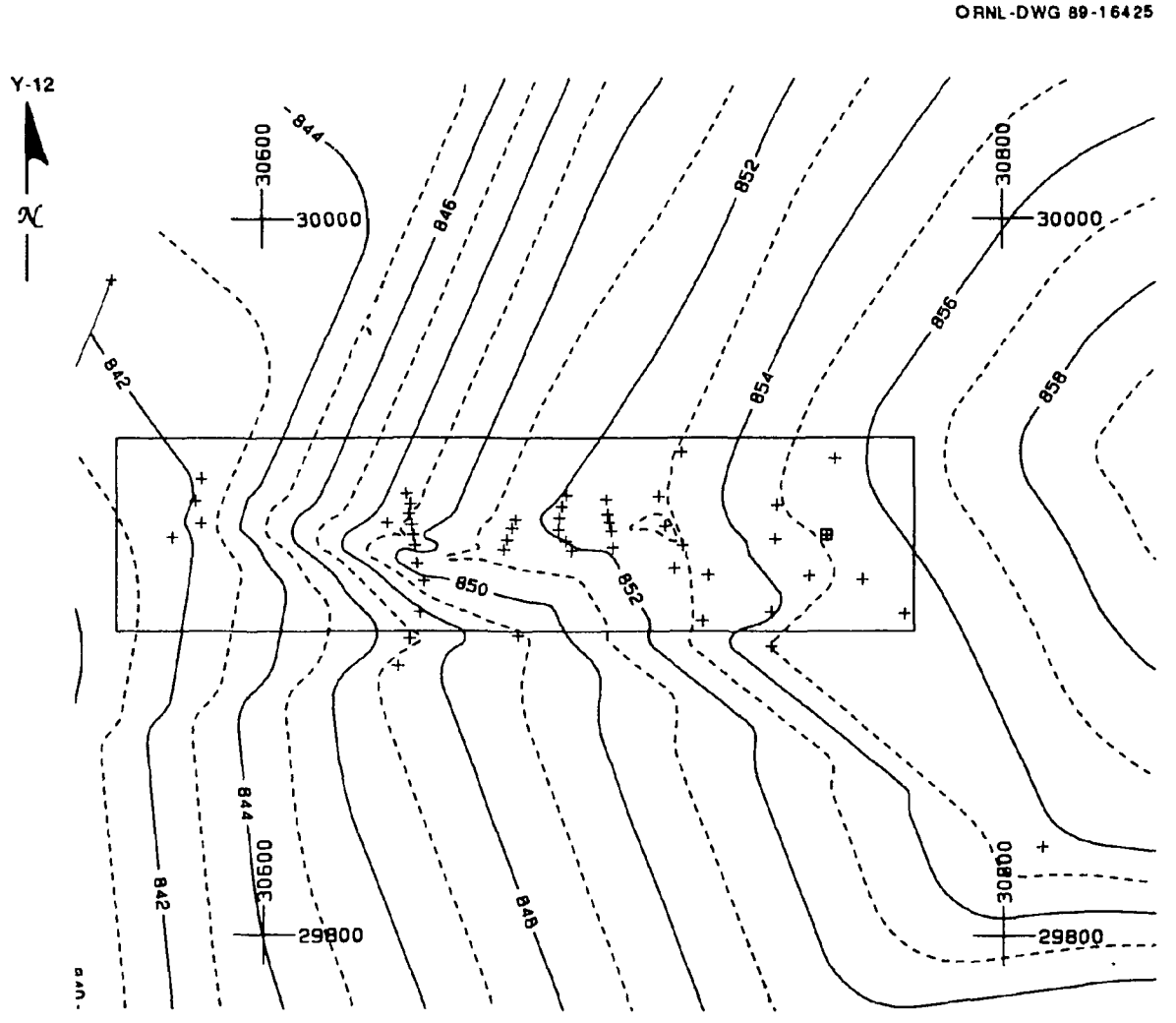

Fig. 23. Computer-generated water table contour map based on January 5, 1989 data. Contour interval 1 ft. Well locations represented by + symbol; square at right represents injection well.

The pore velocity used in the advection-dispersion equation below is taken as

$$Vn = \frac{V}{n} , \tag{4}$$

where n is the effective porosity that is assumed constant, $0 < n < 1$.

6.3.5 The Advection-Dispersion Equation

It is assumed that the tracer concentration may be determined by advection and caused by water movement through porous media. Assuming the steady state velocity found by Eq. (3) and assuming *constant* dispersivity parameters, the concentration is given by Freeze and Cherry (1979).

$$D_x \frac{\partial^2 C}{\partial x^2} + D_y \frac{\partial^2 C}{\partial y^2} = V_x \frac{\partial C}{\partial x} + V_y \frac{\partial C}{\partial y} + F \tag{5}$$

Here, C is concentration, V_x and V_y are velocity components, and D_x and D_y are the dispersion coefficients that were assumed constant, but not necessarily equal. The anisotropy ratios D_x/D_y and K_x/K_y and the effective porosity n were constrained parameters used to tune the computer code for the solution of Eqs. (1) and (5), subject to the appropriate initial/boundary conditions. The initial concentration distribution, $C(x,y,0) = C_o(x,y)$, was taken as either an instantaneous *point* source or an instantaneous *line* source. For the actual tracer simulation, the former was used, and for simulating a larger line source, the latter was used.

The boundary concentrations were assumed homogeneous, that is,

$$C\,(x,y,t) \Big|_{\partial R} = 0 . \tag{6}$$

It was assumed that the injection point remains a continuous weak source over time to simulate the fact that a small amount of highly concentrated tracer remained in place in the injection well over the entire test period. Thus, the concentration was found by solving Eq. (5) with

$$F = \alpha\, C_0\, \delta\,(x - x_1,\, y - y_1) ,$$

and by assuming a predetermined velocity field that, in turn, was driven by hydraulic head data, and the initial, boundary, and source terms. C_o is the initial; δ is the usual Dirac Delta function. The driving term, F, was determined by tuning the free parameter α.

6.4 NUMERICAL SOLUTION OF THE HEAD EQUATION; DATA REQUIREMENTS AND INTERPRETATION

This section describes the solution of the head equation for flow simulation. It includes descriptions of boundary conditions, code selection, sensitivity analysis, and results.

6.4.1 Estimation of Fixed Boundary Conditions

Hydraulic head data for January 5, 1989, were used as input to a computer code that produces a *regular* grid of interpolated and extrapolated values. From this, it is possible to approximate head values at any point on the rectangular domain boundary of the site. The interpolation for needed boundary points used a bicubic spline.

The preliminary conceptual model assumed that the domain for the system consisted of alternating regions parallel to geologic strike with respective hydraulic conductivities varying by approximately one order of magnitude. An initial value of K_x/K_y was taken as 10, based on data obtained by Golder Associates (1988). To obtain the resultant flow, the finite element code SEFTRAN (Version 2.5) was implemented (Ward et al. 1987).

6.4.2 Use of Dirichlet Boundary Conditions

The head equation used to determine a steady state velocity field on the domain discussed above requires values for the hydraulic conductivities K_x and K_y, as well as values for the fixed head and/or flux on the boundary. Because head data were available, it was decided that constant head boundaries would be the most suitable for constructing a data-driven model.

6.4.3 Code for Solution of the Head Equation

To model the flow problem using existing software, it was initially decided to implement the code SEFTRAN. This choice was made because detailed data concerning the stability and accuracy of the flow computations of the code were available from comparisons with analytical results in leaky aquifer theory (T. A. Rizk, personal communication to R. R. Lee, August 1989). Moreover, a user-friendly preprocessor for data input and a locally developed postprocessor for plotting results were available. SEFTRAN is based on a finite element algorithm developed by Huyakorn et al. (1987). The code solves the flow and transport problems in two stages, with output from the integration of the hydraulic head equation being input for the contaminant transport integration. The code performed well in the determination of the steady state head distribution with resultant velocity field and was therefore useful in predicting Darcy flow rates, which could then be compared with the apparent tracer front velocity. Unfortunately, the code produced undesirable oscillations when applied to the transport equation. This point is discussed in Sect. 6.5.2.

Preliminary results indicated that the simulated flow direction closely resembled the tracer migration direction, provided the conductivity anisotropy was sufficiently large. Figures 24, 25, and 26 illustrate flow vectors for anisotropy ratios of 2, 10, and 30, respectively. Anisotropy values near 1 (K_x/K_y=1, 10) produced flow downgradient (Fig. 27) contrary to tracer migration behavior. Subsequent modifications to the preliminary

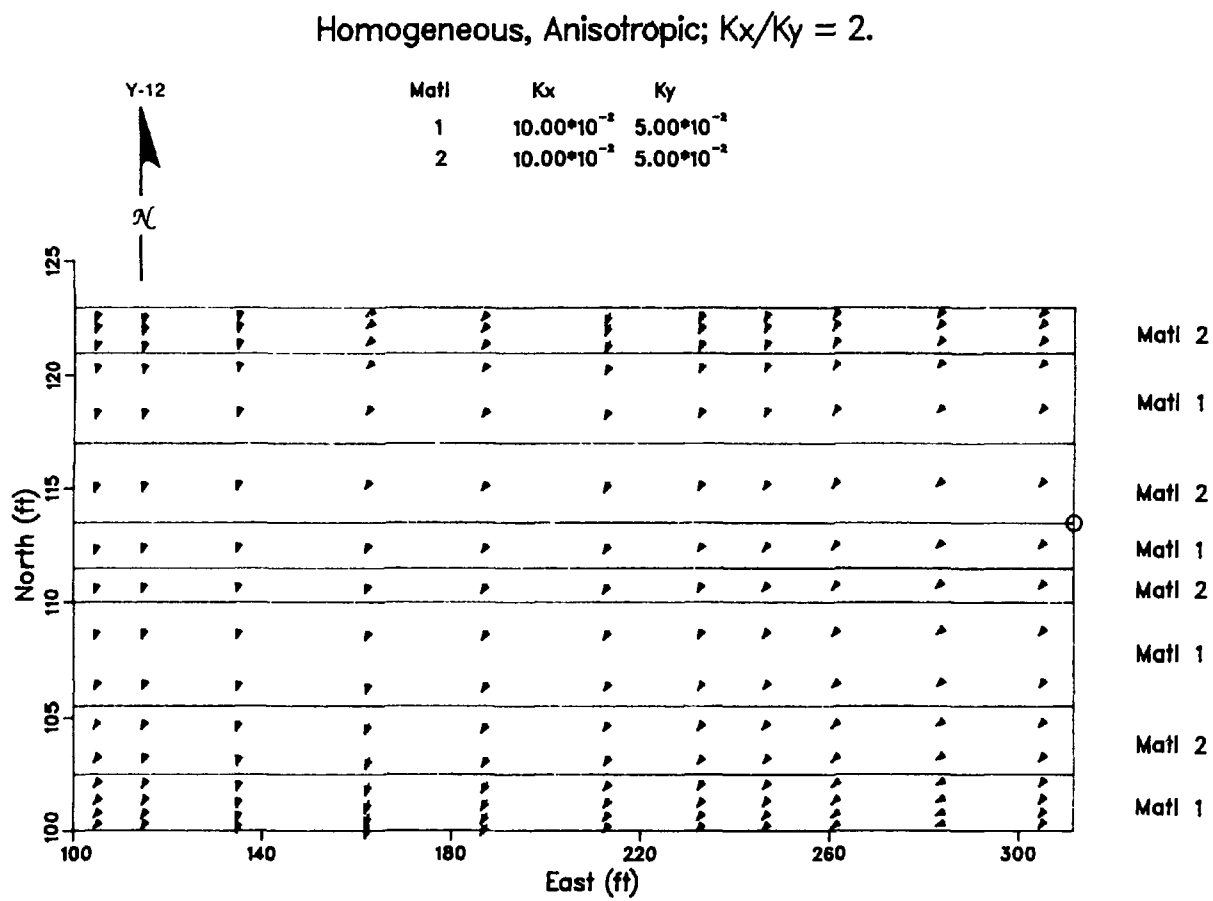

Fig. 24. Flow vectors assuming homogeneous materials and conductivity anisotropy ratio of 2 using SEFTRAN code. Vector length unrelated to flow velocity.

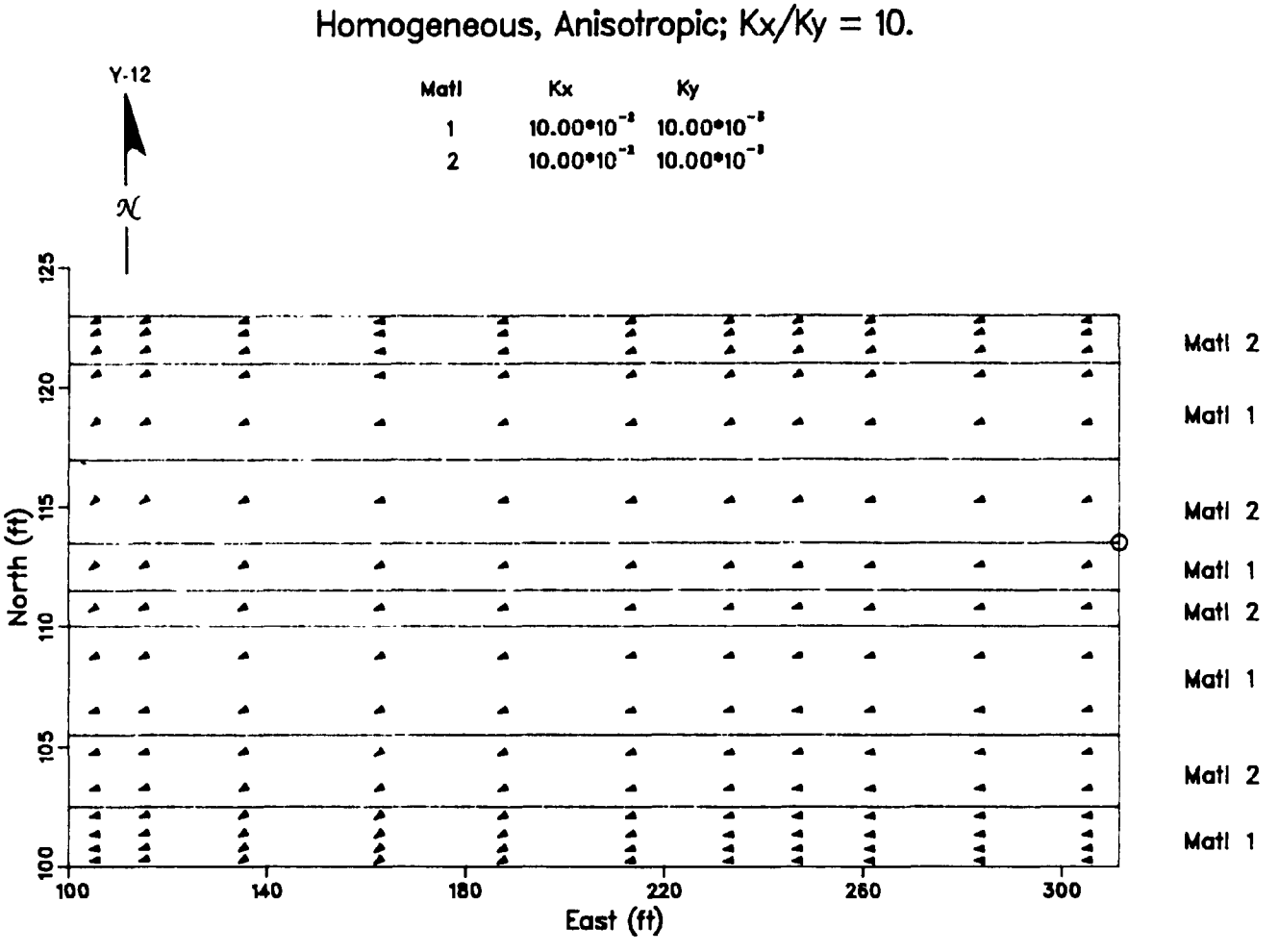

Fig. 25. Flow vectors assuming homogeneous materials and conductivity anisotropy ratio of 10 using SEFTRAN code. Vector length unrelated to flow velocity.

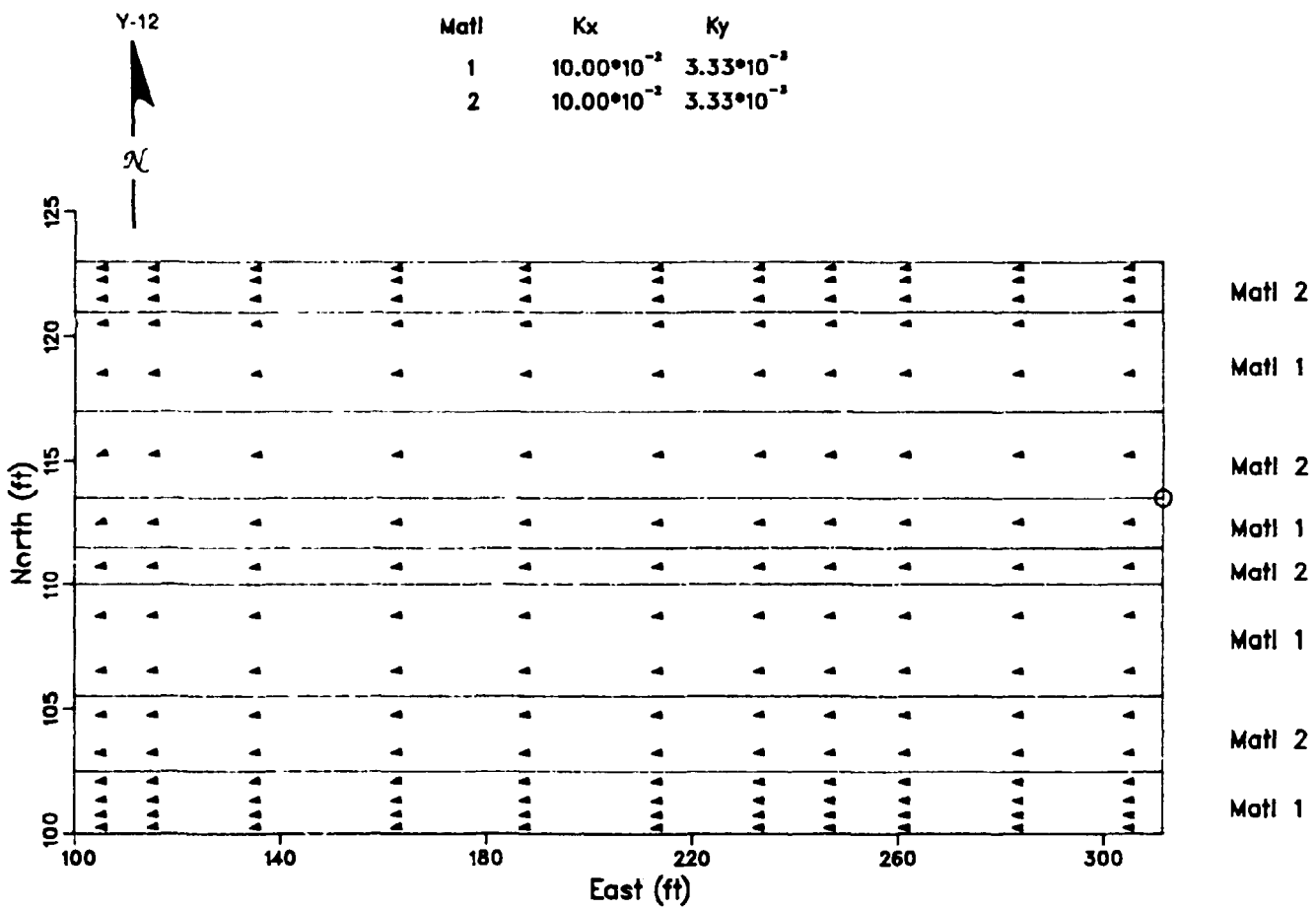

Fig. 26. Flow vectors assuming homogeneous materials and conductivity anisotropy ratio of 30 using SEFTRAN code. Vector length unrelated to flow velocity.

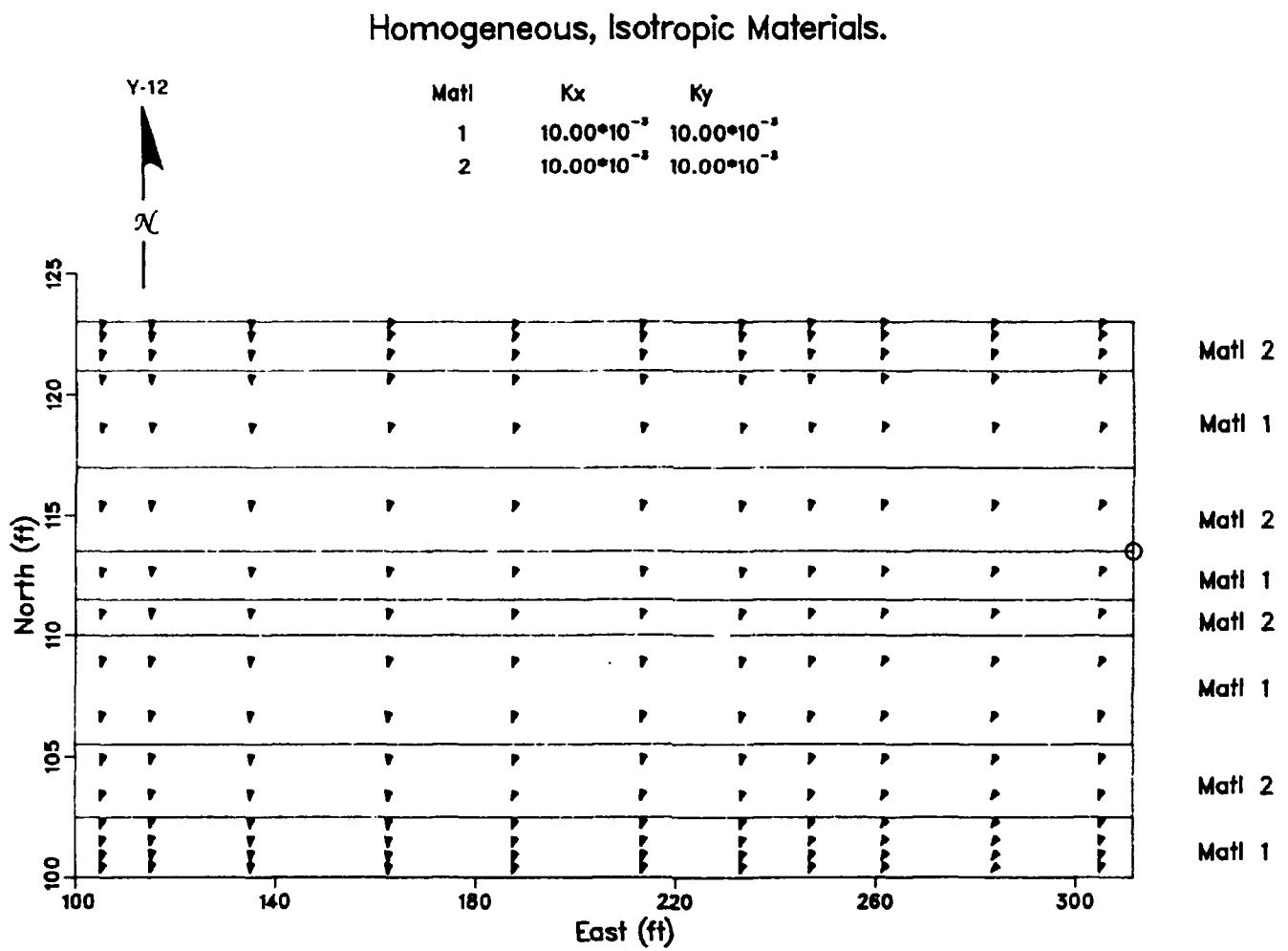

Fig. 27. Flow vectors assuming homogeneous, isotropic materials using SEFTRAN code. Vector length unrelated to flow velocity.

conceptual model and commensurate modifications to the numerical model grid described earlier constituted the final domain.

The basic grid was subdivided with 17 nodes in the x direction (strike) and 21 nodes in the y direction (dip), which produced 320 elements. The input parameters for SEFTRAN are listed in Table 2. The program was run repeatedly to tabulate the root mean square error in comparing computed head values vs measured values at several tracer detection wells. The optimal values for conductivities were thought to be bracketed by previous estimates obtained in FY 1988 modeling.

Table 2. Hydraulic conductivity parameter values used as input to SEFTRAN

	Fast region limestone conductivity (ft/d)	Slow region shale conductivity (ft/d)
Strike	1×10^{-3} ft/d	1×10^{-4} ft/d
Dip	1×10^{-4} ft/d	1×10^{-5} ft/d

Based on a minimum root mean square (RMS),

$$\text{RMS} = \sqrt{\frac{1}{6}\sum_{i=1}^{6}(h_i - \hat{h}_i)^2} \quad .$$

Note: The terms h_i and $\hat{h}_i$ are computed and measured hydraulic heads (respectively), and i is a representative index for detection wells GW-484, -486, -487, -491, -493, and -494.

6.4.4 Iterative Estimates of Hydraulic Conductivity Values

Previous hydraulic conductivity values in various media at the site were published in Golder Associates (1988). Hence, a first task was to verify those values by using similar techniques. After a review of available software to assist in fitting several analytical solutions (Hantush 1964; Theis 1935) to the available head distribution data, several codes were used for nonlinear, curve-fitting analysis. In particular, the code TSSLEAK (Van Der Heijde 1988) was implemented to approximate conductivities based on the Hantush-Jacob formula, and the THEISFIT (Van Der Heijde 1983) code was run to estimate aquifer hydraulic parameters based on an empirical fit to the Theis solution. The values obtained closely approximate the previously determined results.

It was decided that the values obtained by the above analysis should be the starting values used in the code, and SEFTRAN should be run as many times as necessary to refine these values by attempting to find the minimum root mean square error. This produced the values shown in Table 2.

As an alternative in hydraulic conductivity determination, a different analytical expression was used in a constrained optimization exercise. A more common result for a leaky aquifer under pumping conditions (Rizk 1989) was implemented together with a nonlinear optimization code (Crane et al. 1980) to again estimate the hydraulic parameters. This approach consistently produced parameters suggesting that the porous medium should be very anisotropic, on the order of 300. The conclusion was that the values suggested by the RMS minimization with SEFTRAN would be taken as initial inputs to the transport stage of the problem. However, in light of the newer result and tracer migration, an anisotropy value of 30 represented the minimum acceptable value and was used in transport modeling. This value has been reported by Lozier, Spiers, and Pearson (1987) in a similar setting elsewhere in Bear Creek Valley.

6.4.5 Sensitivity of Velocity with Respect to Hydraulic Conductivity and Heterogeneity

A 1-to-2 order of magnitude variation in hydraulic conductivity values indicated that the longitudinal velocity component was not sensitive to small spatial changes in strike-directed conductivity values. Additionally, the sensitivity analysis code GRESS (Horwedel et al. 1988) was implemented for evaluation of the velocity-conductivity relationship. This code, which effectively computes the logarithmic derivative (or relative change) of velocity with respect to conductivity, showed that the solution of the Dirichlet (constant head boundary) problem showed less sensitivity, while the Neumann (constant flux boundary) problem showed more sensitivity.

Concerning conductivity ratios, the GRESS analysis implied that small changes in heterogeneity produce small changes in longitudinal velocity at a fixed point for the Dirichlet problem. However, as before, there was a stronger dependence if the system was driven by Neumann (flux) boundary data. Because a field evaluation of flux conditions was not feasible, fixed head boundary conditions were used.

6.4.6 Simulated Groundwater Flow Using SEFTRAN

The aforementioned parameters were input to SEFTRAN to solve the hydraulic head equation on the 320-element grid described previously. The resulting flow is seen in Fig. 24 where it is noted that the alternating-layer concept produced flow parallel to geologic strike, with flow in the tighter regions showing larger downgradient components. To check the model, the code was run assuming a homogeneous, isotropic domain. The result, in agreement with the previous results in Golder Associates (1988), was flow downgradient. This eventually caused near Gaussian dispersion with sluggish advection downgradient that was contrary to tracer migration data.

With the assumed grid and parameters, the simulated flow along strike appeared consistent with the actual observations of tracer movement. It was therefore decided that these results should be used to solve the advection-dispersion problem.

6.5 NUMERICAL SOLUTION OF THE ADVECTION-DISPERSION EQUATION

This section describes the solution of the advection-dispersion equation [Eq. (5)] for the simulation of contaminant transport. It includes descriptions of parameter and boundary conditions, as well as data-driven and tuning parameters.

6.5.1 Parameter and Initial Boundary Conditions

The advection-diffusion equation [Eq. (5)] was solved with both initial and boundary conditions. Because tracer was injected into well GW-484, it was assumed that a continuous point source existed at the node representing that well. On the basis of how the tracer actually moved, zero concentration was assumed at all boundary points. Since a relatively large concentration of the dye remained in well GW-484, it was decided that an extra degree of freedom would be allowed by assuming that a constant source of smaller magnitude was being input at a very small volumetric rate. Hence, the effort at this stage was to solve Eq. (5) with Dirichlet data,

$$C(x,y,t)\Big|_{\text{boundary}} = 0$$

An effort also was made to determine parameter values in the equation in such a way that the resultant plume showed the major characteristics of the observed concentration distribution at any time from injection to the present. With the exception of porosity, which for modeling purposes was used as a scaling factor for velocity, none of the parameters directly relating to the advection-diffusion equation had been determined by data. Some field results suggested that the porosity n should lie between 2% and 10% (Golder Associates 1988). Therefore, an effort was made to restrict n to this range. The remaining quantities, longitudinal dispersivity (or "characteristic length"), and ratio of longitudinal to transverse dispersivity were considered free parameters for tuning purposes.

6.5.2 Choice of Codes

The code SEFTRAN exhibited nontrivial oscillations in the solution of the contaminant transport portion of the problem. The numerical literature describes such difficulties in solving the advection-dispersion generalized transport equation using the finite element method. (In some cases, adaptive procedures have been successful in remedying the problem.) Other existing groundwater and contaminant transport codes were explored to remedy the difficulty encountered with oscillations.

A finite element program TRAFRAP (Huyakorn et al. 1987) solves the transport equation with an upstream weighing function applied to correct for oscillations. The approach seemed successful only under conditions of high dispersivities (~1000). These values were judged unrealistic because of physical considerations. Thus, TRAFRAP was not selected to solve the transport equation.

Because the domain geometry in the problem was trivial, consideration was given to the analytical code AT123D (Yeh 1981). The code uses eigenfunction expansions to compute solutions in regular domains. The analytical solution technique requires the transport equation to have constant coefficients. Specifically, this meant that the flow velocity components must be constant, and the domain must be homogeneous; however, the conceptual models required consideration of heterogeneity. In addition, the flow velocities are varied throughout the domain. Thus, the analytical code AT123D was not implemented.

It was decided that a code was needed that was fundamentally different from the finite element methods used in SEFTRAN and TRAFRAP but which could take advantage of the simple rectangular geometry without requiring the conductivities in Eq. (1) to be

constant. An additional constraint on the choice of codes was that the code used should be well established and recognized in the groundwater contaminant modeling field. One code that met these conditions was the U.S. Geological Survey (USGS) MOC code (Konikow and Bredehoeft 1988), which uses the finite difference discretization method. This program is based on a nonrigorous assumption that the advection-diffusion equation is solvable by using the Method of Characteristics, a method commonly employed to solve hyperbolic wave equations. The discretization domain must be rectangular, but the coefficients in the hydraulic head equation (i.e., conductivities) need not be constant. Additionally, the USGS code solves the head equation [Eq. (1)] simultaneously with both the advection-diffusion equation [Eq. (5)] and the characteristic curve equations.

The USGS MOC code was implemented using essentially the same domain used with the SEFTRAN runs. The previous velocity field produced by SEFTRAN was used as a quality assurance check on the velocity field that emerges from the MOC calculations; the aforementioned determination of the parameters using SEFTRAN was kept for input into the MOC code with the intention that these values would be tuned further within reasonable limits if needed.

6.5.3 Grid Domain for the USGS MOC Code

The domain for solving the system of equations is taken as the basic rectangular shape shown in Fig. 1. After preliminary tests for repeatability of the velocities produced earlier by SEFTRAN, it was determined that the discretization of the domain should be accomplished by using a 20 x 20 system of nodes, with Δ_x = 12 ft and Δ_y = 3 ft. The system is shown in Fig. 20.

6.5.4 Base Case Parameter Input Values

This section describes the data-driven and tuning parameter values used as input to run the MOC code for the base case simulation.

6.5.4.1 Boundary conditions

Because the MOC code requires the outer rows and columns to be no-flow boundaries, the imposition of Dirichlet data must be accomplished by setting the driving term in Eq. (5) to appropriate values at the adjacent inner rows and columns of the grid. This amounts to groundwater leakage out of the boundary, which just suffices to maintain the constant head at the boundary in Eq. (5) and to maintain zero concentration at the boundary in Eq. (6).

6.5.4.2 Initial conditions

The initial concentrations in the transport equation were taken to be zero except at the node (17,10), which represented the injection well GW-484. There, the concentration was set at 100,000 ppb = 100g/m^3 of dye solution.

6.5.4.3 Choice of remaining parameters in transport equation

Considerable numerical experimentation, using the basic constraints placed on the hydraulic parameters mentioned above and varying the dispersivity coefficients and aquifer thickness within reasonable limits, yielded a base case input set. The parameters that were determined by componentwise tuning are listed in Table 3. A complete listing of the base case input file is displayed in Table 4. The USGS documentation (Konikow and Bredehoeft 1988) is necessary for guidance in the specific details regarding formats. The description of the random assignment of conductivities is discussed in Sect. 6.5.4.4.

Table 3. Range of parameters available for tuning transport code

Description	Assumed range
Effective porosity (Beta)	$1\% < n < 10\%$
Longitudinal dispersivity	$0.01 < \alpha < 5$

Table 4. Base case input parameters to meet USGS code input requirements

Variable name in code	Definition	Value
NTIM	Maximum number of time steps	48
NPMP	Number of pumping periods	1
NX	Number of nodes in x direction	20
NY	Number of nodes in y direction	20
NREC	Number of injection wells	1
PINT	Pumping period in years (yr)	1
POROS	Effective porosity (%)	5
BETA	Longitudinal dispersivity (ft)	3
S	Storage coefficient	0
TIMX	Time increment multiplier (flow)	0
TINIT	Initial time step (flow) (s)	0
XDEL	Width of finite difference cell(x) (ft)	12
YDEL	Width of finite difference cell(y) (ft)	3
DLTRAT	Ratio of transverse to horizontal dispersivity	0.01
ANFCTR	Ratio of transverse to horizontal transmissivity	0.03
REC	Injection rate at Well GW-484 (ft^3/s)	10**(-8)
CNREC	Concentration of injected water (ppb)	10**4
THCK	Saturated thickness of aquifer (ft)	10

6.5.4.4 Determination of hydraulic conductivity values

The preliminary conceptual model required alternating layers along strike with conductivities alternating between two assumed values (Fig. 28). However, as described in Sect. 5, an attempt to verify that construct by analysis of field data failed. It was then hypothesized that the medium may be so heterogeneous that it could be represented only by random conductivities at each node. Because an empirical population of values was known, it was decided to assign conductivity values at each node by sampling that population. The result is shown in Table 5, in which the actual conductivity value is obtained by multiplying the indicated value by 3.28×10^{-6} ft/s.

Table 5. Base case randomized hydraulic conductivity grid domain

.0	.0	.0	.0	.0	.0	.0	.0	.0	.0	.0	.0	.0	.0	.0	.0	.0	.0	.0	.0
.0	.8	3.8	2.2	.6	2.6	2.2	2.3	9.1	7.7	2.5	3.1	1.9	2.3	4.2	5.9	.6	1.1	4.9	.0
.0	2.3	3.3	2.6	2.6	5.0	3.6	.6	3.1	7.2	1.0	3.5	3.5	3.4	3.3	.8	4.8	4.7	2.0	.0
.0	2.7	2.3	1.0	1.0	3.6	9.1	3.3	3.3	1.9	1.4	1.6	8.9	2.2	.9	3.3	4.6	9.5	2.3	.0
.0	4.7	8.9	1.4	.5	1.1	1.3	2.3	2.6	3.3	1.5	3.6	2.2	3.5	6.8	.6	1.8	.8	4.7	.0
.0	2.5	1.0	2.0	4.7	3.3	1.9	.7	3.1	8.4	.6	3.5	2.9	8.9	3.2	3.4	3.4	1.0	3.3	.0
.0	5.1	3.1	2.4	3.5	4.6	2.2	11.4	11.4	11.4	4.6	2.6	9.5	8.8	.5	2.2	3.4	9.1	3.3	.0
.0	8.9	1.7	1.4	3.3	4.7	2.4	1.0	2.2	.6	4.9	1.3	4.4	.5	2.3	1.0	3.5	3.5	1.0	.0
.0	3.1	3.6	2.9	2.3	3.3	.6	3.3	3.4	1.0	1.0	5.6	2.9	2.5	3.3	8.9	5.2	3.5	1.3	.0
.0	1.5	2.6	1.0	.5	10.5	.6	3.4	9.2	2.3	1.7	2.7	1.4	4.1	11.4	11.4	11.4	11.4	2.9	.0
.0	4.6	3.4	.5	3.4	5.2	1.1	9.1	3.4	6.2	2.1	7.8	2.6	3.5	1.0	8.5	2.6	2.6	1.0	.0
.0	1.7	3.5	1.1	1.1	11.1	5.2	.7	2.7	2.1	11.4	6.7	.6	2.6	2.3	3.5	5.2	3.4	2.6	.0
.0	1.0	4.7	5.2	3.3	2.3	8.9	11.4	11.4	11.4	3.4	1.0	10.8	9.0	.6	4.7	10.8	3.3	1.1	.0
.0	3.4	.6	.5	4.7	3.3	7.9	.6	1.9	5.3	1.1	2.0	1.0	3.4	.7	2.5	1.0	1.7	4.6	.0
.0	2.6	6.6	2.5	2.1	3.4	1.6	2.0	4.7	.6	3.5	8.6	2.4	.5	4.7	3.5	2.0	4.9	5.2	.0
.0	4.4	3.5	2.6	3.1	4.4	3.4	4.5	6.4	8.5	4.7	3.3	4.7	4.5	.5	3.3	4.9	2.6	1.0	.0
.0	3.5	3.4	2.8	4.7	5.2	1.1	9.9	3.4	.6	3.7	5.6	4.5	4.9	1.0	3.5	6.4	2.2	2.4	.0
.0	3.5	9.8	.6	6.2	2.3	.8	1.7	5.2	3.5	8.1	.6	1.2	8.8	.5	4.7	8.8	3.8	4.7	.0
.0	3.4	3.3	4.0	5.2	3.4	.4	1.0	2.2	9.7	5.7	2.6	1.8	2.3	4.3	1.1	.4	2.3	4.7	.0
.0	.0	.0	.0	.0	.0	.0	.0	.0	.0	.0	.0	.0	.0	.0	.0	.0	.0	.0	.0

6.5.4.5 Summary of data-driven and constrained parameter values

Relative to the entire coupled boundary value problem that was solved for the tracer concentration C (x,y,t), the inputs were determined by field data as follows:

- The grid orientation is based on the conceptual model that the principal direction of flow is parallel to geologic strike suggested by geologic and tracer data.
- The boundary conditions were taken as fixed hydraulic head values that were interpolated directly from a global interpolating spline that was fitted to all data taken at a date that represents the entire simulation time of 12 months. Figure 22 compares the hydraulic gradient for data representative of January 5, 1989, with data from other times during the 12-month period.
- Hydraulic conductivities in general were randomly sampled at each node, based on an empirical cumulative distribution function cdf of field data (Fig. 29). Letting $p = F(k)$ denote the cdf, a cubic spline interpolation S, passing through the data points [k(j),p(j)], was constructed. For any subregion of the original domain for which random conductivity is required, a *uniformly* distributed random number r on

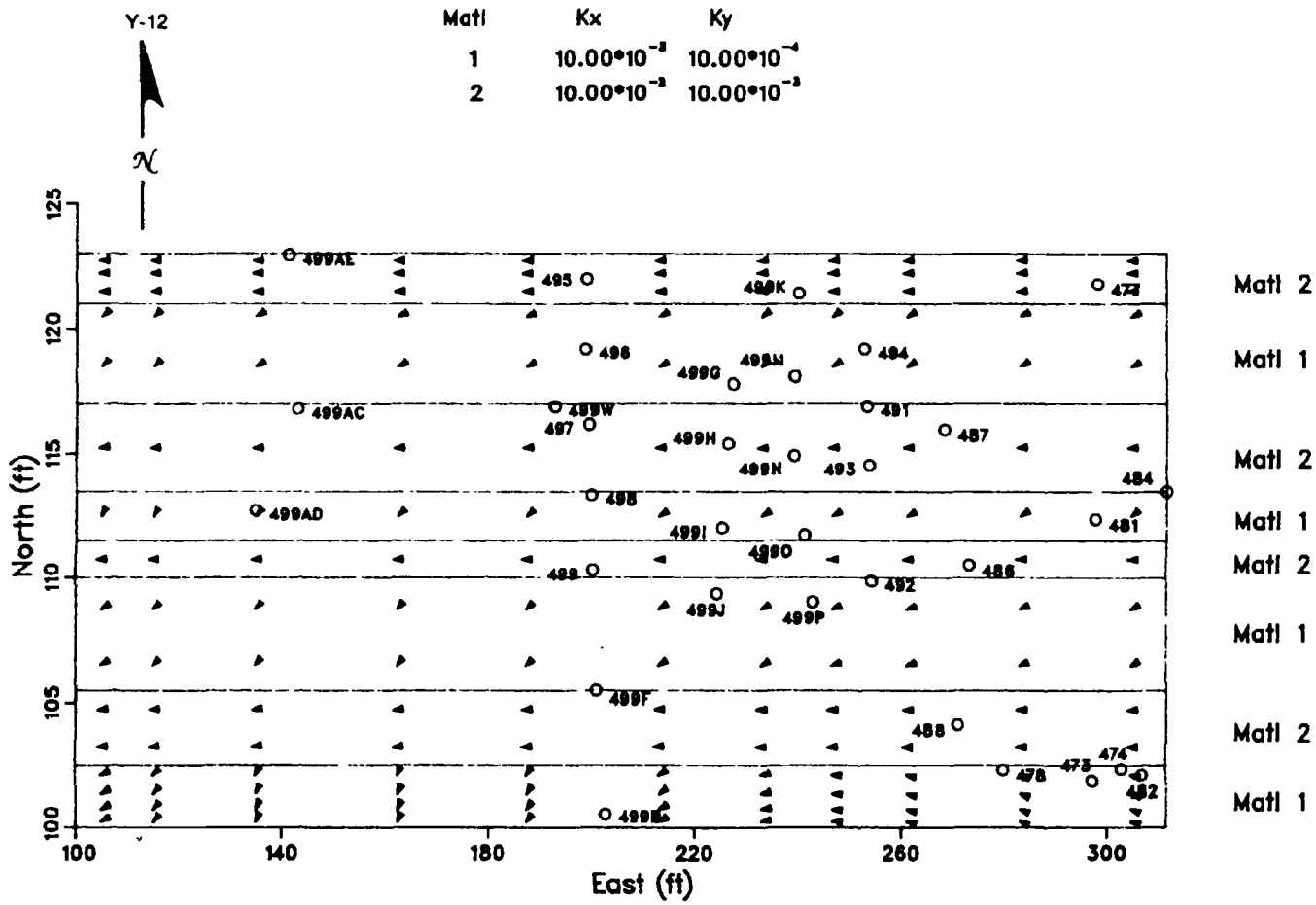

Fig. 28. Base case SEFTRAN flow simulation assuming heterogeneous materials and conductivity anisotropy ratio of 10. Vector length related to flow velocity.

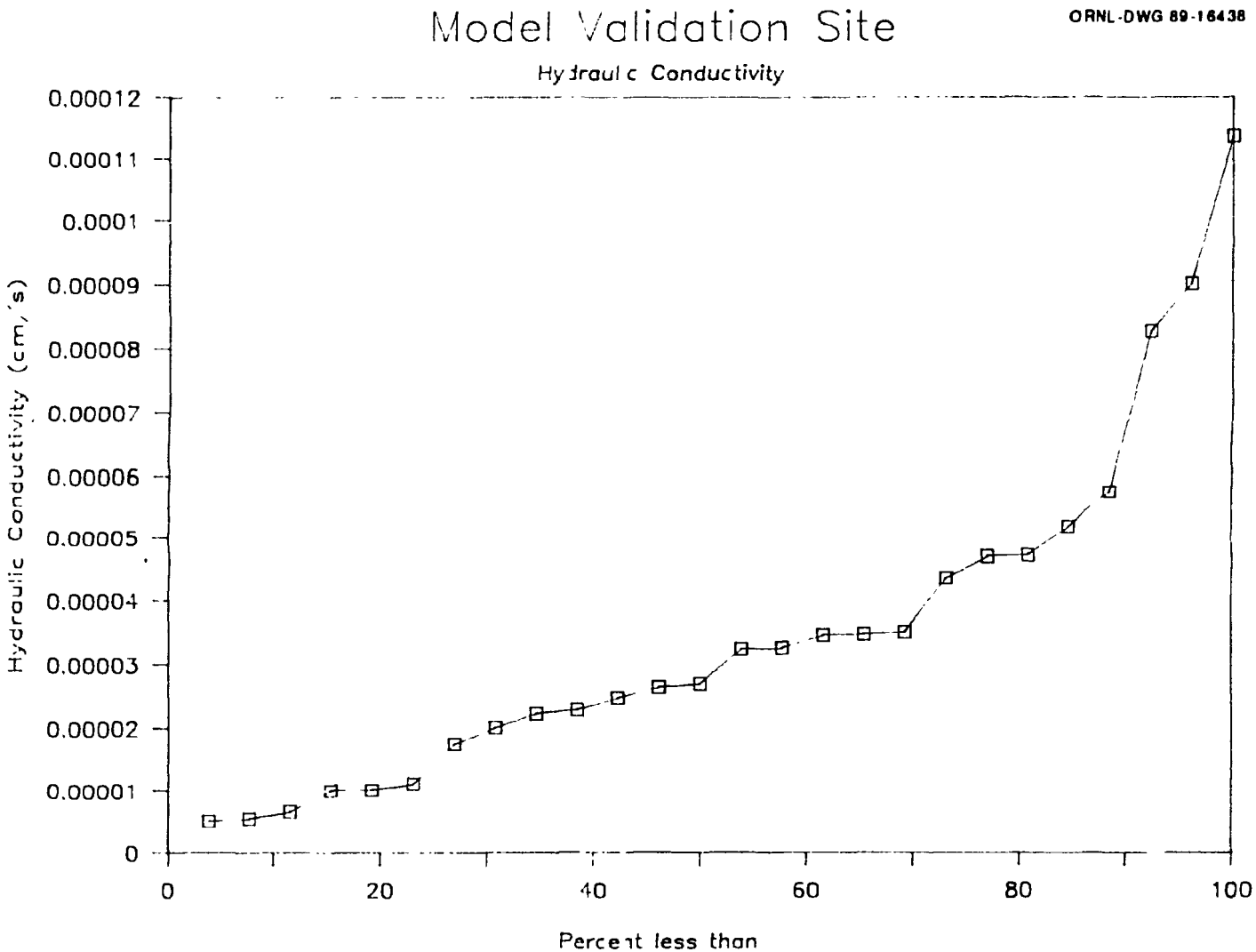

Fig. 29. Empirical cumulative distribution function of hydraulic conductivity values.

(0,1) is generated. Then, the determination of conductivity for that region is taken as

$$k = S^{-1}(p).$$

For numerical purposes, this is done for all nodes except those for which a maximum conductivity is required, such as conduits. Even for these particular nodes, the conductivity used does not exceed the maximum measured value of 1.0×10^{-4} cm/s.

- The boundary values used in Eq. (5) are taken as zero (Dirichlet), and the initial concentration distribution is taken as

$$C(x,y,0) = C_o \text{ for GW-484 ,}$$

and

$$C(x,y,0) = 0 \text{ elsewhere .}$$

The best approximation for C_o was 100,000 ppb ($\log C_o = 5.0$), which coincides within one-half order of magnitude of what was actually injected.

- The constrained parameters used to tune the numerical solution were

porosity $1\% <= p <= 10\%$,
longitudinal dispersivity $0 <= \text{ALPHA}(1) <= 10$,
conductivity anisotropy $1 <= K_x/K_y <= 30$, and
dispersivity anisotropy $1 <= \text{ALPHA}(1)/\text{ALPHA}(t) <= 100$.

Porosity was used to adjust the tracer migration velocity. Longitudinal and transverse dispersivity values were used to adjust the spread of the plume. The hydraulic conductivity anisotropy was used to adjust the direction of the center of mass of the plume.

6.5.5 Model Sensitivity Analysis

The principal parameters used in simulating groundwater flow and tracer migration are those put into the partial differential Eqs. (1) and (5), which determine the contours described above. To understand how errors in the assigned values of these input parameters may affect the numerical solutions of the equations, a study of relative stability was conducted using the computer code GRESS. The quantity used to evaluate parameter sensitivity of the USGS MOC code was the quotient of relative change in concentration to relative change in the parameter under consideration. That is, if p represents the parameter, then the sensitivity of the concentration computation at a given point in the domain and at a given time is given as

$$\frac{d(C)/p}{d(p)/p} .$$

If this quantity is less than 1, then a relative error in the parameter p (such as porosity, dispersivity, conductivity, or anisotropy) is not magnified in the overall computation for concentration. The smaller the ratio, the less sensitive C is to errors in the parameter. The GRESS code, in conjunction with the USGS MOC code, performs this computation.

Figures 30 and 31 show the results from that analysis for two detection wells (GW-493 and GW-495, located near the plume axis and margin, respectively) at time t = 12 months. The sensitivity varied with concentration, and several observations were made.

- The transport was only moderately sensitive to all the parameters, with the exception of longitudinal dispersivity, which evidently drove the system at all concentrations. This parameter was less influential at higher concentrations.
- As concentration increased, the porosity (which mathematically is a scale factor for velocity) became more influential; however, it never produced a sensitivity as large as 10×10^{-2}.
- Anisotropy of both hydraulic conductivity and dispersivity contributed to moderate sensitivity, with the effect of dispersivity being larger. The anisotropies produced similar sensitivity curves; in fact, the curves for GW-495 were virtually coincident.
- The effect of modeling with one or three conduits of elevated hydraulic conductivity produced no important differences in sensitivity.

The choice of the longitudinal dispersivity parameter D(L) produced significant effects on concentration, especially when the concentration was relatively low. This parameter and its anisotropy D(T)/D(L), which were tuned to duplicate the aspect ratio of the tracer plume, were given order-of-magnitude weight equal to that of the advection term obtained by running the SEFTRAN code earlier in the study. With increased concentration, sensitivity decreased with respect to longitudinal dispersivity and increased with respect to porosity. This suggests that the model may err in resolving details of the leading edge of the tracer plume. Hence, while the inclusion of elevated conductivity conduits produced more realistic front velocities as well as basic plume characteristics, the details of lower-concentration fingering may be sensitive to dispersion coefficient errors. On the other hand, for predicting the basic orientation and evolution of tracer migration, it is believed that lower sensitivity values that relate to the center of mass, direction, and velocity of the plume add confidence in describing the theoretical model.

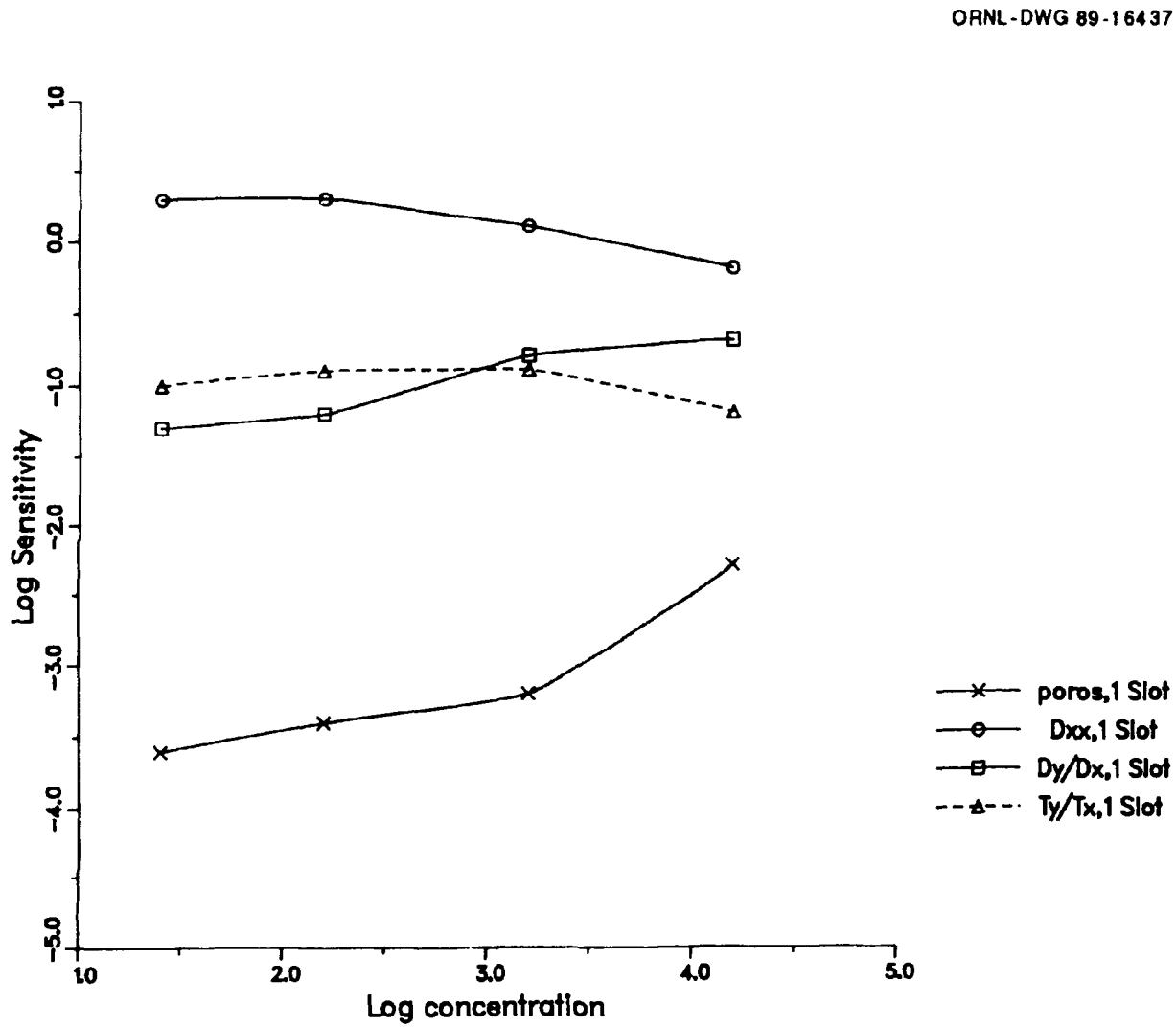

Fig. 30. Log concentration at well GW-493 for various parameters using the GRESS code.

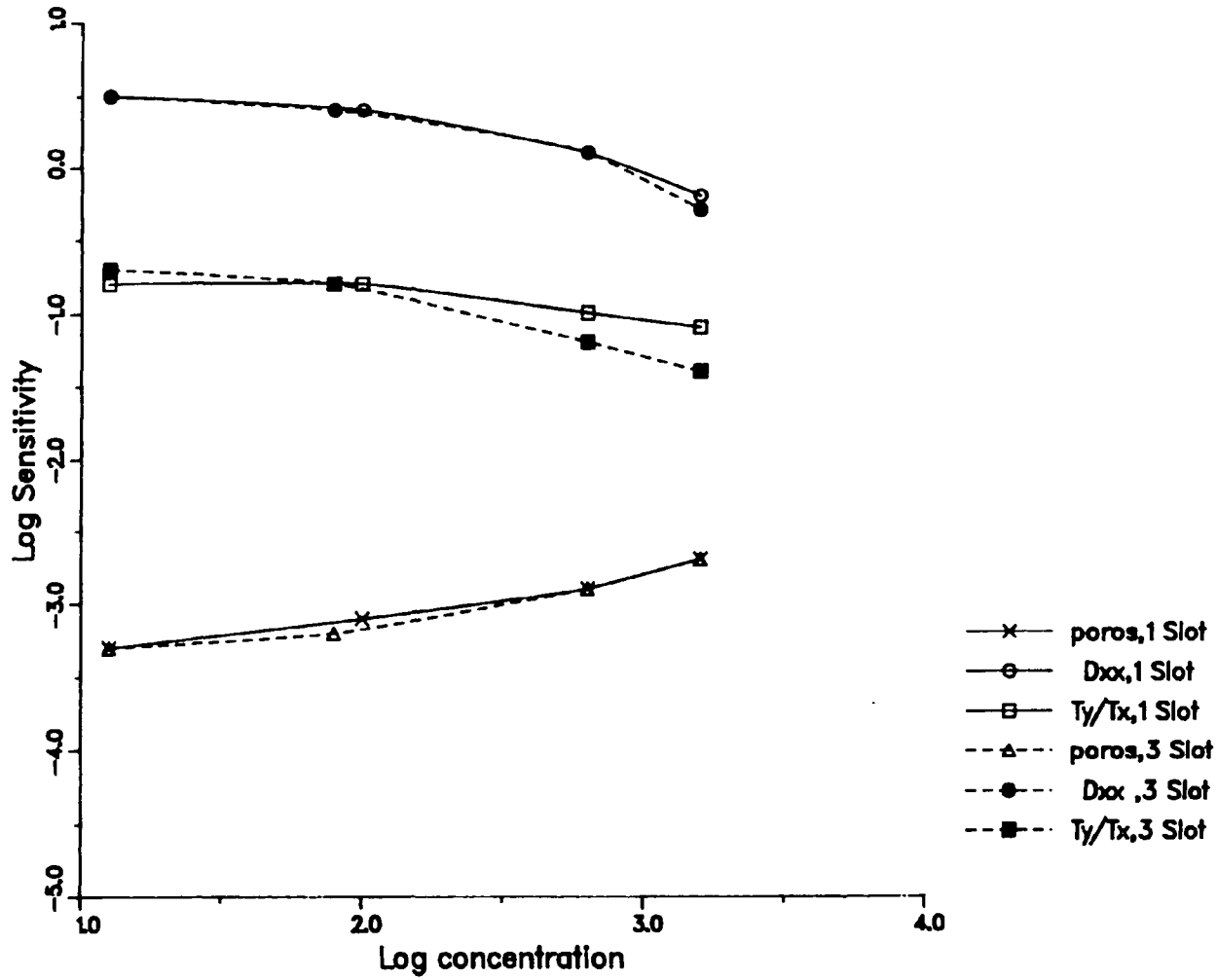

Fig. 31. Log concentration at well GW-495 for various parameters using the GRESS code.

7. COMPARISON OF MODEL SIMULATION WITH TRACER MIGRATION DATA

Figures 32 through 37 compare contours of site tracer concentration data with model simulation results for six time steps during a 1-year period. In these base case simulations (using an 11-m-long elevated hydraulic-conductivity conduit at the tracer injection point to achieve calibration to near-field tracer migration), the simulated direction and rate of migration closely resemble contours of site tracer data. Following the interpreted presence of two additional conduits in the flow field based on site water-table elevation and tracer-concentration data, they too were superimposed on the model grid. Figures 38 to 41 illustrate results of those simulations for four time steps during a 1-year period. The comparison shows a remarkable, detailed similarity between the 100- and 1000-ppb contours of tracer concentration data and the model simulation. Figure 42 illustrates a representative transport simulation assuming homogeneous, isotropic aquifer conditions. In contrast to observed tracer migration, it can be seen (like the SEFTRAN flow simulation in Fig. 26) that the direction of solute transport is coincident with the maximum gradient.

To simulate the effects of a larger-scale source, a solute line source was input at the north-south grid row equivalent to the tracer injection well location. Several simulations were performed, including no discontinuous high-conductivity conduits and one conduit. The results suggest that flow in those cases results in local fingering of solute with little effect on the long-term (12-month), long-distance (50 plus meters) transport rate. Multiple closely spaced, longitudinal-but-discontinuous conduits act as continuous preferential conductors of solute that can greatly affect transport rate (Figs. 43 to 46).

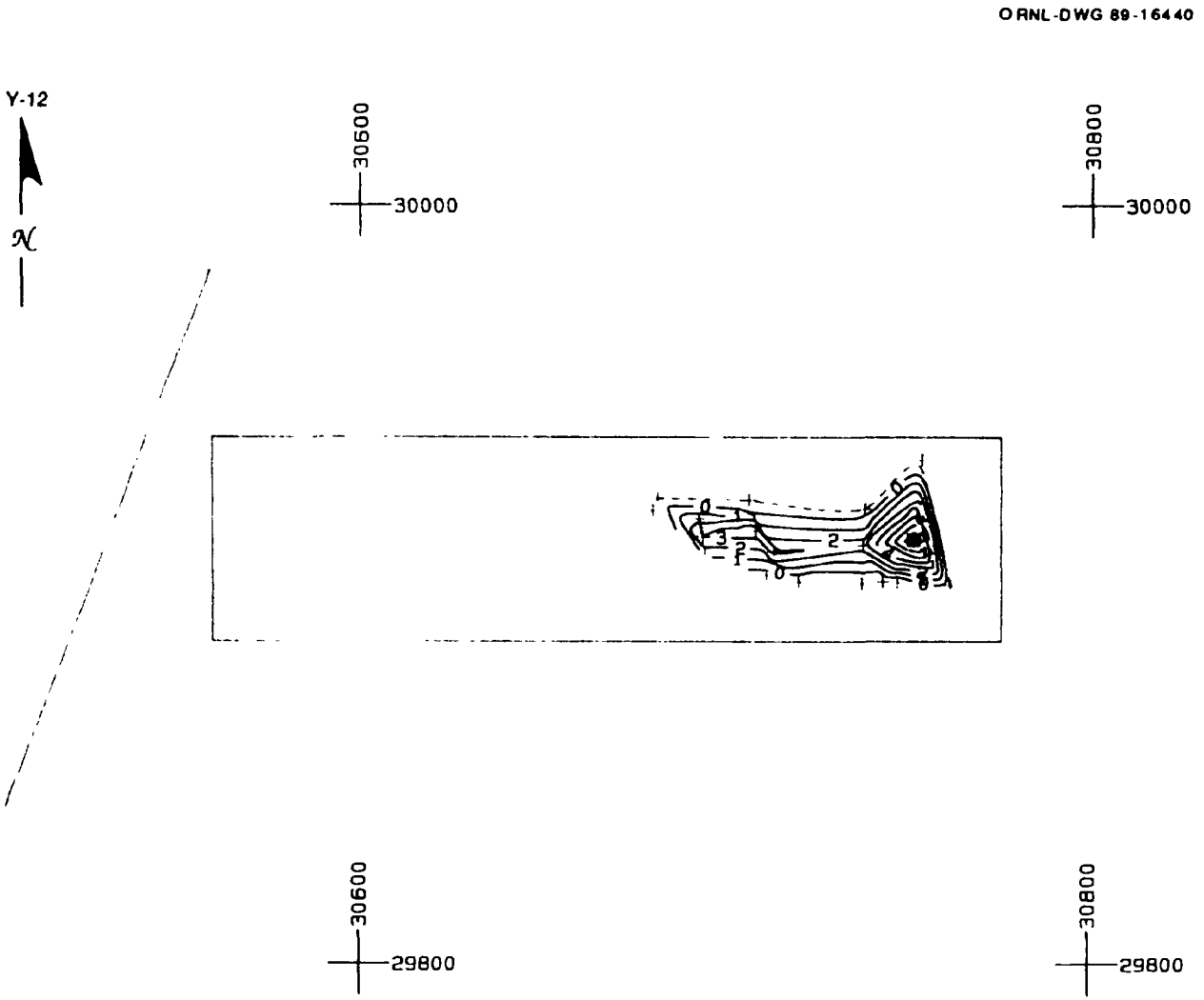

Fig. 32. Computer-generated contour map of log tracer concentration day 26 after injection. Contour interval log tracer concentration (ppb). Well locations represented by + symbol. Injection well within closed contours at right. Rectangle represents computer code grid domain. Creek represented by line at left.

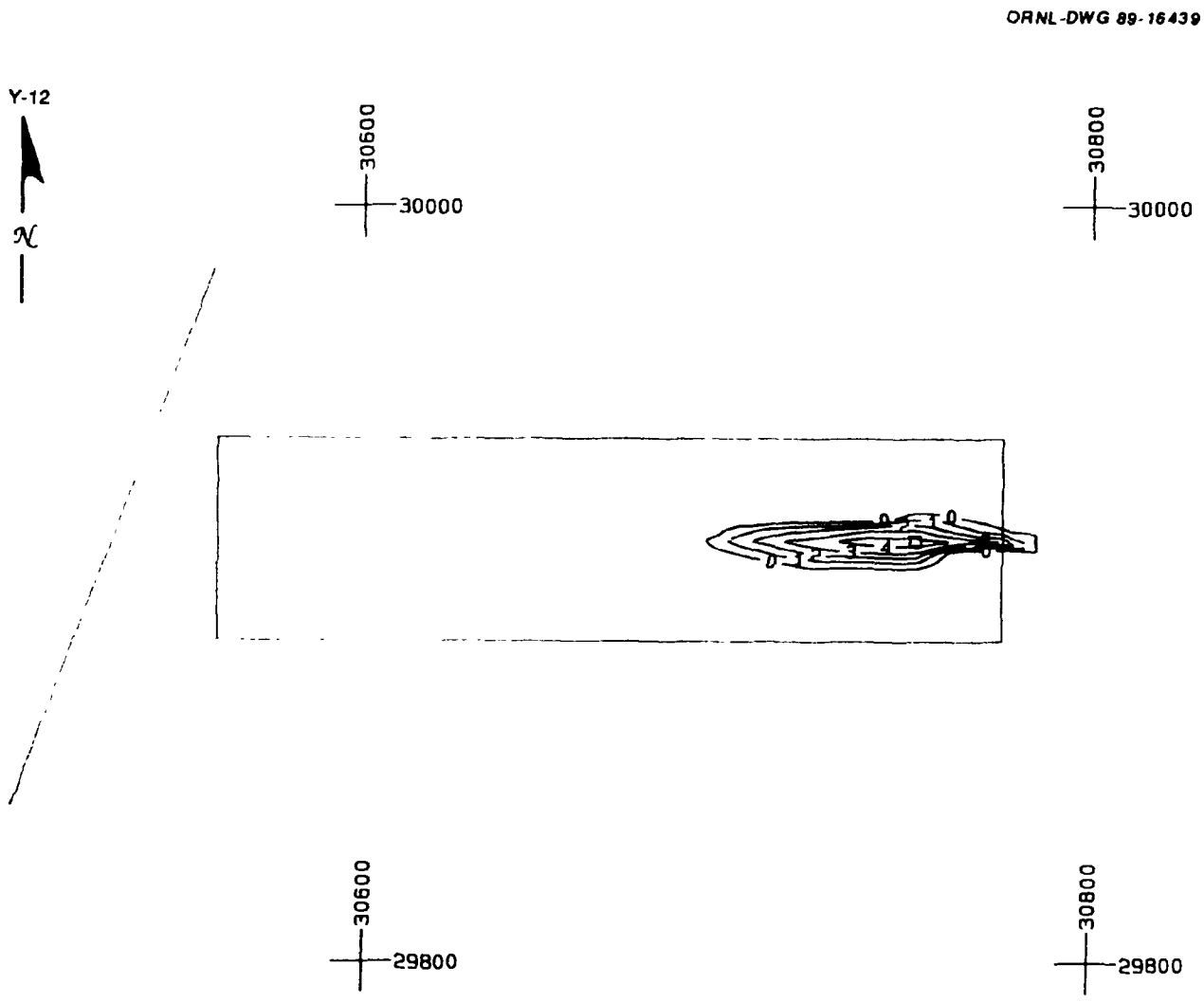

Fig. 33. Base case simulation contour map of log tracer concentration 1 month after injection. Contour interval log tracer concentration (ppb). Rectangle represents computer code grid domain. Injection well symbolized by square. Creek represented by line at left.

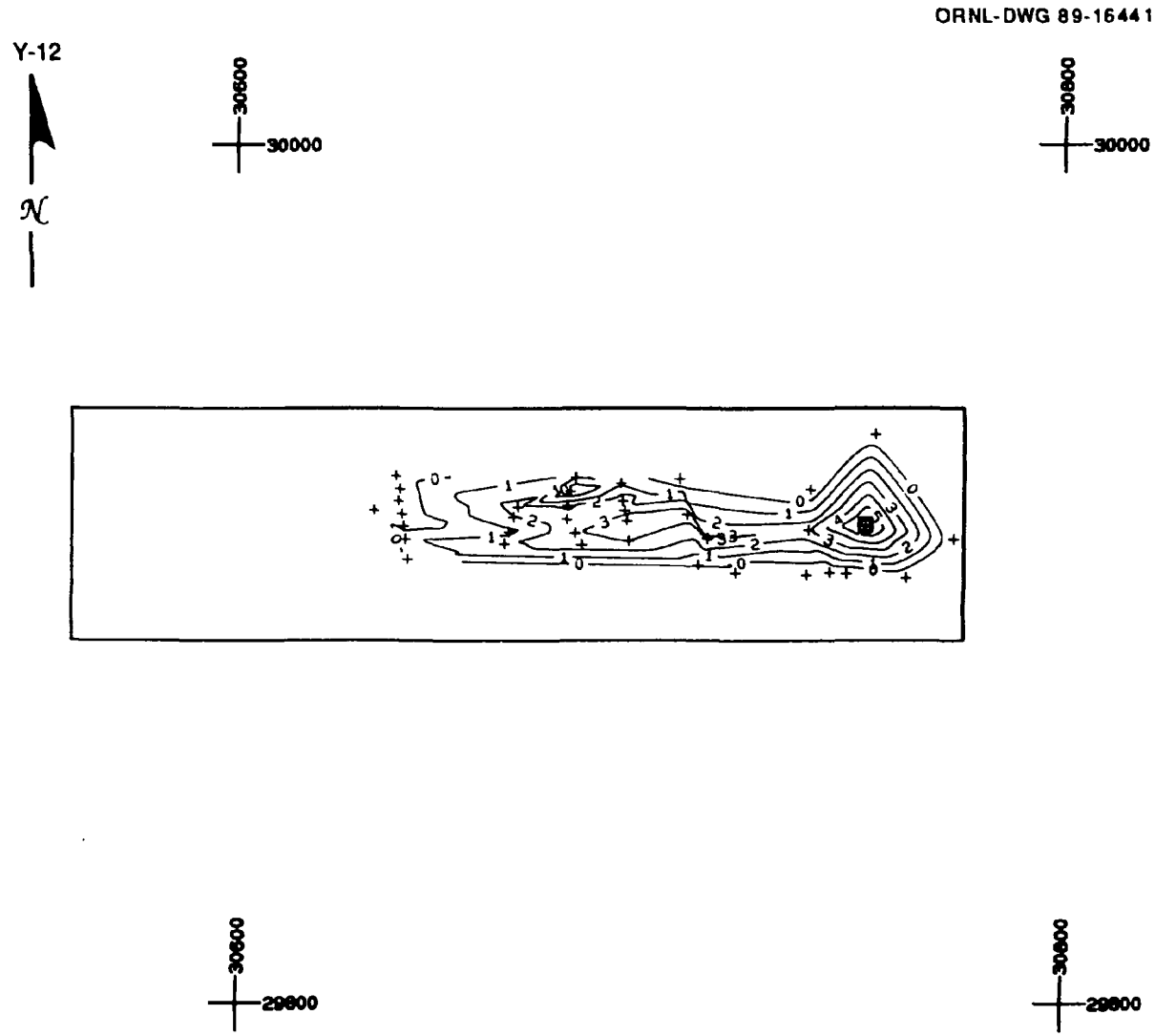

Fig. 34. Computer-generated contour map of log tracer concentration day 182 after injection. Contour interval log tracer concentration (ppb). Well locations represented by + symbol. Injection well within closed contours at right. Rectangle represents computer code grid domain.

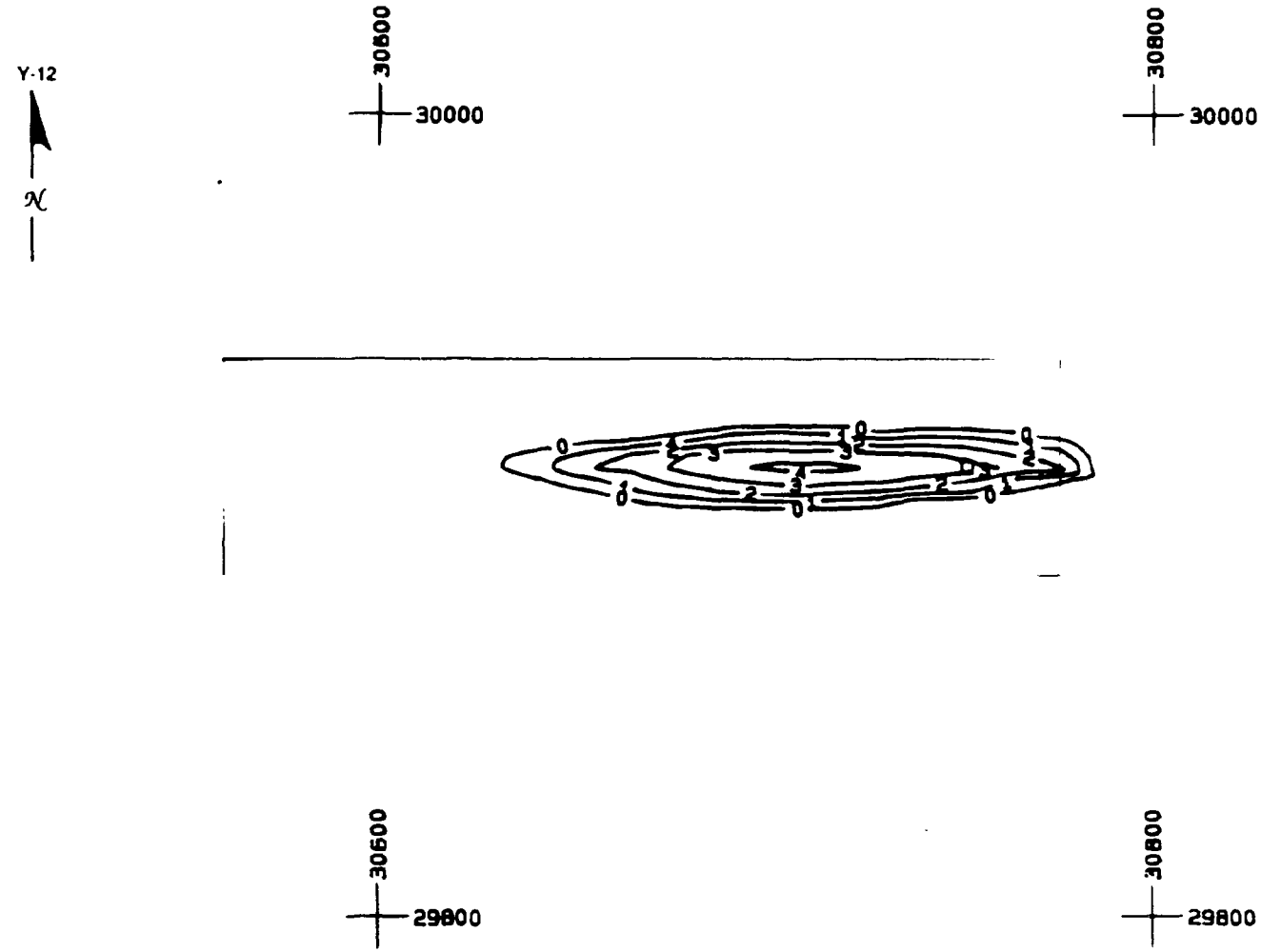

Fig. 35. Base case simulation contour map of log tracer concentration 6 months after injection. Contour interval log tracer concentration (ppb). Rectangle represents computer code grid domain. Injection well symbolized by square. Creek represented by line at left.

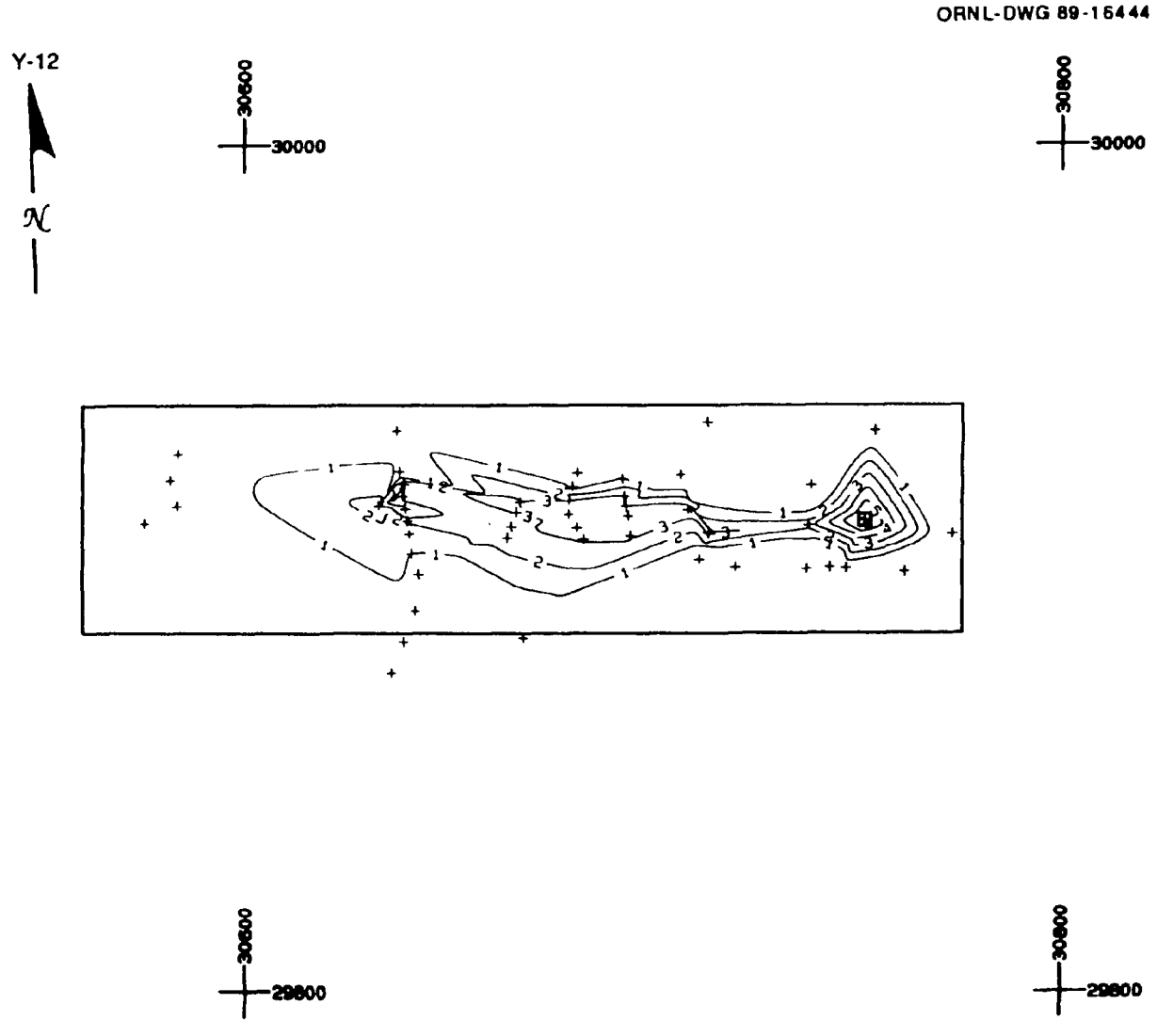

Fig. 36. Computer-generated contour map of log tracer concentration day 372 after injection. Contour interval log tracer concentration (ppb). Well locations represented by + symbol. Injection well within closed contours at right. Rectangle represents computer code grid domain.

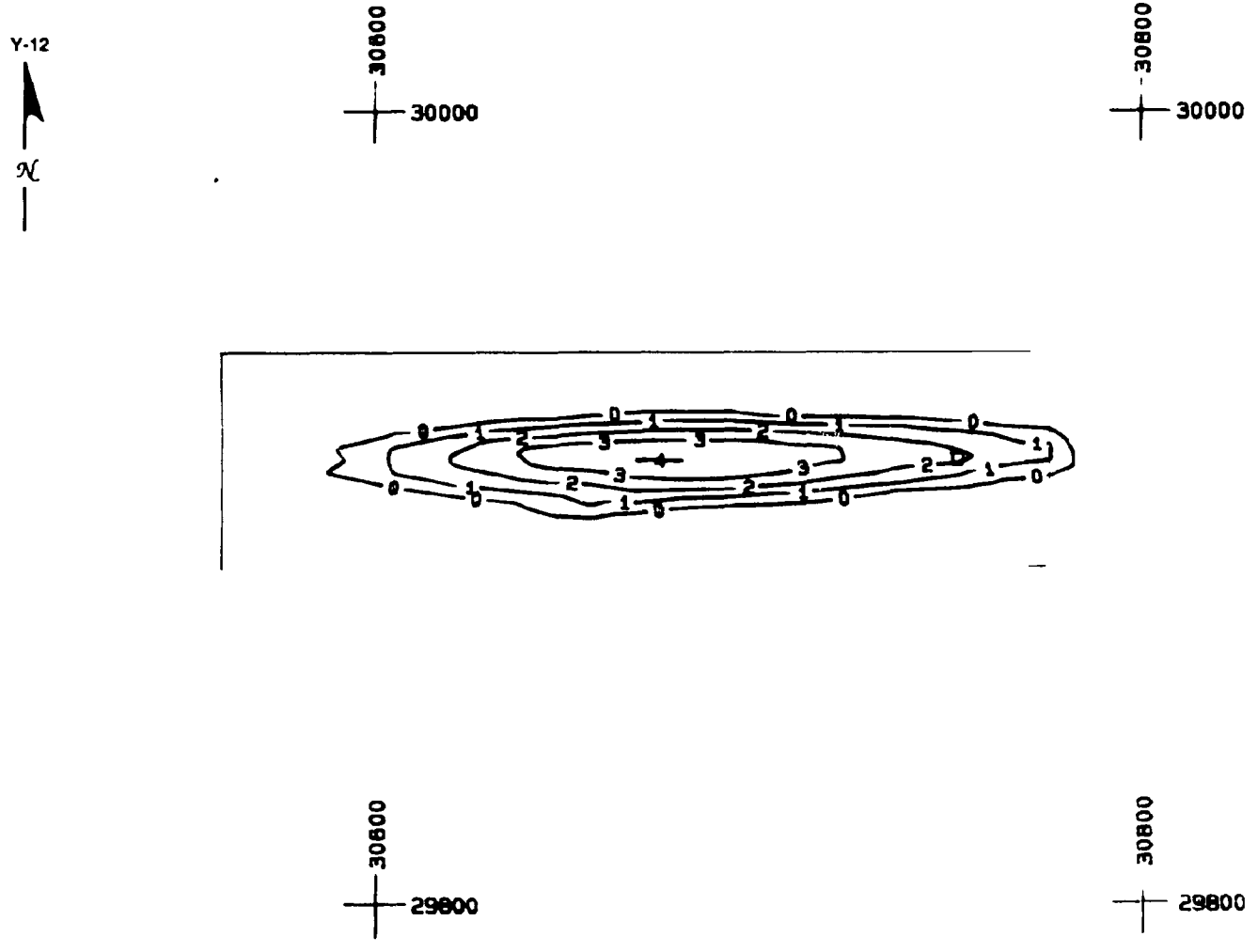

Fig. 37. Base case simulation contour map of log tracer concentration 12 months after injection. Contour interval log tracer concentration (ppb). Rectangle represents computer code grid domain. Injection well symbolized by square. Creek represented by line at left.

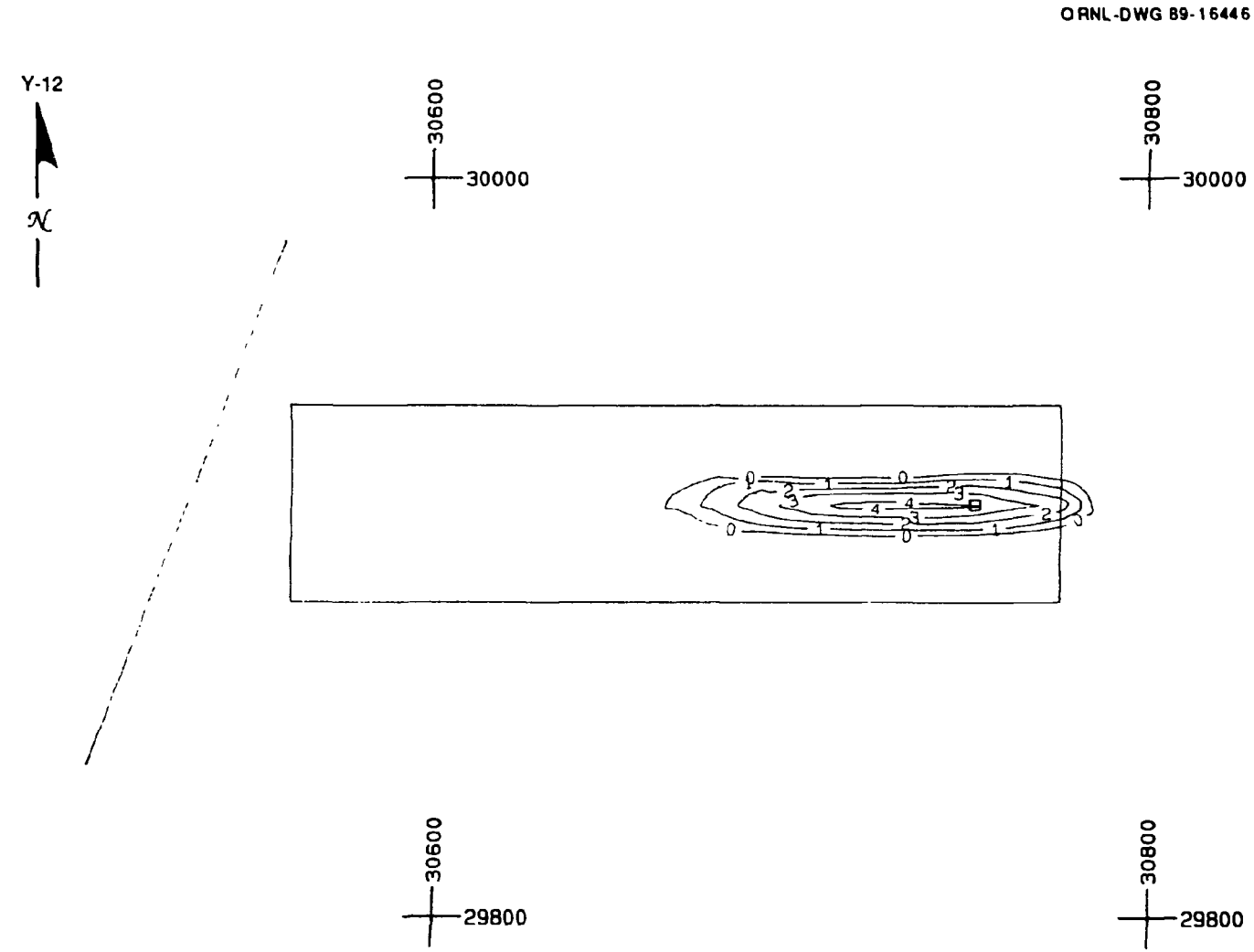

Fig. 38. Final case simulation contour map of log tracer concentration 3 months after injection. Contour interval log tracer concentration (ppb). Rectangle represents computer code grid domain. Injection well symbolized by square. Creek represented by line at left.

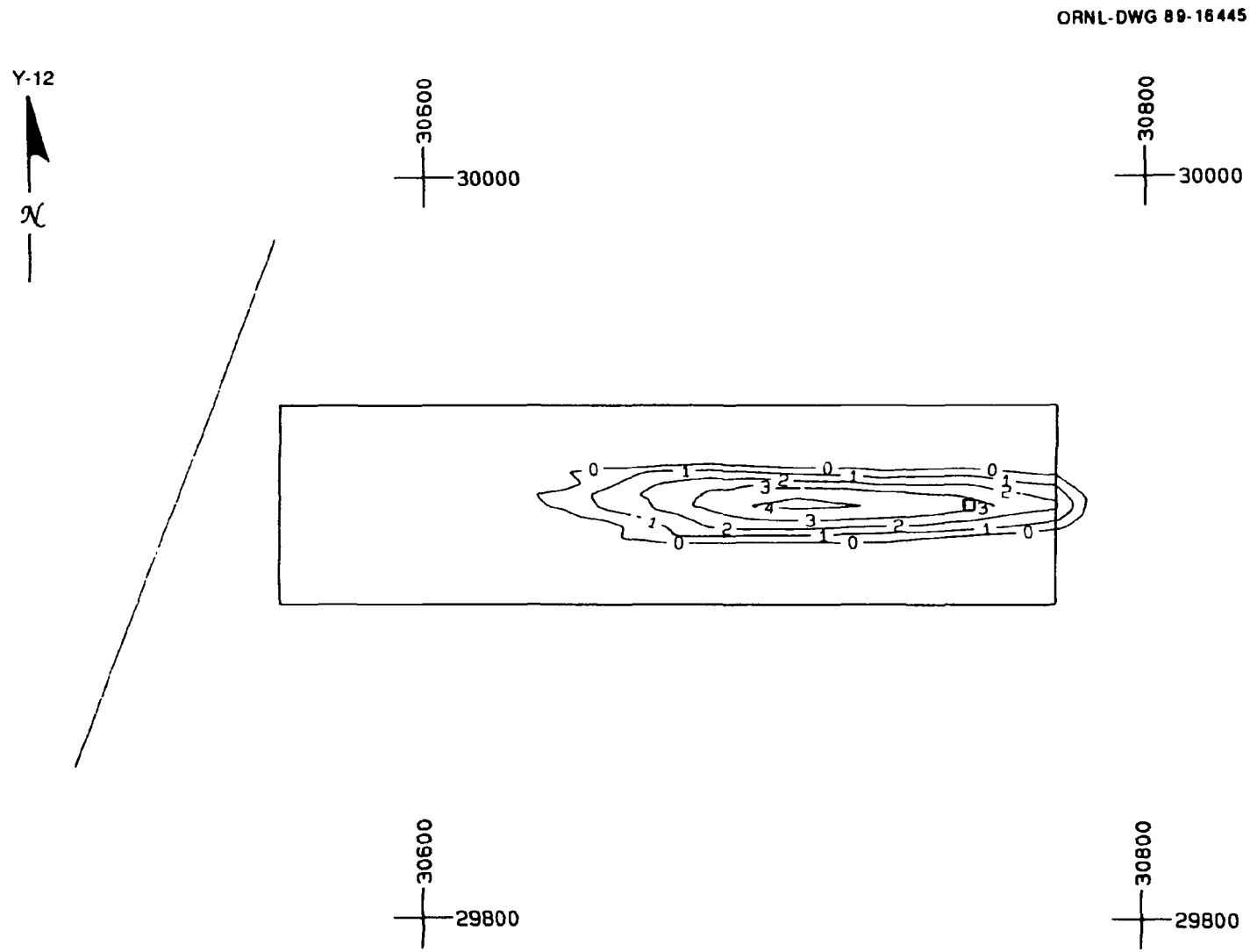

Fig. 39. Final case simulation contour map of log tracer concentration 6 months after injection. Contour interval log tracer concentration (ppb). Rectangle represents computer code grid domain. Injection well symbolized by square. Creek represented by line at left.

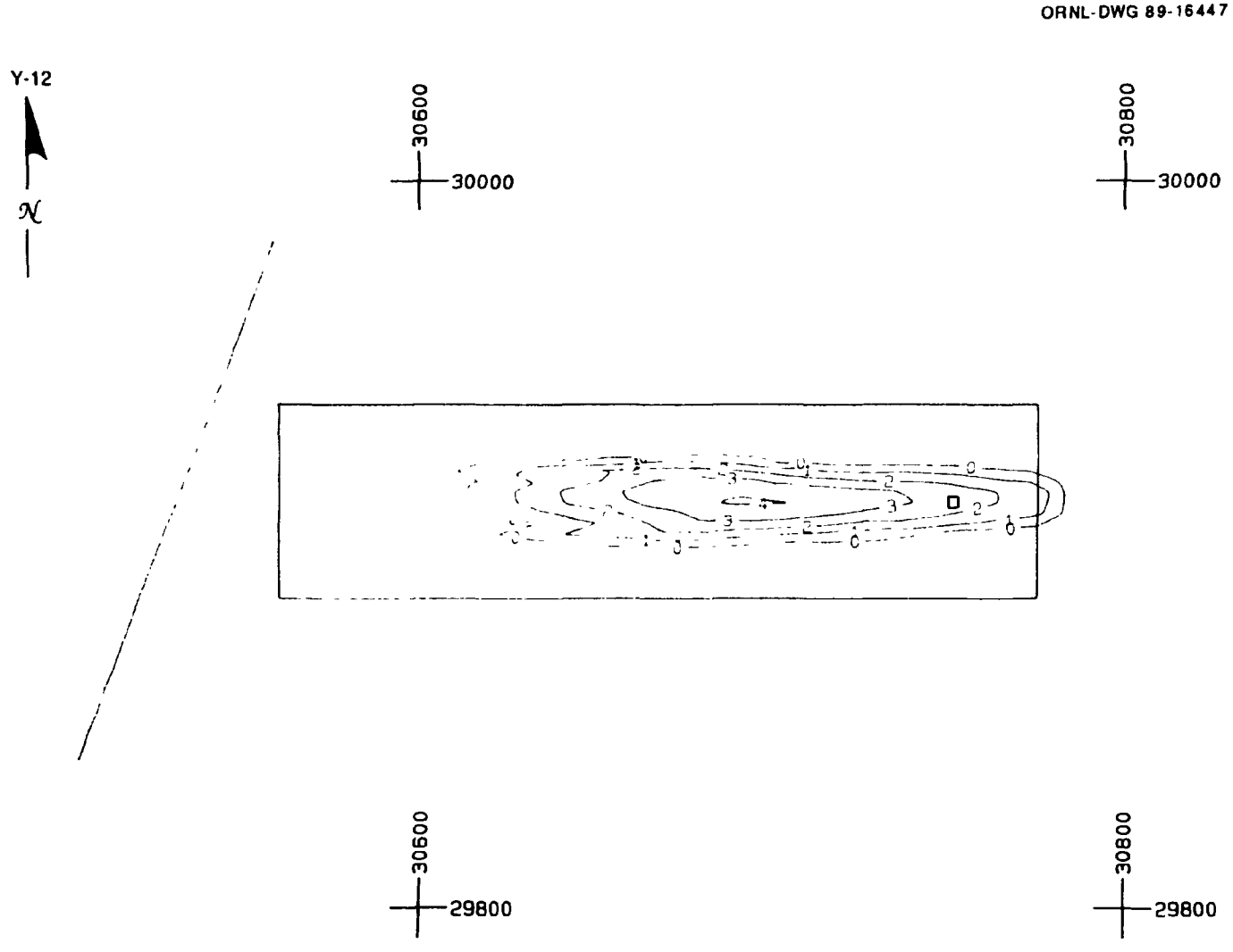

Fig. 40. Final case simulation contour map of log tracer concentration 9 months after injection. Contour interval log tracer concentration (ppb). Rectangle represents computer code grid domain. Injection well symbolized by square. Creek represented by line at left.

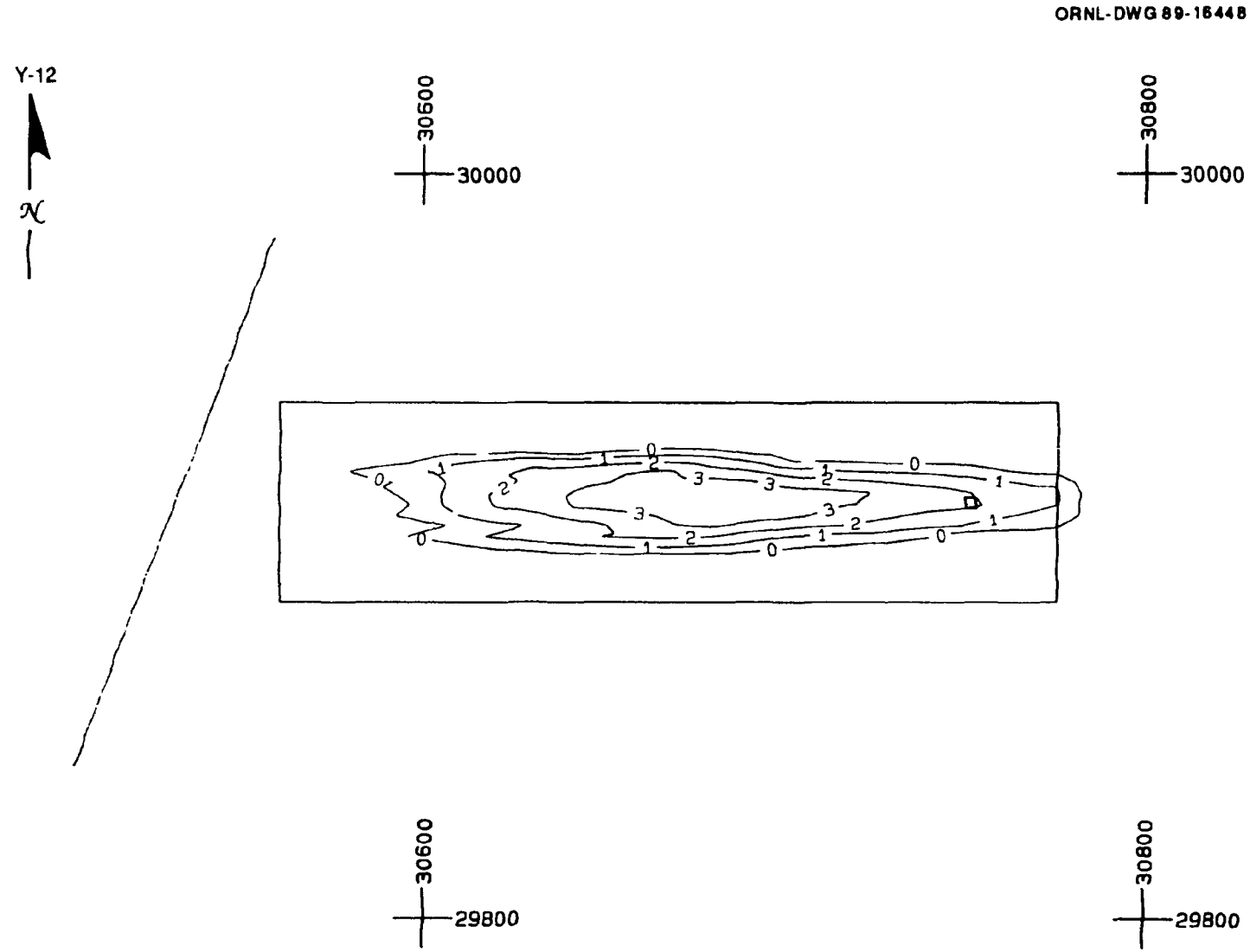

Fig. 41. Final case simulation contour map of log tracer concentration 12 months after injection. Contour interval log tracer concentration (ppb). Rectangle represents computer code grid domain. Injection well symbolized by square. Creek represented by line at left.

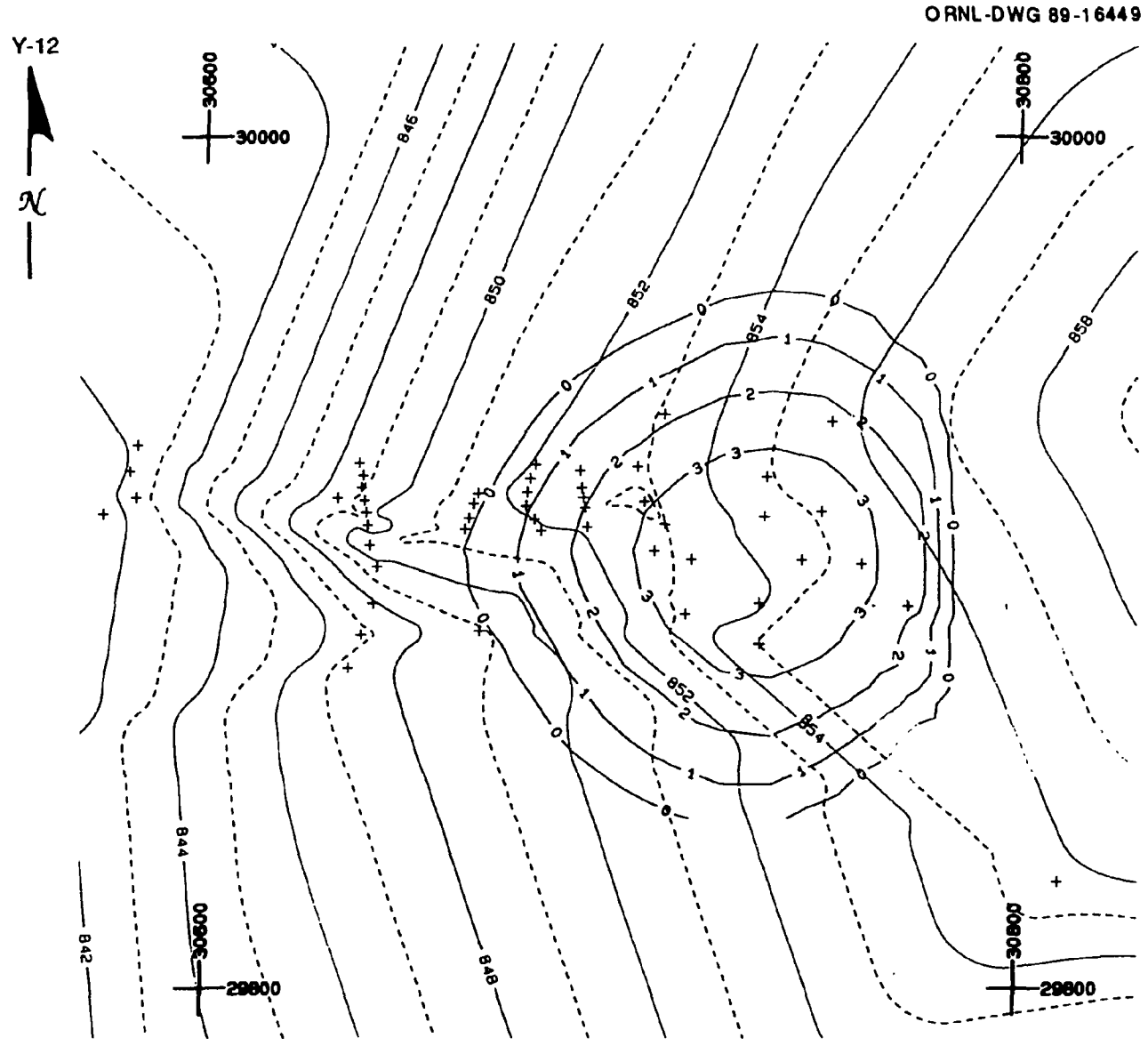

Fig. 42. Solute transport simulation assuming homogeneous, isotropic aquifer properties

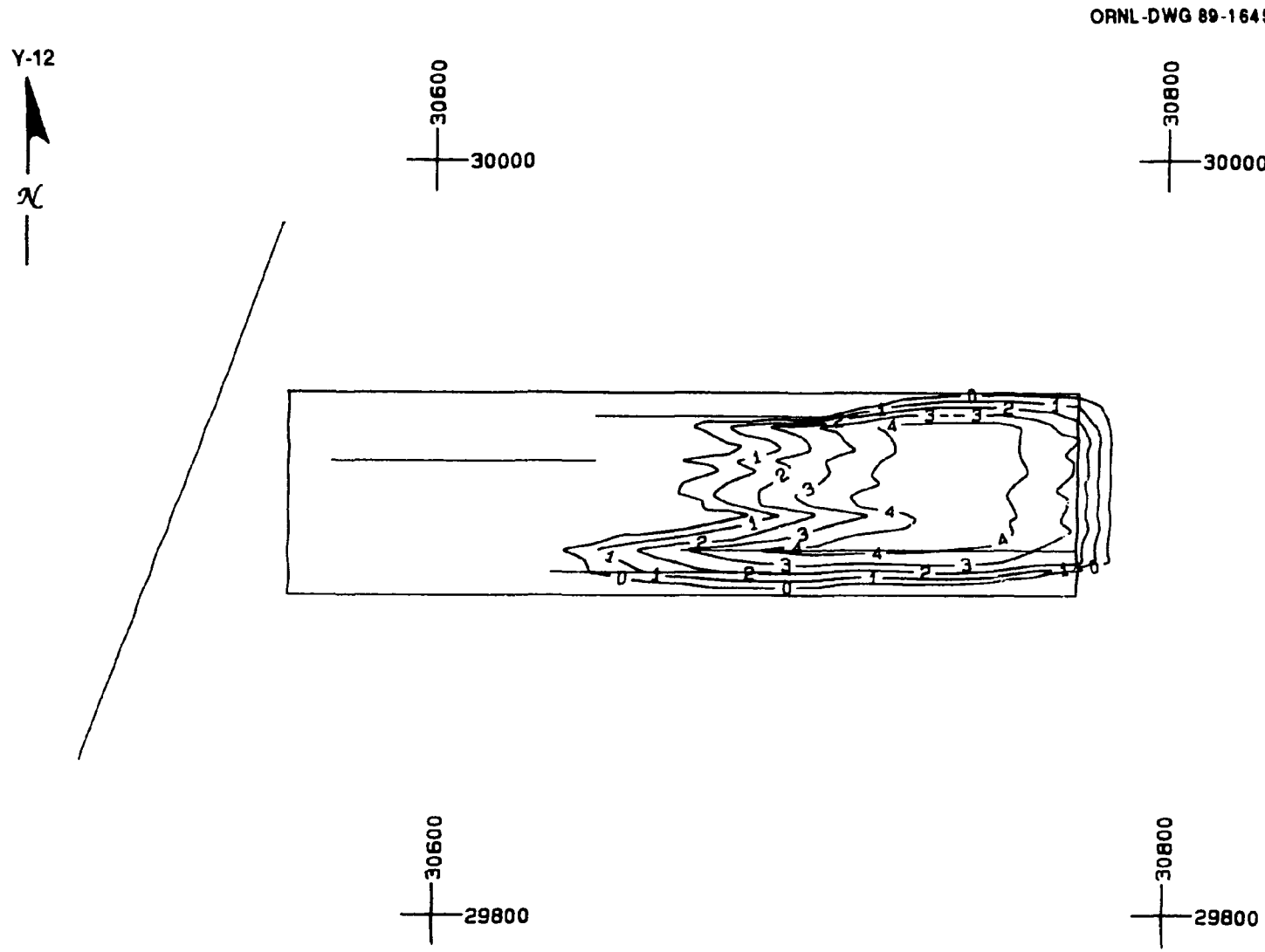

Fig. 43. Simulation assuming line source injection at injection well location, randomly distributed hydraulic conductivity values, and randomly distributed conduits of elevated hydraulic conductivity 3 months after injection. Contour interval log tracer concentration (ppb). Rectangle represents computer code grid domain. Creek represented by line at left.

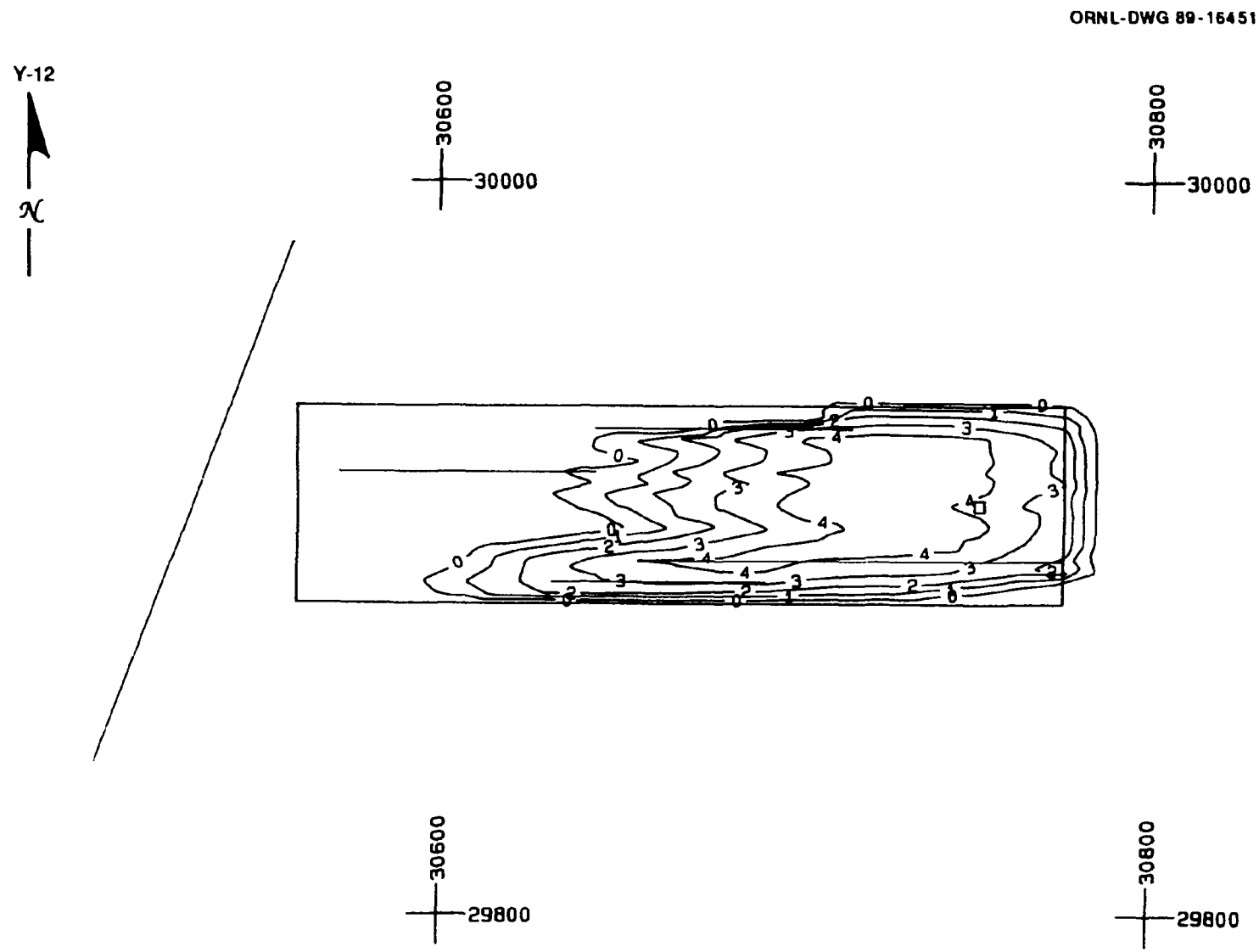

Fig. 44. Simulation assuming line source injection at injection well location, randomly distributed hydraulic conductivity values, and randomly distributed conduits of elevated hydraulic conductivity 6 months after injection. Contour interval log tracer concentration (ppb). Rectangle represents computer code grid domain. Creek represented by line at left.

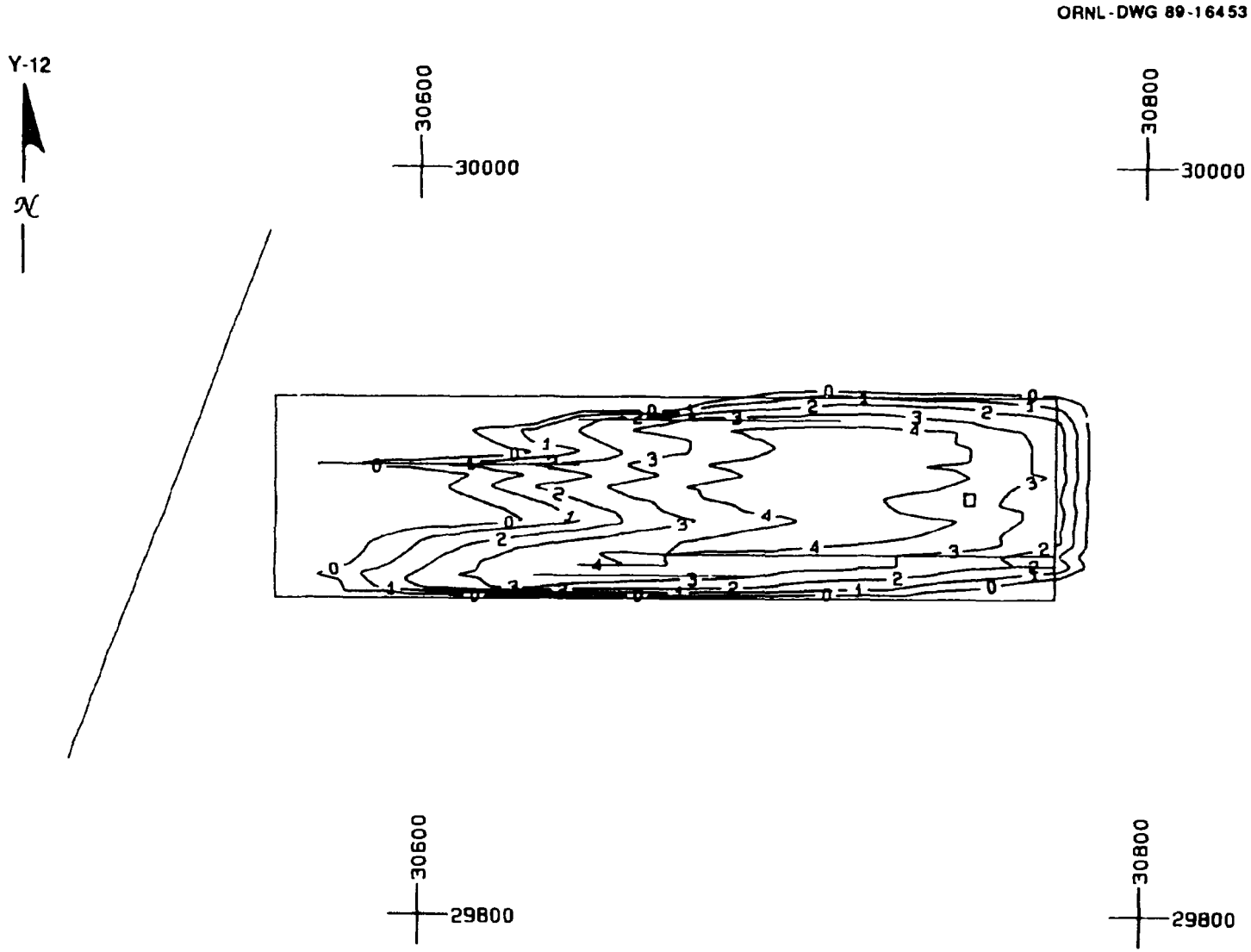

Fig. 45. Simulation assuming line source injection at injection well location, randomly distributed hydraulic conductivity values, and randomly distributed conduits of elevated hydraulic conductivity 9 months after injection. Contour interval log tracer concentration (ppb). Rectangle represents computer code grid domain. Creek represented by line at left.

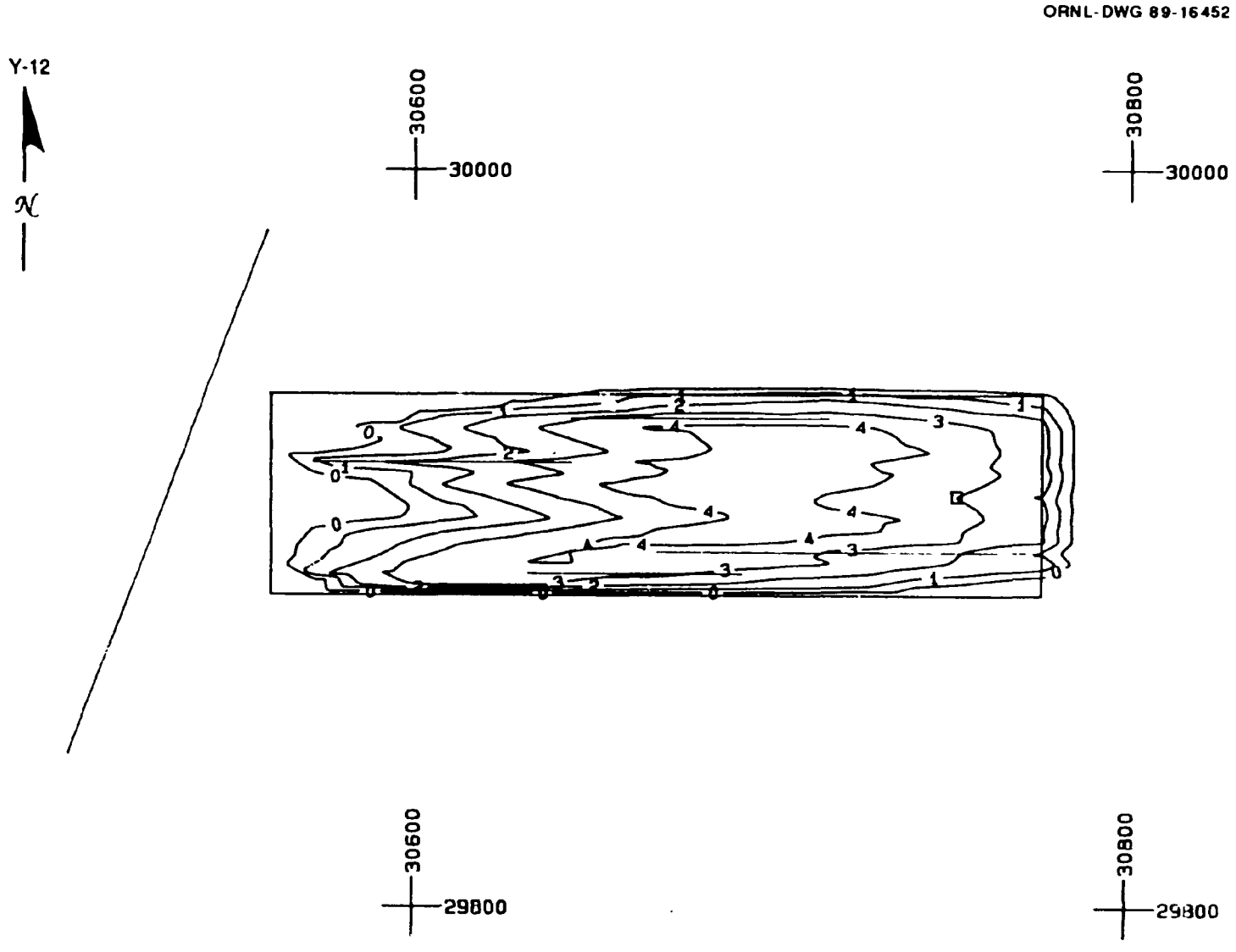

Fig. 46. Simulation assuming line source injection at injection well location, randomly distributed hydraulic conductivity values, and randomly distributed conduits of elevated hydraulic conductivity 12 months after injection. Contour interval log tracer concentration (ppb). Rectangle represents computer code grid domain. Creek represented by line at left.

8. DISCUSSION

One of the principal objectives of FY 1989 activities was to evaluate the legitimacy of the preliminary conceptual model for flow and transport that was developed from the FY 1988 model validation task by site testing, data analysis, and model simulation. Successful performance of the task was due in part to the approach to problem solution. In contrast to the typical method of performing such tasks in which site data interpretations are provided to modelers for model input after data analyses have been completed, this task was performed by developing and testing hypotheses in parallel throughout task performance. The approach allowed for simultaneous hypothesis development, testing, modification, and verification from field specialists, theoreticians, and mathematicians. The approach is regarded as merely an application of the scientific method, but it is seldom applied to multidisciplinary problems of this nature. The investigators believe that the results of the model validation task provide specific examples that demonstrate the benefits of the approach.

Hydrologic test data analyses do not support the concept of a hydraulic conductivity contrast between bedrock lithologies; no statistically significant contrast is evident either between bedrock lithologies or between weathered and unweathered bedrock. Preliminary FY 1989 computer flow simulations, however, indicated that the flow field at the site could be successfully simulated by incorporating the preliminary conceptual model in grid construction and grid element parameter value assignment. Although successful model simulations were performed with the heterogeneous lithology concept, the hydrologic test data designed to demonstrate the validity of the concept failed to do so. Alternatively, those data also failed to disprove the concept. Cross-sectional contouring of water elevation data suggests that the hydraulic head profile is related to bedrock attitude. With uncertainties associated with hydrologic test data interpretation and analysis, the concept may remain viable. It may be that available methods for analyzing field data are incapable of resolving the level of detail required to perform an adequate test. It also may be that water-producing zones in the principal aquifer exceed the limited testing scale.

The observed transient tracer-migration rate at intermediate distances from the injection well combined with rapid shallow aquifer response to rainfall (Figs. 15a and 15b) indicates that aquifer recharge/discharge flux may be more important than gradient in determining groundwater flow velocity. Rapid (less than 24 h) aquifer recharge followed by several days of discharge suggests that site soils allow rapid infiltration of rainfall directly to the aquifer, which then requires days of discharge flow to reach pre-rainfall head conditions. Section 5.3.5 describes the relationship between observed pulses in the rate of tracer migration and accompanying increases in tracer concentration in response to precipitation. It is projected that when tracer reaches the stream, aquifer response to event precipitation will result in tracer discharge to the stream in similar pulses.

The role of the hydraulic gradient profile on the transient tracer-migration rate is unclear; the tracer-migration rate is not always related to the slope of the gradient. Tracer migration and water elevation indicate the presence of discontinuous, nearly strike-parallel zones of elevated head potential and hydraulic conductivity, which have a dominating influence on both the direction and rate of flow and transport. To perform simulations of tracer migration, these zones were represented as conduits of elevated hydraulic conductivity and were assigned values at the upper end of values measured in the field (1×10^{-4} cm/s).

It may be that with sufficient data, a solution to the transient problem without the use of conduits might produce results similar to the steady-state solution performed in this study.

Although the site flow field can be successfully simulated using the preliminary conceptual model, the bulk of the data suggest that modification of the model is necessary. The revised conceptual model for flow and transport based on the analysis of site data is a refinement of the preliminary conceptual model developed prior to FY 1989 activities. In the shallow aquifer, flow direction is dominated by local and regional geologic fractures. Head that drives flow is derived largely from depth or from an undetermined off-site location at lesser depths. The transient tracer-migration rate is related to a complex interplay between fracture connectedness, zones of elevated hydraulic head potential and hydraulic conductivity, and an overall changing site hydraulic head gradient related to precipitation events and the annual precipitation cycle.

As stated in Sect. 1, tracer arrival in the far field at the initiation of the FY 1989 task precludes results of this study from constituting a complete demonstration of model validation. However, the authors believe that the results constitute a model validation in the following manner. First, the base case tracer simulation (one conduit) was calibrated to flow in the near field and was allowed to run for 12 months. That case predicted that the average tracer-migration rate for the time period was 0.4 ft/d; the actual migration rate for the 100-ppb isopleth during that time period was 0.33 ft/d. In addition, modeling and conceptual model development from field activities proceeded in parallel. The model was intended to examine the legitimacy of ideas developed from the analysis and interpretation of field data. The computer code simulation of tracer migration validates those ideas.

Clearly, the next step (model validation) is for the calibrated model to perform accurate predictions of tracer location, time of arrival, and concentration in the absence of a priori field data. Such an exercise could be performed at this site by predicting tracer arrival at the perennial creek to the west of the site. Such a task is under consideration and may be performed pending determinations regarding the ability of such an exercise to meet program needs. Alternatively, another tracer test could be performed at another site with the objective of evaluating predictive model accuracy.

9. CONCLUSIONS

This study demonstrates that the level of resolution provided by a groundwater tracer test can be simulated as an equivalent porous medium by using model input parameter values constrained by field data interpretations. The results (model calibration) constitute the first necessary step in predictive model accuracy (model validation). In part, the successful simulation is attributed to use of a systematic approach to site characterization, conceptual model formulation, hypothesis testing, and modeling through an iterative feedback process. Simulating tracer-migration behavior over short time periods (weeks) is limited by our ability to conceptually integrate the effects of bedrock fractures, fluctuations in the local hydraulic head configuration, and precipitation on the flow field. Simulations over longer time periods (months) smooth the short-term fluctuations in these effects for more accurate comparison with tracer-migration behavior.

Conventional site data interpretation and groundwater modeling practices that assume steady-state, homogeneous conditions do not accurately represent the flow field on the ORR. Simulations that use those conditions predict an unrealistic plume shape and migration pathway. A set of extensive tracer concentration and water elevation data indicates that the direction of groundwater flow and solute transport is related to the presence of bedrock fractures. The rate of migration is altered locally by the presence and lateral extent of these fractures (conduits) and is weakly related to the hydraulic gradient profile. Depending on the time of year, tracer migration in the shallow aquifer responds almost immediately to rainfall events of ~20 mm and greater.

Accurate simulations during a 1-year period can be achieved by assigning randomly distributed values of hydraulic conductivity and conduit geometry in the flow field within the constraints of site data interpretations. Future use of this constrained randomization approach to problem solution at the scale of the surrounding Bear Creek Valley site may reduce uncertainties associated with site-wide pathways analysis and performance assessment.

10. REFERENCES

Akima, H. 1978. "A Method of Bivariate Interpolation and Smooth Surface Fitting for Irregularly Distributed Data Points," *ACM Transactions on Mathematical Software* 4, 148–159.

Crane, [illegible] and M. Minkoff 1980. *Solution of the General Nonlinear [illegible] MCON*, ANL-80-64, Argonne National [illegible]

Davis, [illegible] *Characterization Techniques at a Low-Level Waste Shallow Land Burial Field Demonstration Facility*, ORNL/TM-9146, Oak Ridge National Laboratory, Oak Ridge, Tenn., July.

Freeze, R. and J. Cherry 1979. *Groundwater*, Prentice-Hall, Englewood Cliffs, N.J.

Golder Associates, Inc. 1988. *Contaminant Transport Model Validation*, ORNL/Sub/88-SA706/5 1, Oak Ridge National Laboratory, Oak Ridge, Tenn.

Hantush, M. 1964. "Hydraulics of Wells," *Advances in Hydroscience*, Vol. 1, Academic Press, N.Y.

Horwedel, J. E., et al. October 1988. *GRESS Version 0.0 User's Manual*, ORNL/TM-10835, Oak Ridge National Laboratory, Oak Ridge, Tenn.

Huyakorn, P. S., H. O. White, Jr., and T. D. Wadsworth 1987. *TRAFRAP-WT: A Two-Dimensional Finite Element Code for Fluid Flow and Transport in Fractured Porous Media*, Hydrogeologic, Inc., Va., July.

Huyakorn, P. S. and G. F. Pinder 1988. *Computational Methods in Subsurface Flow*, Academic Press, Inc., N.Y.

Konikow, L. F. and J. D. Bredehoeft 1988. *Computer Model of Two-Dimensional Solute Transport and Dispersion in Ground Water, Version 2.5*, Book 7, Chapter C-2, USGS.

Lee, R. R. and R. H. Ketelle 1988. *Contaminant Transport Model Validation*, ORNL/TM-10972, Oak Ridge National Laboratory, Oak Ridge, Tenn., September.

Lee, R. R. and R. H. Ketelle 1989. *Geology of the West Bear Creek Site*, ORNL/TM-10887, Oak Ridge National Laboratory, Oak Ridge, Tenn., January.

Lozier, W. B., C. A. Spiers, and R. Pearson 1987. *Aquifer Pump Test with Tracers*, ORNL/Sub/86-32136/2, Oak Ridge National Laboratory, Oak Ridge, Tenn., October.

Rafalko, Leonard G. and Mark E. Hawley 1989. "Uncertainty in Transport Predictions," in papers from the *NWWA Conference on Solving Ground Water Problems with Models, Feb. 7-9, 1989, Indianapolis, Indiana*.

Theis, C. V. 1935. "The Relationship Between the Lowering of the Piezometric Surface and the Rate of Discharge of a Well Using Groundwater Storage," *Trans. of the Am. Geophys. Union*, 2, 519–524.

Van Der Heijde, P. K. M. 1983. *THEISFIT*, International Groundwater Modeling Center, Holcomb Research Institute, Butler University, Indianapolis, September.

Van Der Heijde, P. K. M. 1988. *TSSLEAK*, International Groundwater Modeling Center, Holcomb Research Institute, Butler University, Indianapolis, November.

Waldrop, W. R., J. M. Boggs, and S. C. Young 1988. *A Field Experiment of Groundwater Transport in a Heterogeneous Aquifer*, proceedings of the USATHAMA 13th Annual Environmental Quality R&D Symposium held at Williamsburg, Va. on Nov. 15–17, 1988.

Ward, D. S., B. H. Lester, and J. Mercer 1987. *SEFTRAN: A Simple and Efficient Two-Dimensional Groundwater Flow and Transport Model,* Geotrans, Inc.

Webster, D. A. 1976. *A Review of Hydrologic and Geologic Conditions Related to the Radioactive Solid-Waste Burial Grounds at Oak Ridge National Laboratory, Oak Ridge, Tennessee,* USGS Open-File Report 76-727.

Webster, D. A. and M. W. Bradley 1988. *Hydrology of the Melton Valley Radioactive-Waste Burial Grounds at Oak Ridge National Laboratory, Oak Ridge, Tennessee,* USGS Open-File Report 87-686.

Yeh, G. T. 1981. *AT123D: Analytical Transient 1-2-3-D Simulation of Waste Transport in the Aquifer System, Oak Ridge National Laboratory, Oak Ridge, Tennessee,* ORNL/TM-5602, March.

APPENDIX A

WELL HYDROGRAPHS

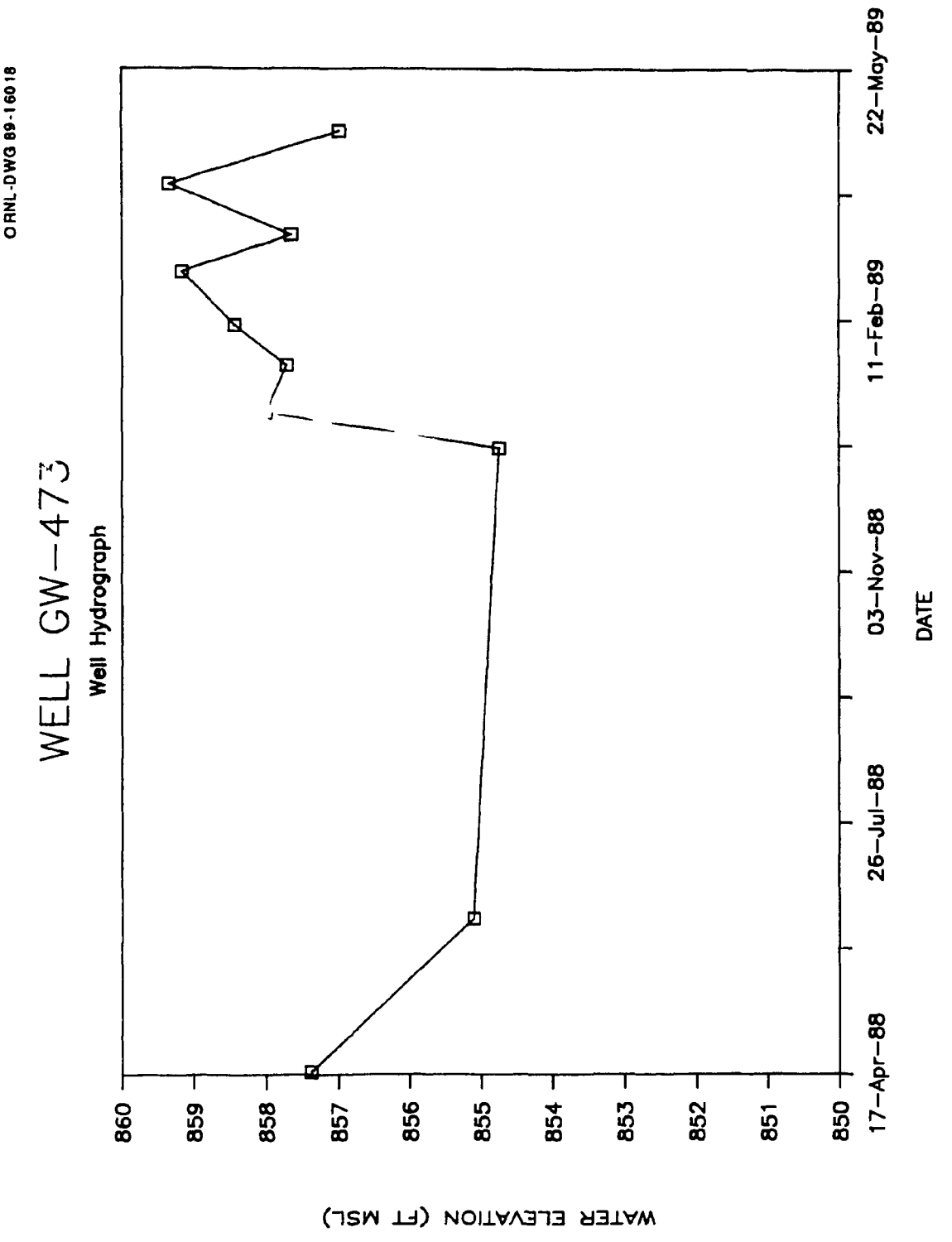
ORNL-DWG 89-16018
WELL GW-473
Well Hydrograph
WATER ELEVATION (FT MSL)
860
859
858
857
856
855
854
853
852
851
850
17-Apr-88
26-Jul-88
03-Nov-88
11-Feb-89
22-May-89
DATE

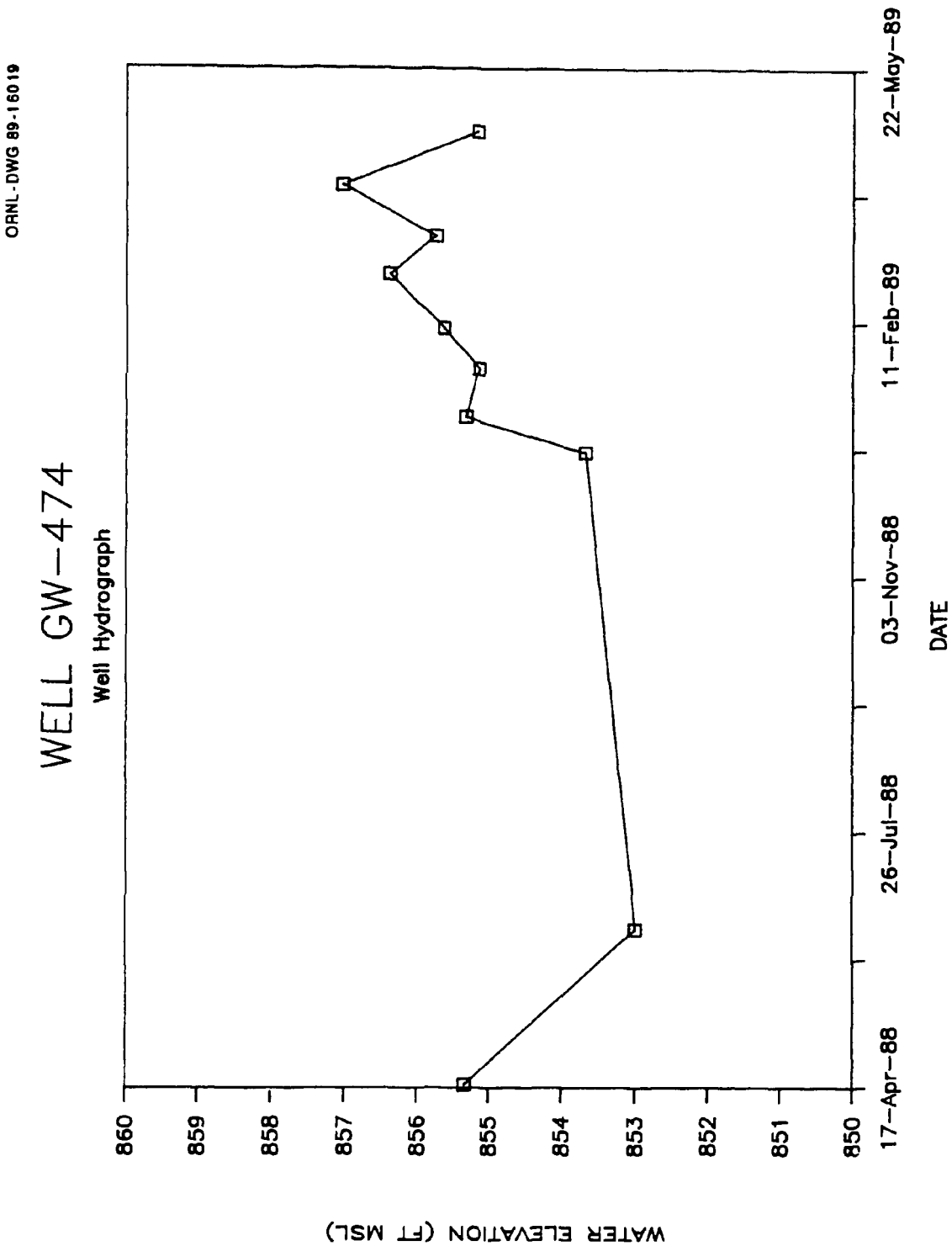
ORNL-DWG 89-16019
WELL GW-474
Well Hydrograph
WATER ELEVATION (FT MSL)
860
859
858
857
856
855
854
853
852
851
850
17-Apr-88
26-Jul-88
03-Nov-88
11-Feb-89
22-May-89
DATE

ORNL-DWG 89-16020

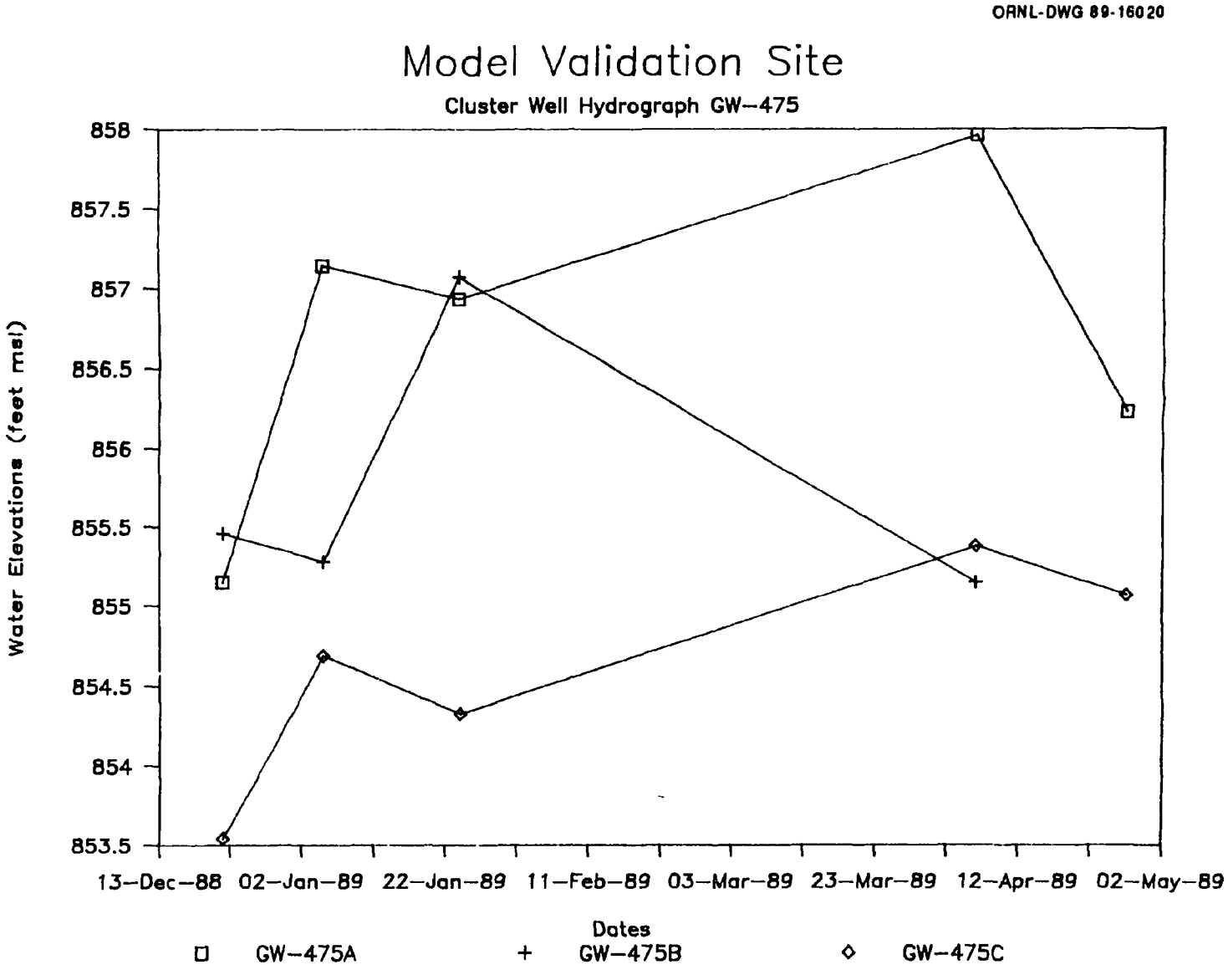

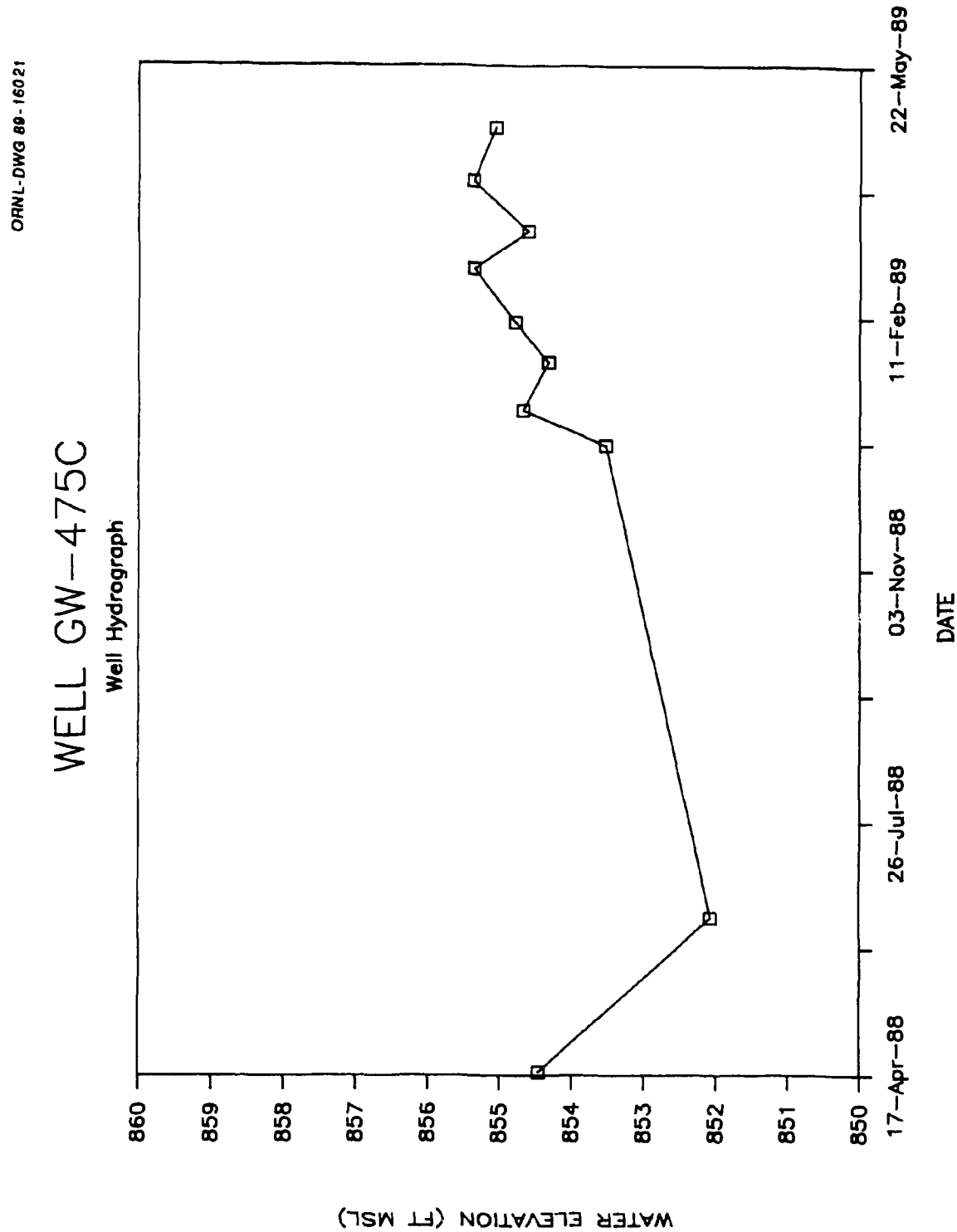
ORNL-DWG 89-16021
WELL GW-475C
Well Hydrograph
WATER ELEVATION (FT MSL)
860
859
858
857
856
855
854
853
852
851
850
17-Apr-88
26-Jul-88
03-Nov-88
11-Feb-89
22-May-89
DATE

ORNL-DWG 89-16022

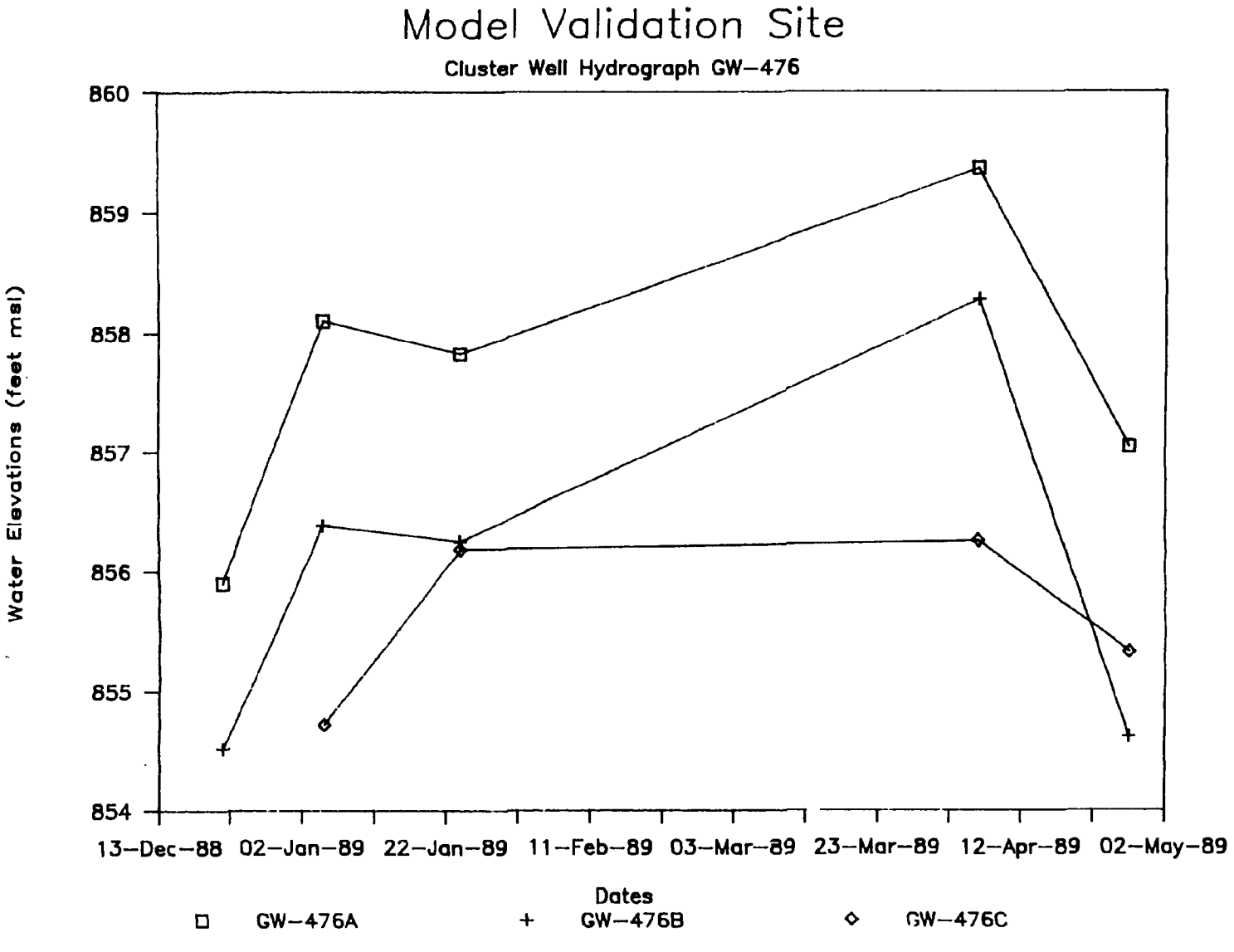

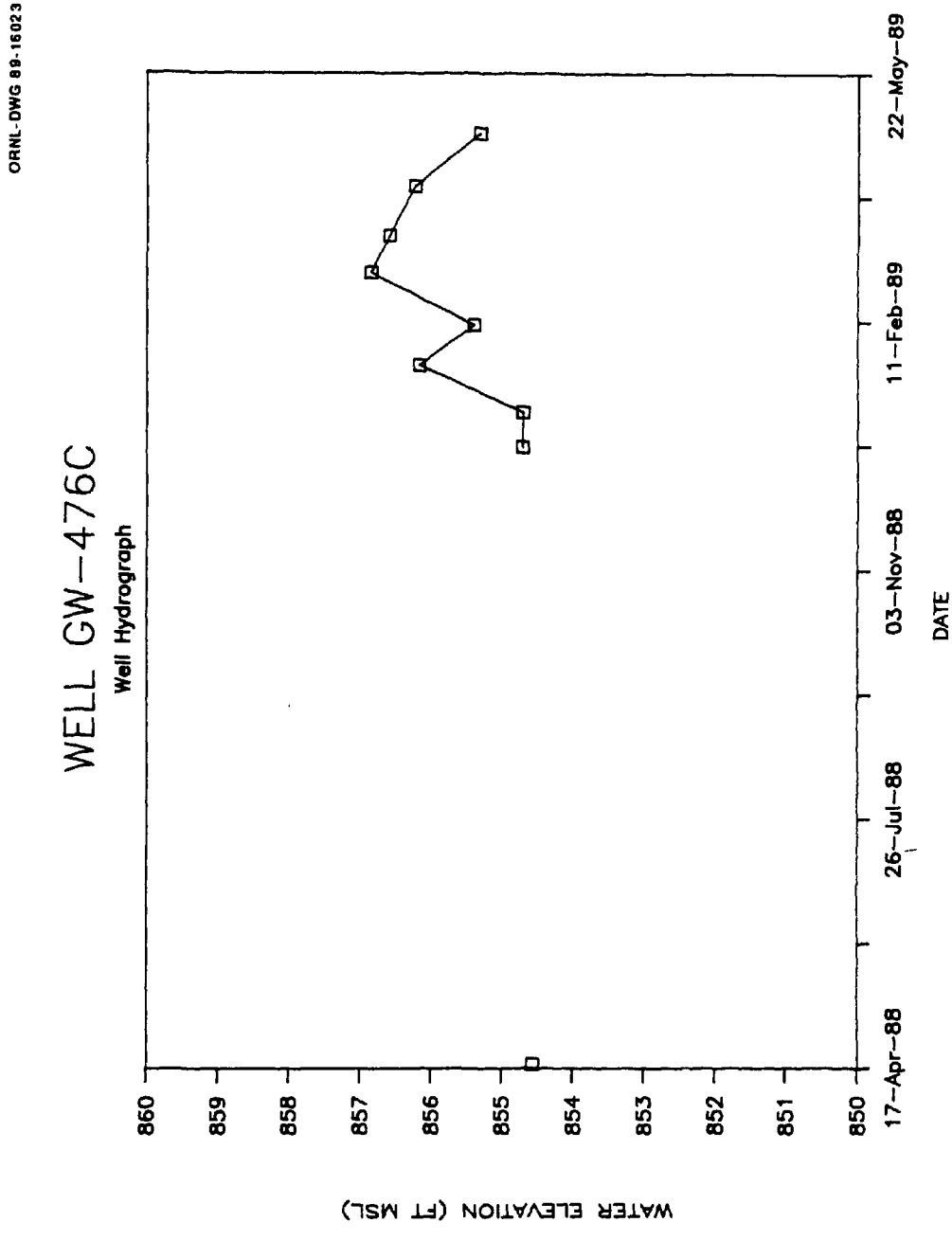
ORNL-DWG 89-16023
WELL GW-476C
Well Hydrograph
WATER ELEVATION (FT MSL)
860
859
858
857
856
855
854
853
852
851
850
17-Apr-88
26-Jul-88
03-Nov-88
11-Feb-89
22-May-89
DATE

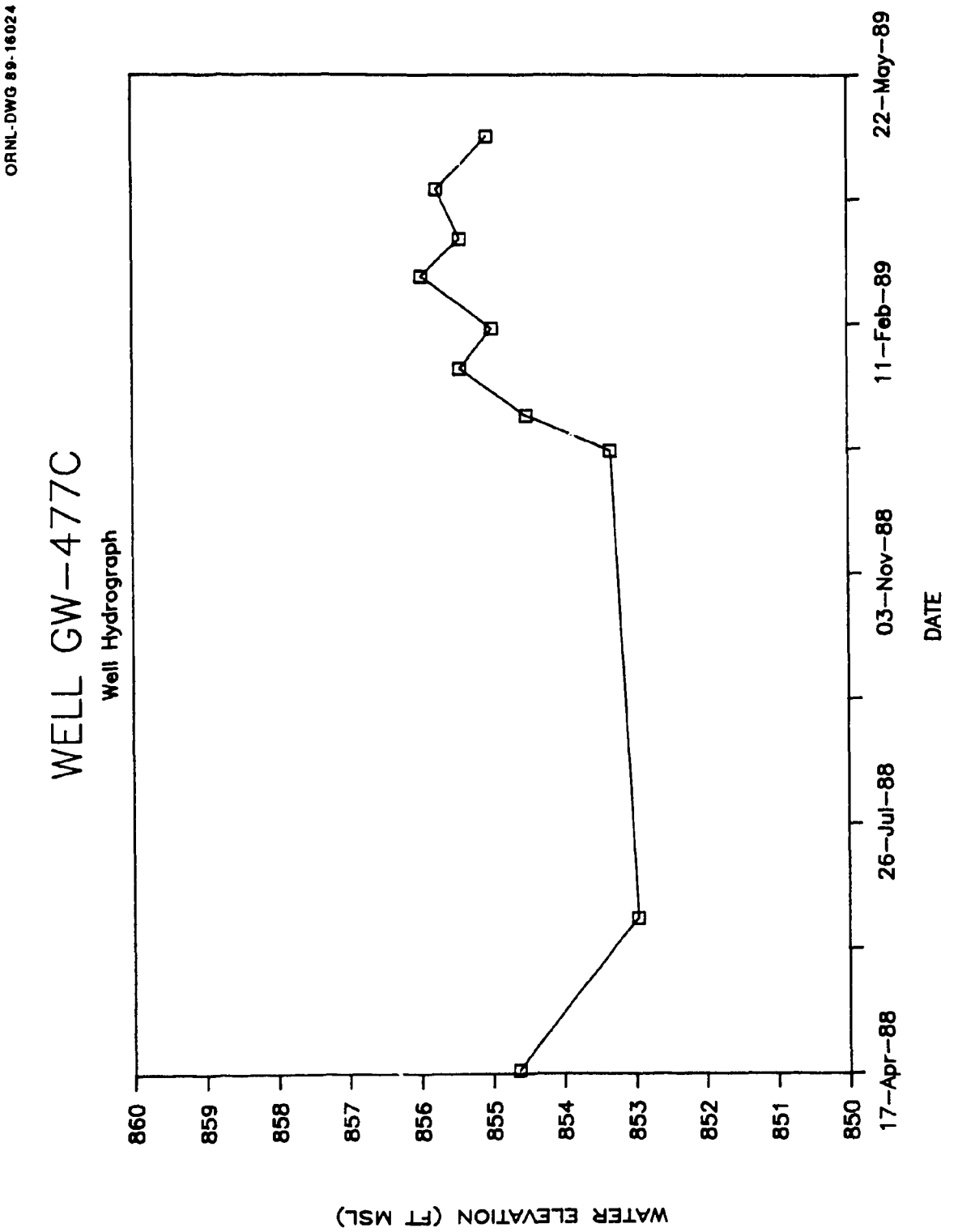
ORNL-DWG 89-16024
WELL GW-477C
Well Hydrograph
WATER ELEVATION (FT MSL)
860
859
858
857
856
855
854
853
852
851
850
17-Apr-88
26-Jul-88
03-Nov-88
11-Feb-89
22-May-89
DATE

ORNL-DWG 89-16025

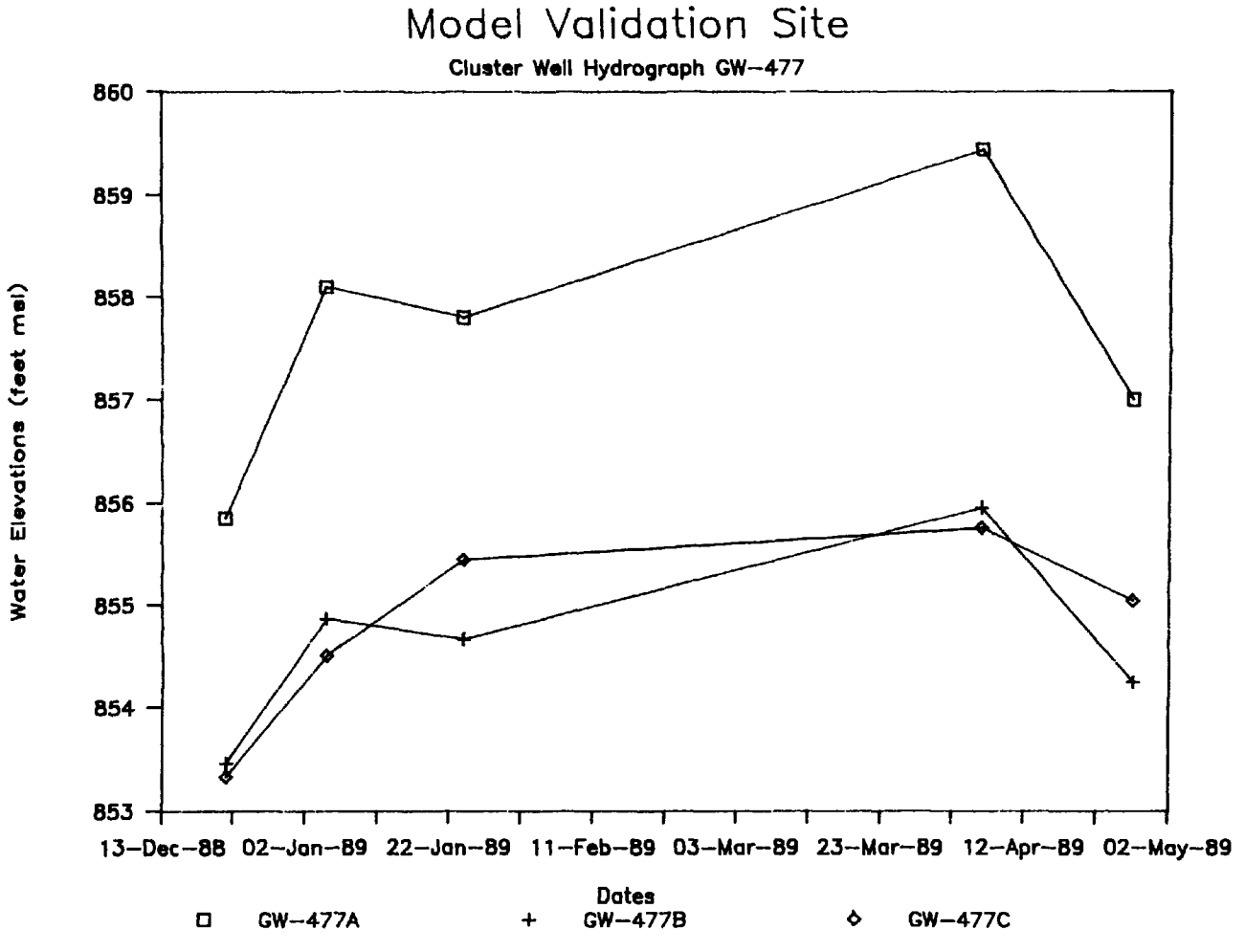

ORNL-DWG 89-16026

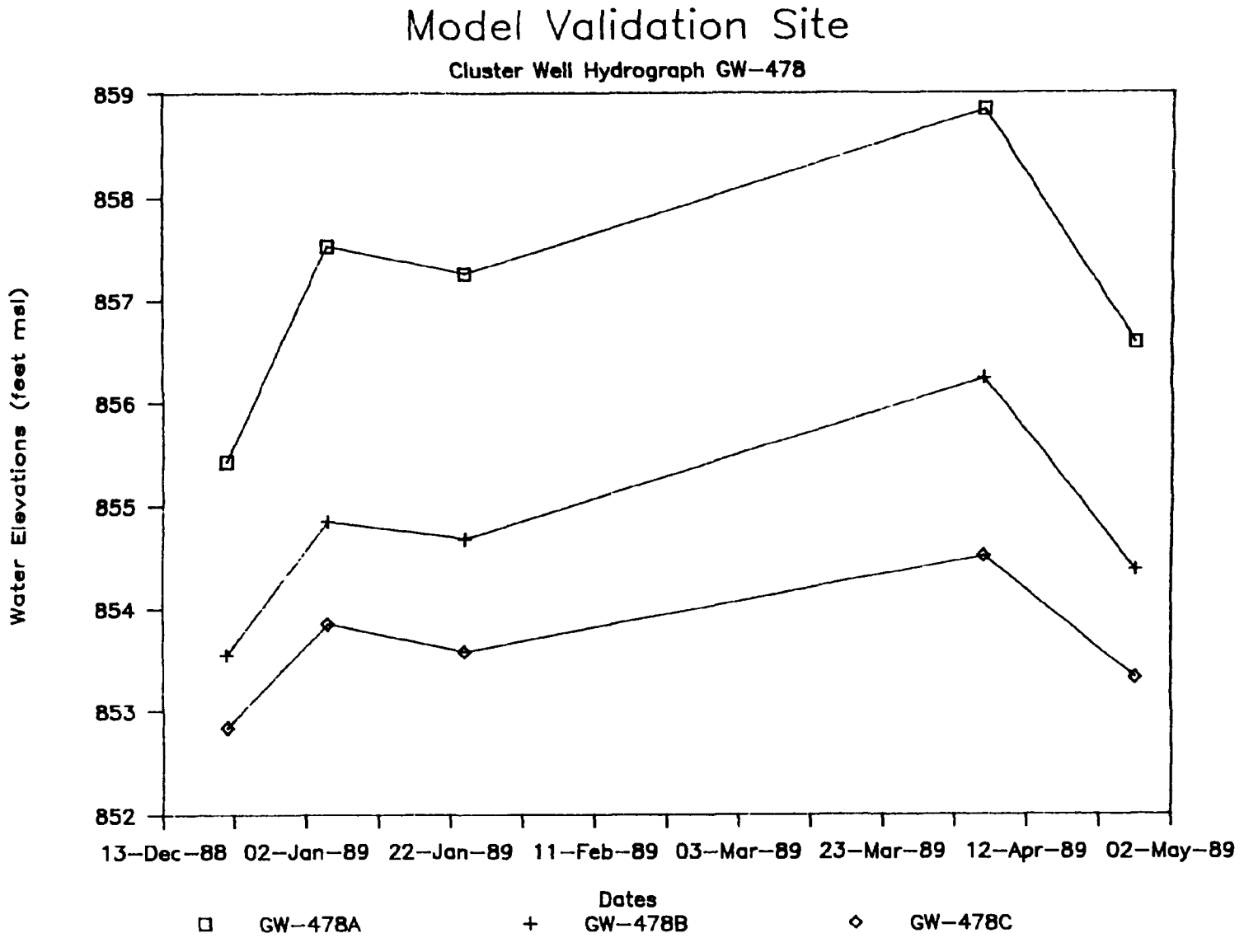

ORNL-DWG 89-16027

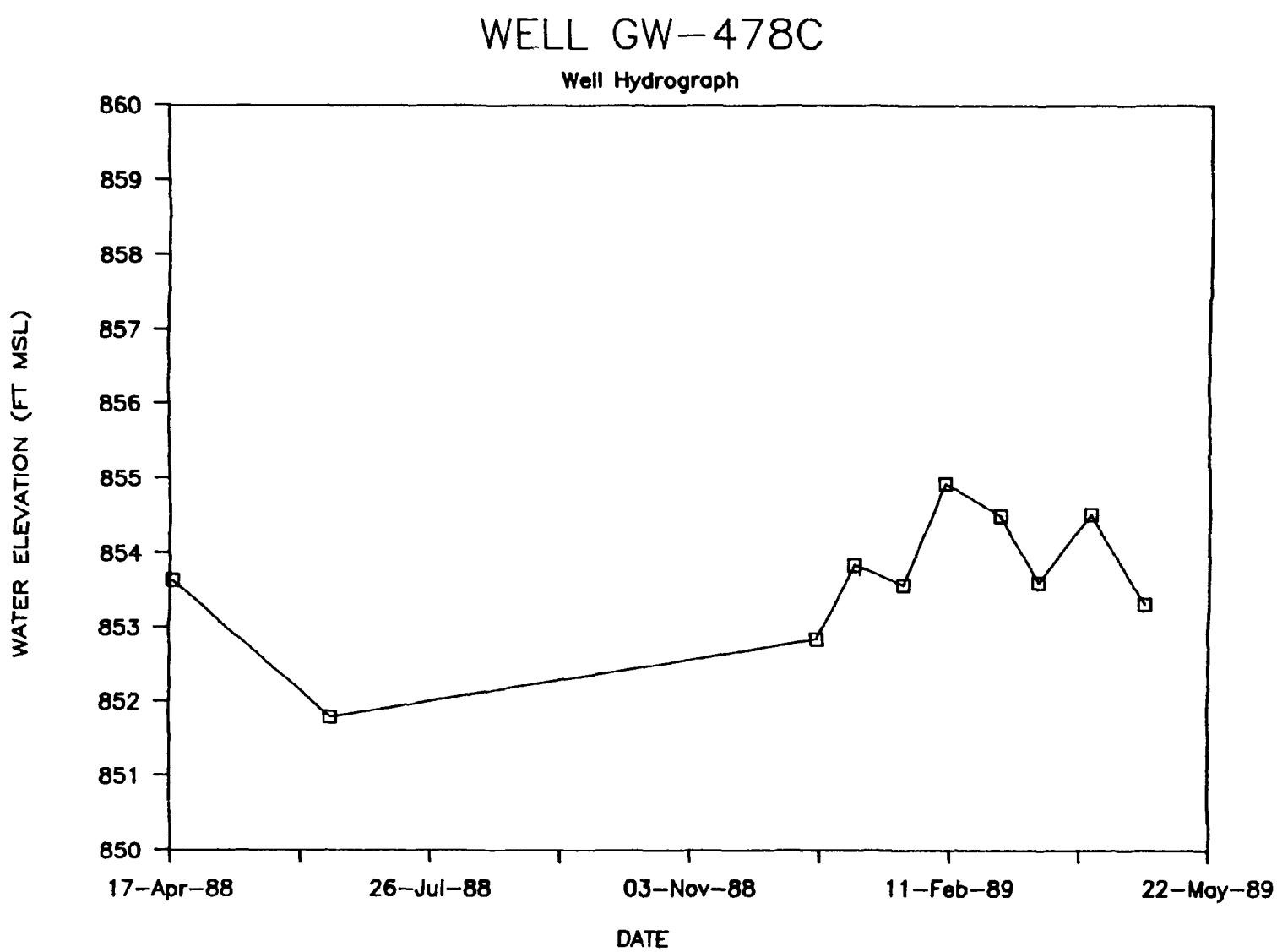

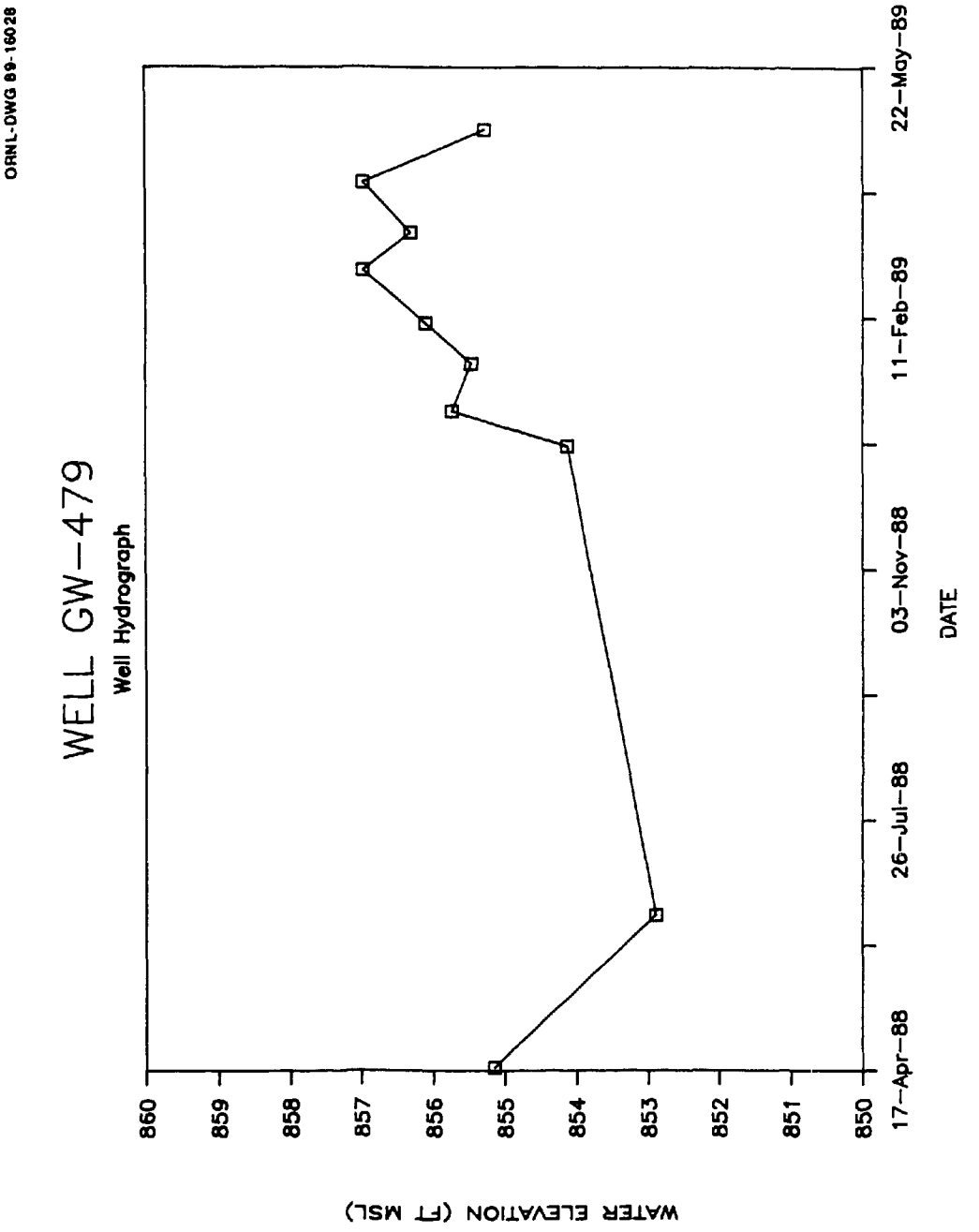
ORNL-DWG 89-16028
WELL GW-479
Well Hydrograph
WATER ELEVATION (FT MSL)
860
859
858
857
856
855
854
853
852
851
850
17-Apr-88
26-Jul-88
03-Nov-88
11-Feb-89
22-May-89
DATE

ORNL-DWG 89-16029

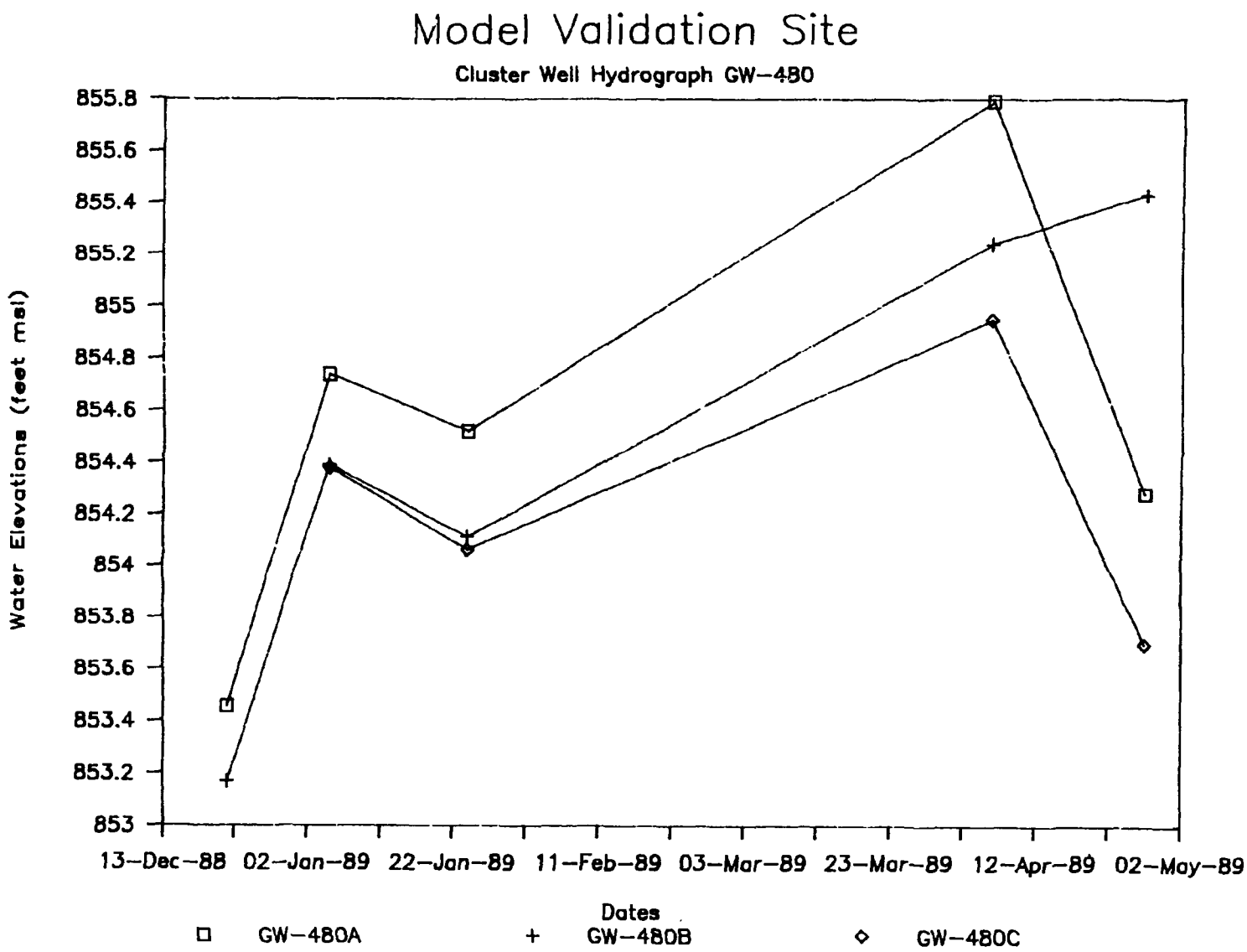

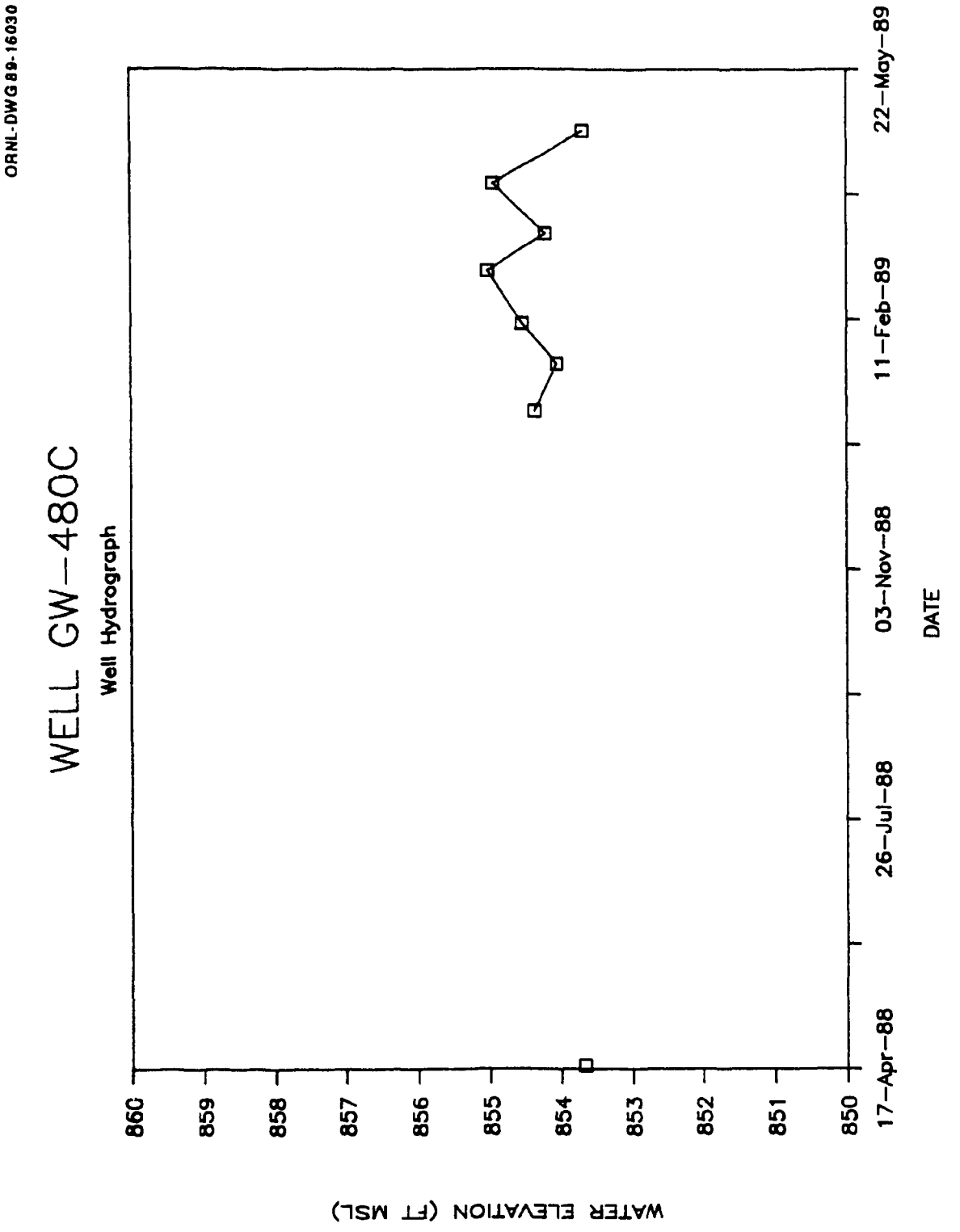
ORNL-DWG 89-16030
WELL GW-480C
Well Hydrograph
WATER ELEVATION (FT MSL)
860
859
858
857
856
855
854
853
852
851
850
17-Apr-88
26-Jul-88
03-Nov-88
11-Feb-89
22-May-89
DATE

ORNL-DWG 89-16031

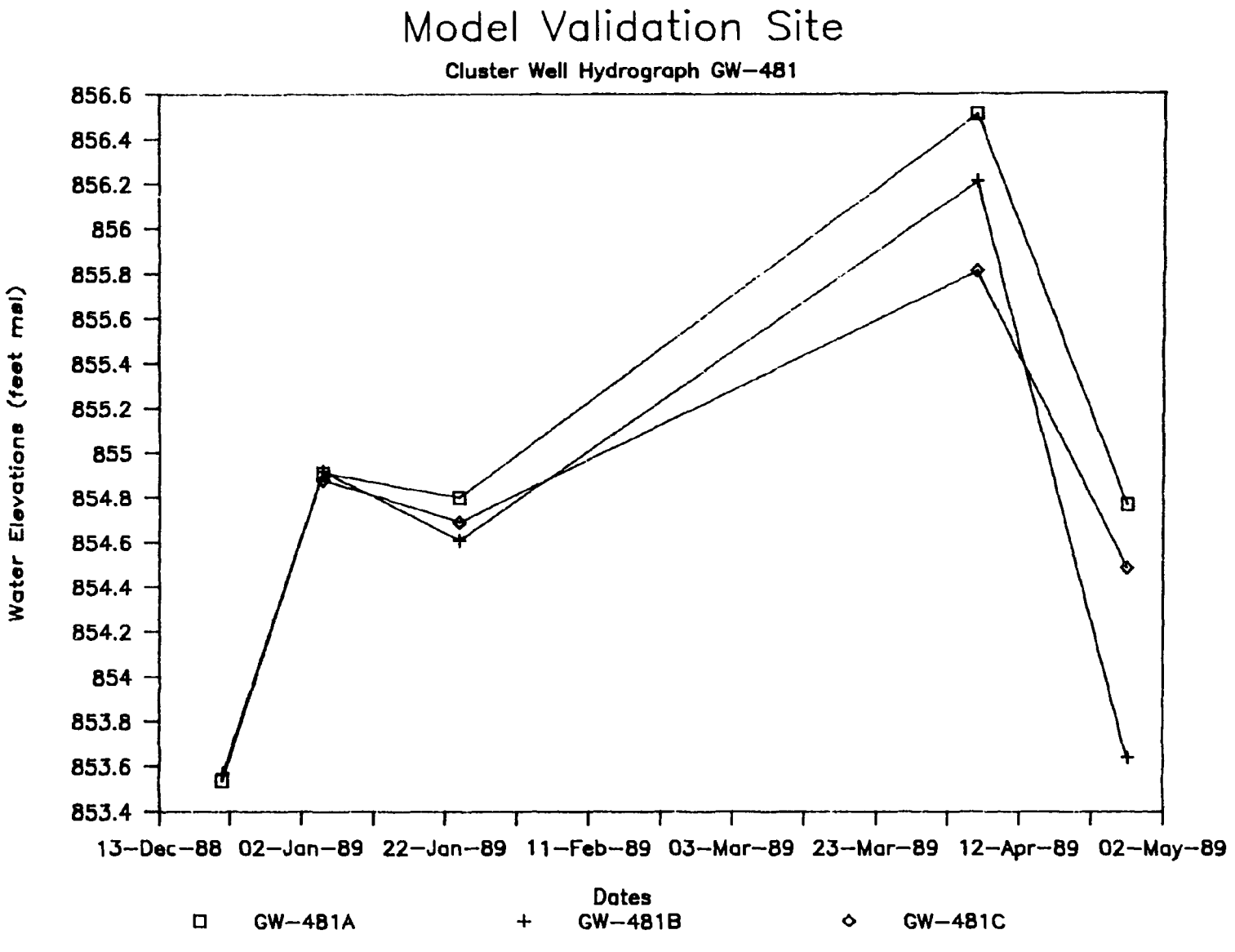

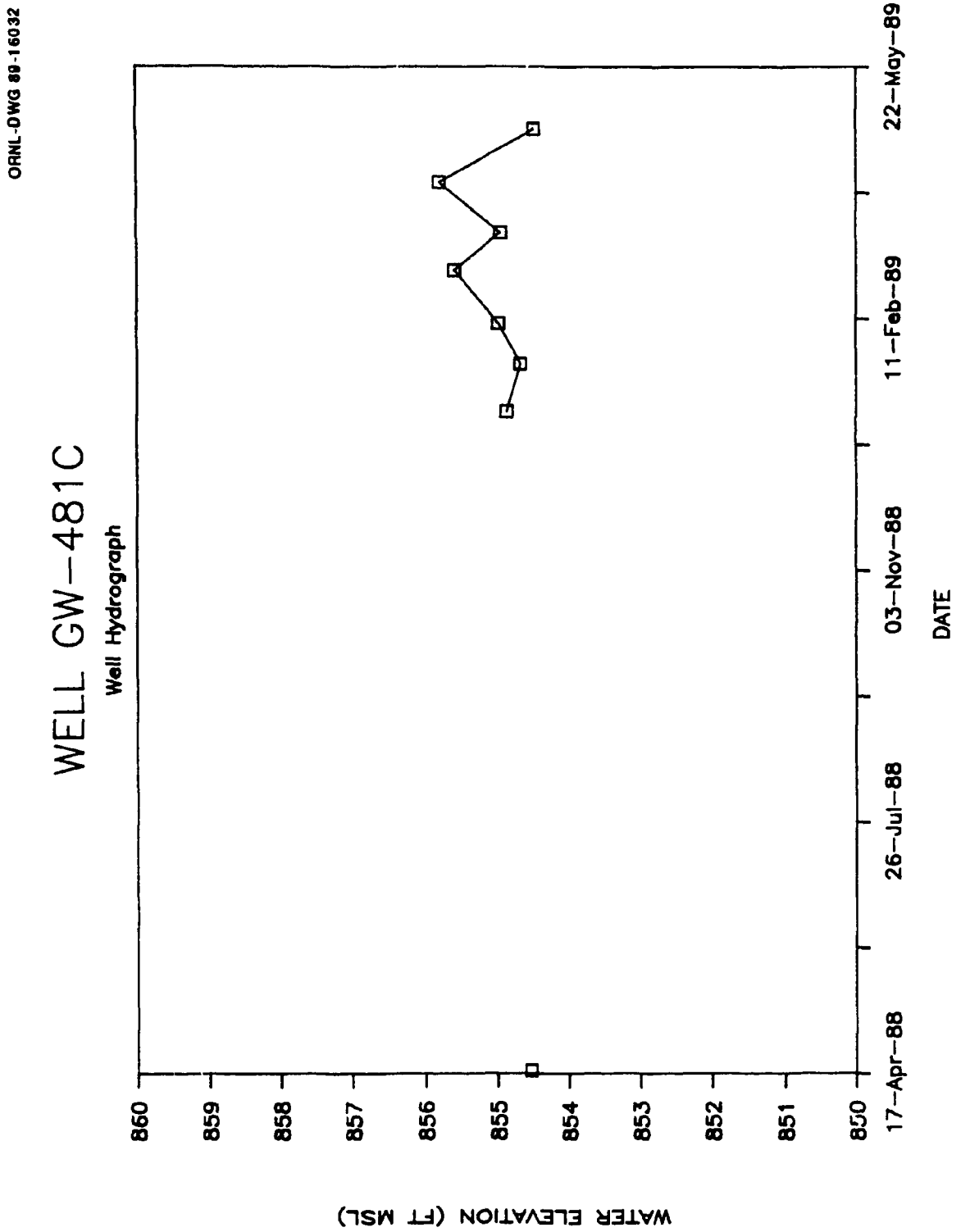
ORNL-DWG 89-16032
WELL GW-481C
Well Hydrograph
WATER ELEVATION (FT MSL)
860
859
858
857
856
855
854
853
852
851
850
17-Apr-88
26-Jul-88
03-Nov-88
11-Feb-89
22-May-89
DATE

ORNL-DWG 89-16033

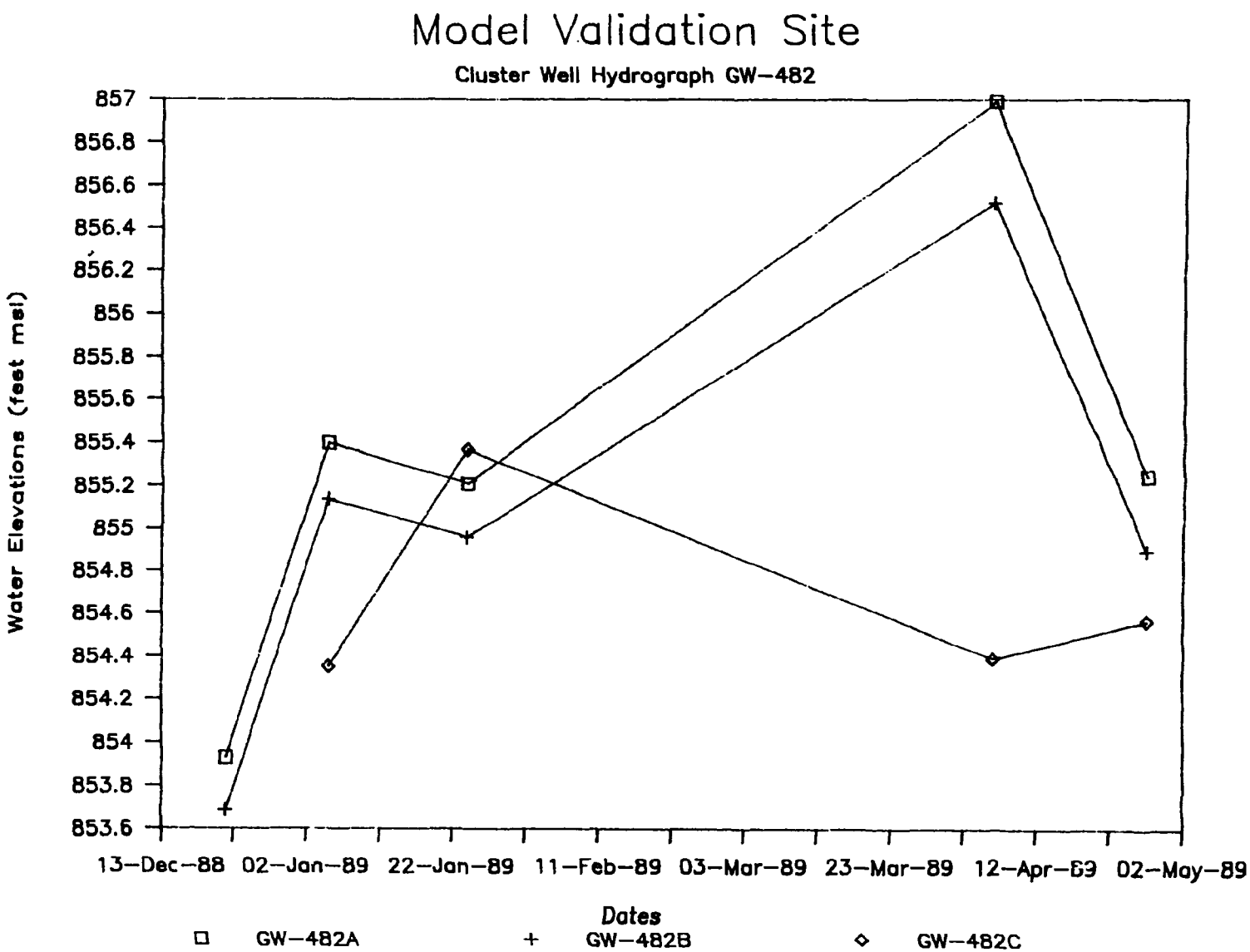

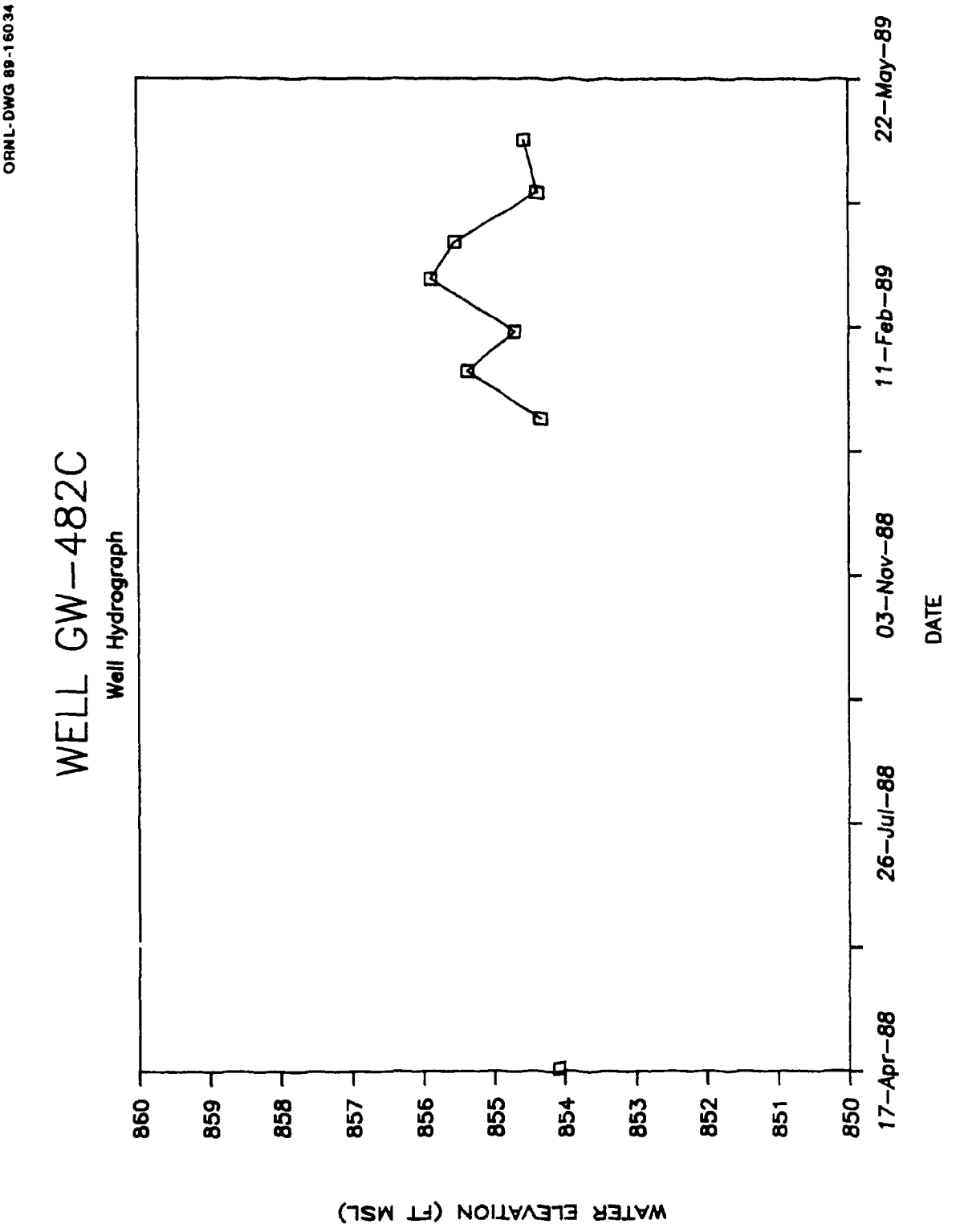
ORNL-DWG 89-16034
WELL GW-482C
Well Hydrograph
WATER ELEVATION (FT MSL)
860
859
858
857
856
855
854
853
852
851
850
17-Apr-88
26-Jul-88
03-Nov-88
11-Feb-89
22-May-89
DATE

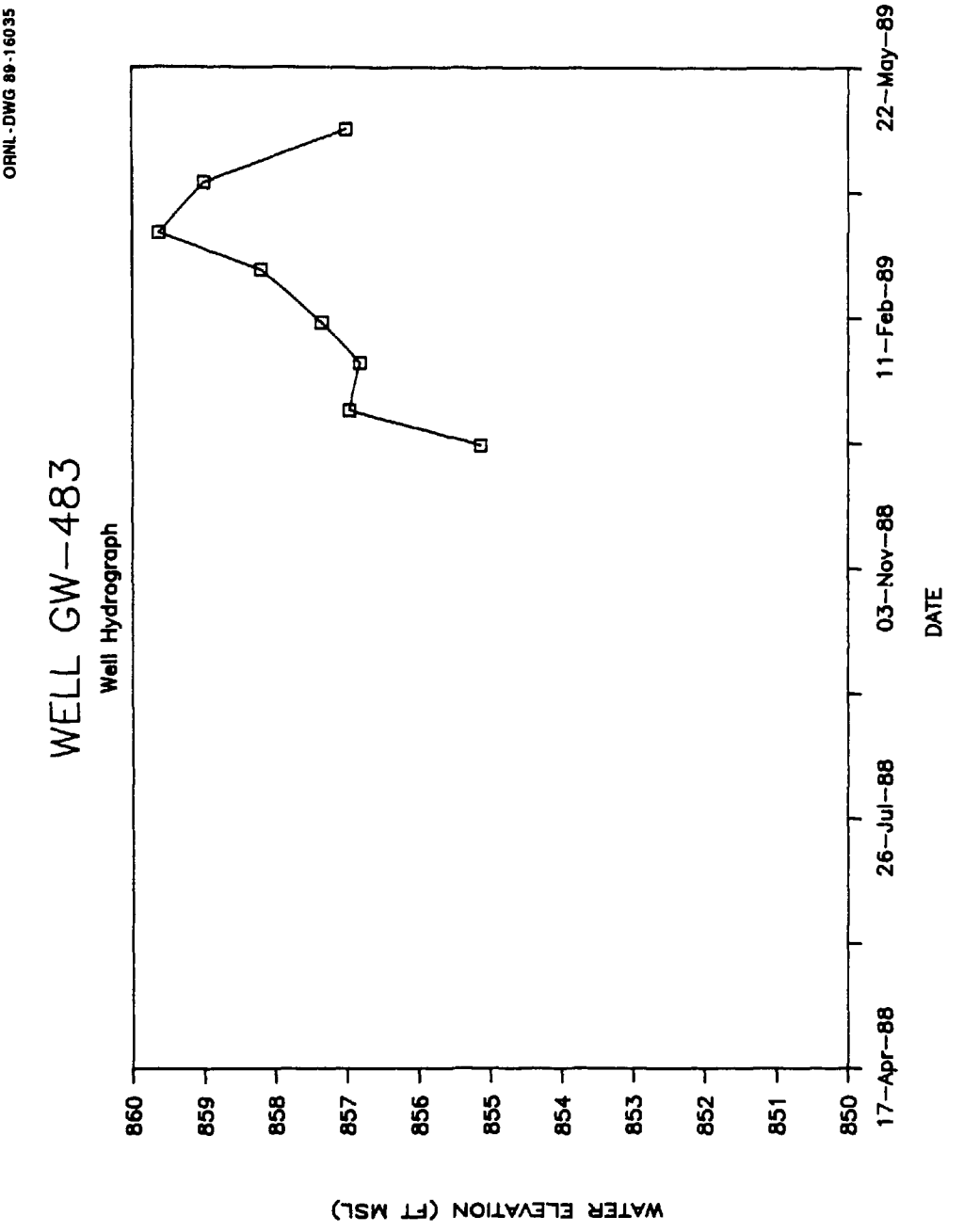
ORNL-DWG 89-16035
WELL GW-483
Well Hydrograph
WATER ELEVATION (FT MSL)
860
859
858
857
856
855
854
853
852
851
850
17-Apr-88
26-Jul-88
03-Nov-88
11-Feb-89
22-May-89
DATE

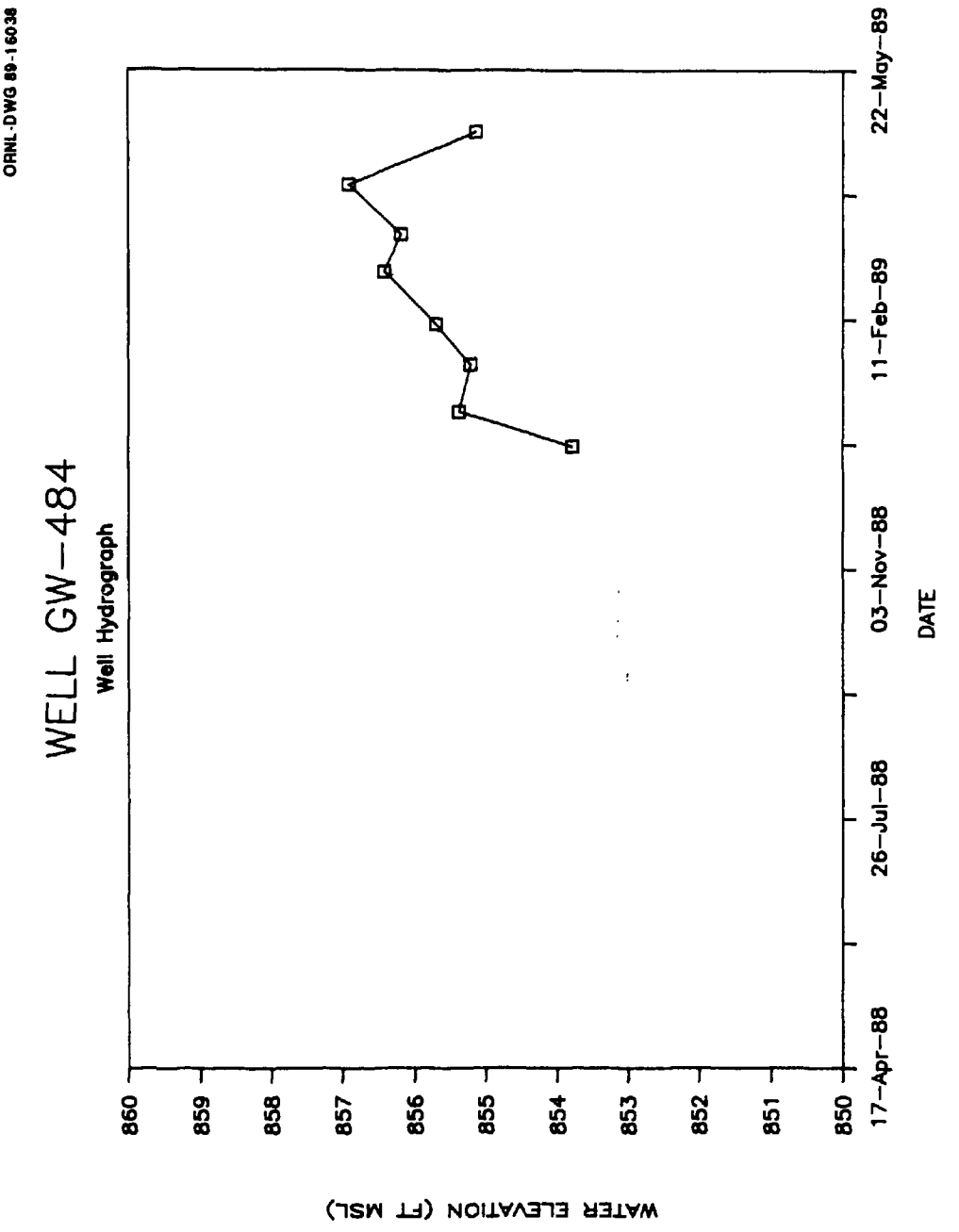
ORNL-DWG 89-16038
WELL GW-484
Well Hydrograph
WATER ELEVATION (FT MSL)
860
859
858
857
856
855
854
853
852
851
850
17-Apr-88
26-Jul-88
03-Nov-88
11-Feb-89
22-May-89
DATE

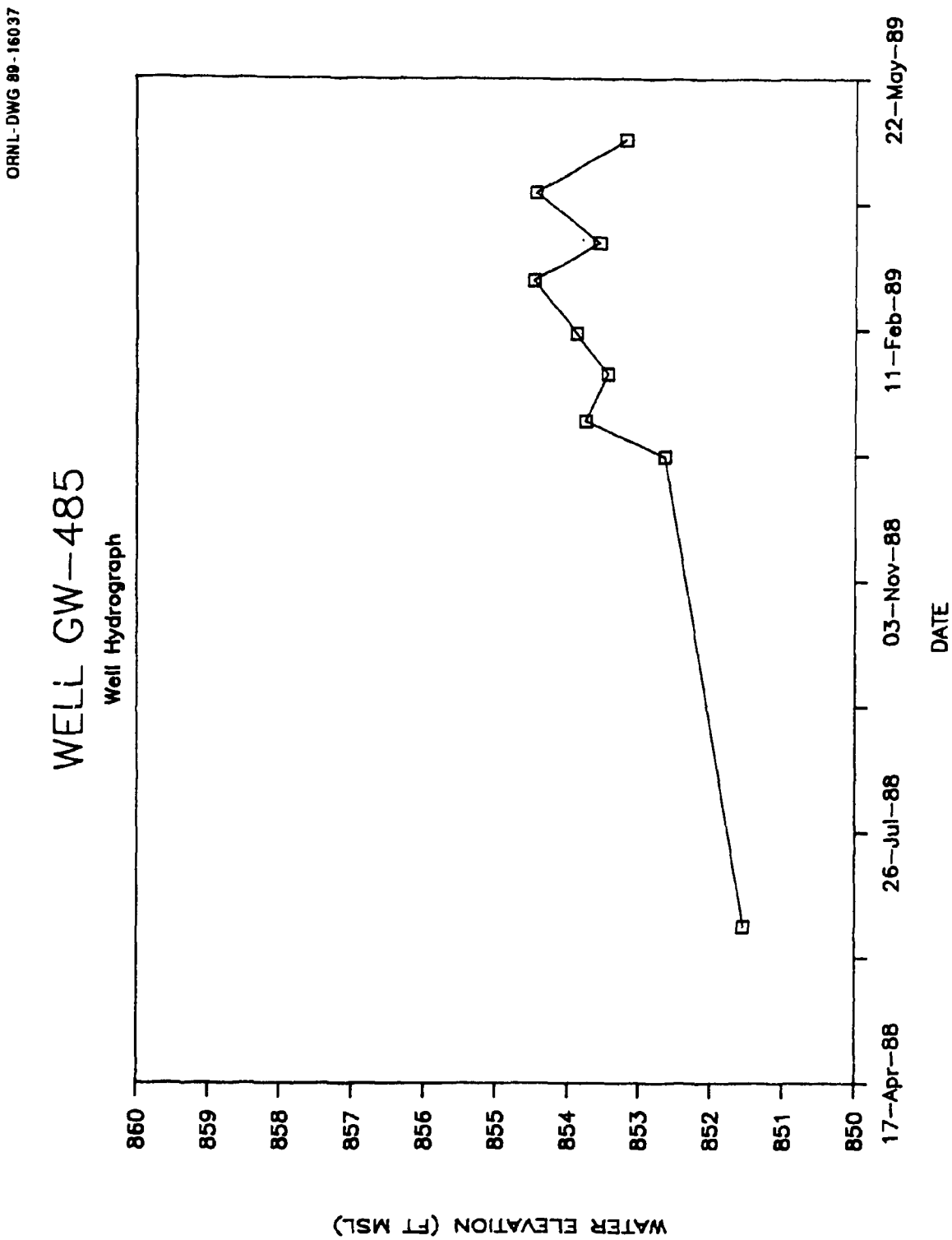
ORNL-DWG 89-16037
WELL GW-485
Well Hydrograph
WATER ELEVATION (FT MSL)
860
859
858
857
856
855
854
853
852
851
850
17-Apr-88
26-Jul-88
03-Nov-88
11-Feb-89
22-May-89
DATE

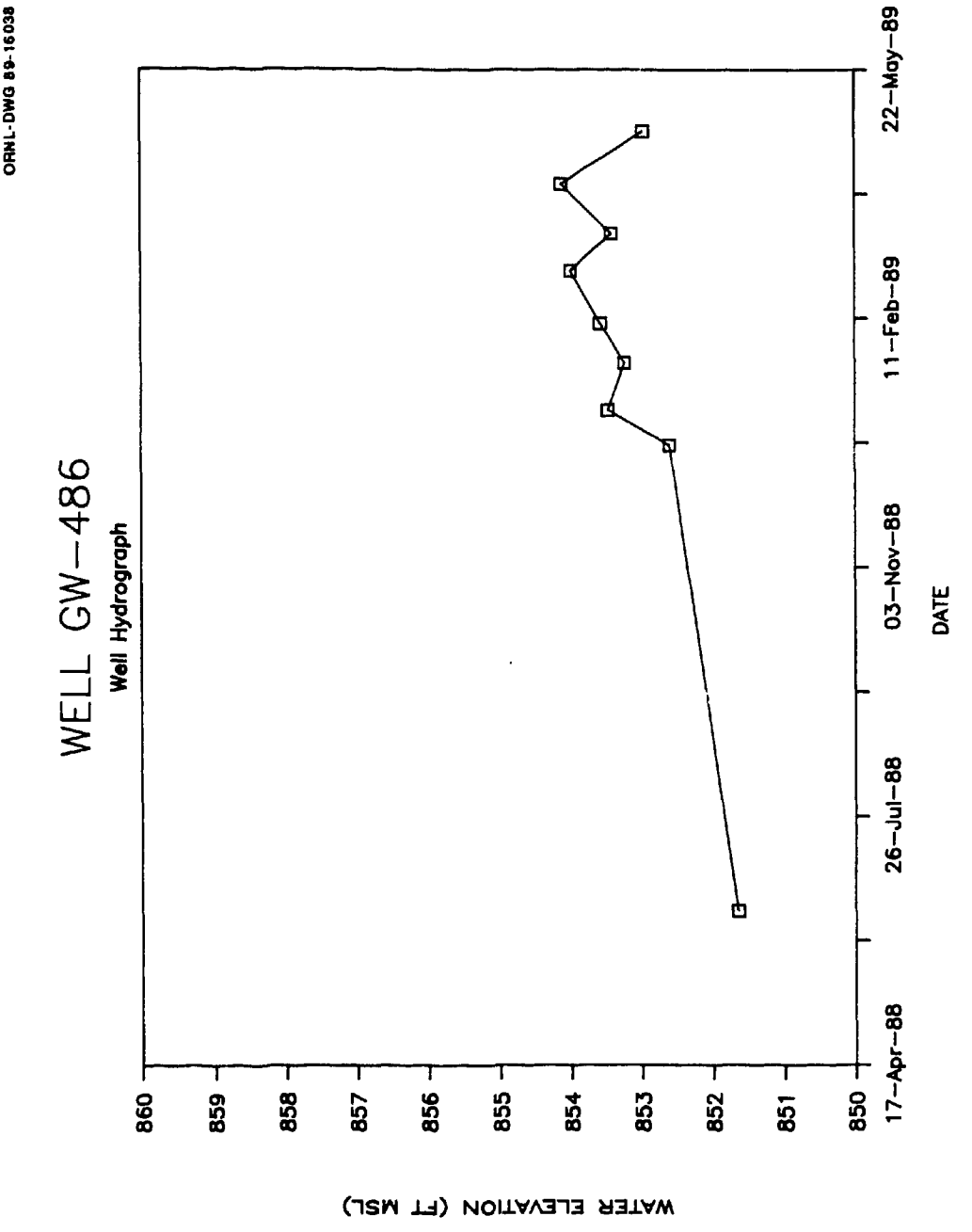
ORNL-DWG 89-16038
WELL GW-486
Well Hydrograph
WATER ELEVATION (FT MSL)
860
859
858
857
856
855
854
853
852
851
850
17-Apr-88
26-Jul-88
03-Nov-88
11-Feb-89
22-May-89
DATE

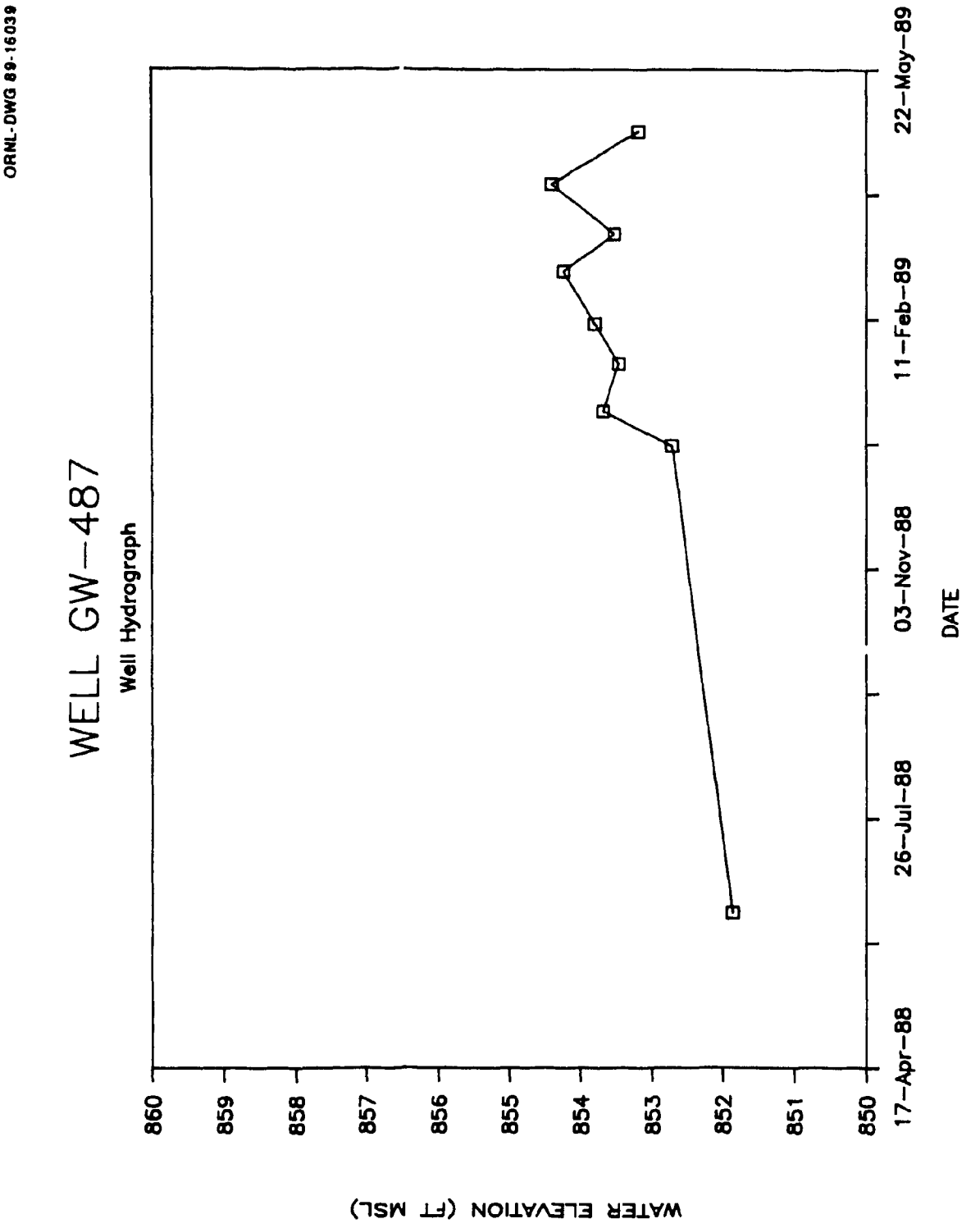
ORNL-DWG 89-16039
WELL GW-487
Well Hydrograph
WATER ELEVATION (FT MSL)
860
859
858
857
856
855
854
853
852
851
850
17-Apr-88
26-Jul-88
03-Nov-88
11-Feb-89
22-May-89
DATE

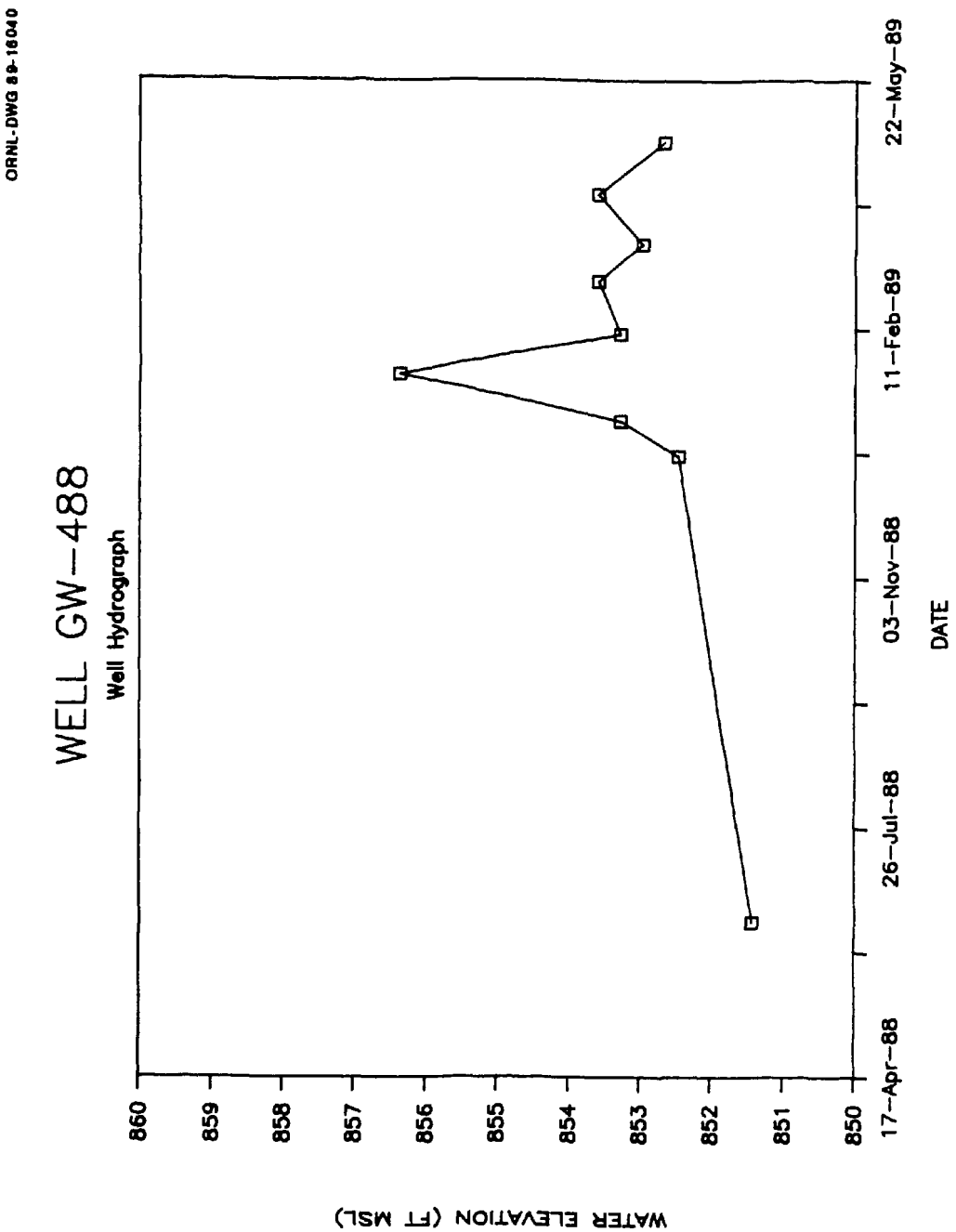
ORNL-DWG 89-16040
WELL GW-488
Well Hydrograph
WATER ELEVATION (FT MSL)
860
859
858
857
856
855
854
853
852
851
850
17-Apr-88
26-Jul-88
03-Nov-88
11-Feb-89
22-May-89
DATE

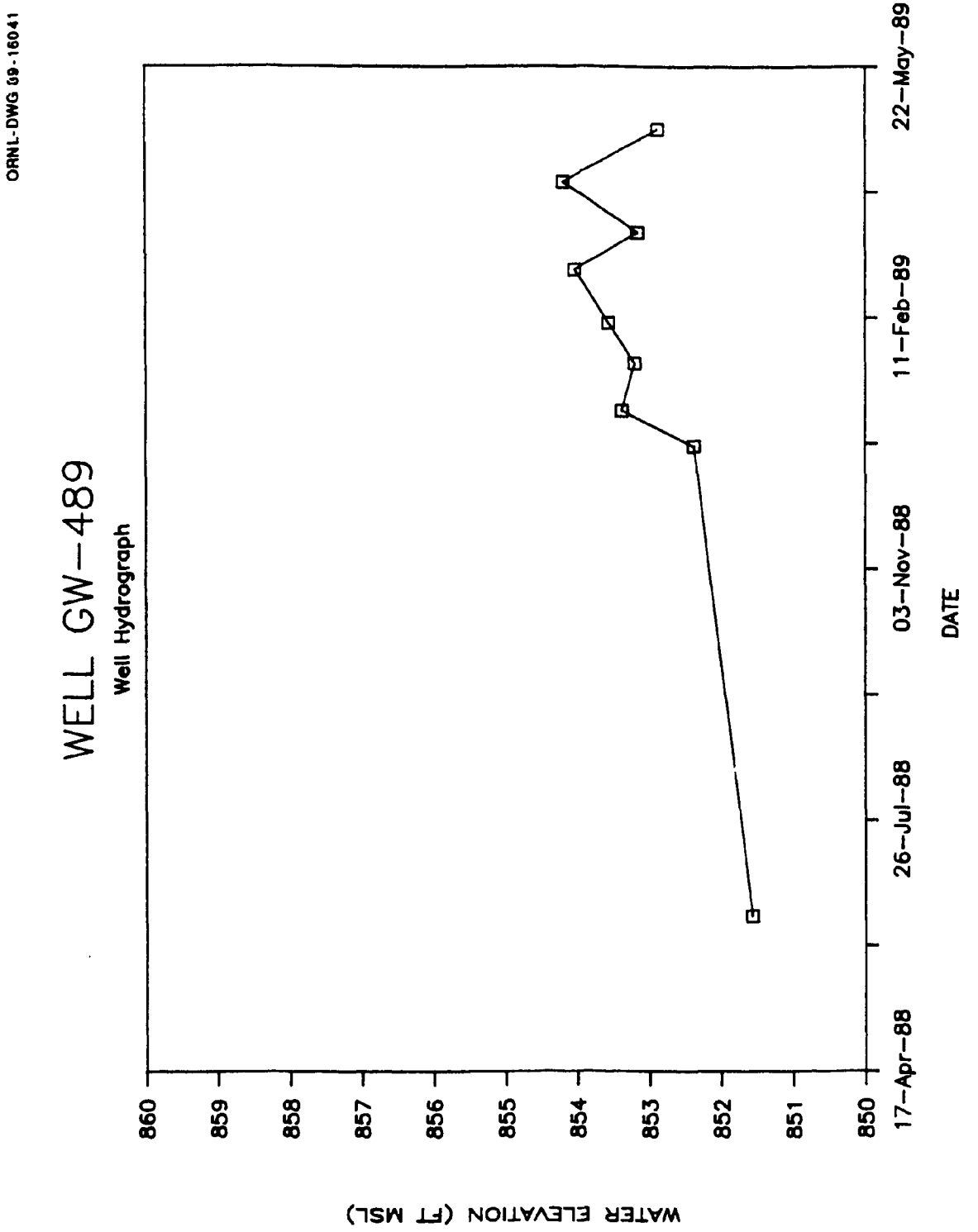
ORNL-DWG 89-16041
WELL GW-489
Well Hydrograph
WATER ELEVATION (FT MSL)
860
859
858
857
856
855
854
853
852
851
850
17-Apr-88
26-Jul-88
03-Nov-88
11-Feb-89
22-May-89
DATE

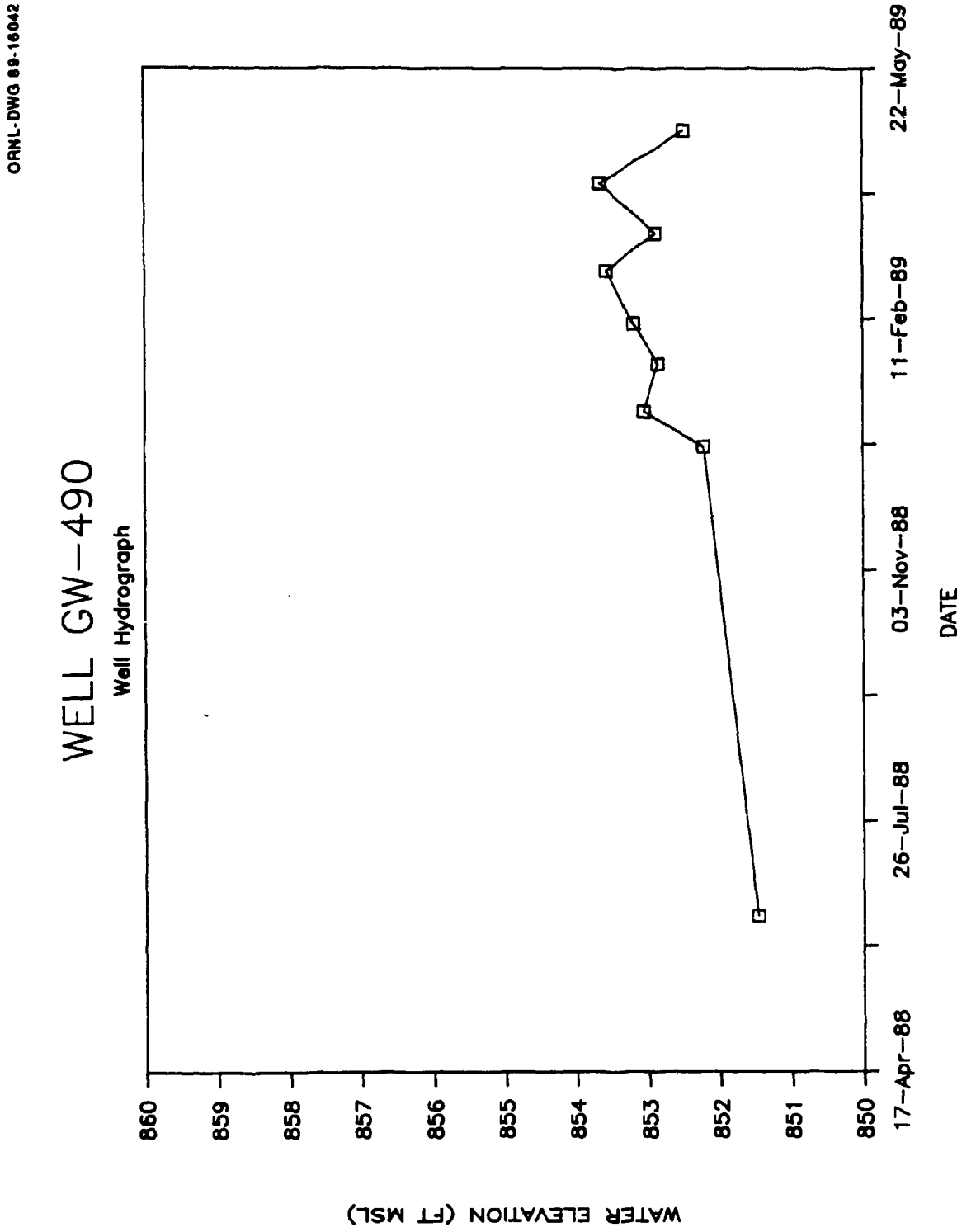
ORNL-DWG 89-16042
WELL GW-490
Well Hydrograph
WATER ELEVATION (FT MSL)
860
859
858
857
856
855
854
853
852
851
850
17-Apr-88
26-Jul-88
03-Nov-88
11-Feb-89
22-May-89
DATE

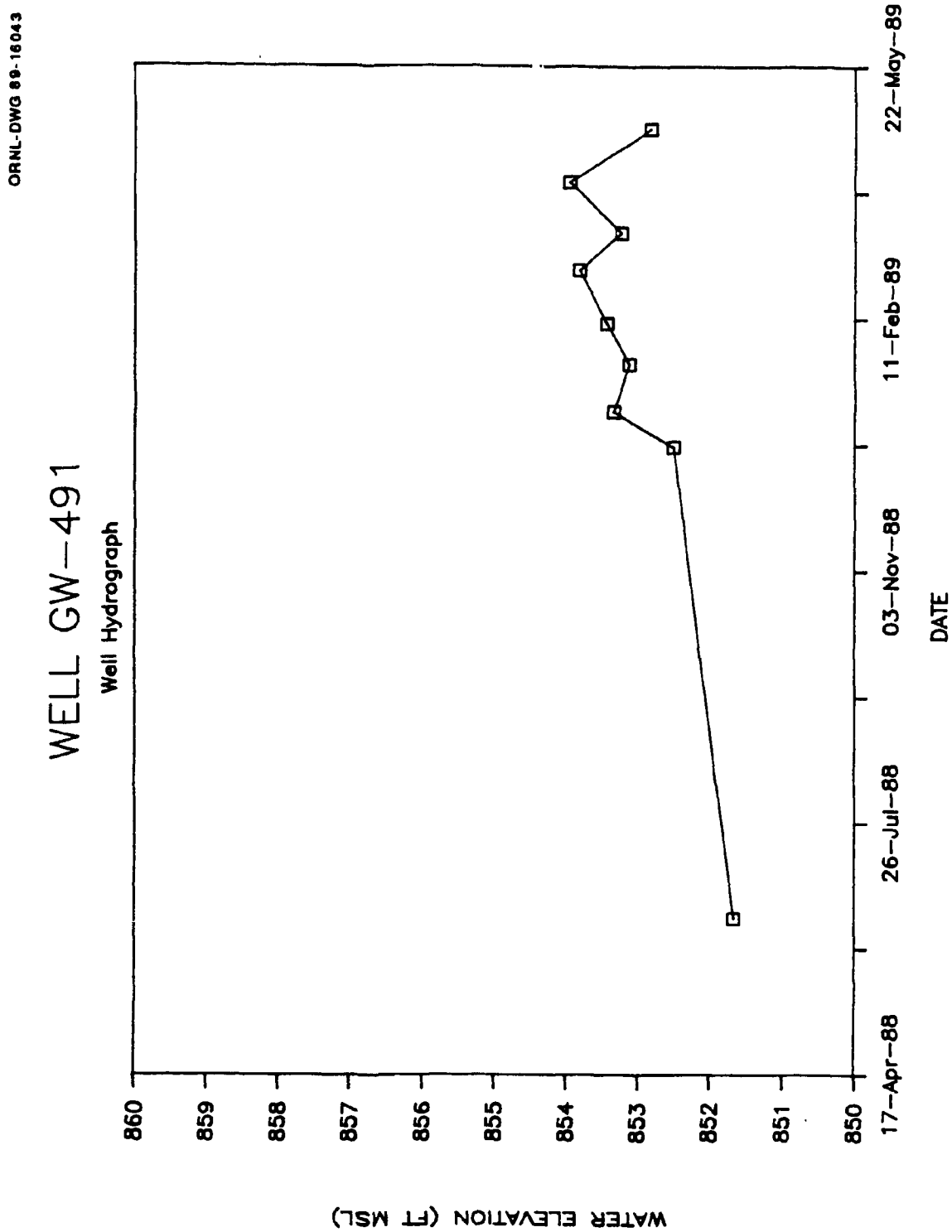
ORNL-DWG 89-16043
WELL GW-491
Well Hydrograph
WATER ELEVATION (FT MSL)
860
859
858
857
856
855
854
853
852
851
850
17-Apr-88
26-Jul-88
03-Nov-88
11-Feb-89
22-May-89
DATE

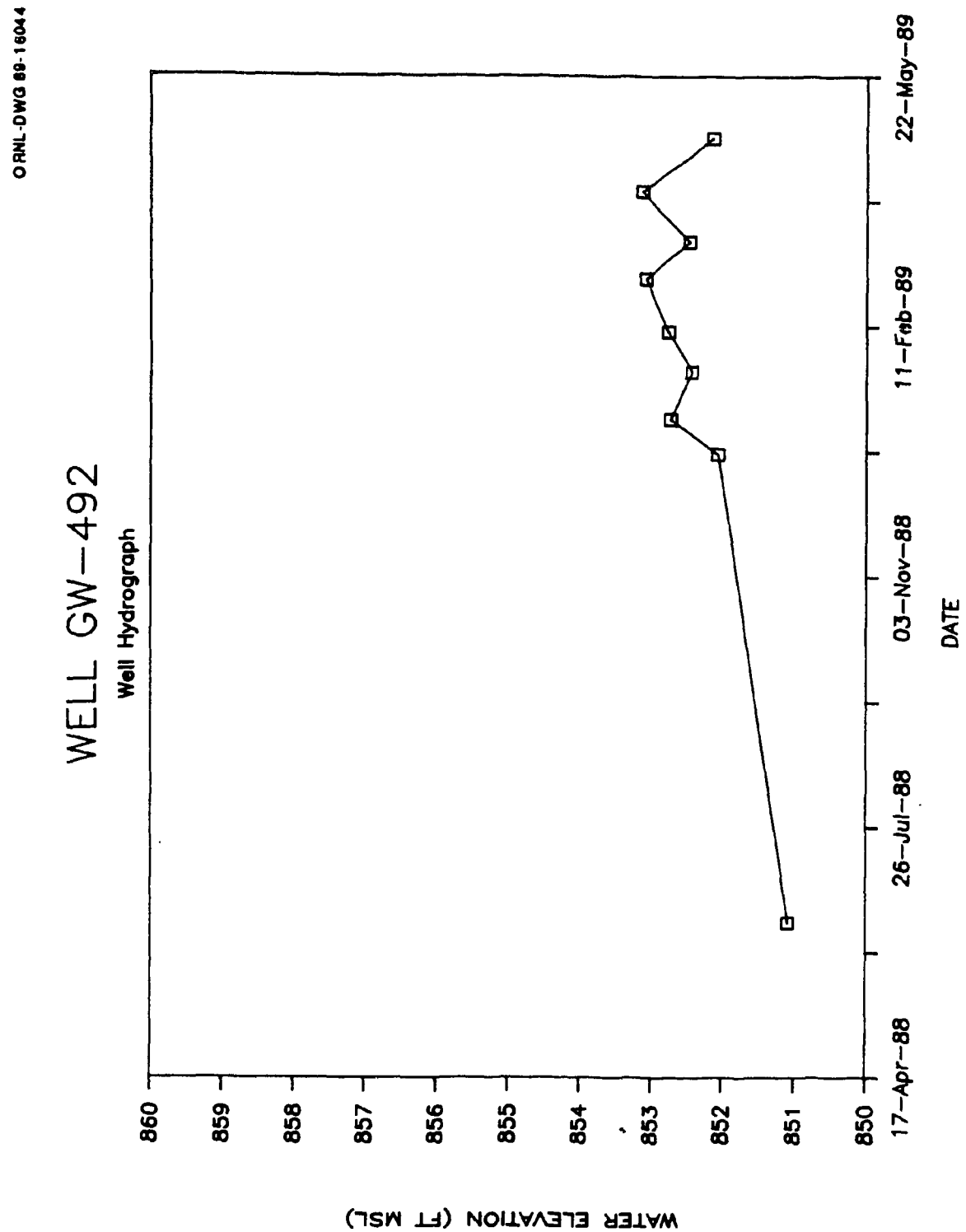
ORNL-DWG 89-16044
WELL GW-492
Well Hydrograph
WATER ELEVATION (FT MSL)
860
859
858
857
856
855
854
853
852
851
850
17-Apr-88
26-Jul-88
03-Nov-88
11-Feb-89
22-May-89
DATE

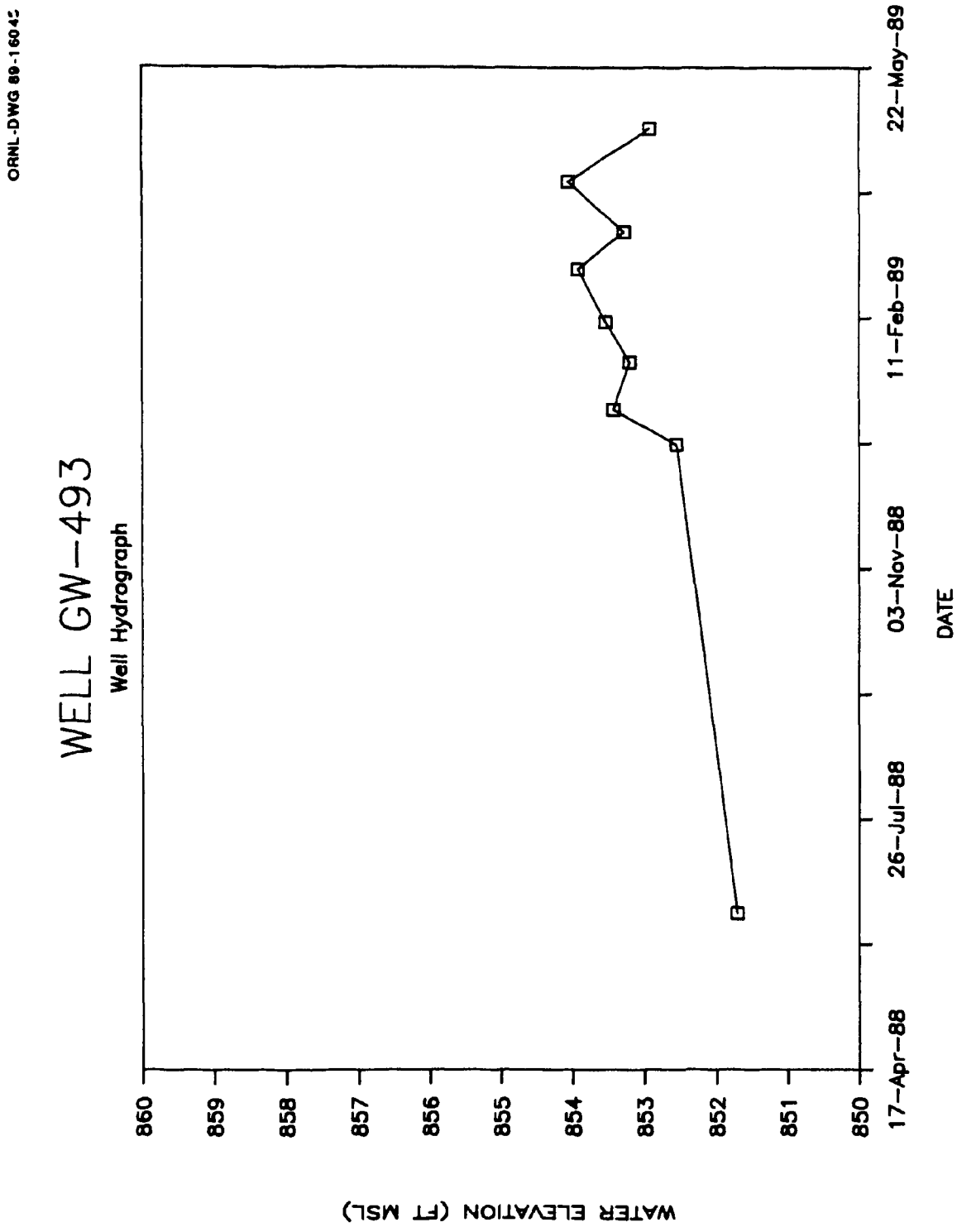
ORNL-DWG 89-16045
WELL GW-493
Well Hydrograph
WATER ELEVATION (FT MSL)
860
859
858
857
856
855
854
853
852
851
850
17-Apr-88
26-Jul-88
03-Nov-88
11-Feb-89
22-May-89
DATE

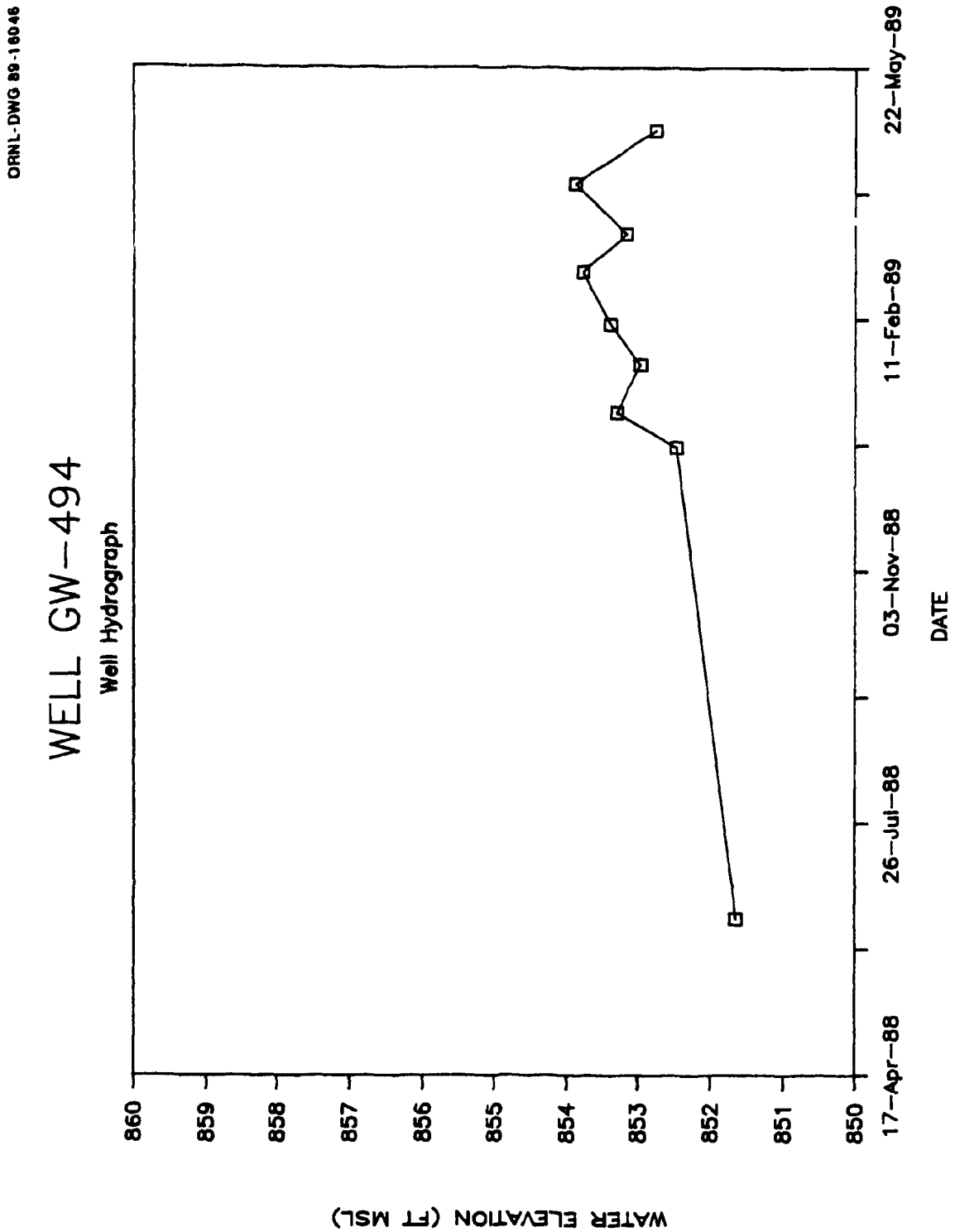
ORNL-DWG 89-16046
WELL GW-494
Well Hydrograph
WATER ELEVATION (FT MSL)
860
859
858
857
856
855
854
853
852
851
850
17-Apr-88
26-Jul-88
03-Nov-88
11-Feb-89
22-May-89
DATE

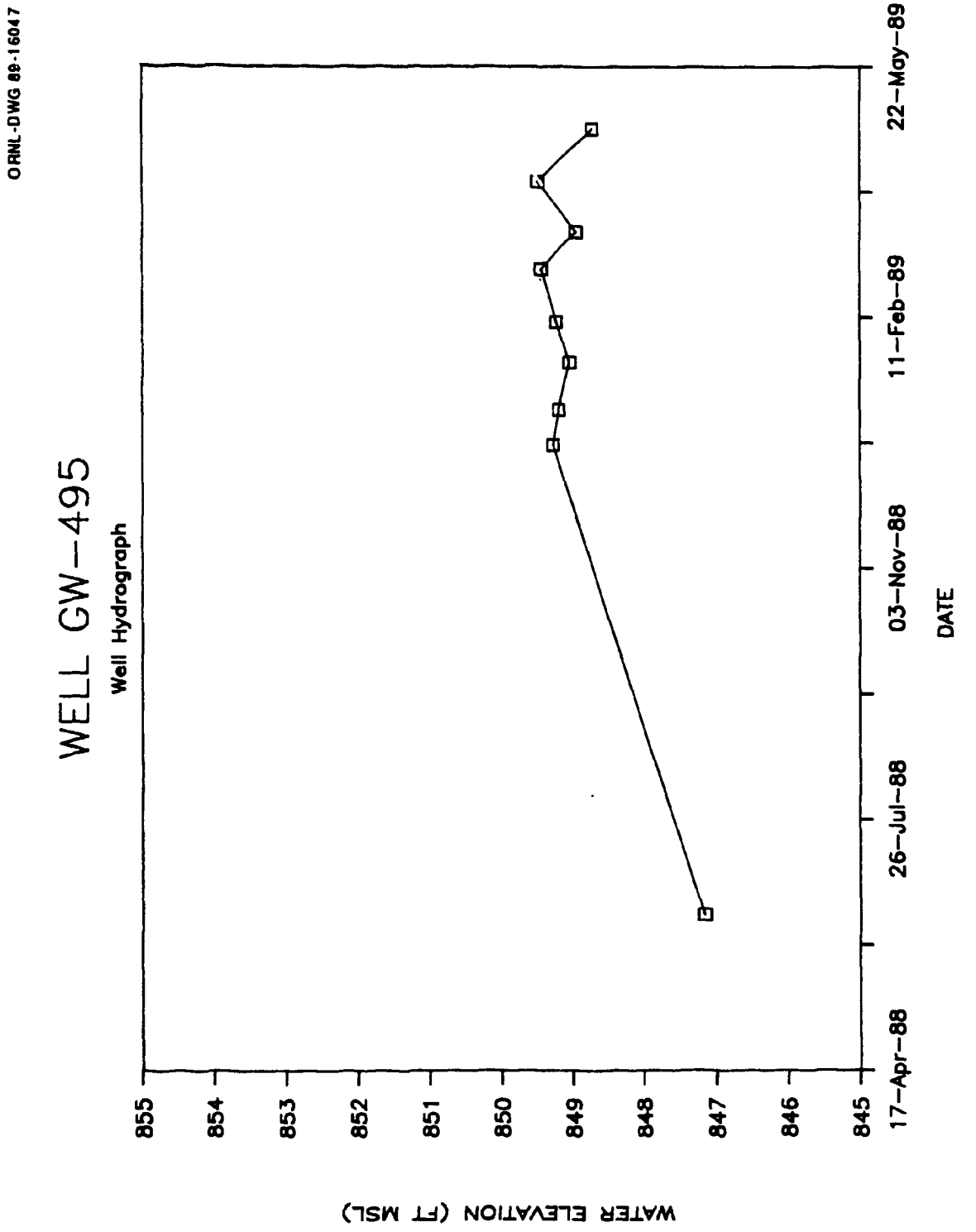
ORNL-DWG 89-16047
WELL GW-495
Well Hydrograph
WATER ELEVATION (FT MSL)
855
854
853
852
851
850
849
848
847
846
845
17-Apr-88
26-Jul-88
03-Nov-88
11-Feb-89
22-May-89
DATE

ORNL-DWG 89-16048

WELL GW-496

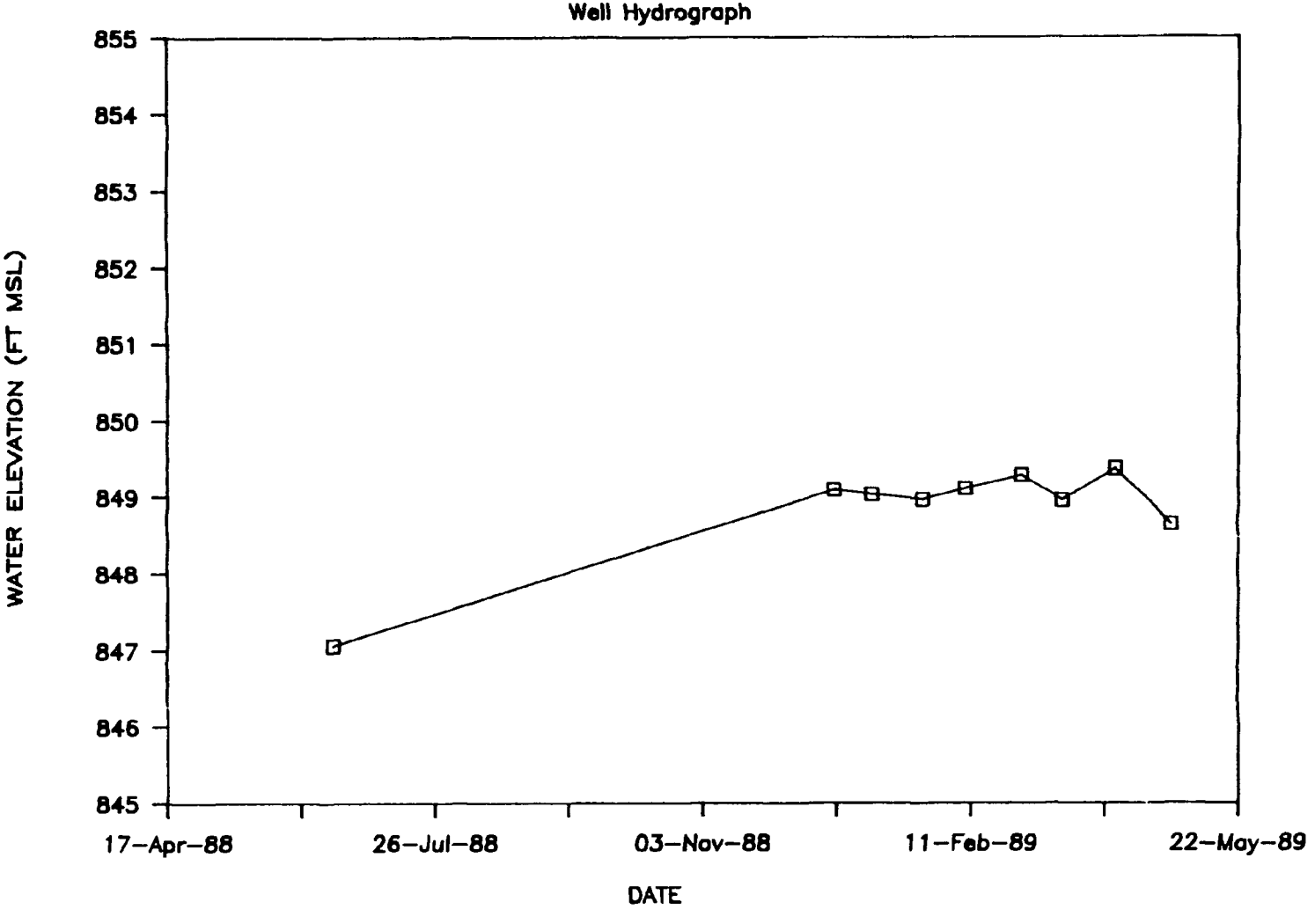

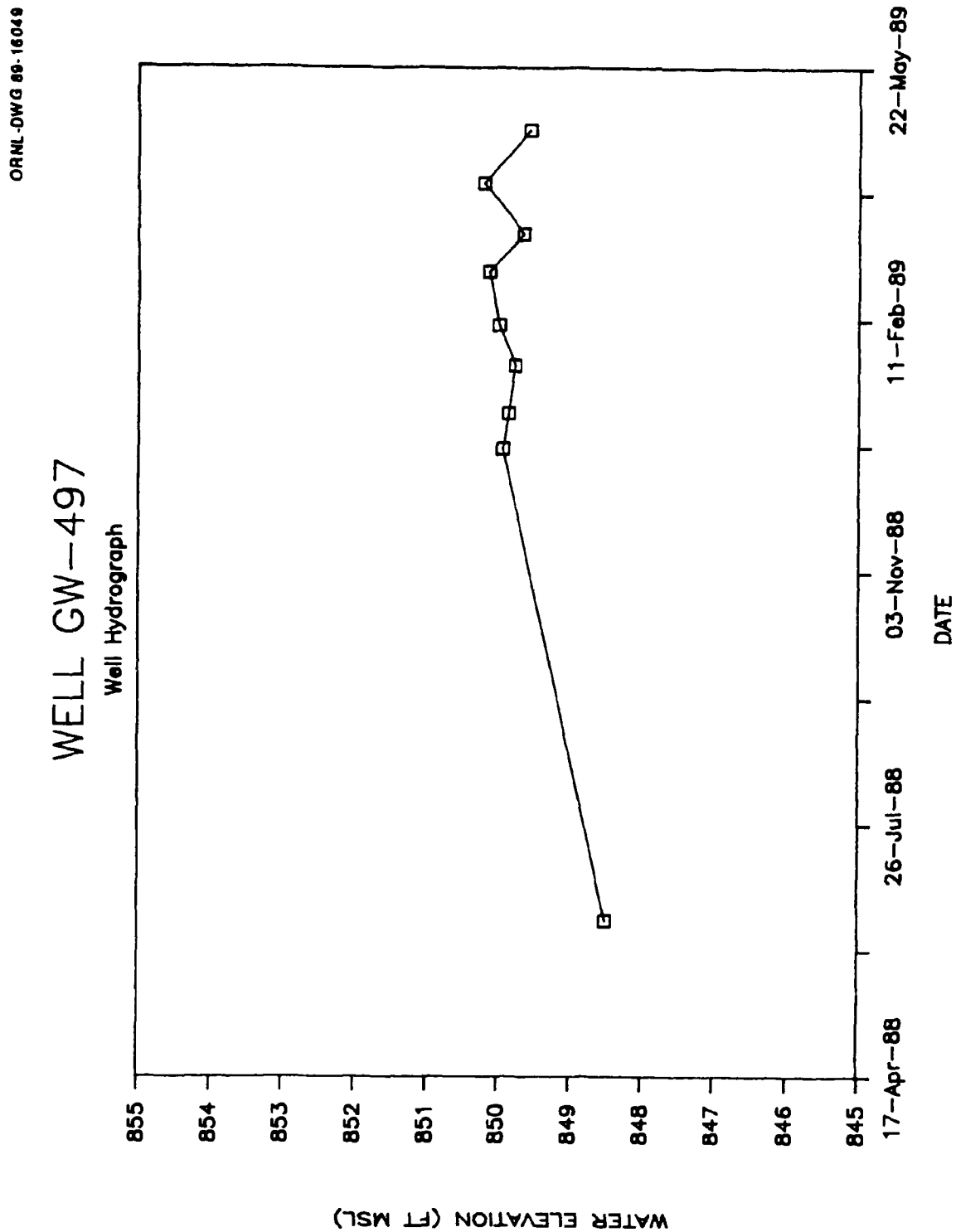
ORNL-DWG 89-16049
WELL GW-497
Well Hydrograph
WATER ELEVATION (FT MSL)
855
854
853
852
851
850
849
848
847
846
845
17-Apr-88
26-Jul-88
03-Nov-88
11-Feb-89
22-May-89
DATE

ORNL-DWG 89-16050

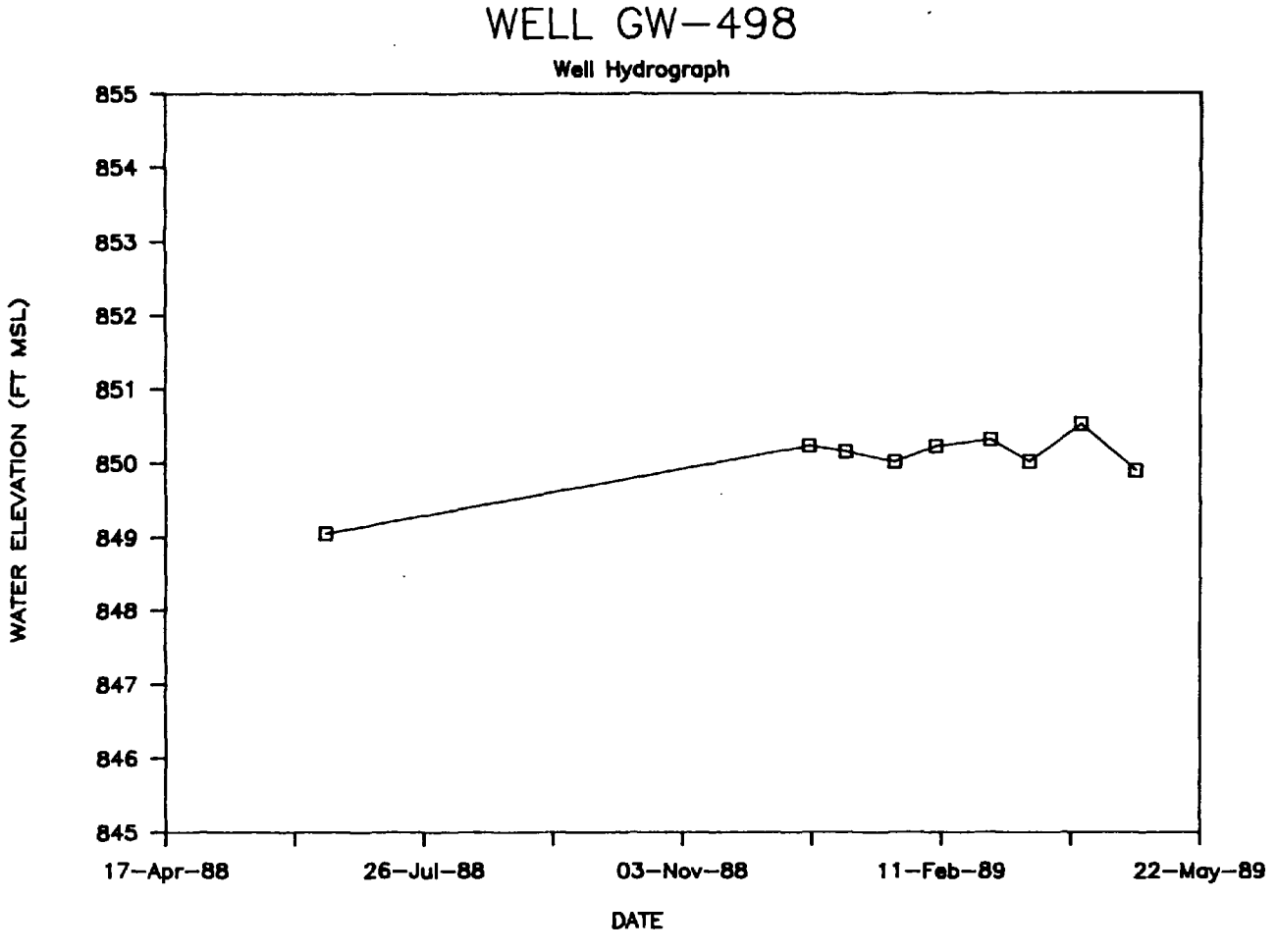

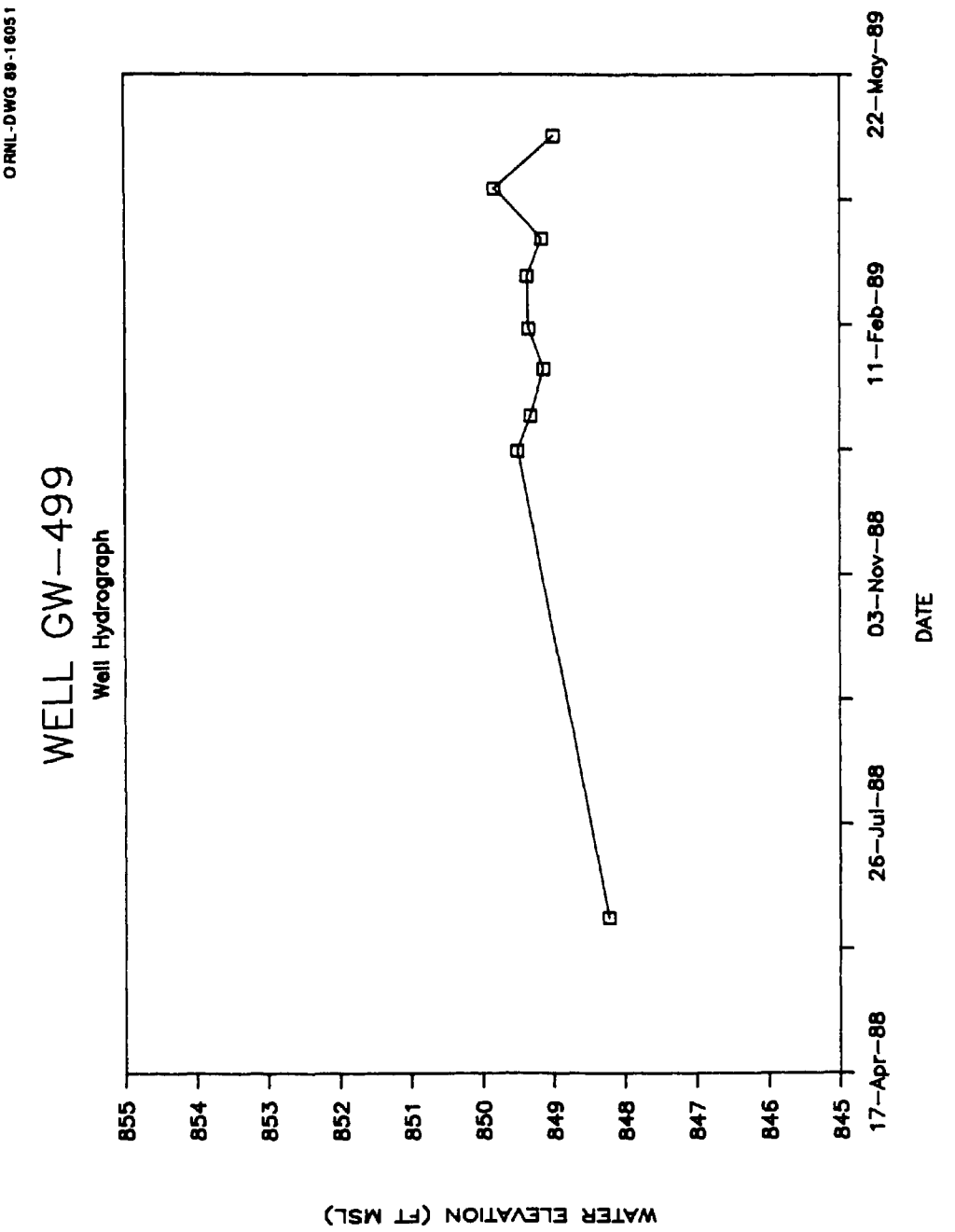
ORNL-DWG 89-16051
WELL GW-499
Well Hydrograph
WATER ELEVATION (FT MSL)
855
854
853
852
851
850
849
848
847
846
845
17-Apr-88
26-Jul-88
03-Nov-88
11-Feb-89
22-May-89
DATE

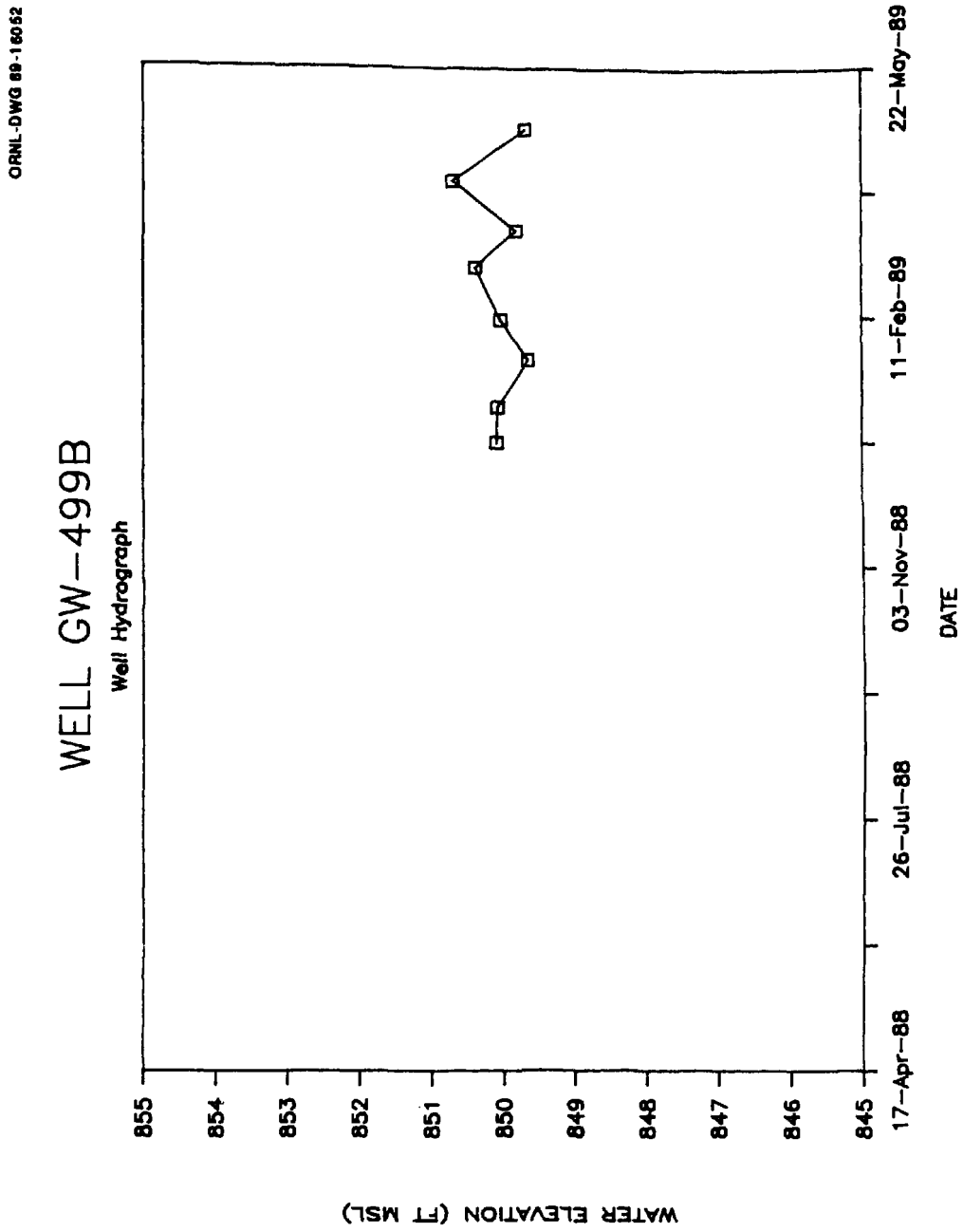
ORNL-DWG 89-16052
WELL GW-499B
Well Hydrograph
WATER ELEVATION (FT MSL)
855
854
853
852
851
850
849
848
847
846
845
17-Apr-88
26-Jul-88
03-Nov-88
11-Feb-89
22-May-89
DATE

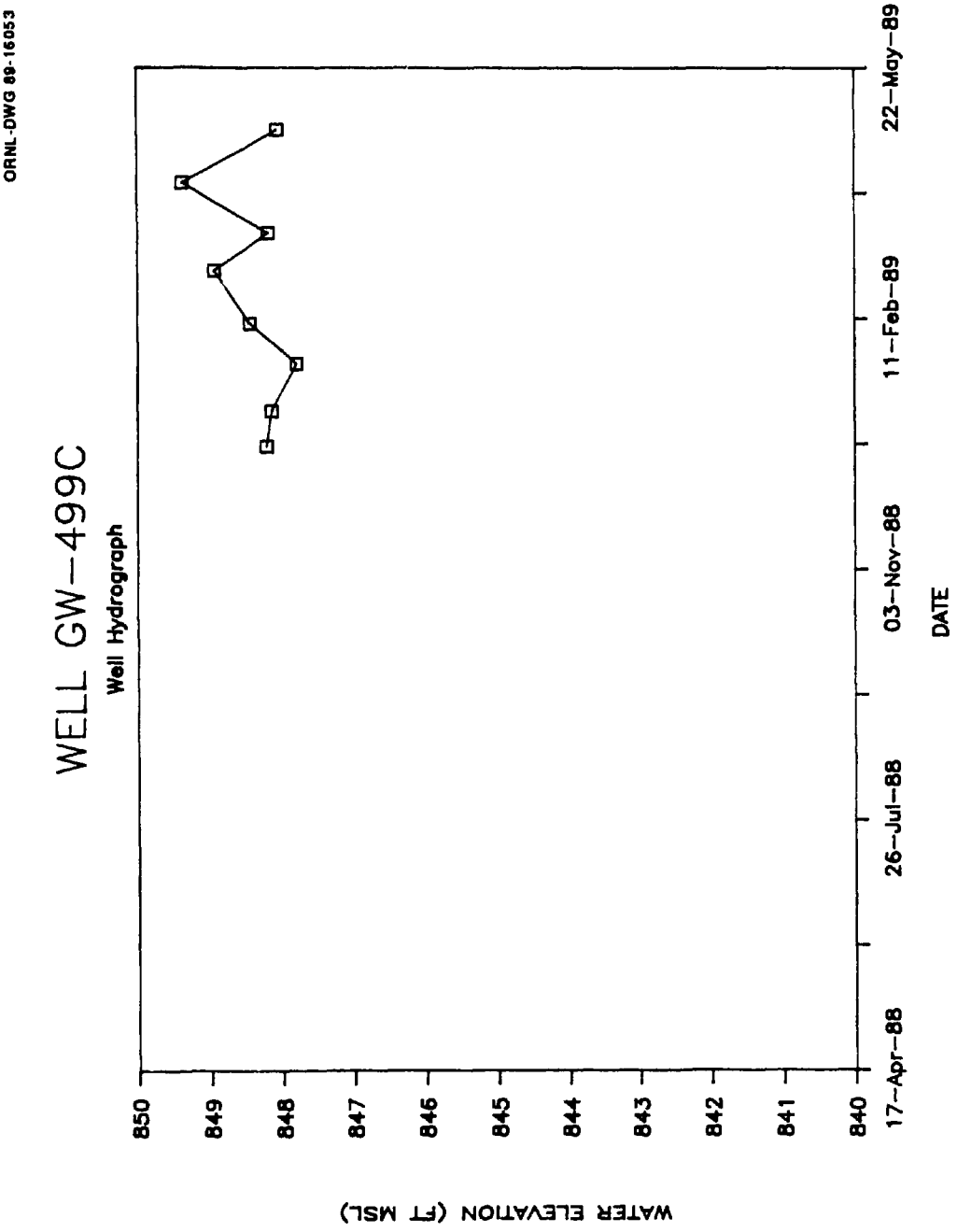
ORNL-DWG 89-16053
WELL GW-499C
Well Hydrograph
WATER ELEVATION (FT MSL)
850
849
848
847
846
845
844
843
842
841
840
17-Apr-88
26-Jul-88
03-Nov-88
11-Feb-89
22-May-89
DATE

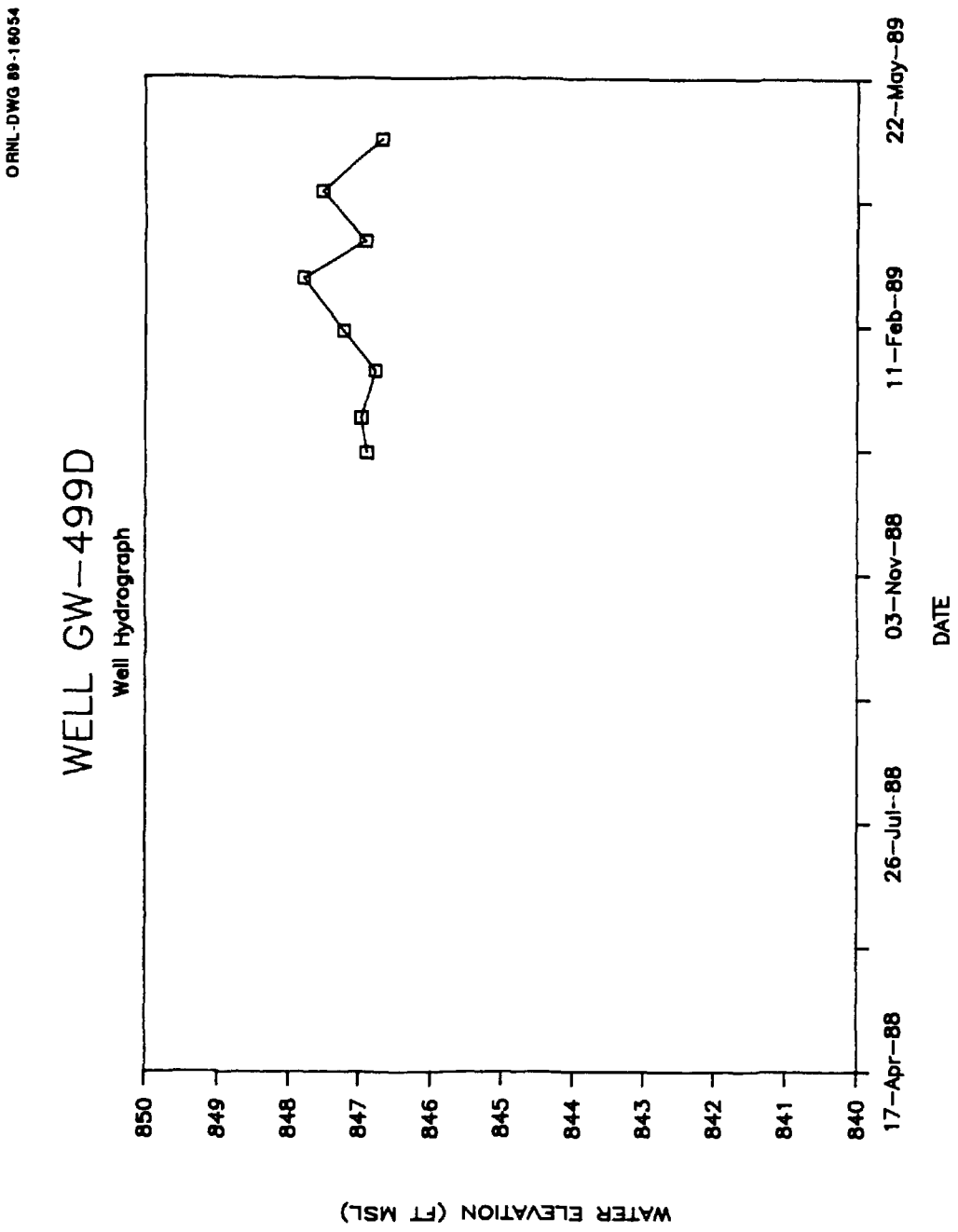
ORNL-DWG 89-16054
WELL GW-499D
Well Hydrograph
WATER ELEVATION (FT MSL)
850
849
848
847
846
845
844
843
842
841
840
17-Apr-88
26-Jul-88
03-Nov-88
11-Feb-89
22-May-89
DATE

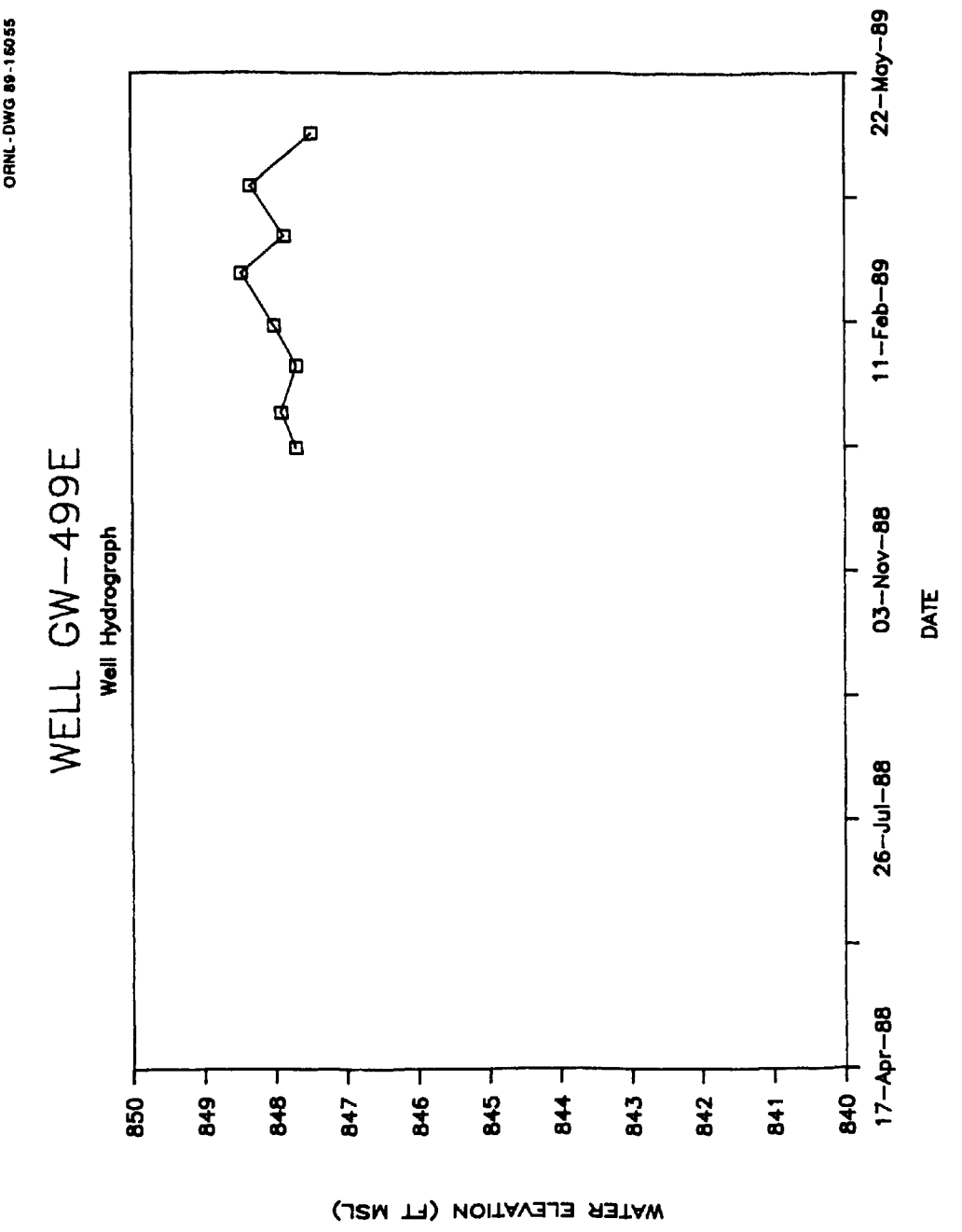
ORNL-DWG 89-16055
WELL GW-499E
Well Hydrograph
WATER ELEVATION (FT MSL)
850
849
848
847
846
845
844
843
842
841
840
17-Apr-88
26-Jul-88
03-Nov-88
11-Feb-89
22-May-89
DATE

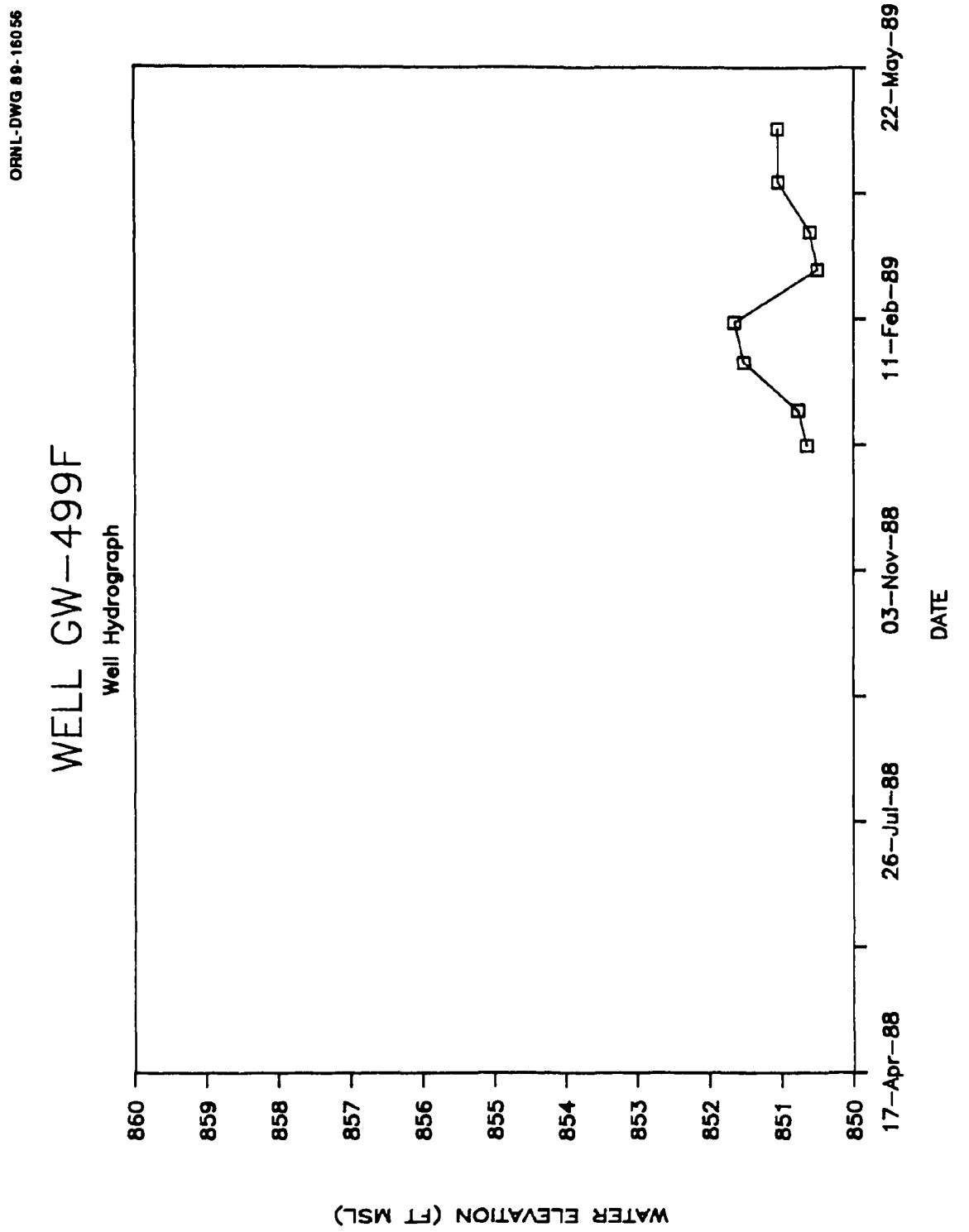
ORNL-DWG 89-16056
WELL GW-499F
Well Hydrograph
WATER ELEVATION (FT MSL)
860
859
858
857
856
855
854
853
852
851
850
17-Apr-88
26-Jul-88
03-Nov-88
11-Feb-89
22-May-89
DATE

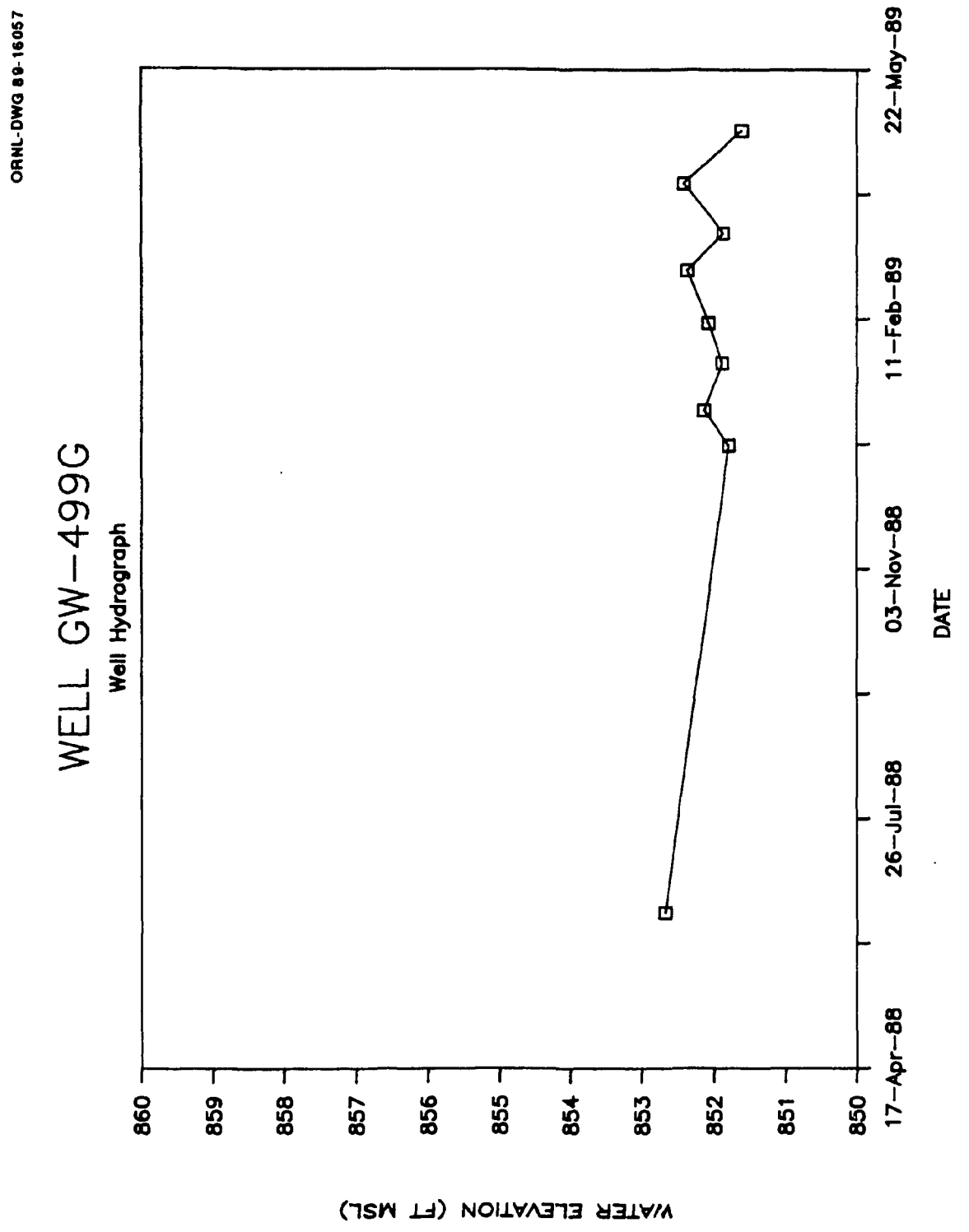
ORNL-DWG 89-16057
WELL GW-499G
Well Hydrograph
WATER ELEVATION (FT MSL)
860
859
858
857
856
855
854
853
852
851
850
17-Apr-88
26-Jul-88
03-Nov-88
11-Feb-89
22-May-89
DATE

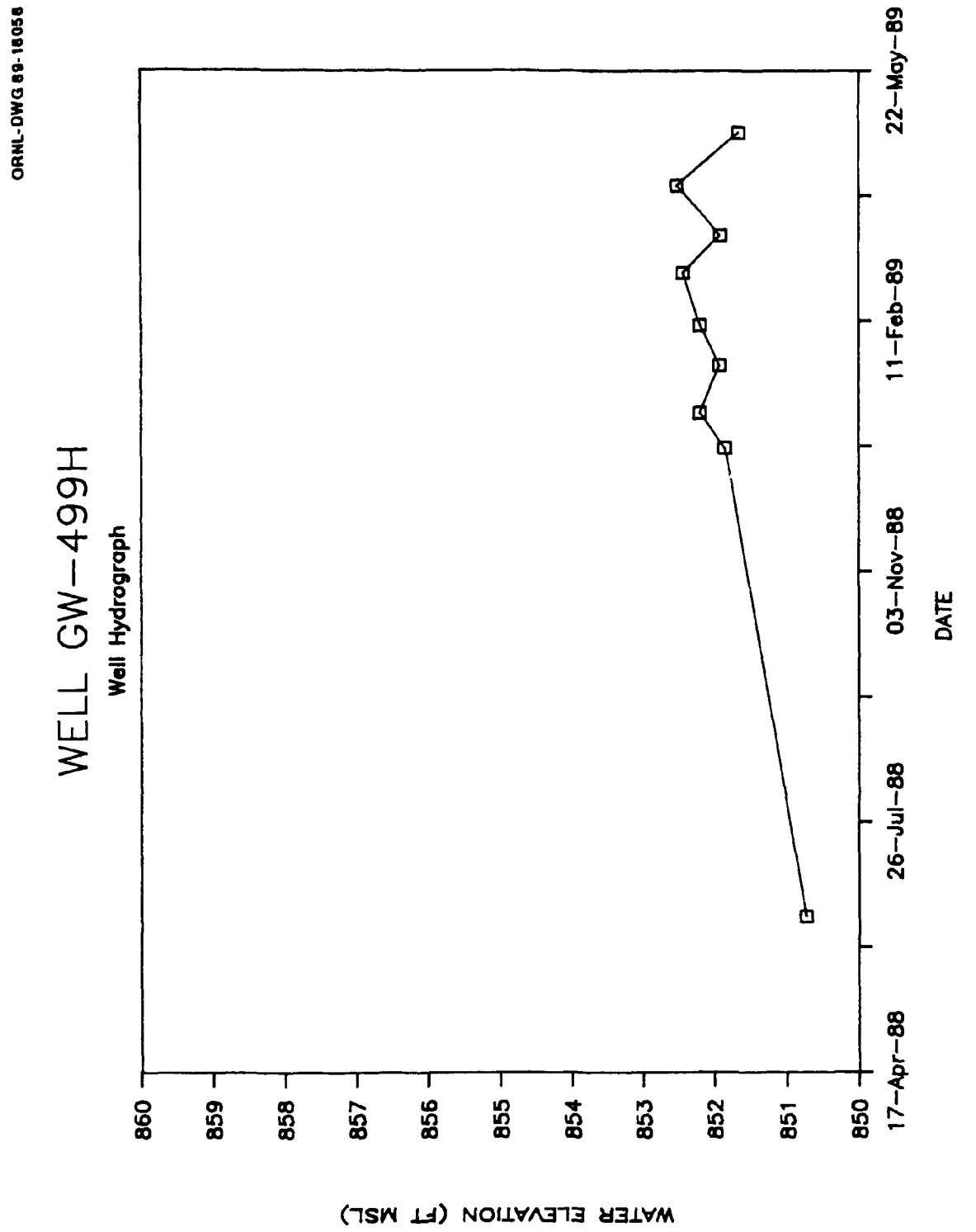
ORNL-DWG 89-18058
WELL GW-499H
Well Hydrograph
WATER ELEVATION (FT MSL)
860
859
858
857
856
855
854
853
852
851
850
17-Apr-88
26-Jul-88
03-Nov-88
11-Feb-89
22-May-89
DATE

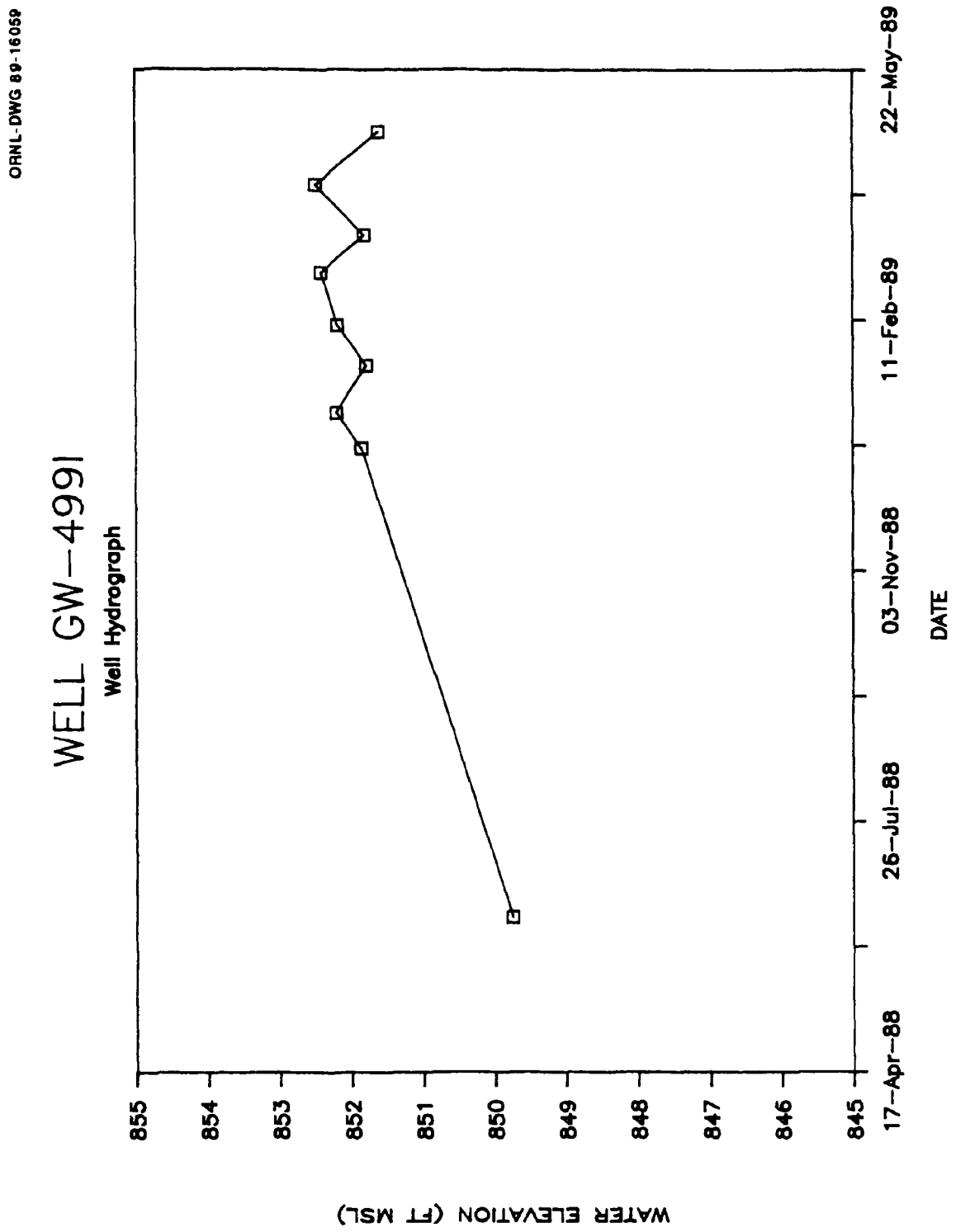
ORNL-DWG 89-16059
WELL GW-4991
Well Hydrograph
WATER ELEVATION (FT MSL)
855
854
853
852
851
850
849
848
847
846
845
17-Apr-88
26-Jul-88
03-Nov-88
11-Feb-89
22-May-89
DATE

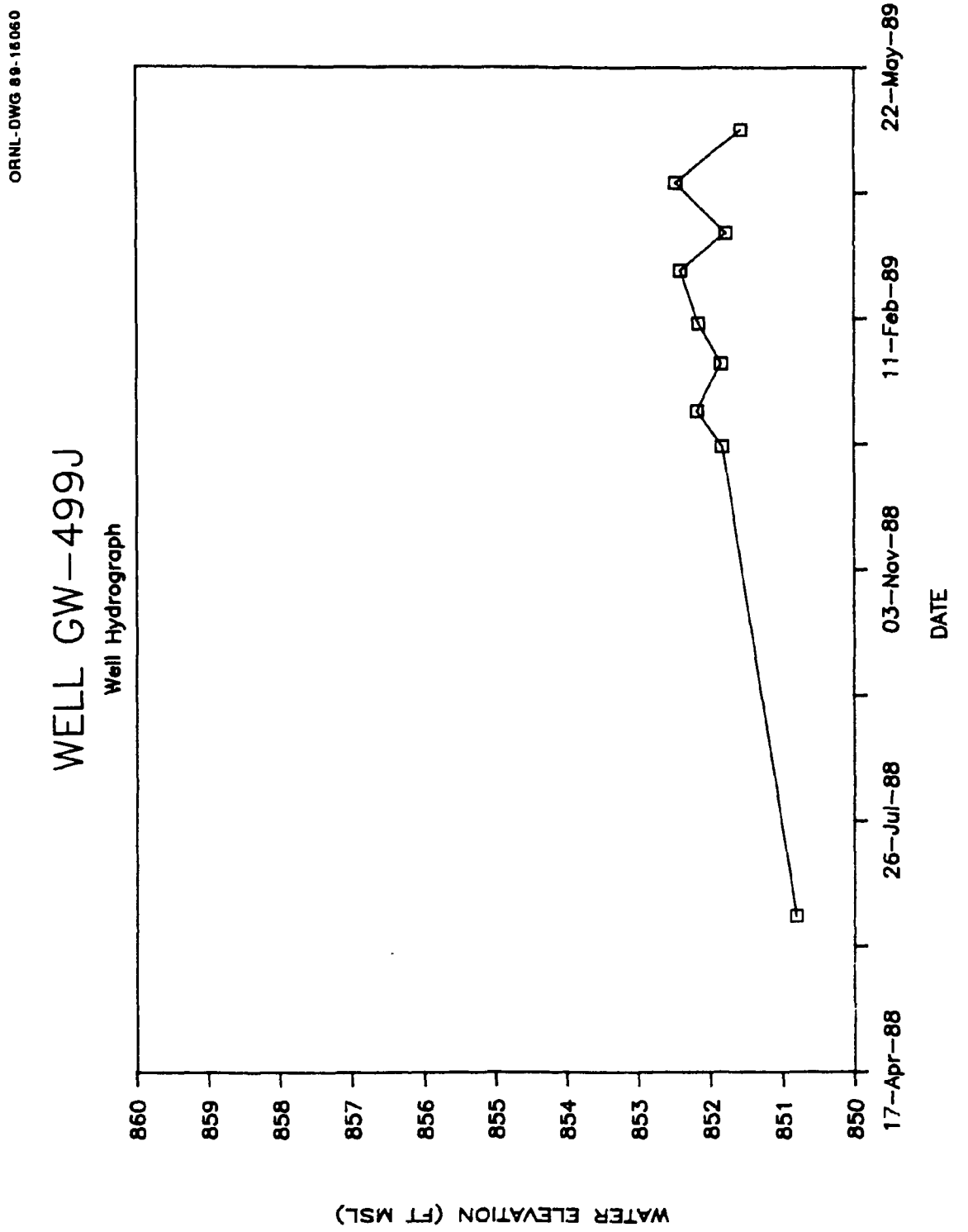
ORNL-DWG 89-15060
WELL GW-499J
Well Hydrograph
WATER ELEVATION (FT MSL)
860
859
858
857
856
855
854
853
852
851
850
17-Apr-88
26-Jul-88
03-Nov-88
11-Feb-89
22-May-89
DATE

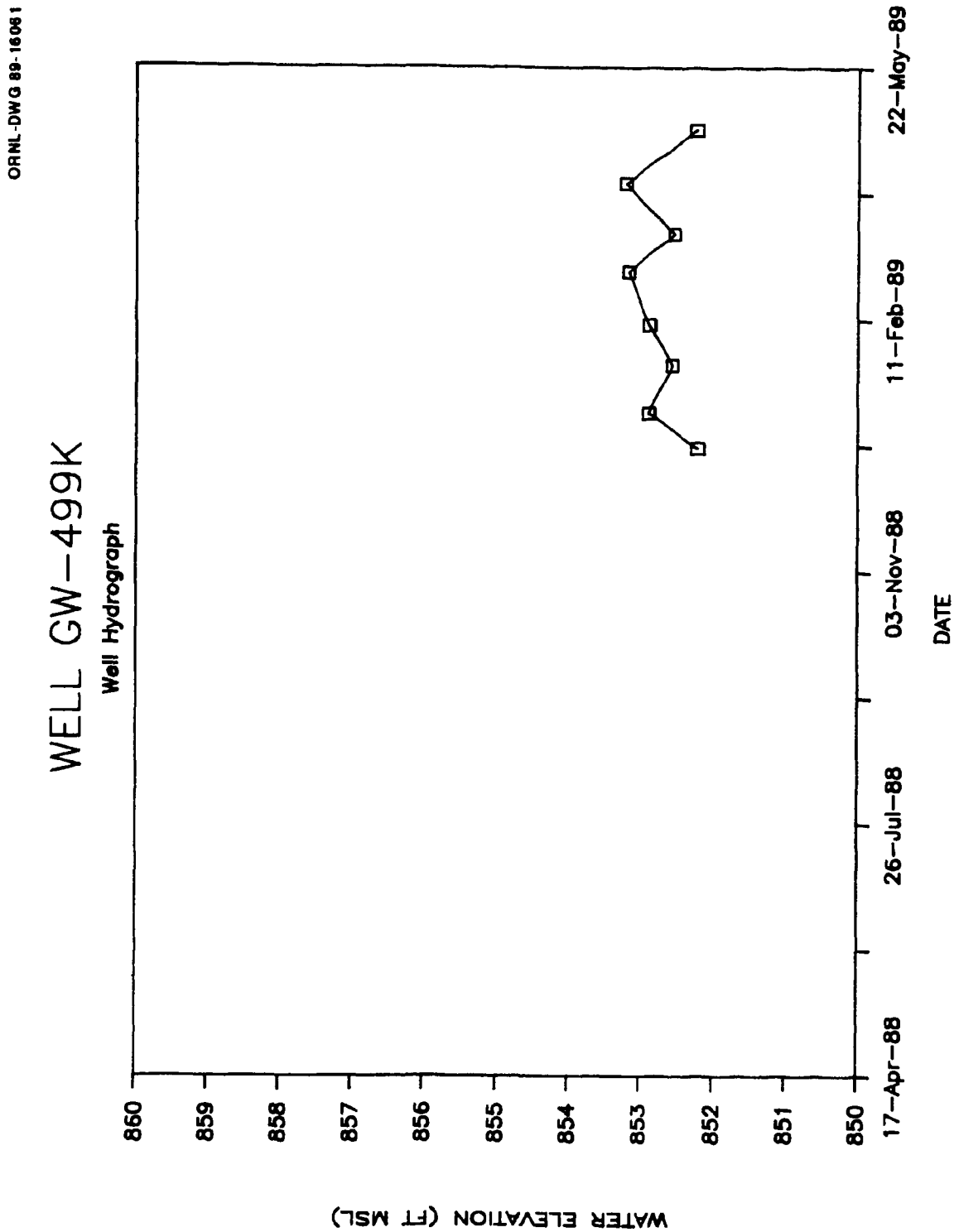
ORNL-DWG 89-16061
WELL GW-499K
Well Hydrograph
WATER ELEVATION (FT MSL)
860
859
858
857
856
855
854
853
852
851
850
17-Apr-88
26-Jul-88
03-Nov-88
11-Feb-89
22-May-89
DATE

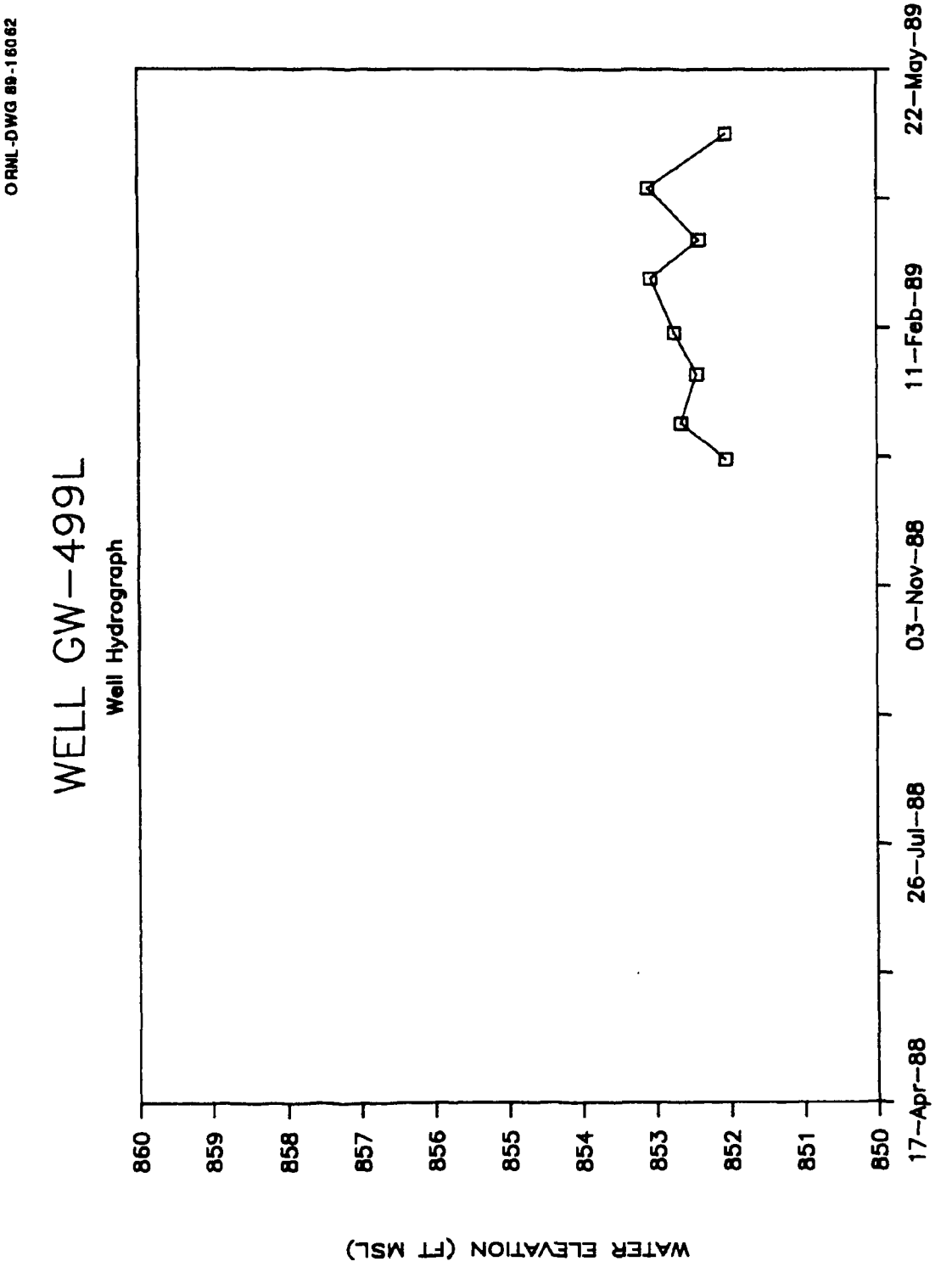
ORNL-DWG 89-16062
WELL GW-499L
Well Hydrograph
WATER ELEVATION (FT MSL)
860
859
858
857
856
855
854
853
852
851
850
17-Apr-88
26-Jul-88
03-Nov-88
11-Feb-89
22-May-89
DATE

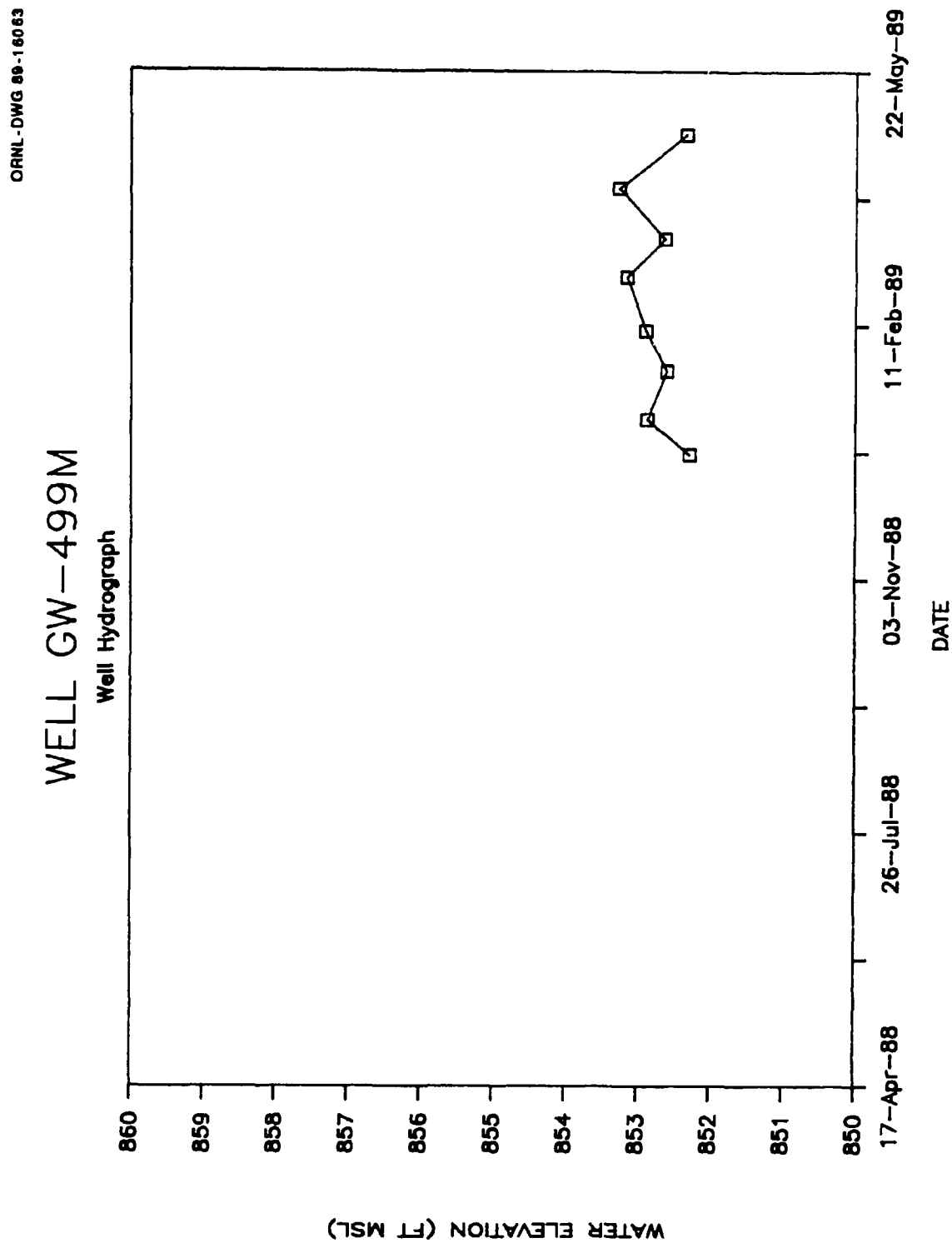
ORNL-DWG 89-16063
WELL GW-499M
Well Hydrograph
WATER ELEVATION (FT MSL)
860
859
858
857
856
855
854
853
852
851
850
17-Apr-88
26-Jul-88
03-Nov-88
11-Feb-89
22-May-89
DATE

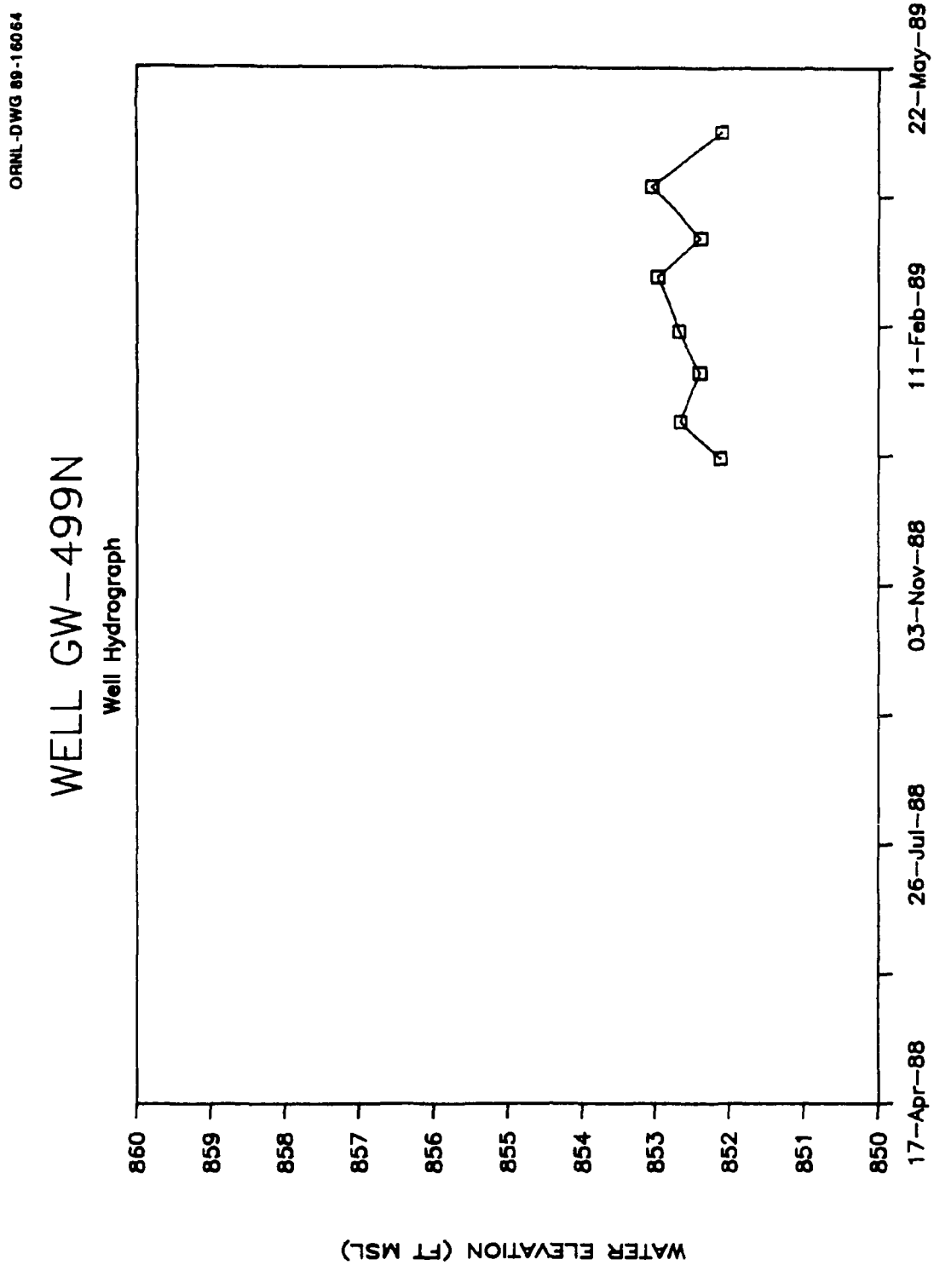
ORNL-DWG 89-16064
WELL GW-499N
Well Hydrograph
WATER ELEVATION (FT MSL)
860
859
858
857
856
855
854
853
852
851
850
17-Apr-88
26-Jul-88
03-Nov-88
11-Feb-89
22-May-89
DATE

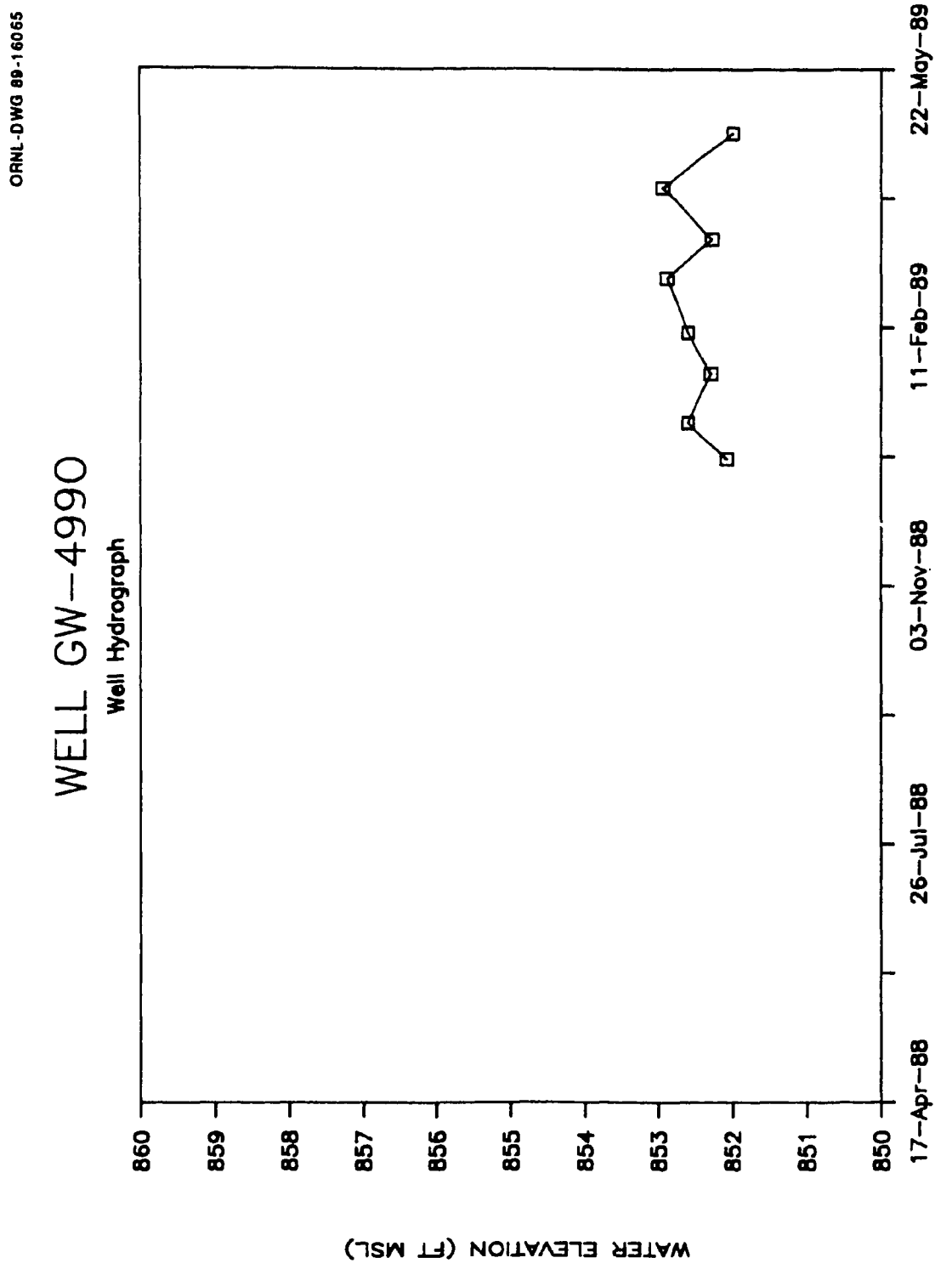
ORNL-DWG 89-16065
WELL GW-4990
Well Hydrograph
WATER ELEVATION (FT MSL)
860
859
858
857
856
855
854
853
852
851
850
17-Apr-88
26-Jul-88
03-Nov-88
11-Feb-89
22-May-89
DATE

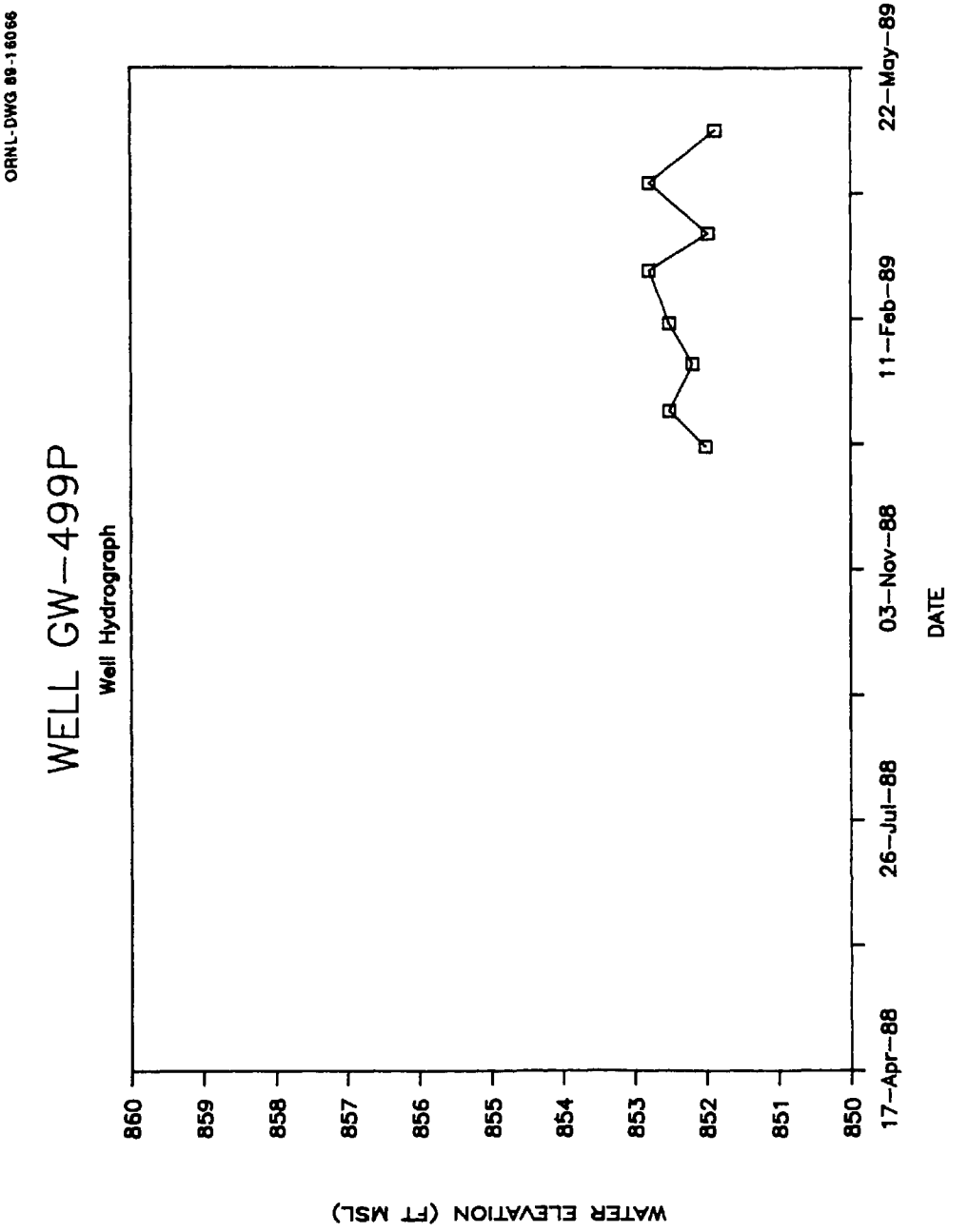
ORNL-DWG 89-18066
WELL GW-499P
Well Hydrograph
WATER ELEVATION (FT MSL)
860
859
858
857
856
855
854
853
852
851
850
17-Apr-88
26-Jul-88
03-Nov-88
11-Feb-89
22-May-89
DATE

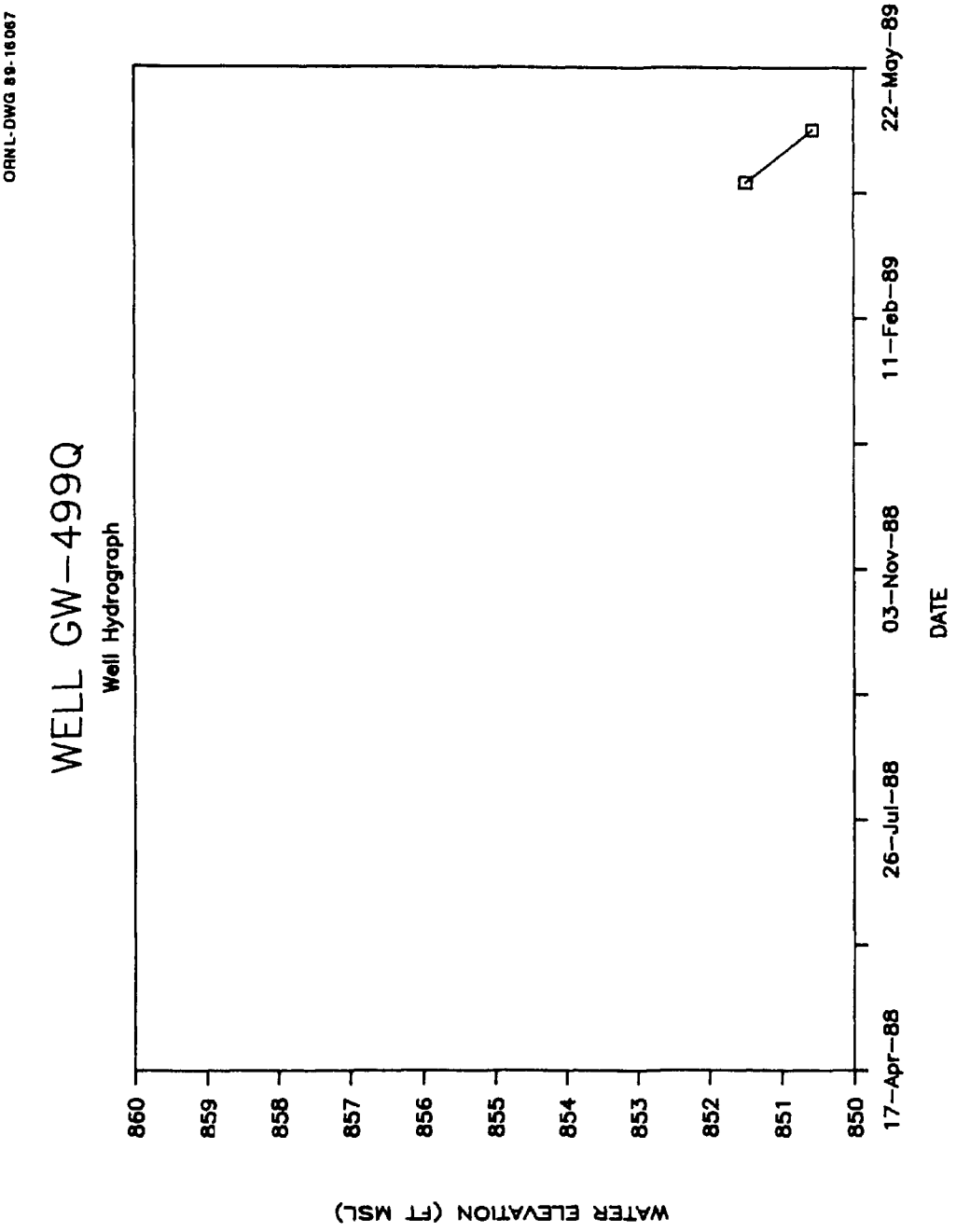
ORNL-DWG 89-16067
WELL GW-499Q
Well Hydrograph
WATER ELEVATION (FT MSL)
860
859
858
857
856
855
854
853
852
851
850
17-Apr-88
26-Jul-88
03-Nov-88
11-Feb-89
22-May-89
DATE

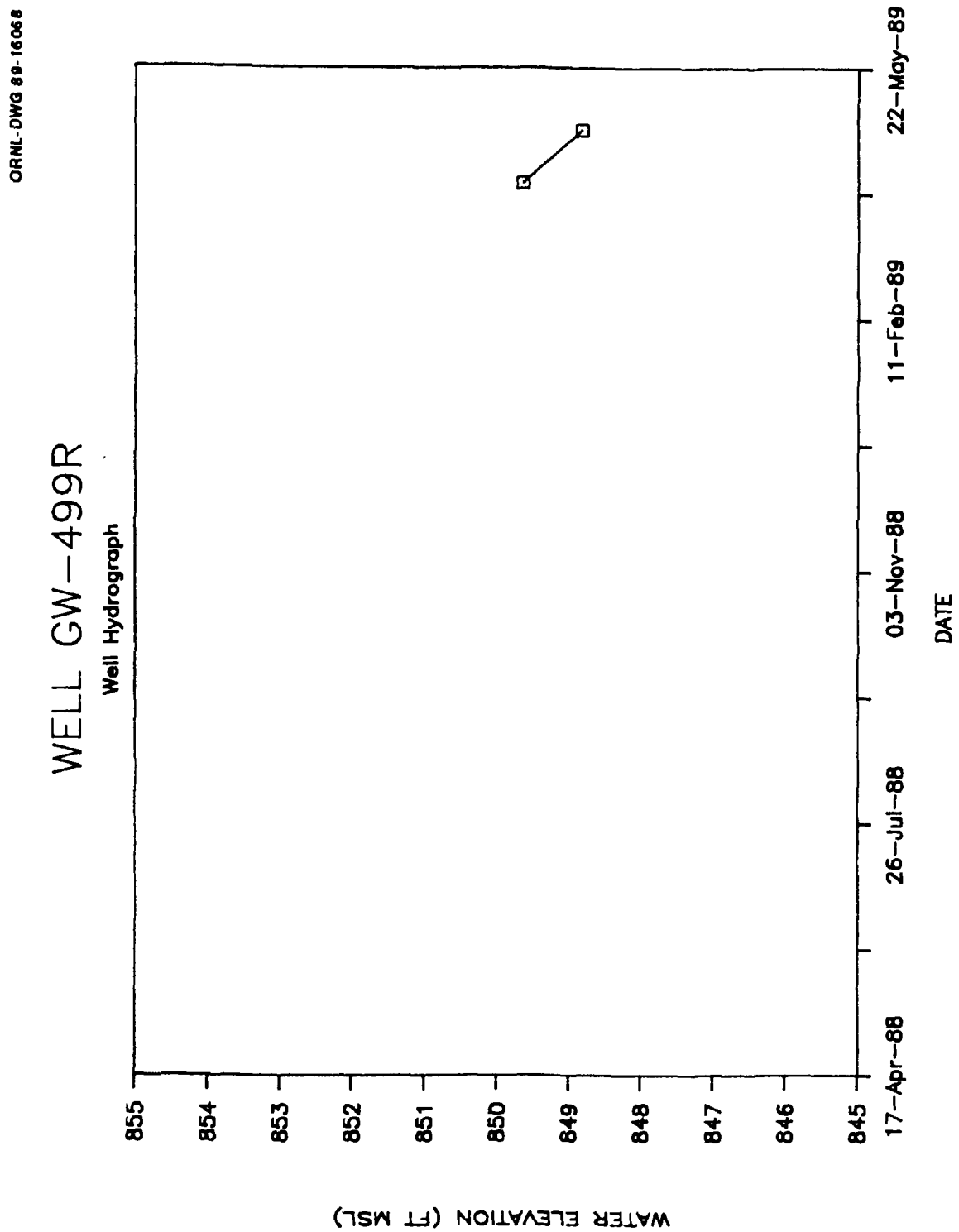
ORNL-DWG 89-16068
WELL GW-499R
Well Hydrograph
WATER ELEVATION (FT MSL)
855
854
853
852
851
850
849
848
847
846
845
17-Apr-88
26-Jul-88
03-Nov-88
11-Feb-89
22-May-89
DATE

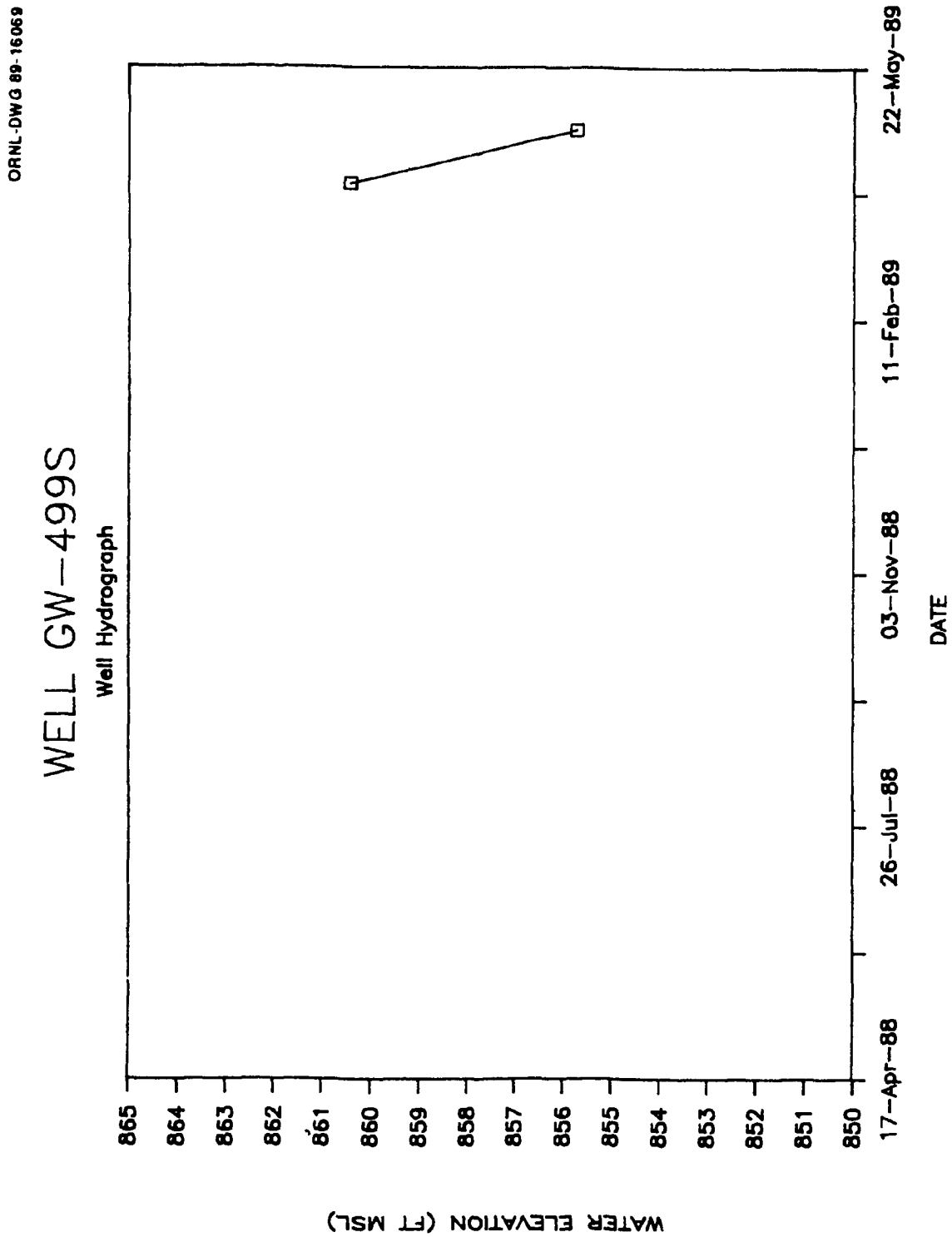
ORNL-DWG 89-16069
WELL GW-499S
Well Hydrograph
WATER ELEVATION (FT MSL)
865
864
863
862
861
860
859
858
857
856
855
854
853
852
851
850
17-Apr-88
26-Jul-88
03-Nov-88
11-Feb-89
22-May-89
DATE

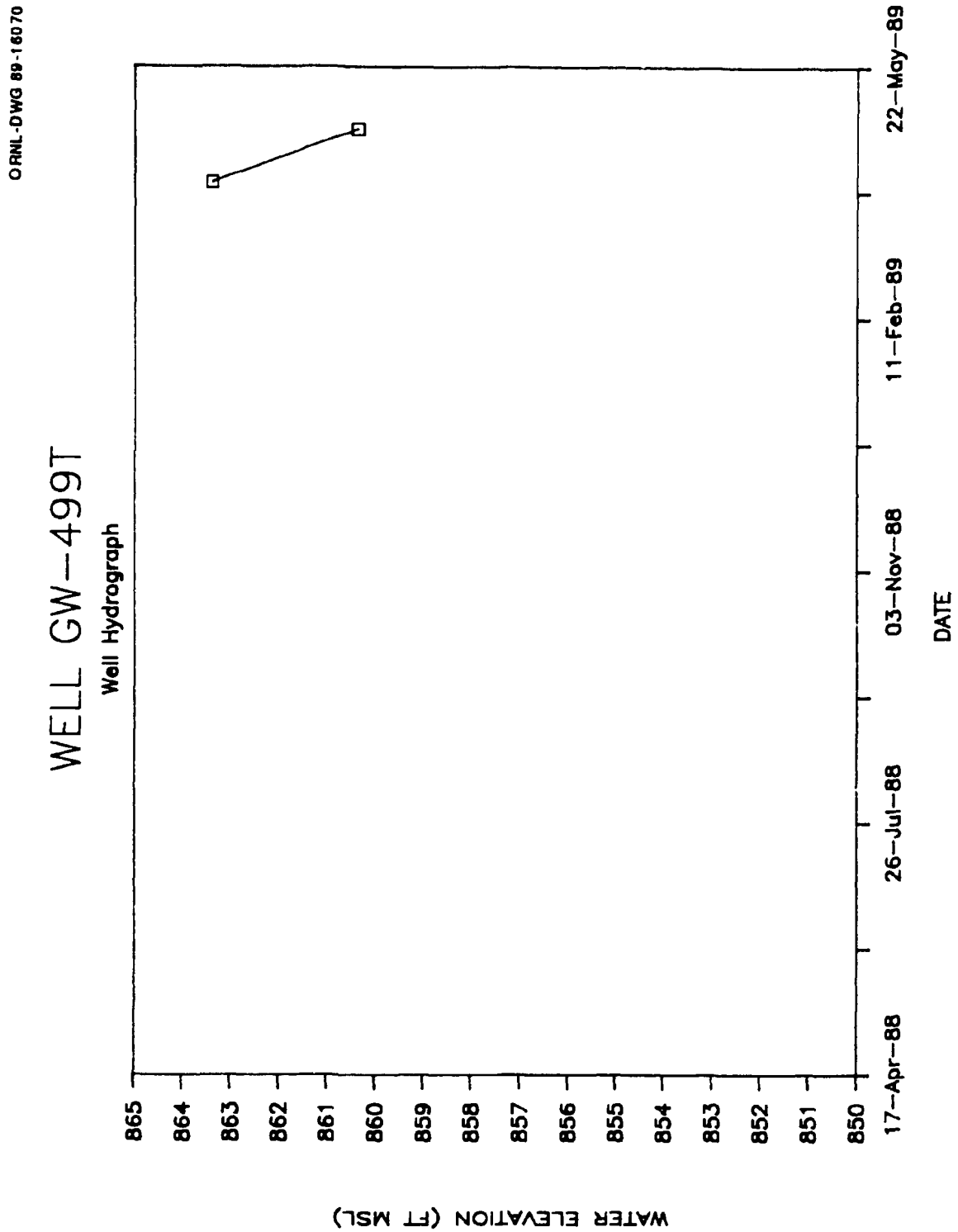
ORNL-DWG 89-16070
WELL GW-499T
Well Hydrograph
WATER ELEVATION (FT MSL)
865
864
863
862
861
860
859
858
857
856
855
854
853
852
851
850
17-Apr-88
26-Jul-88
03-Nov-88
11-Feb-89
22-May-89
DATE

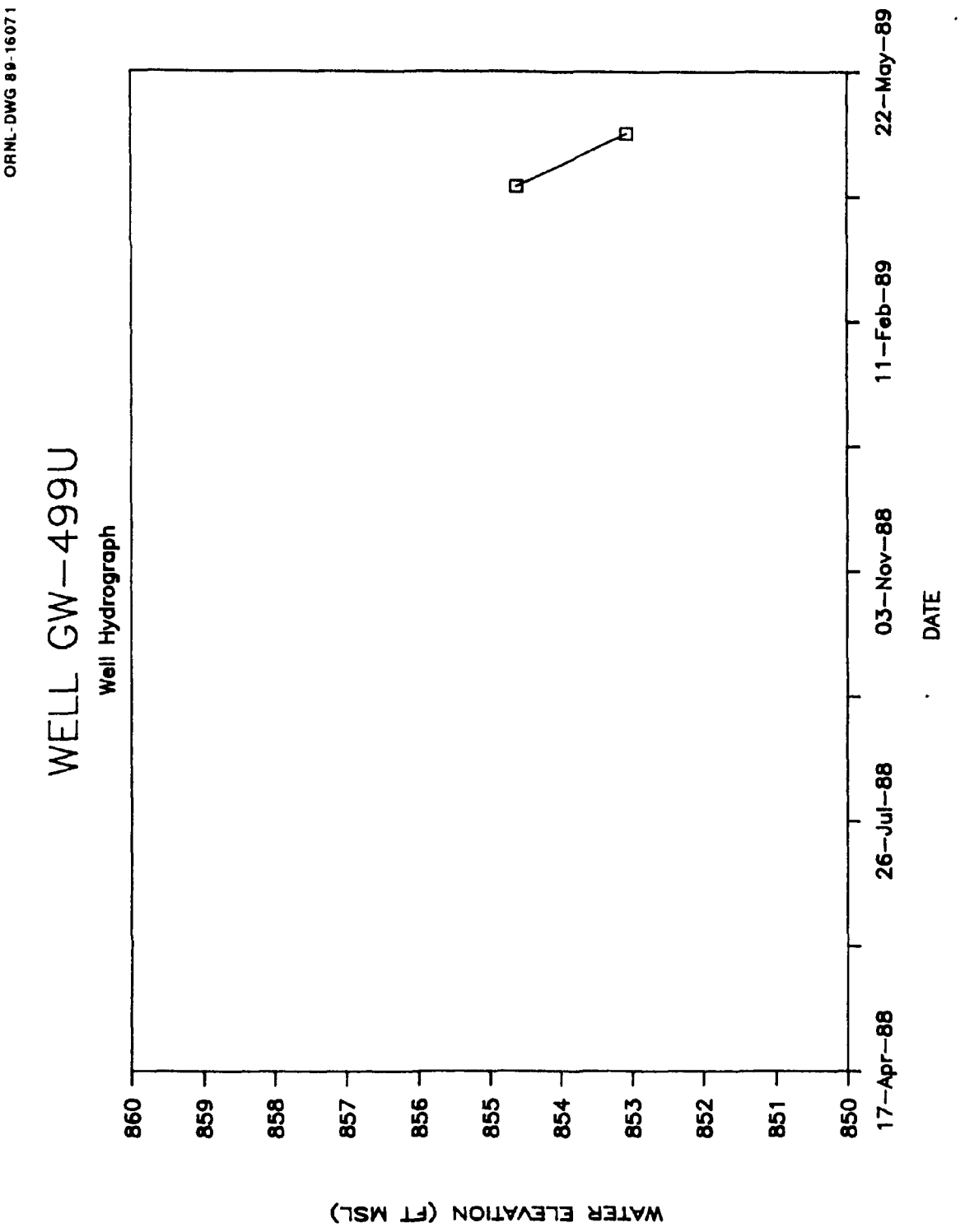
ORNL-DWG 89-16071
WELL GW-499U
Well Hydrograph
WATER ELEVATION (FT MSL)
860
859
858
857
856
855
854
853
852
851
850
17-Apr-88
26-Jul-88
03-Nov-88
11-Feb-89
22-May-89
DATE

ORNL-DWG 89-16072

WELL GW-499V

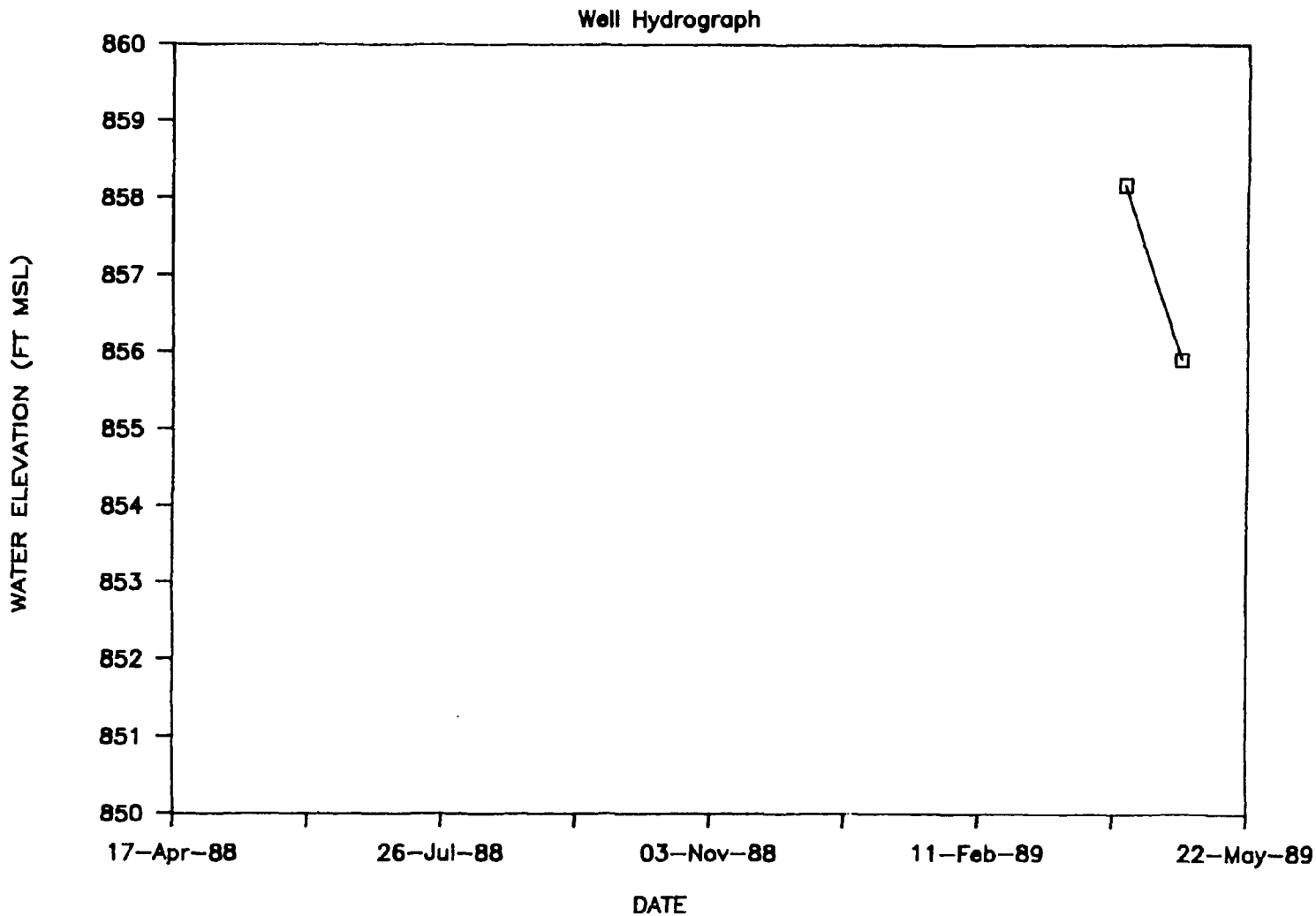

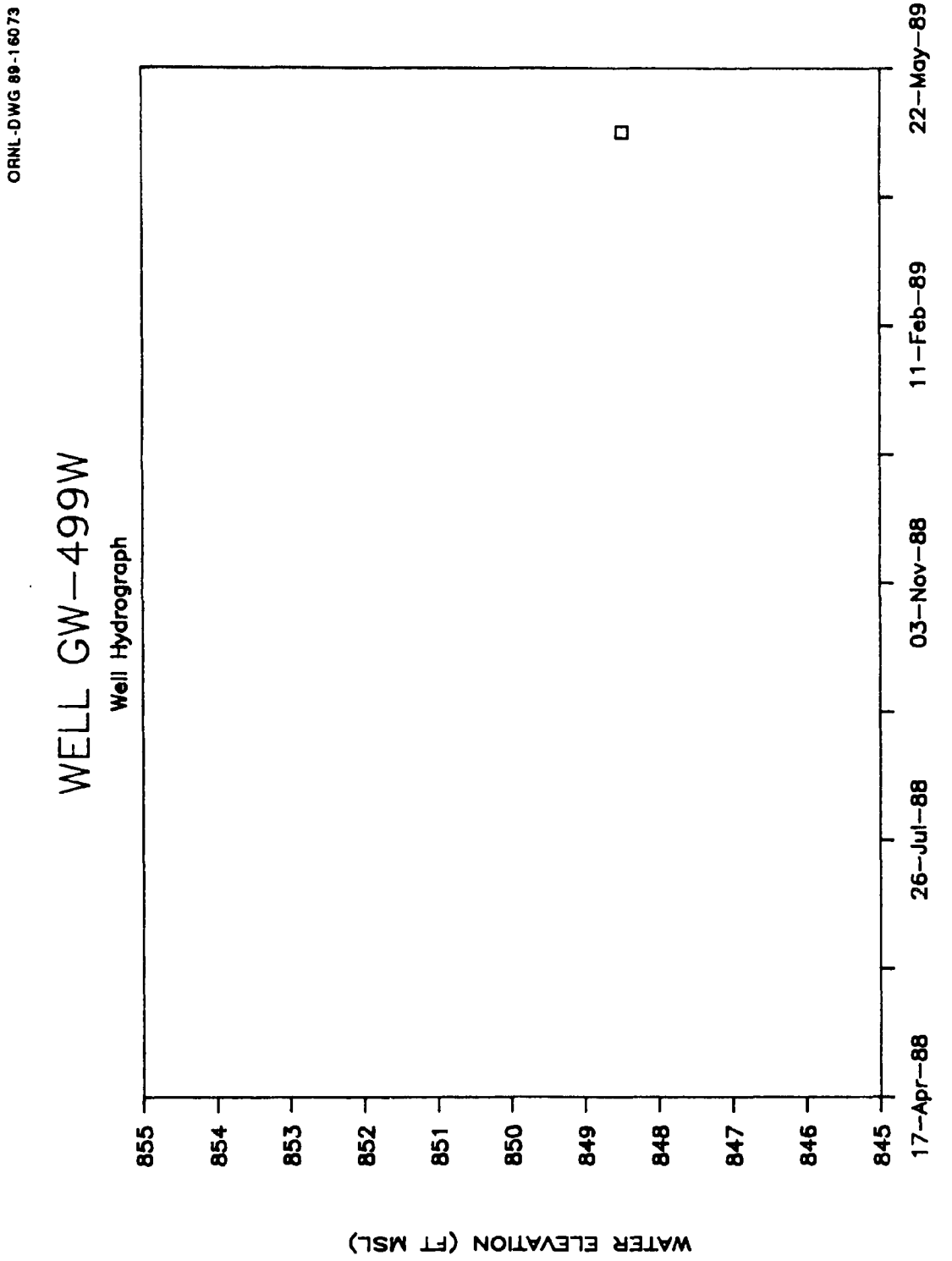
ORNL-DWG 89-16073
WELL GW-499W
Well Hydrograph
WATER ELEVATION (FT MSL)
855
854
853
852
851
850
849
848
847
846
845
17-Apr-88
26-Jul-88
03-Nov-88
11-Feb-89
22-May-89
DATE

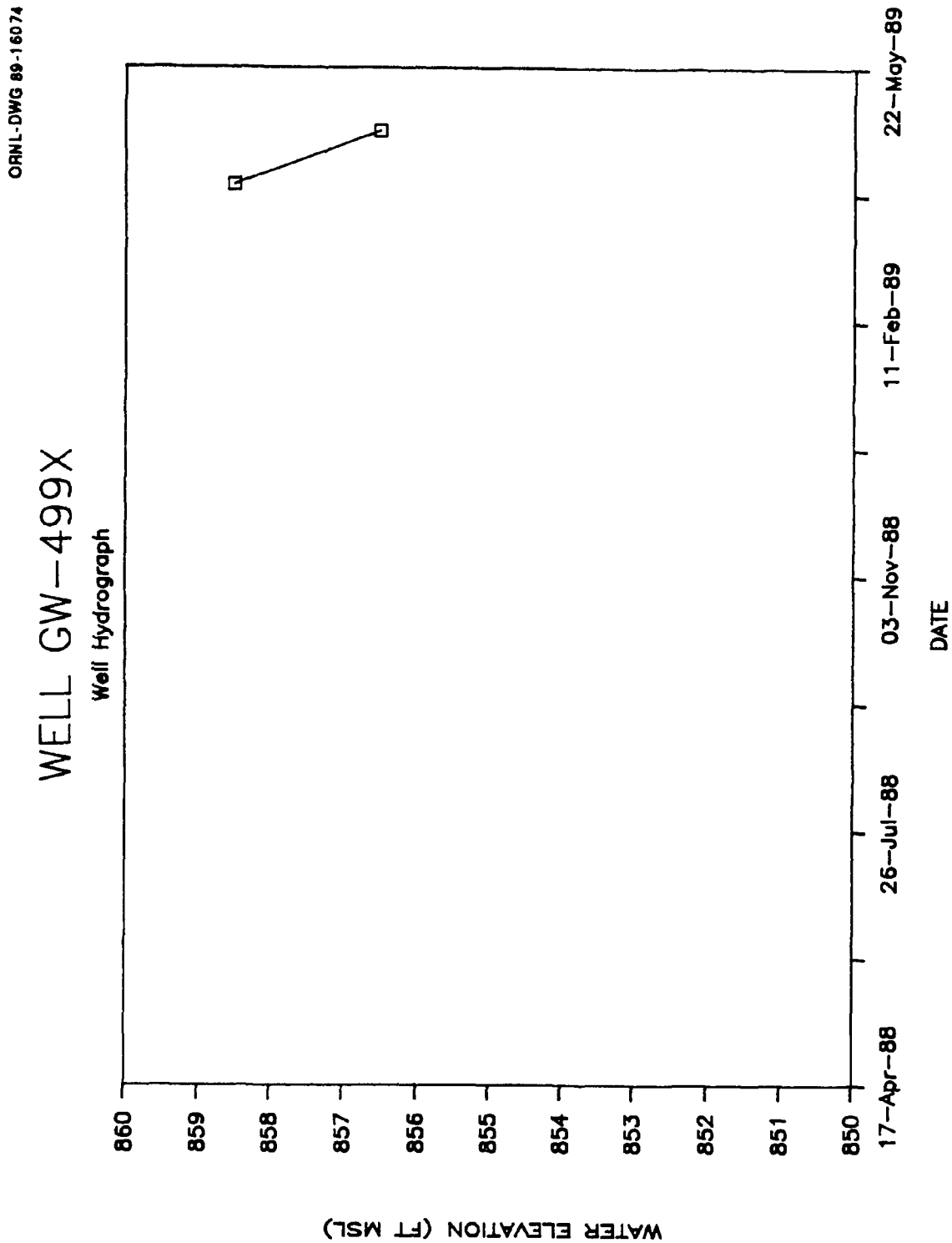
ORNL-DWG 89-16074
WELL GW-499X
Well Hydrograph
WATER ELEVATION (FT MSL)
860
859
858
857
856
855
854
853
852
851
850
17-Apr-88
26-Jul-88
03-Nov-88
11-Feb-89
22-May-89
DATE

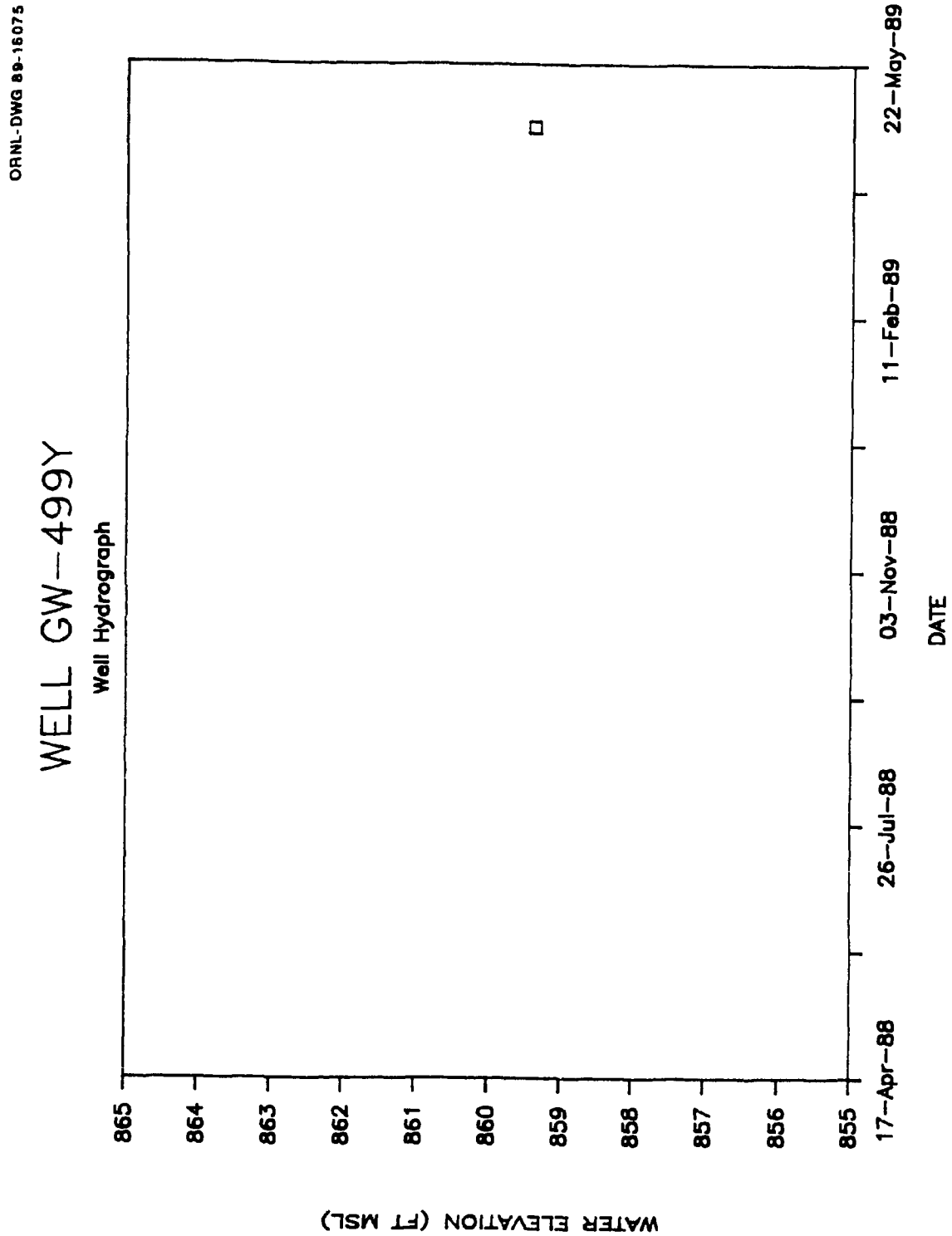
ORNL-DWG 89-16075
WELL GW-499Y
Well Hydrograph
WATER ELEVATION (FT MSL)
865
864
863
862
861
860
859
858
857
856
855
17-Apr-88
26-Jul-88
03-Nov-88
11-Feb-89
22-May-89
DATE

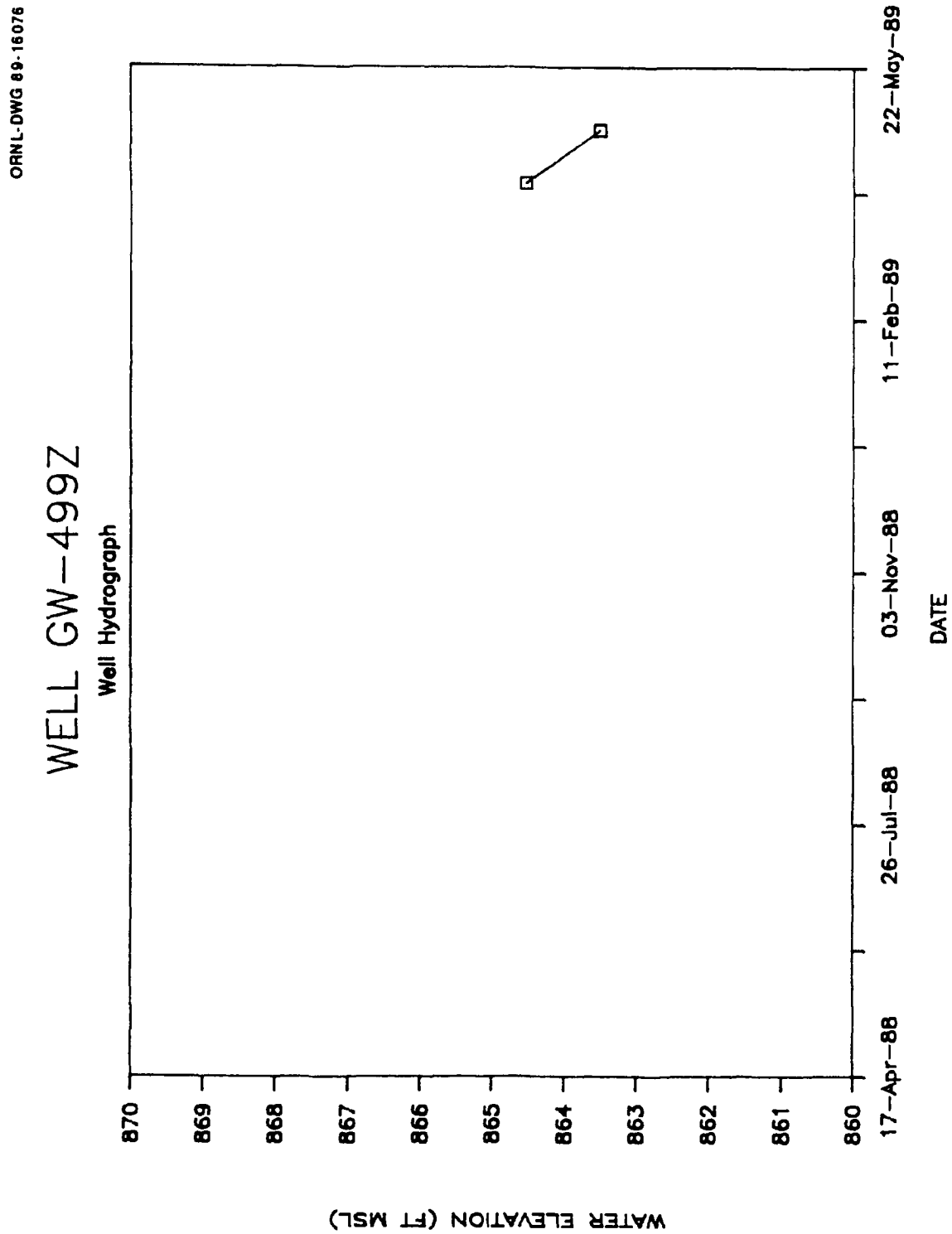
ORNL-DWG 89-16076
WELL GW-499Z
Well Hydrograph
WATER ELEVATION (FT MSL)
870
869
868
867
866
865
864
863
862
861
860
17-Apr-88
26-Jul-88
03-Nov-88
11-Feb-89
22-May-89
DATE

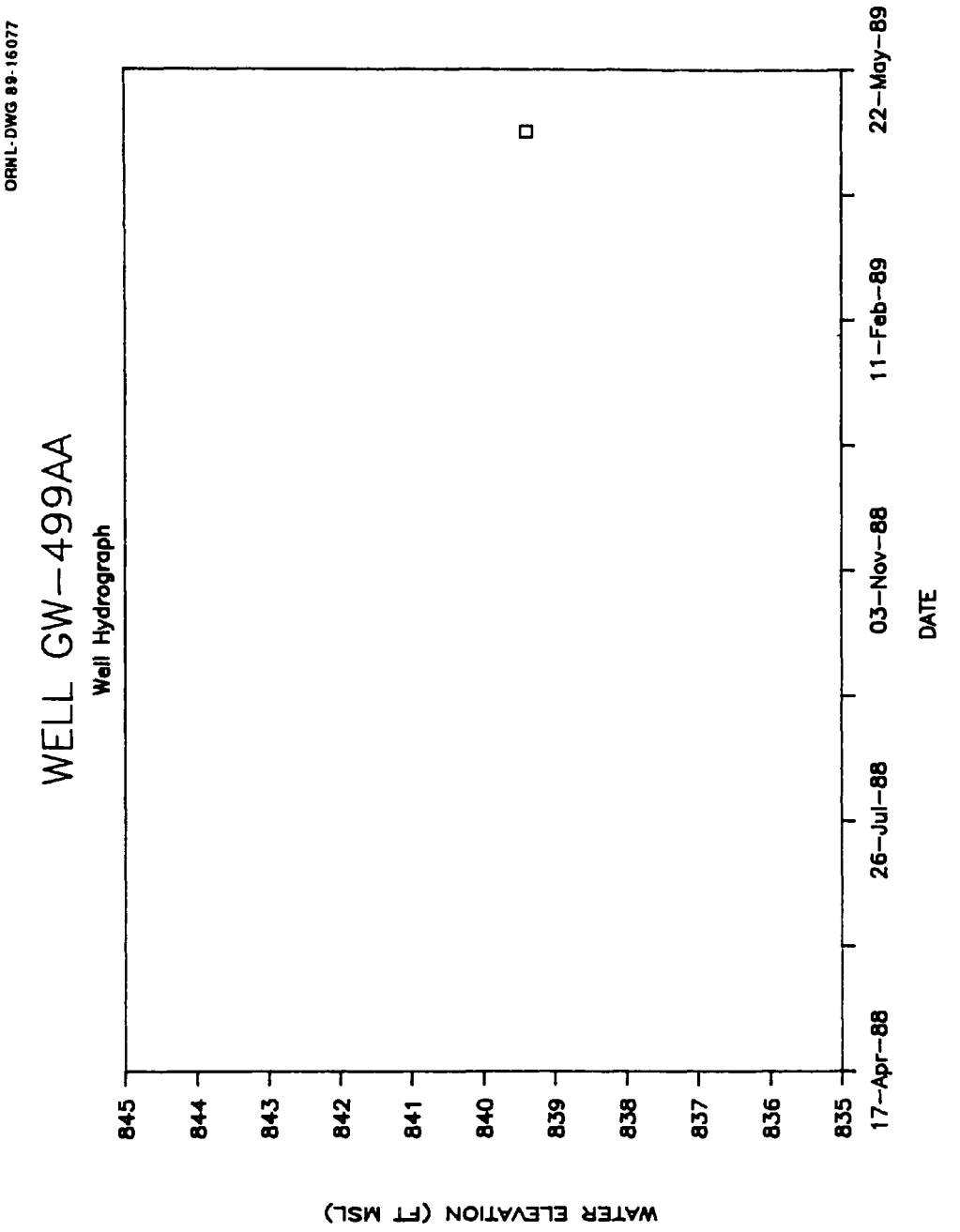
ORNL-DWG 89-16077
WELL GW-499AA
Well Hydrograph
WATER ELEVATION (FT MSL)
845
844
843
842
841
840
839
838
837
836
835
17-Apr-88
26-Jul-88
03-Nov-88
11-Feb-89
22-May-89
DATE

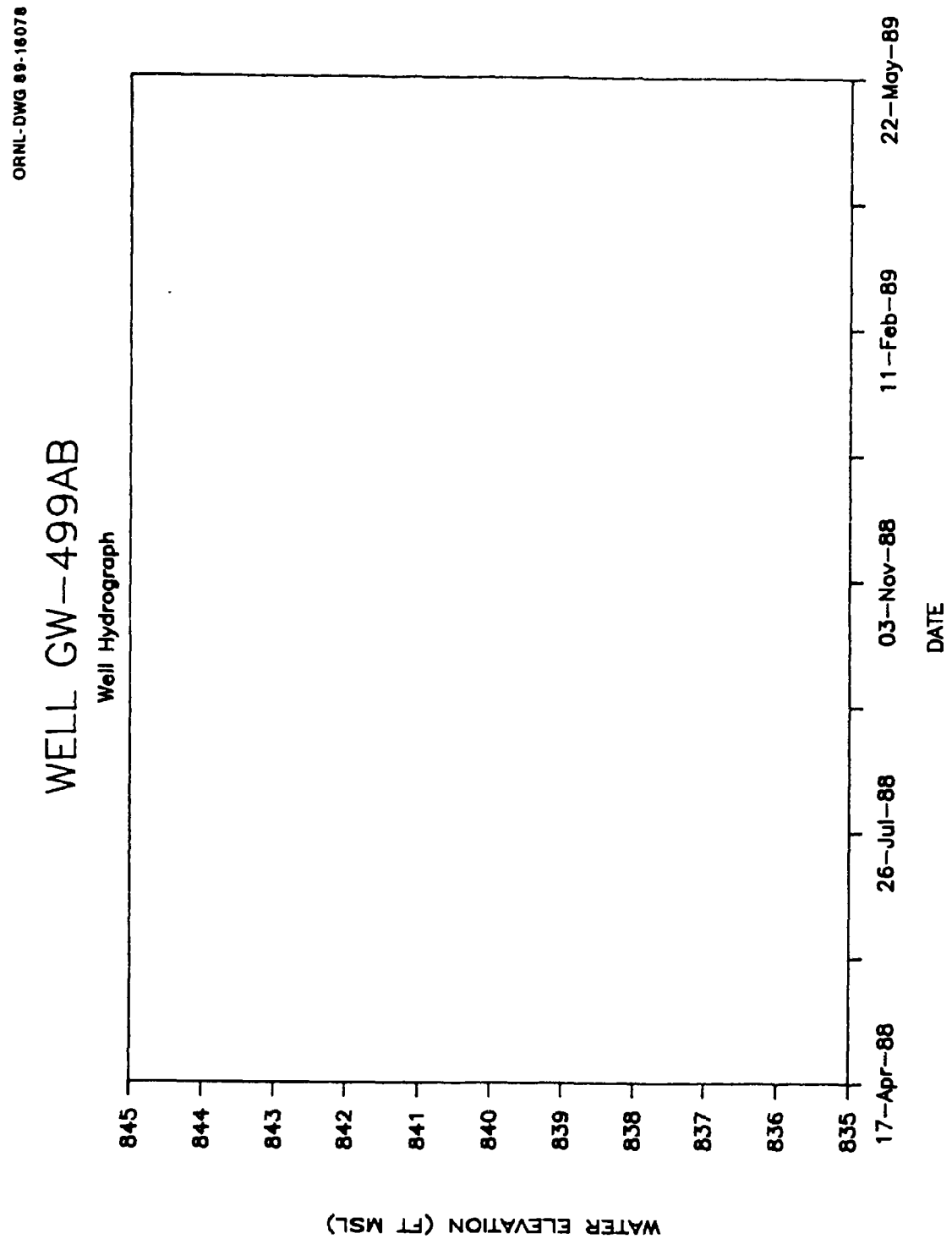
ORNL-DWG 89-16078
WELL GW-499AB
Well Hydrograph
WATER ELEVATION (FT MSL)
845
844
843
842
841
840
839
838
837
836
835
17-Apr-88
26-Jul-88
03-Nov-88
11-Feb-89
22-May-89
DATE

ORNL-DWG 89-16079

WELL GW-499AC

Well Hydrograph

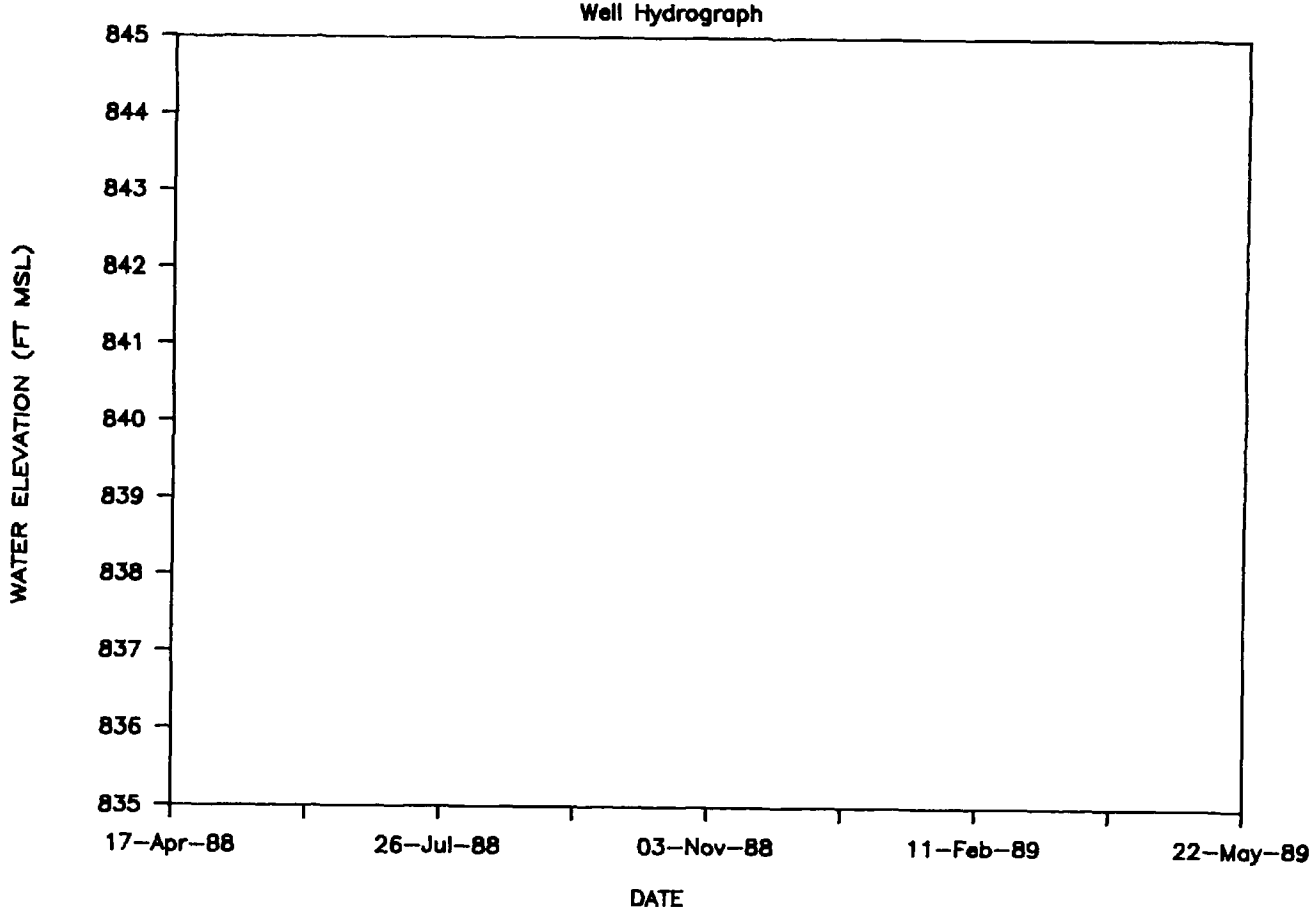

ORNL-DWG 89-16080

WELL GW-499AD

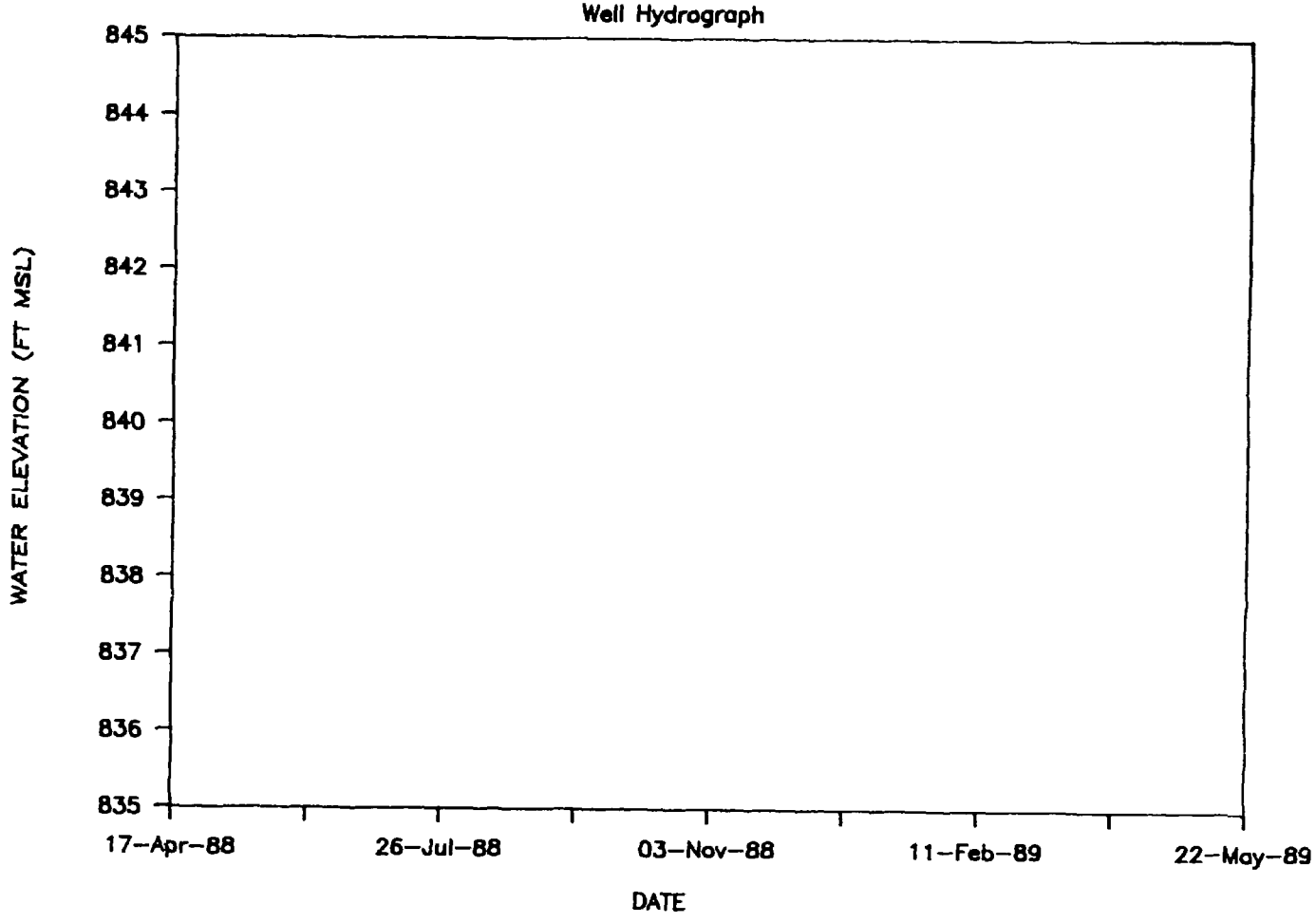

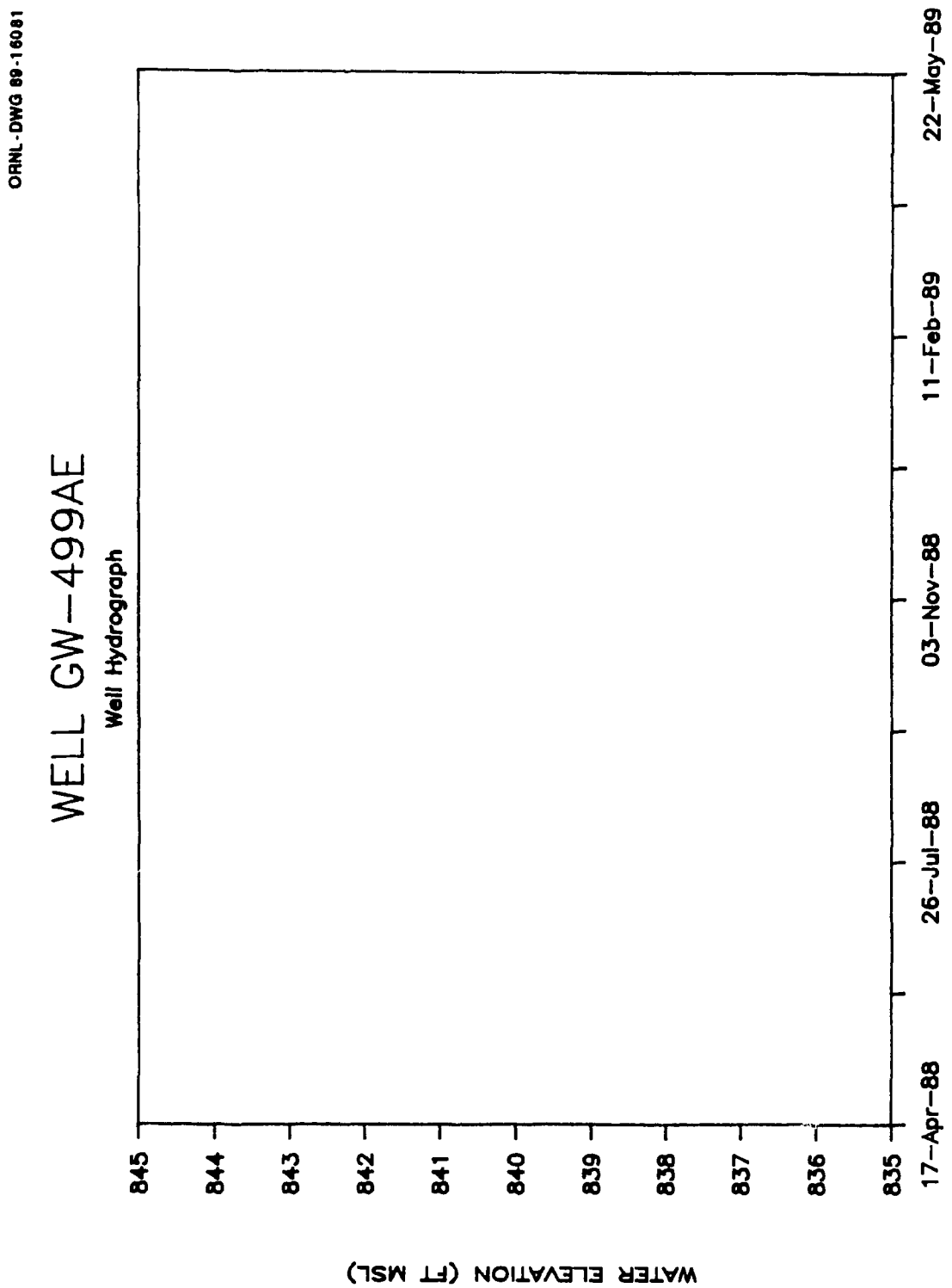
ORNL-DWG 89-16081
WELL GW-499AE
Well Hydrograph
WATER ELEVATION (FT MSL)
845
844
843
842
841
840
839
838
837
836
835
17-Apr-88
26-Jul-88
03-Nov-88
11-Feb-89
22-May-89
DATE

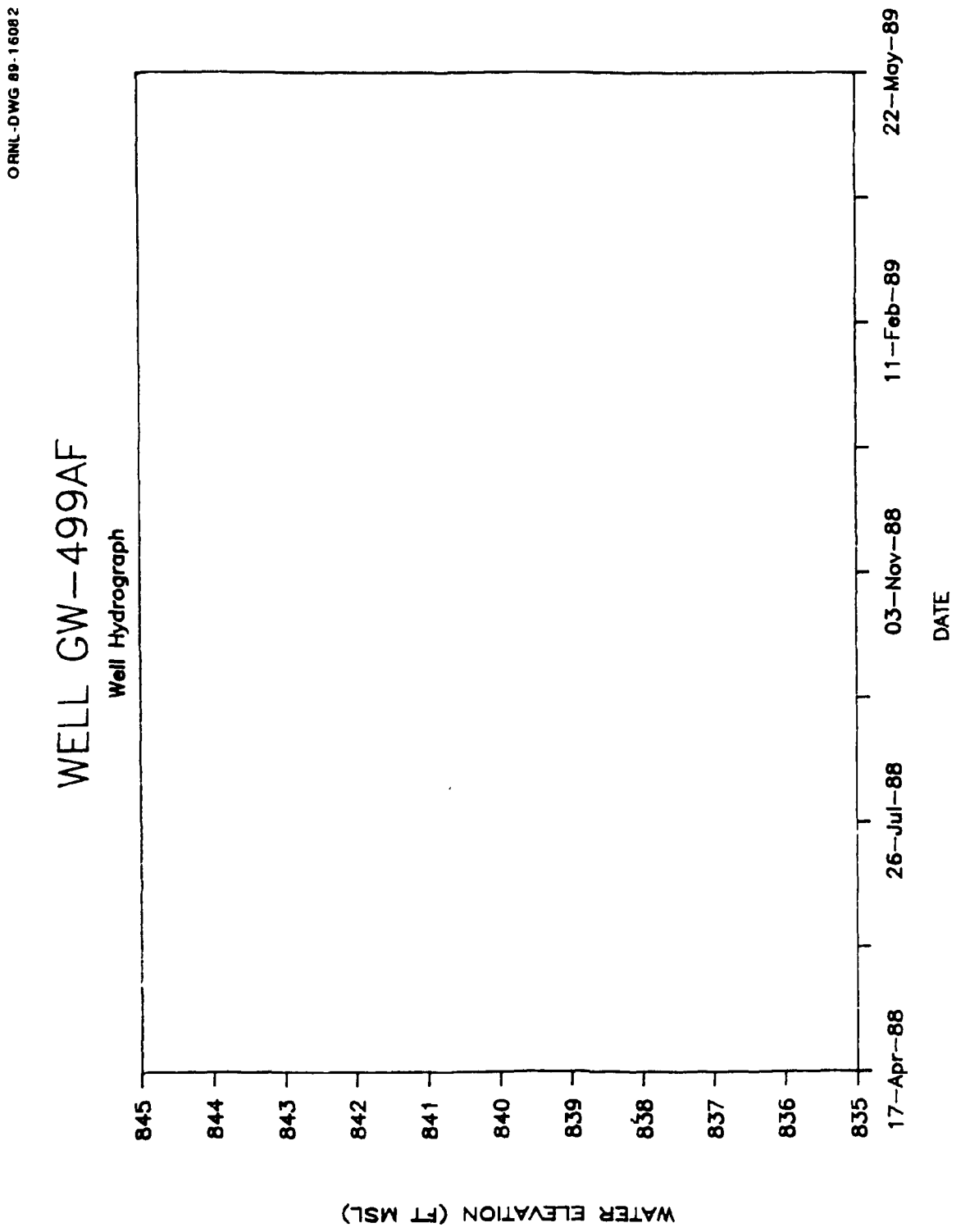
ORNL-DWG 89-16082
WELL GW-499AF
Well Hydrograph
WATER ELEVATION (FT MSL)
845
844
843
842
841
840
839
838
837
836
835
17-Apr-88
26-Jul-88
03-Nov-88
11-Feb-89
22-May-89
DATE

APPENDIX B

TRACER ARRIVAL CURVES

ORNL-DWG 89-15993

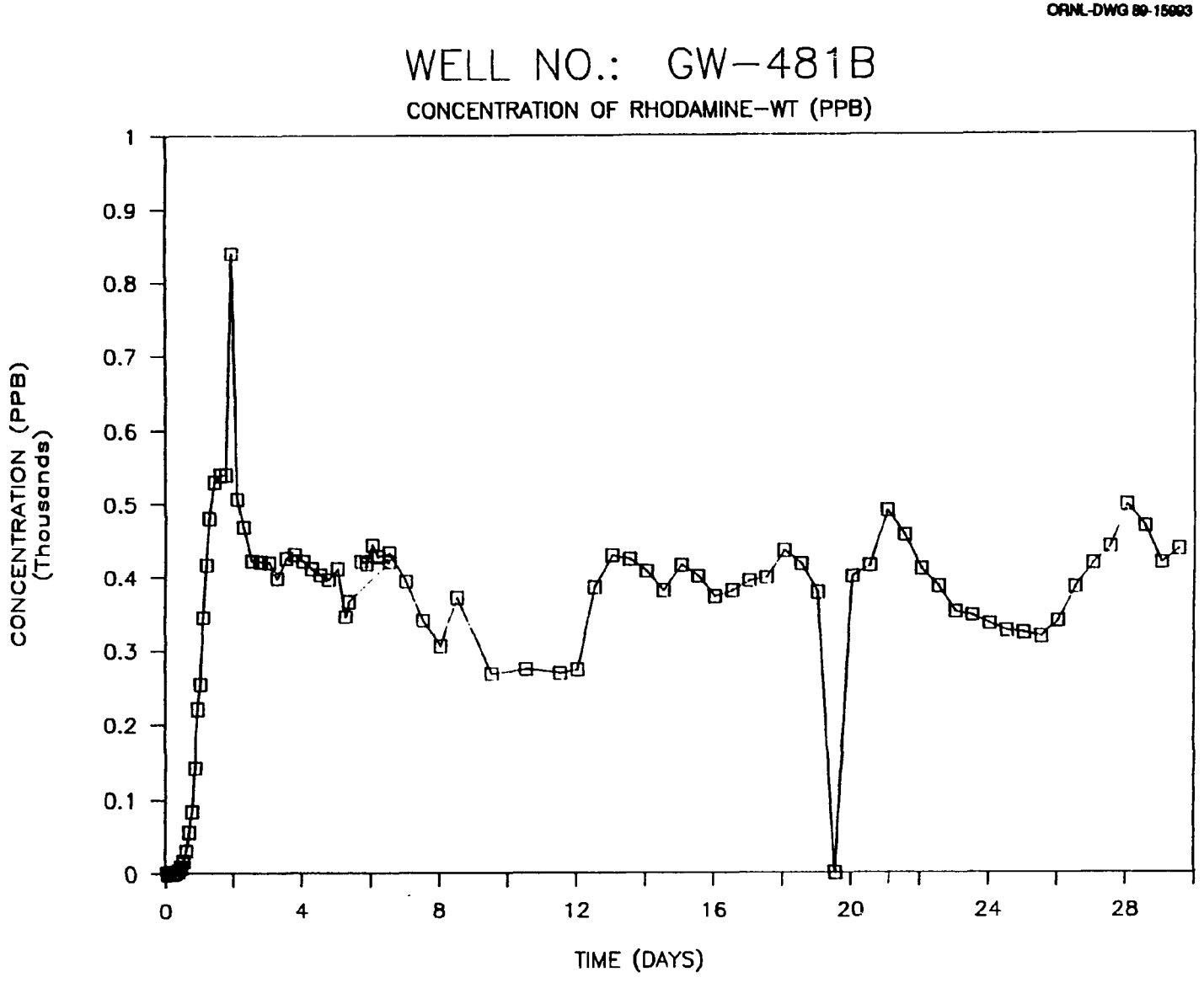

ORNL-DWG 89-15994

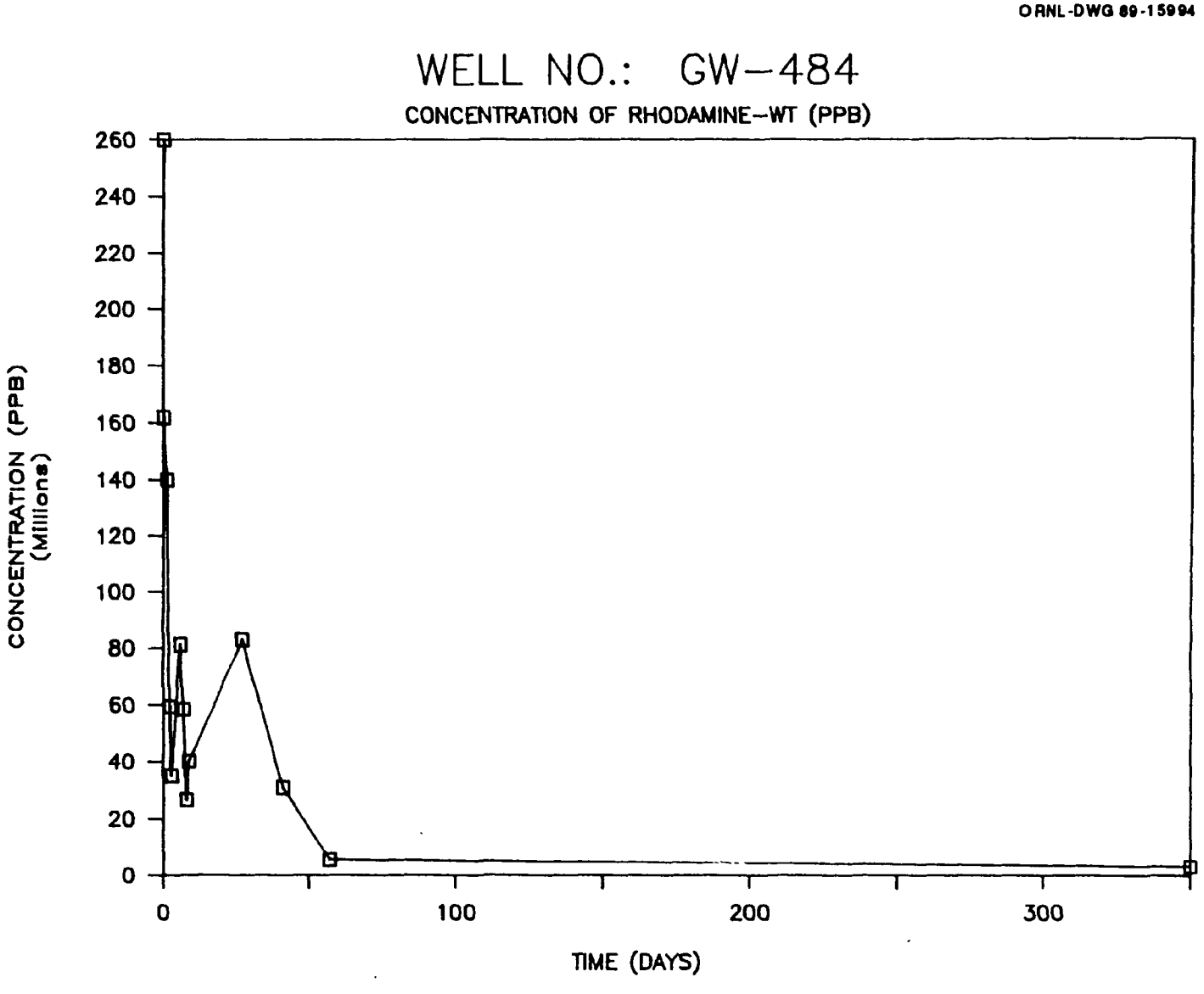

ORNL-DWG 89-15095

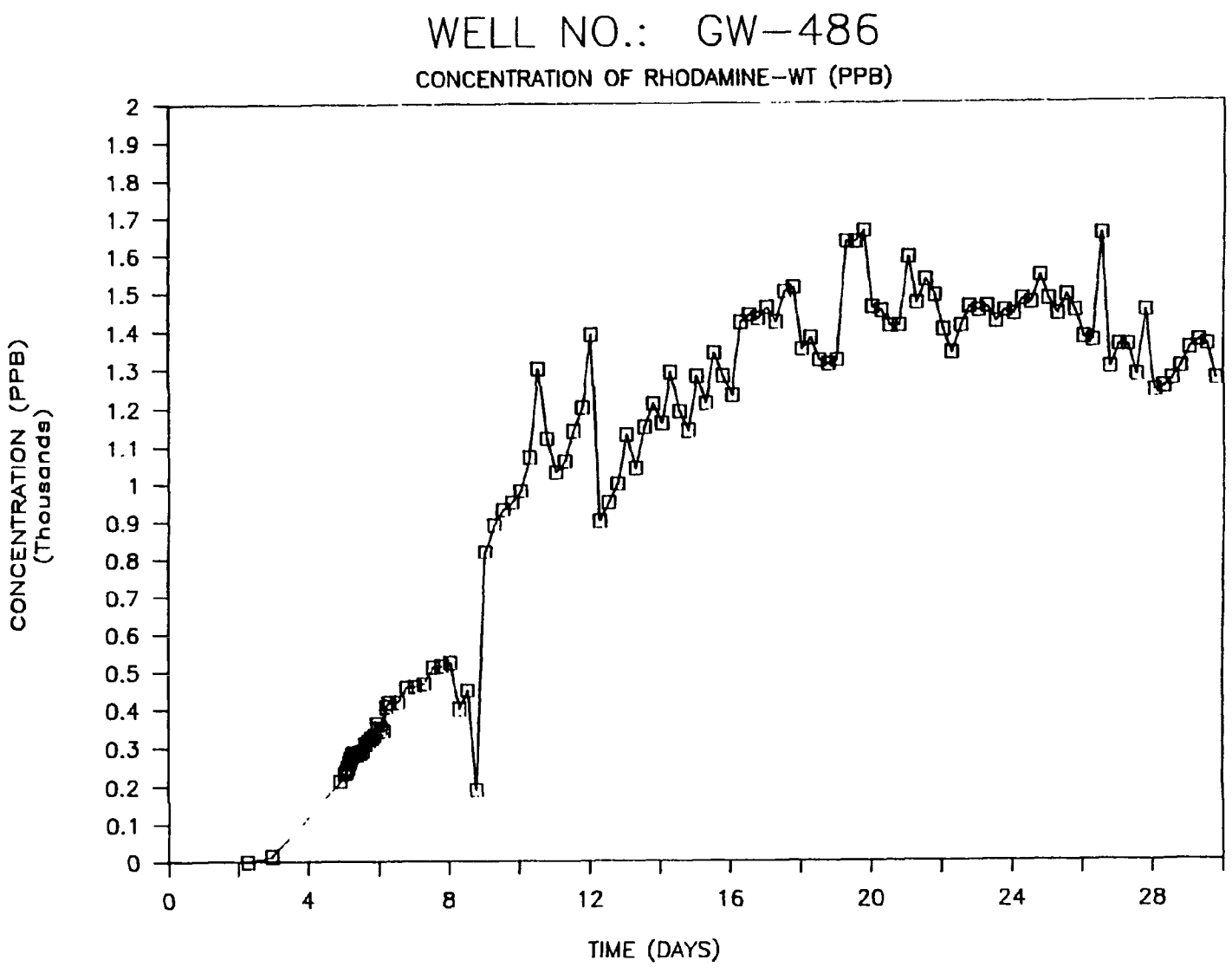

ORNL-DWG 89-15997

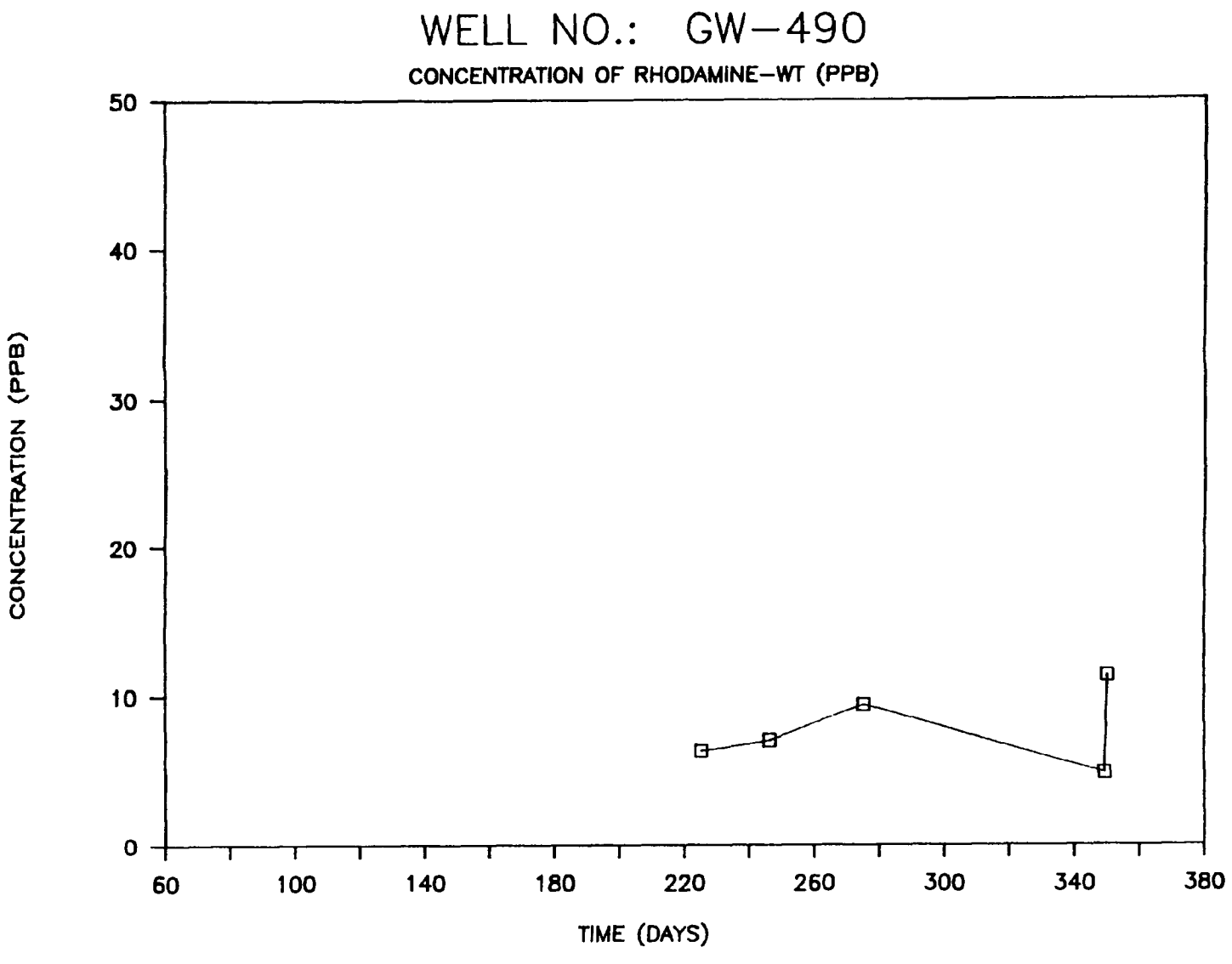

ORNL-DWG 89-15998

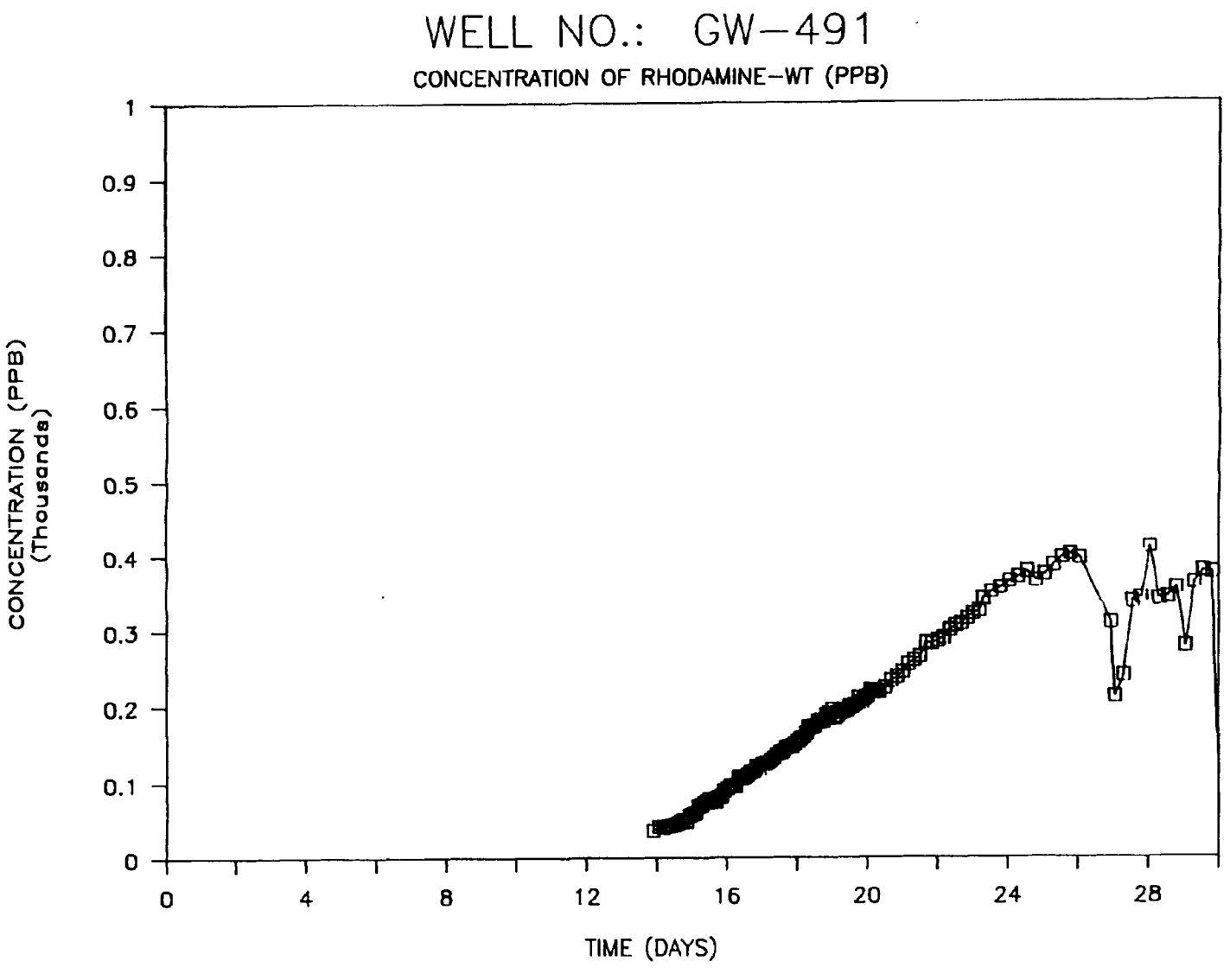

ORNL-DWG 89-15999

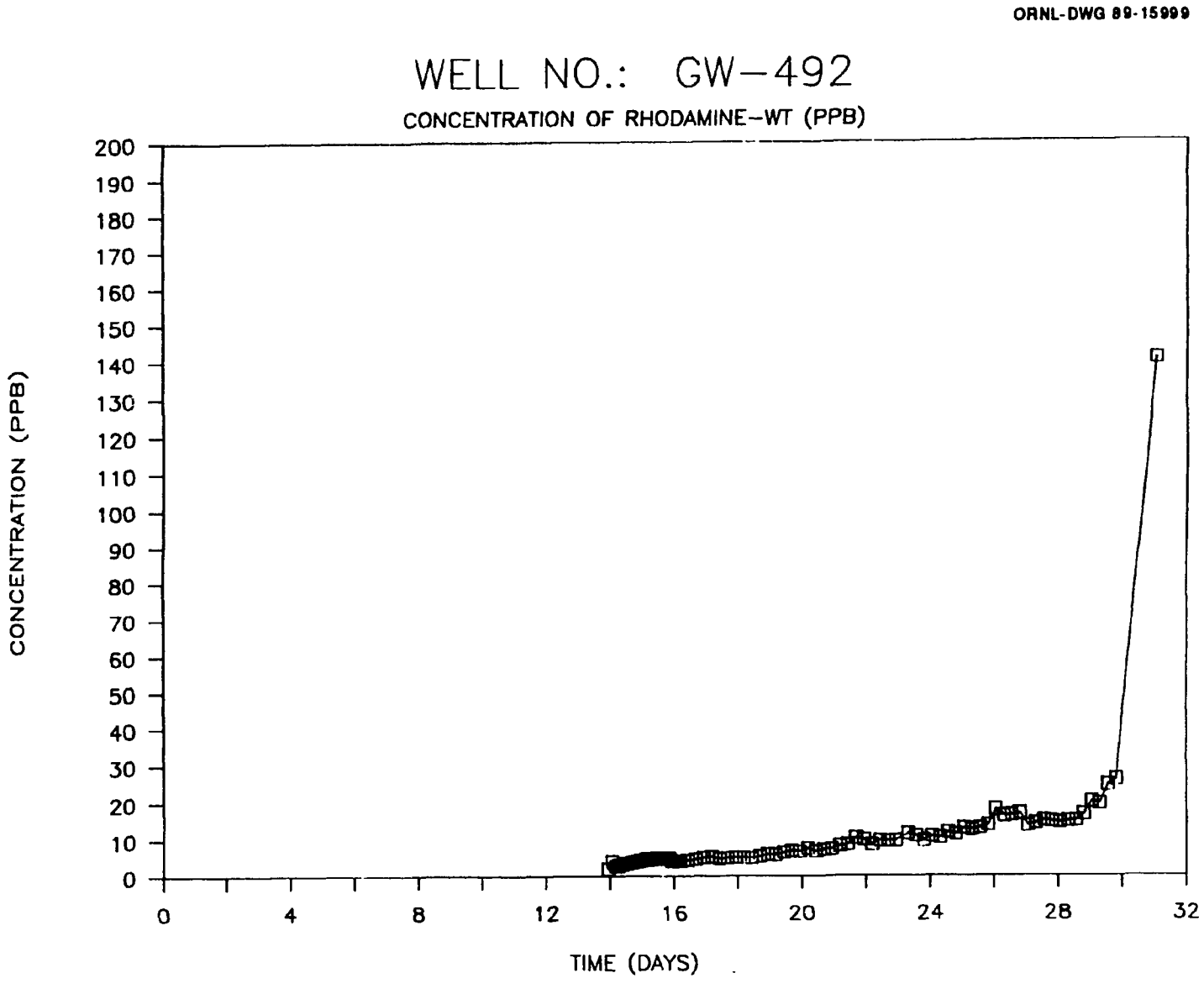

ORNL-DWG 89-16000

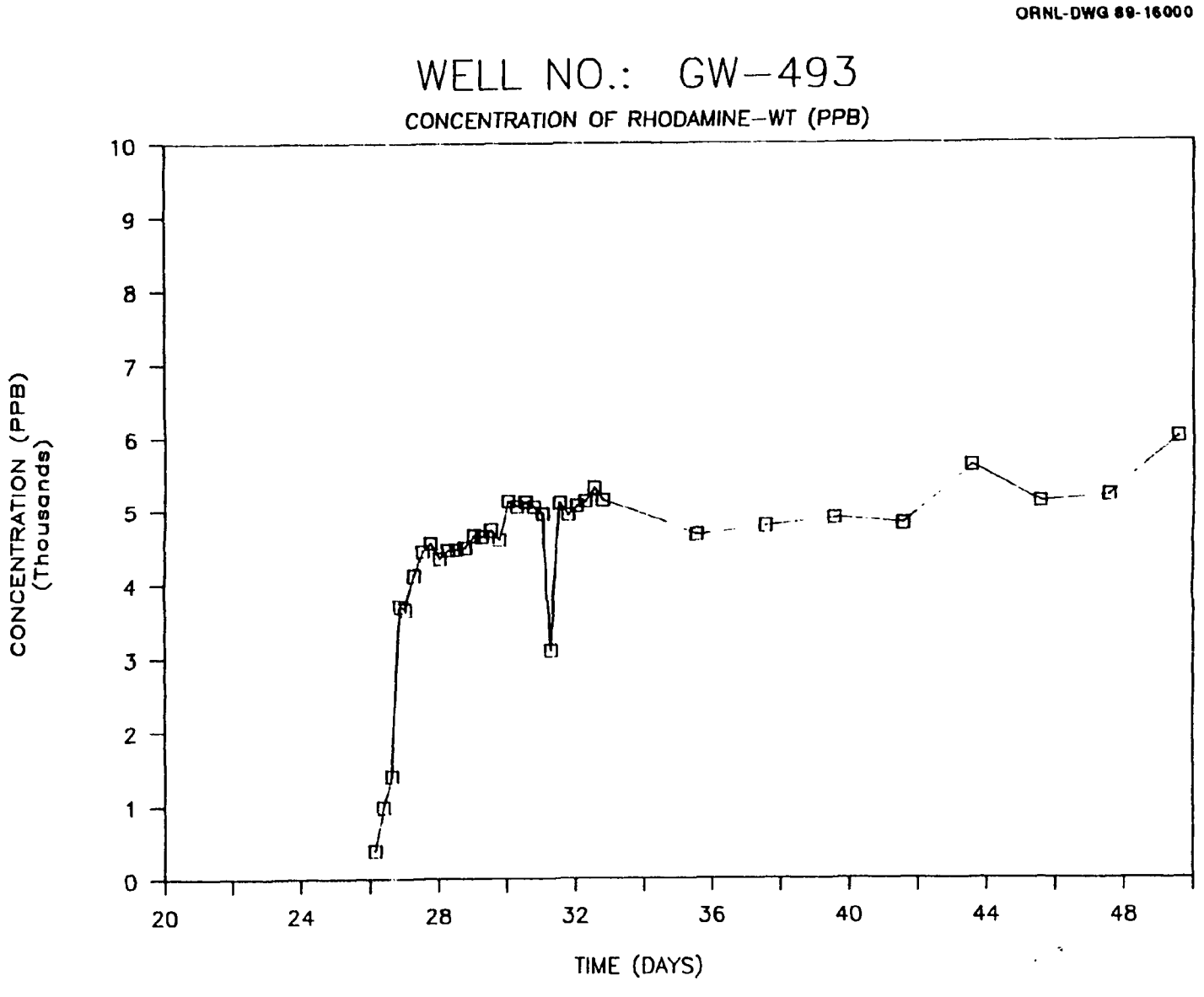

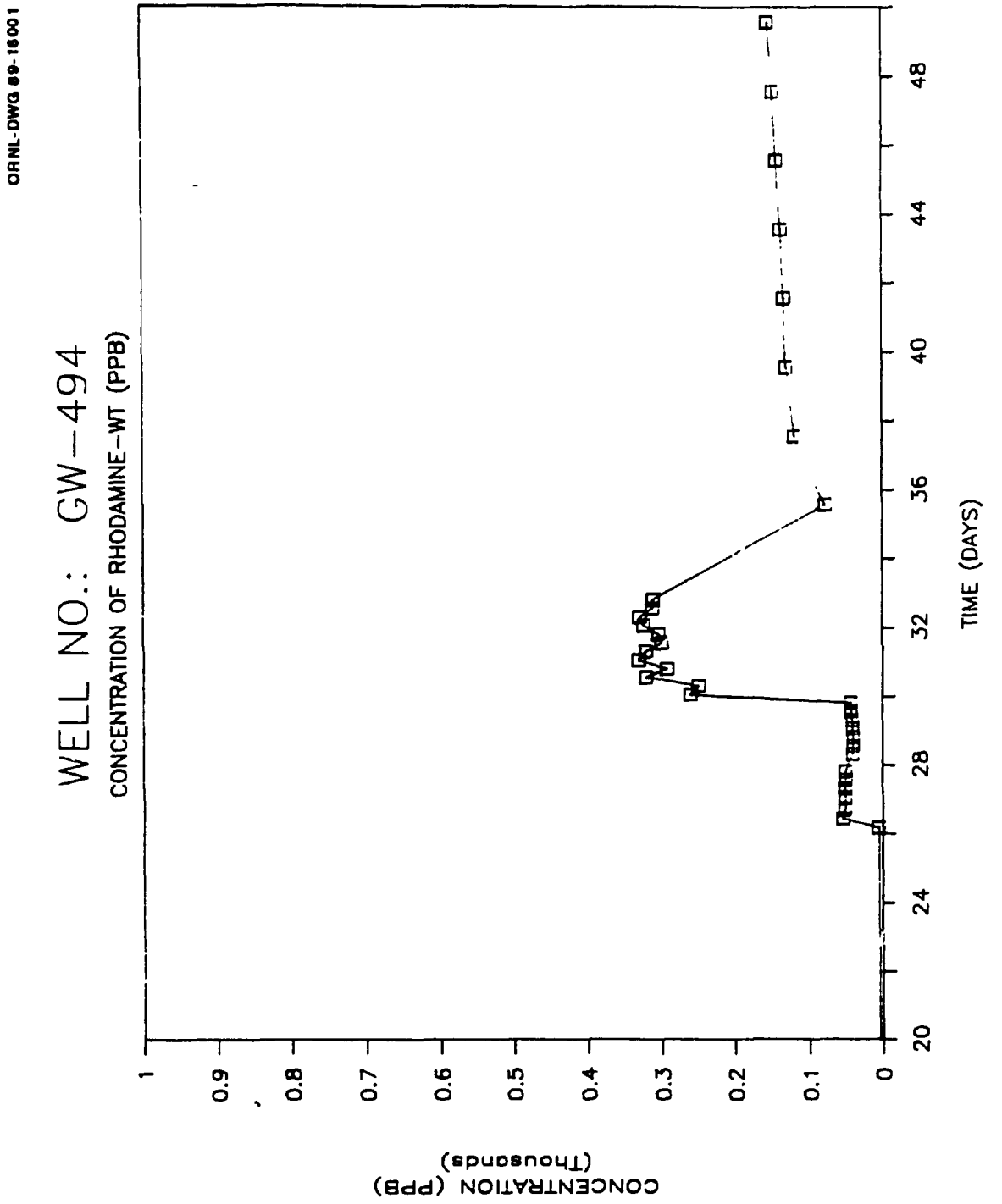
ORNL-DWG 89-16001
WELL NO.: GW-494
CONCENTRATION OF RHODAMINE-WT (PPB)
CONCENTRATION (PPB)
(Thousands)
1
0.9
0.8
0.7
0.6
0.5
0.4
0.3
0.2
0.1
0
20
24
28
32
36
40
44
48
TIME (DAYS)

ORNL-DWG 89-16002

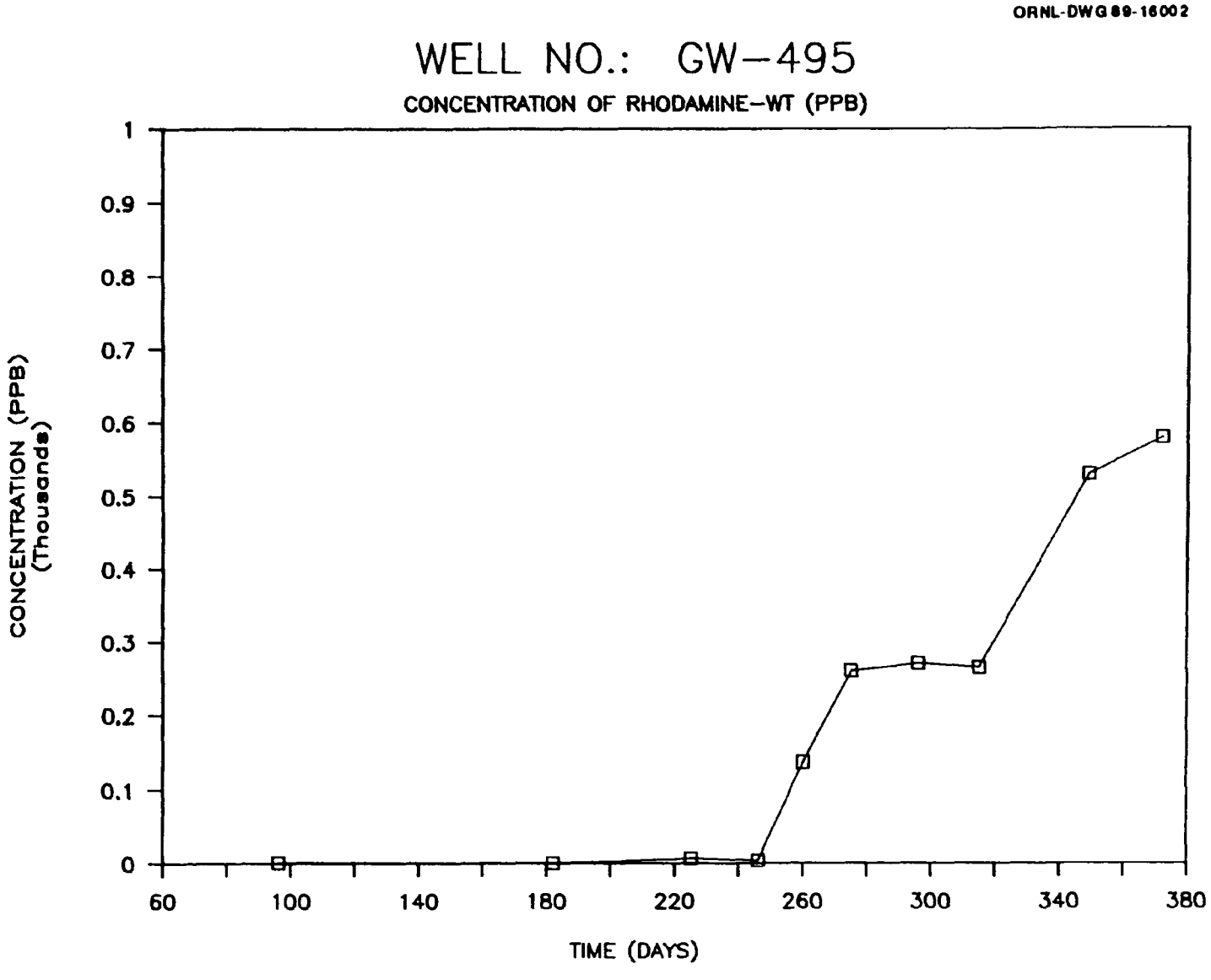

ORNL-DWG 89-16003

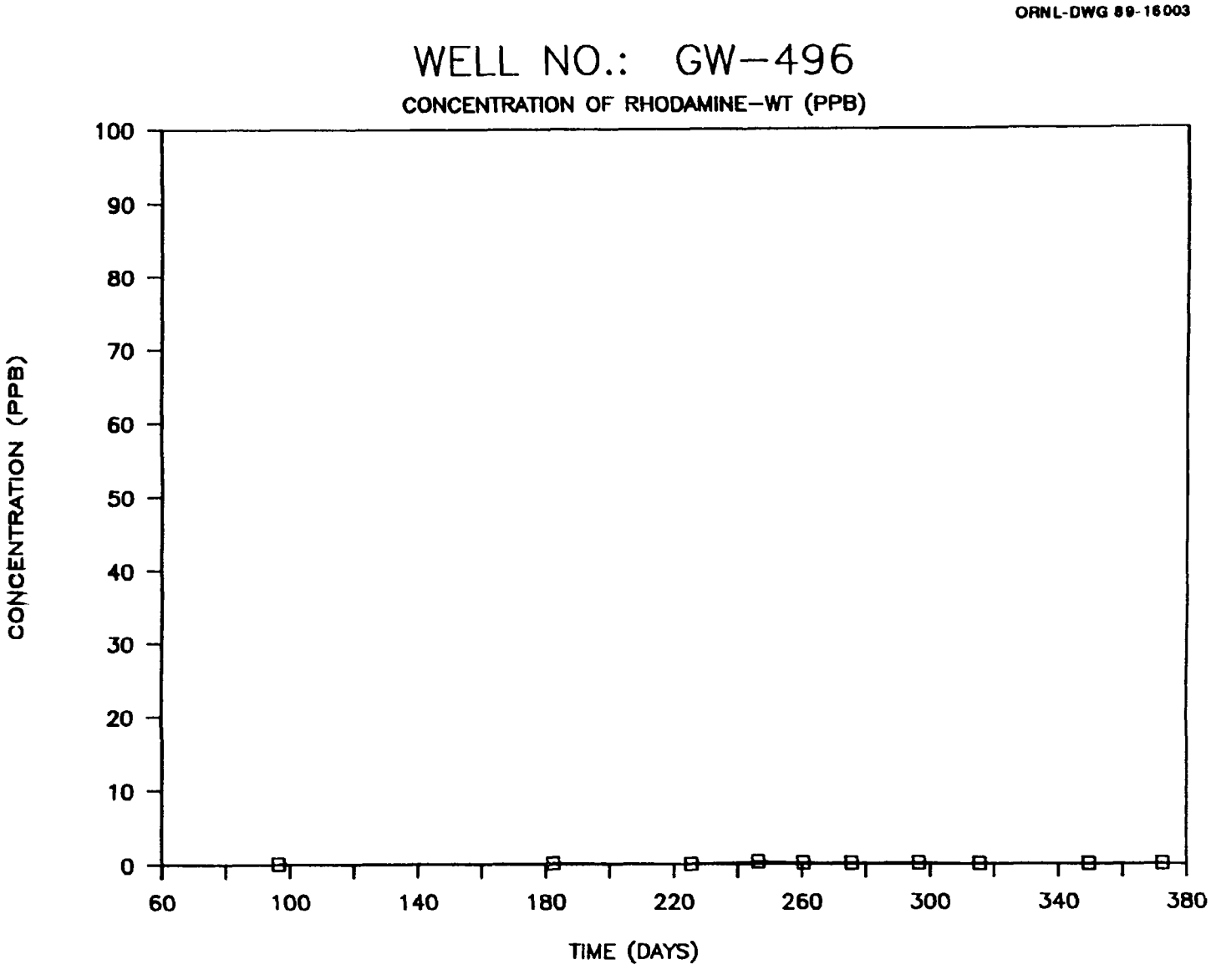

ORNL-DWG 89-16004

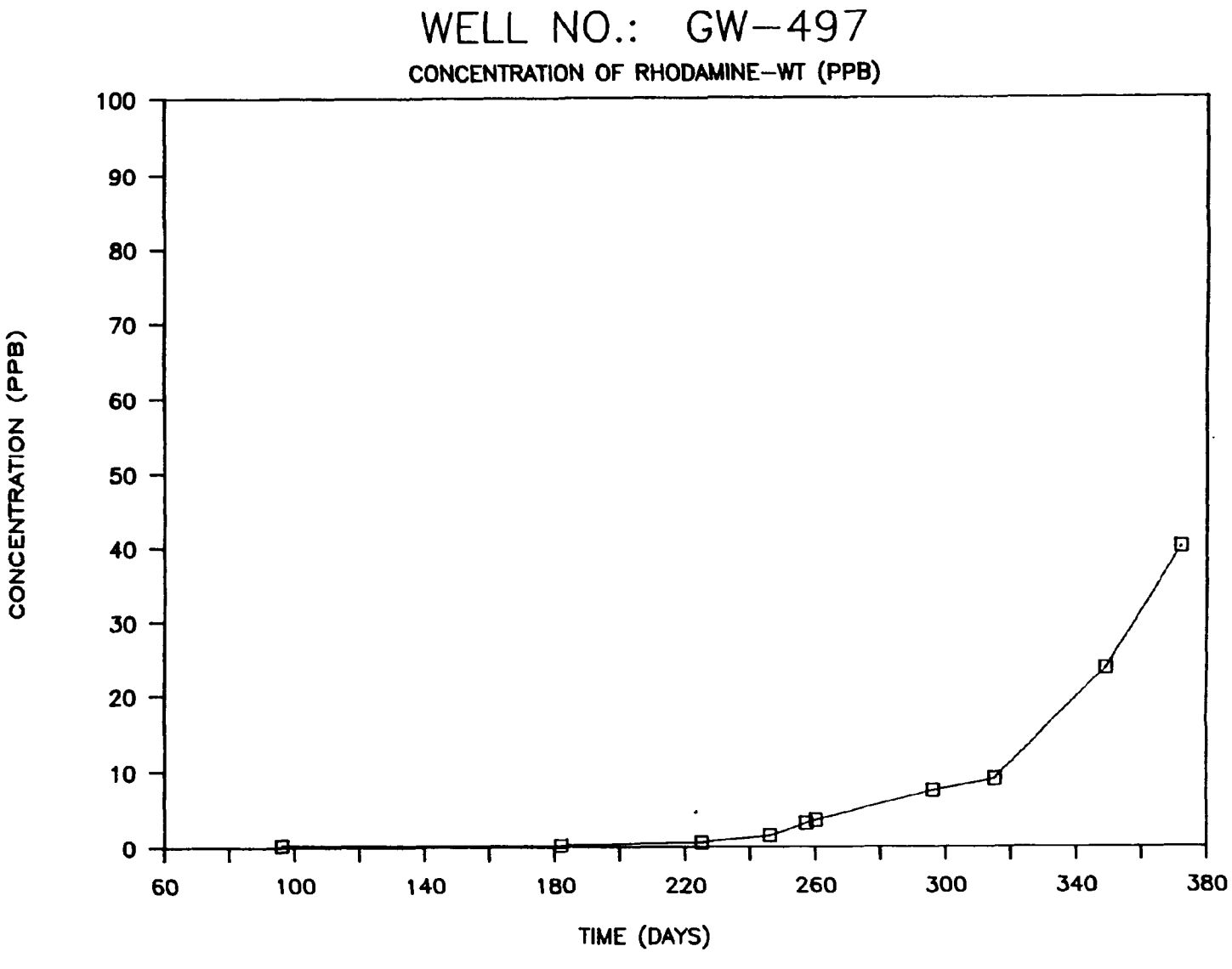

ORNL-DWG 89-16005

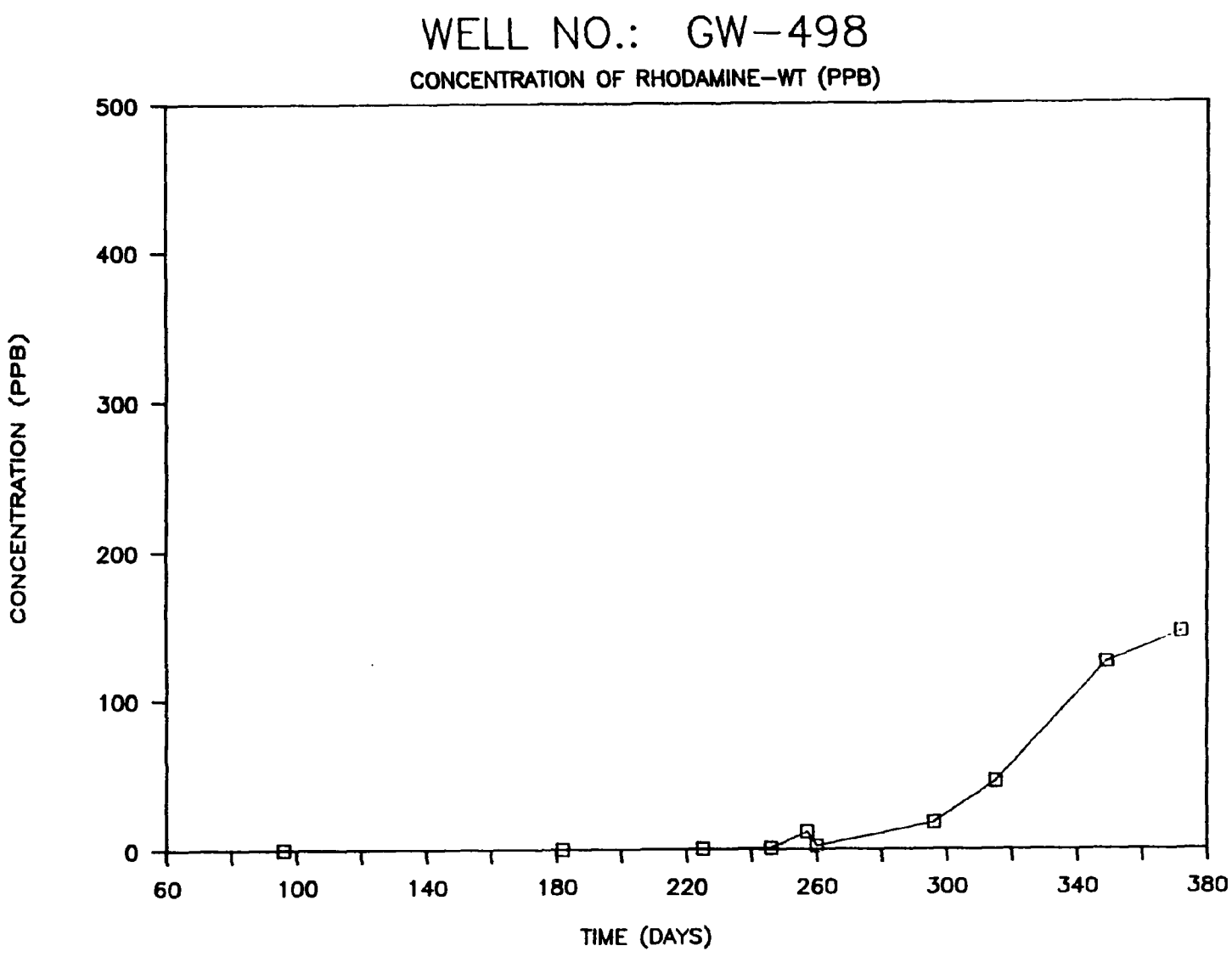

ORNL-DWG 89-16006

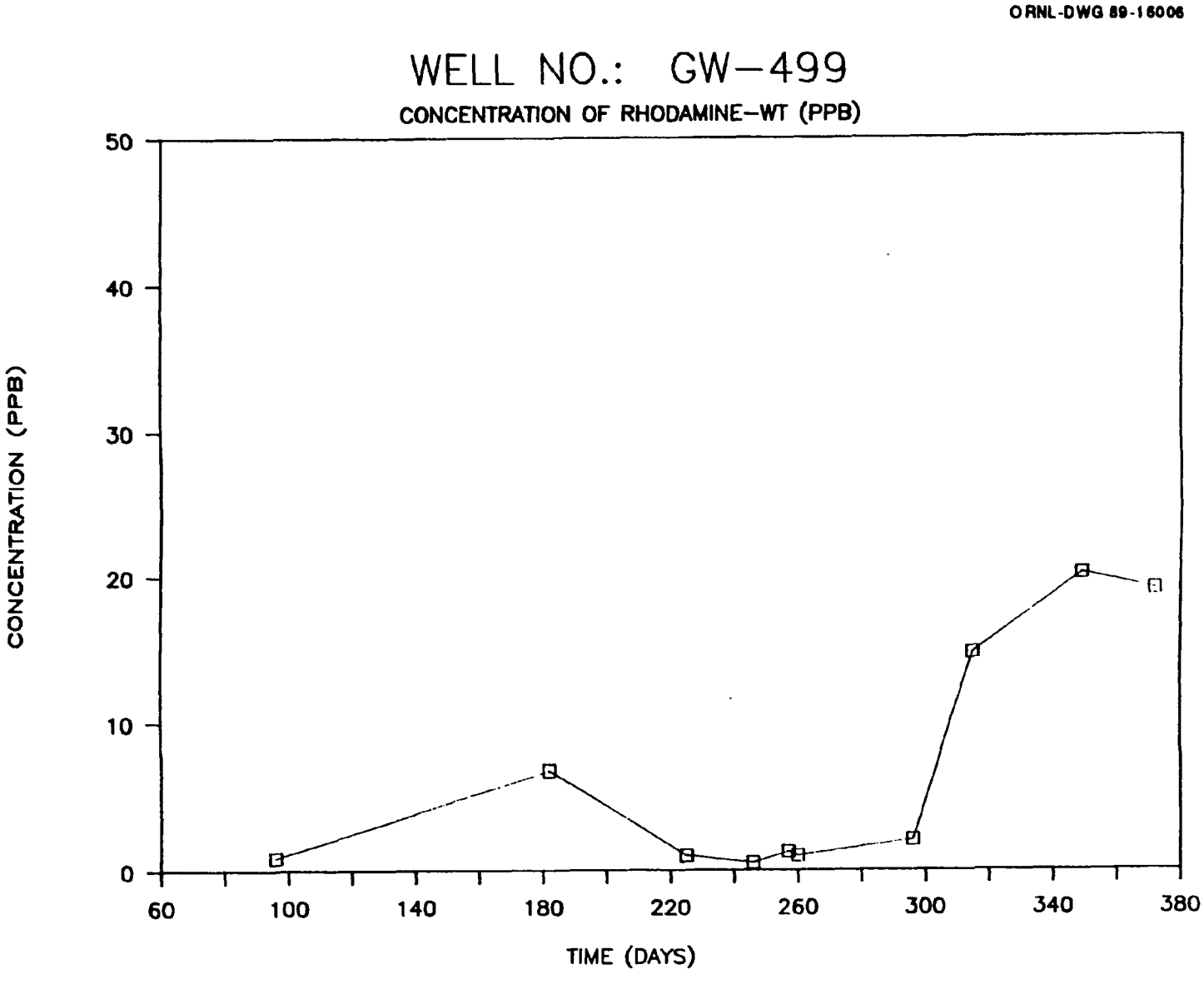

ORNL-DWG 89-16007

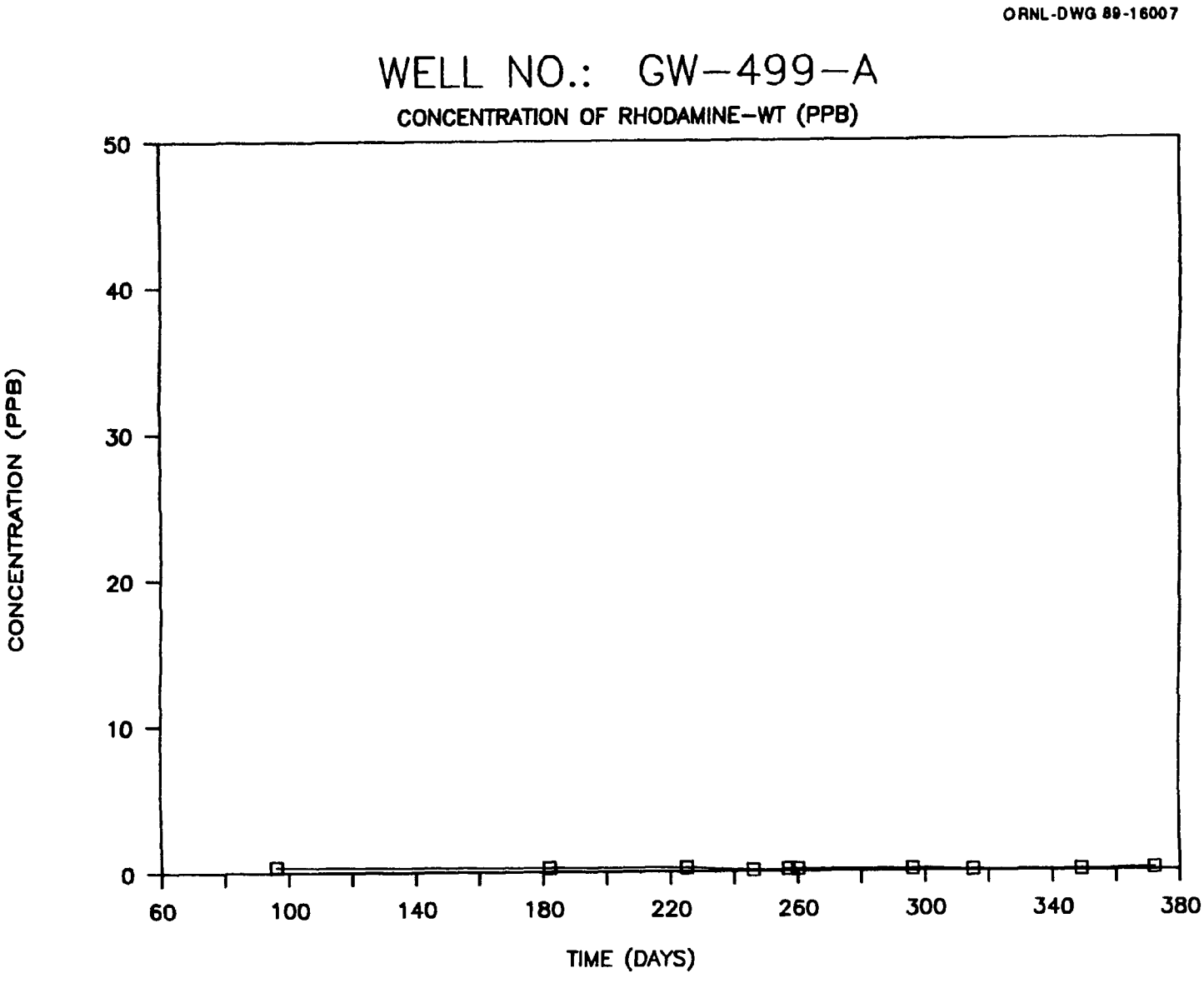

ORNL-DWG 89-16008

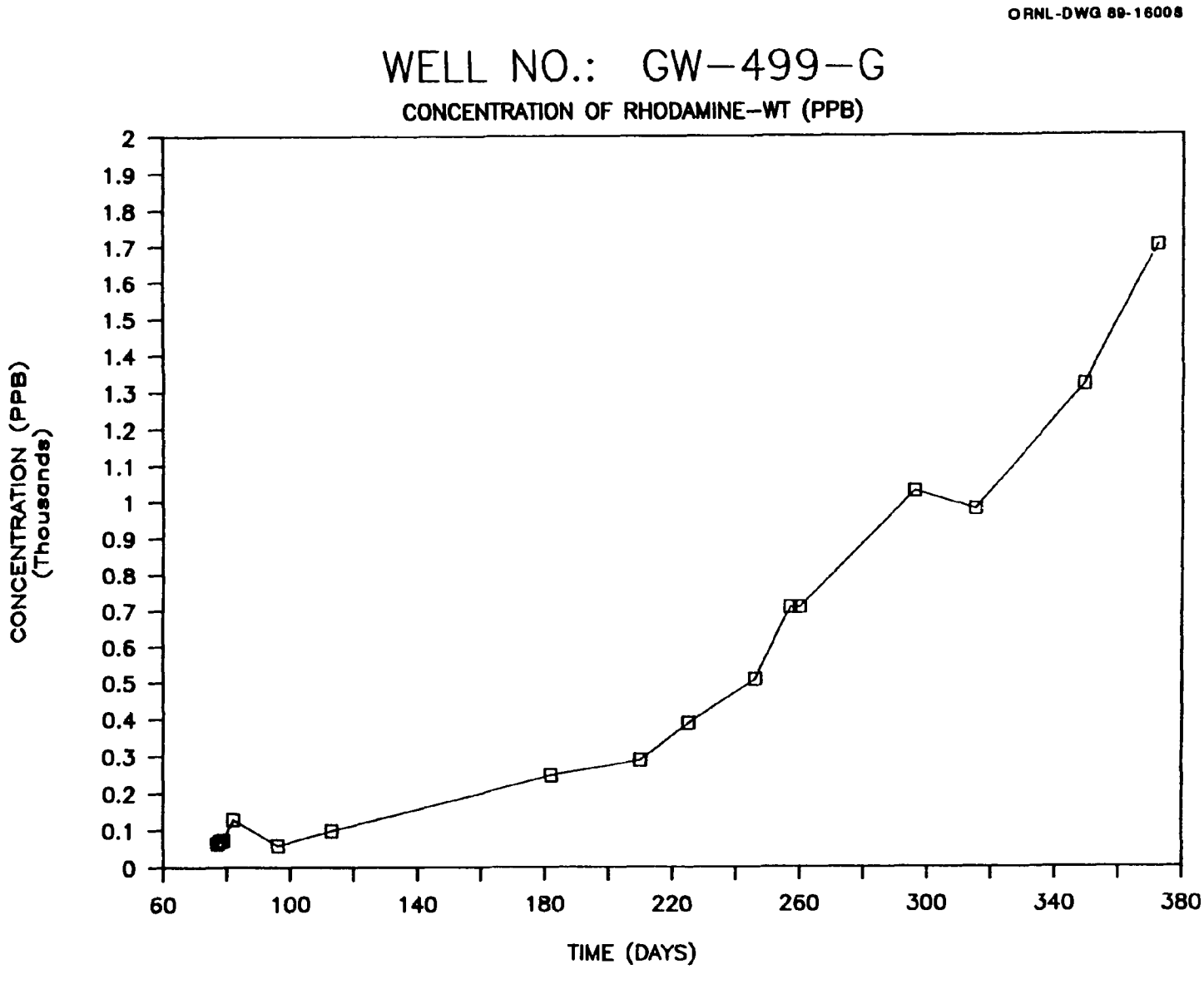

ORNL-DWG 89-16009

WELL NO.: GW-499-H

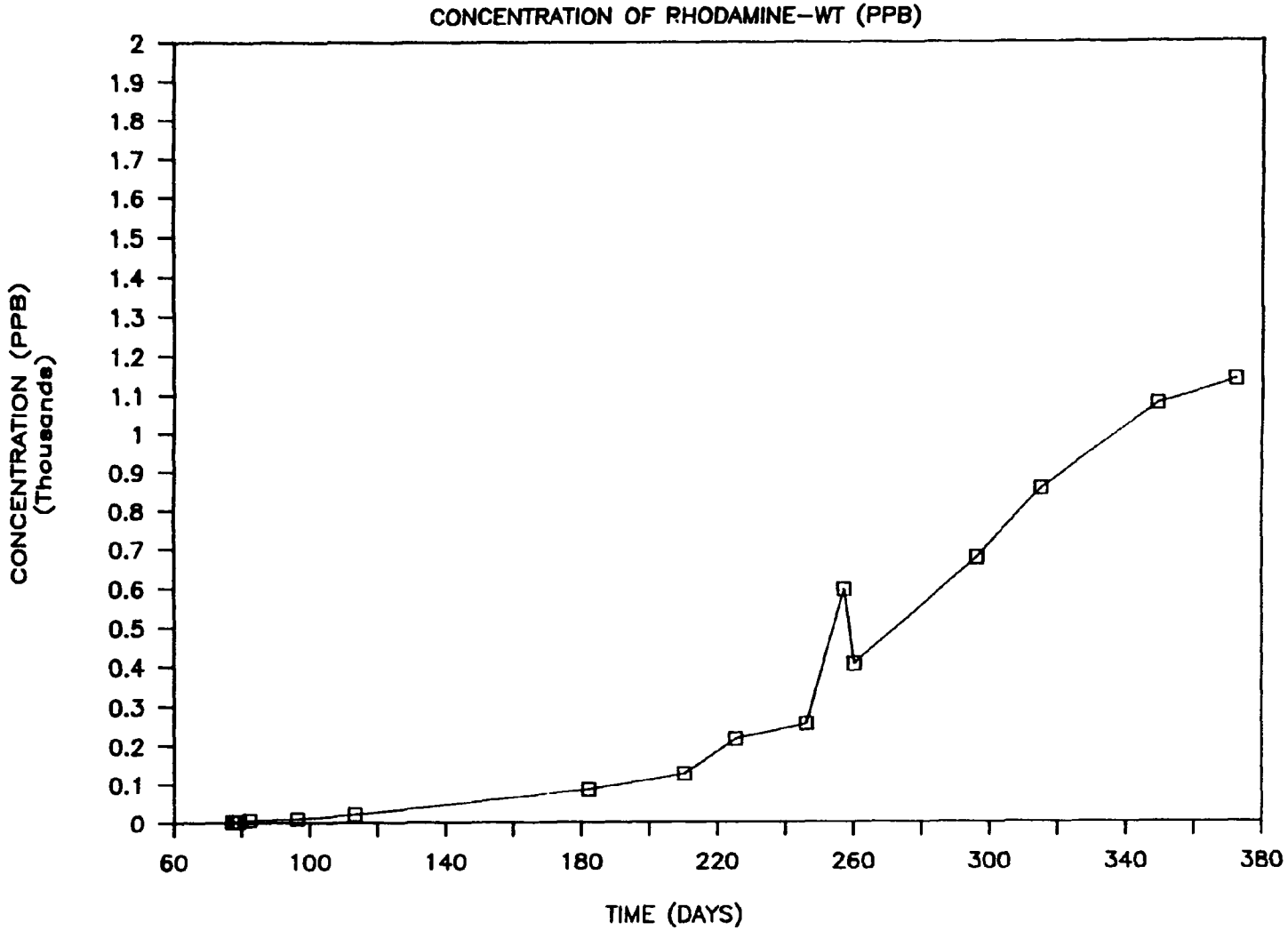

ORNL-DWG 89-16010

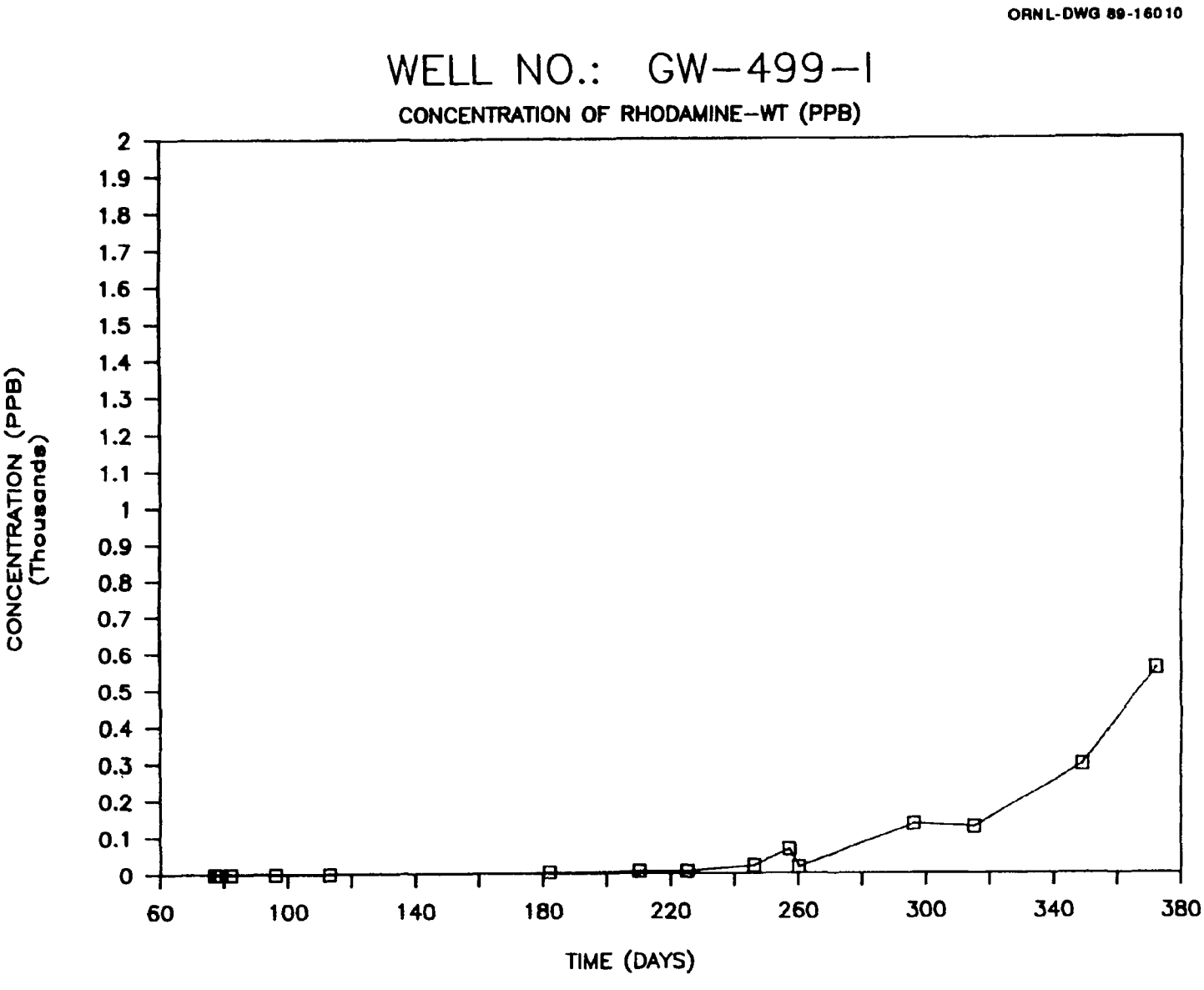

ORNL-DWG 89-16011

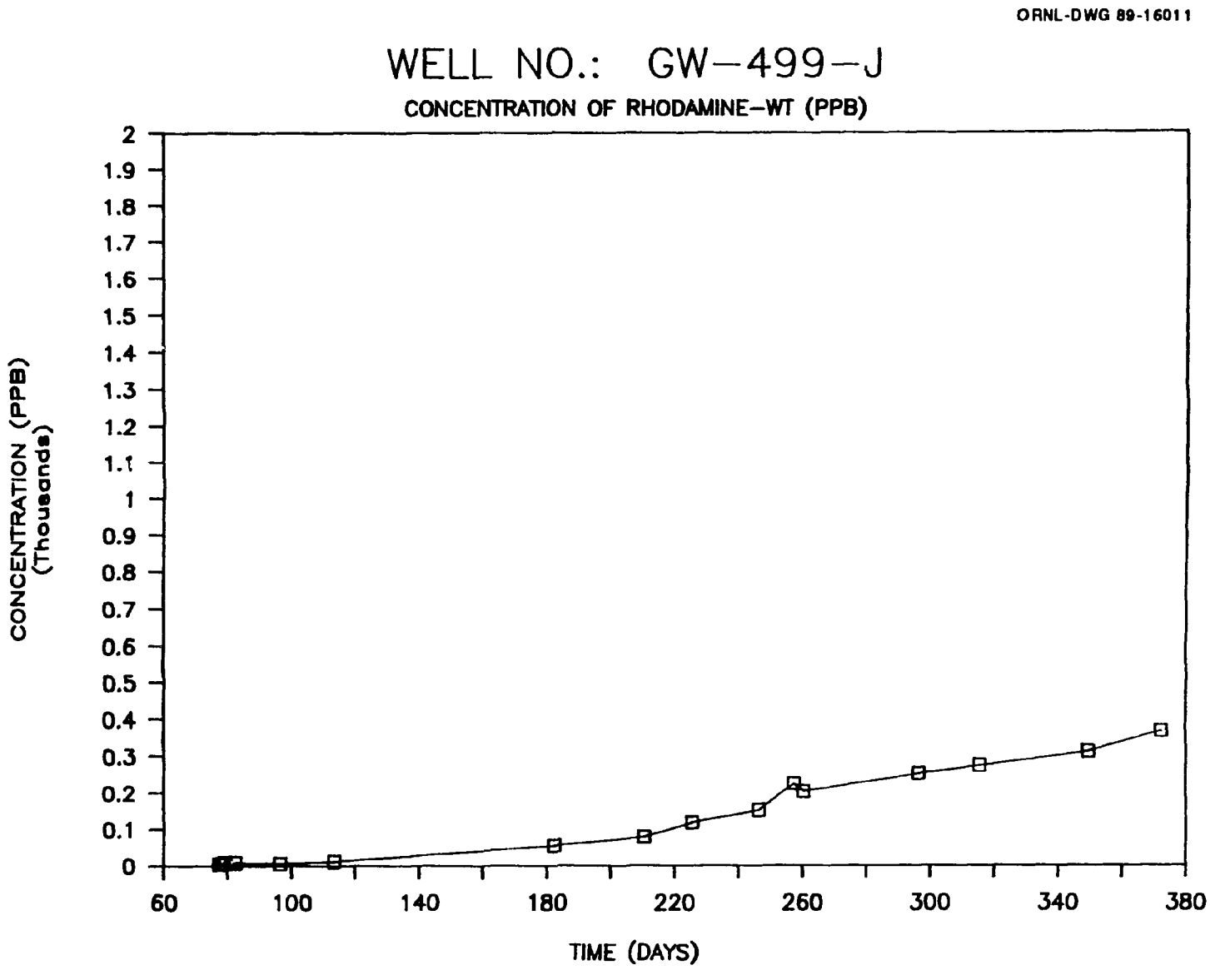

ORNL-DWG 89-16012

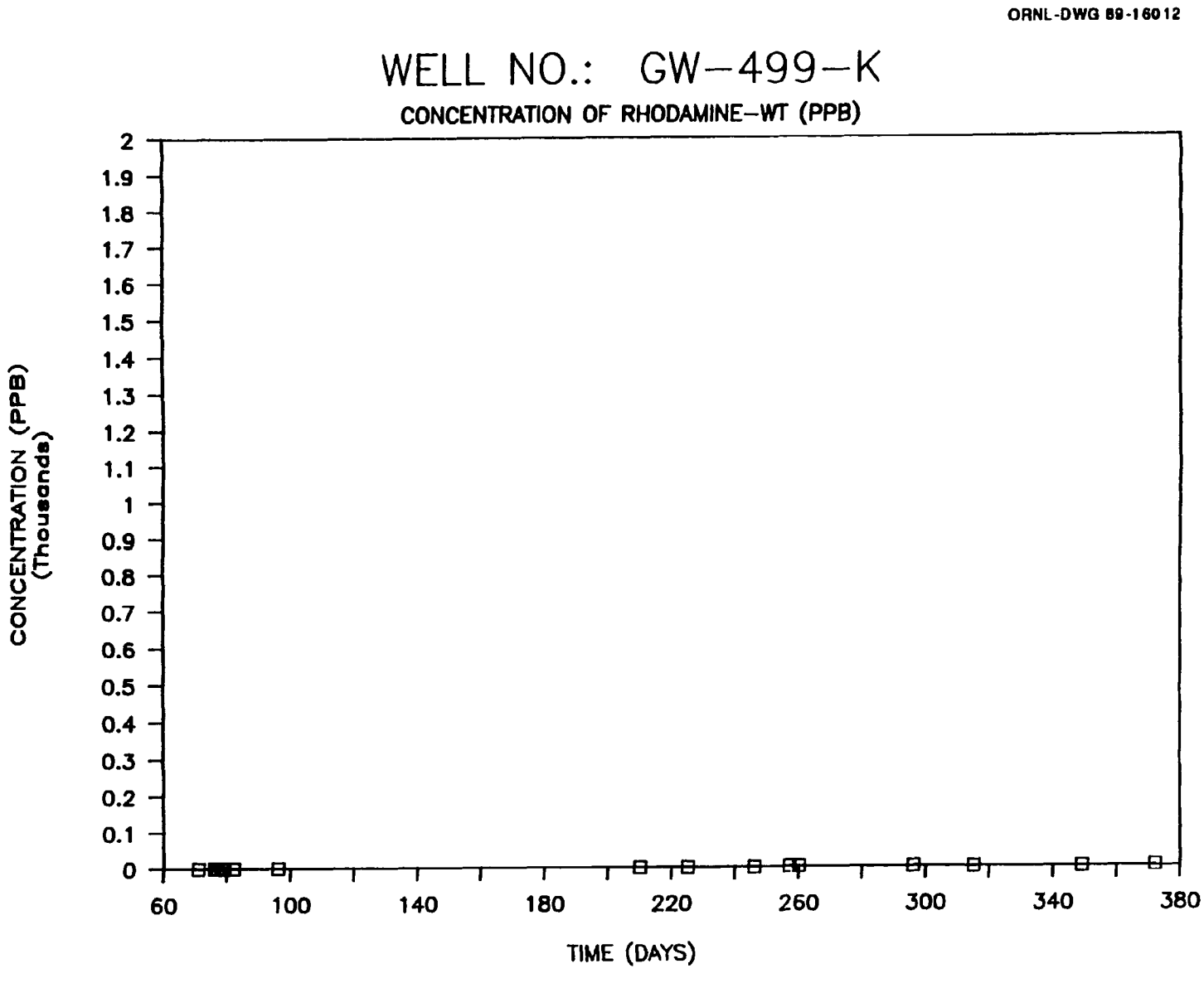

ORNL-DWG 89-16013

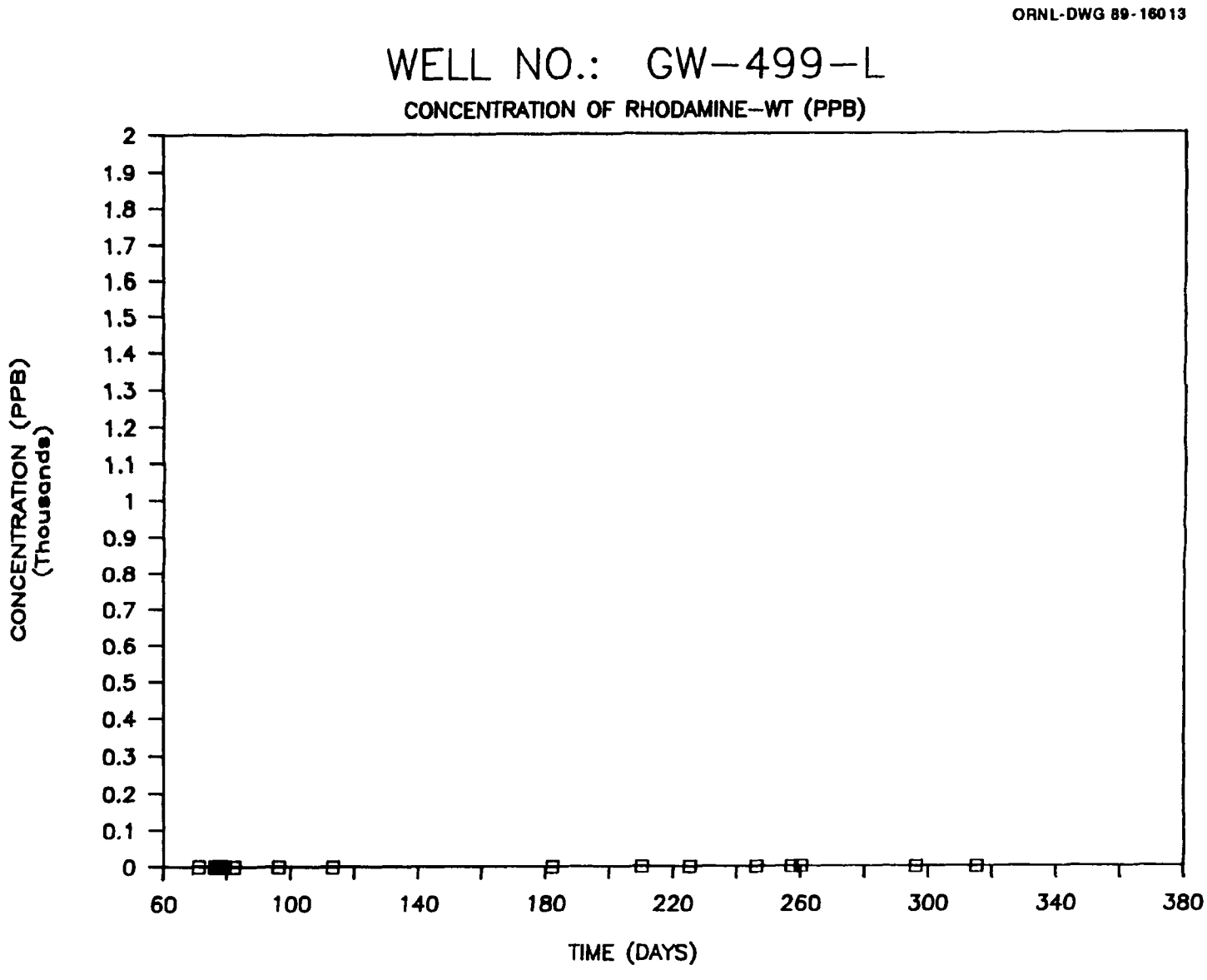

ORNL-DWG 89-16014

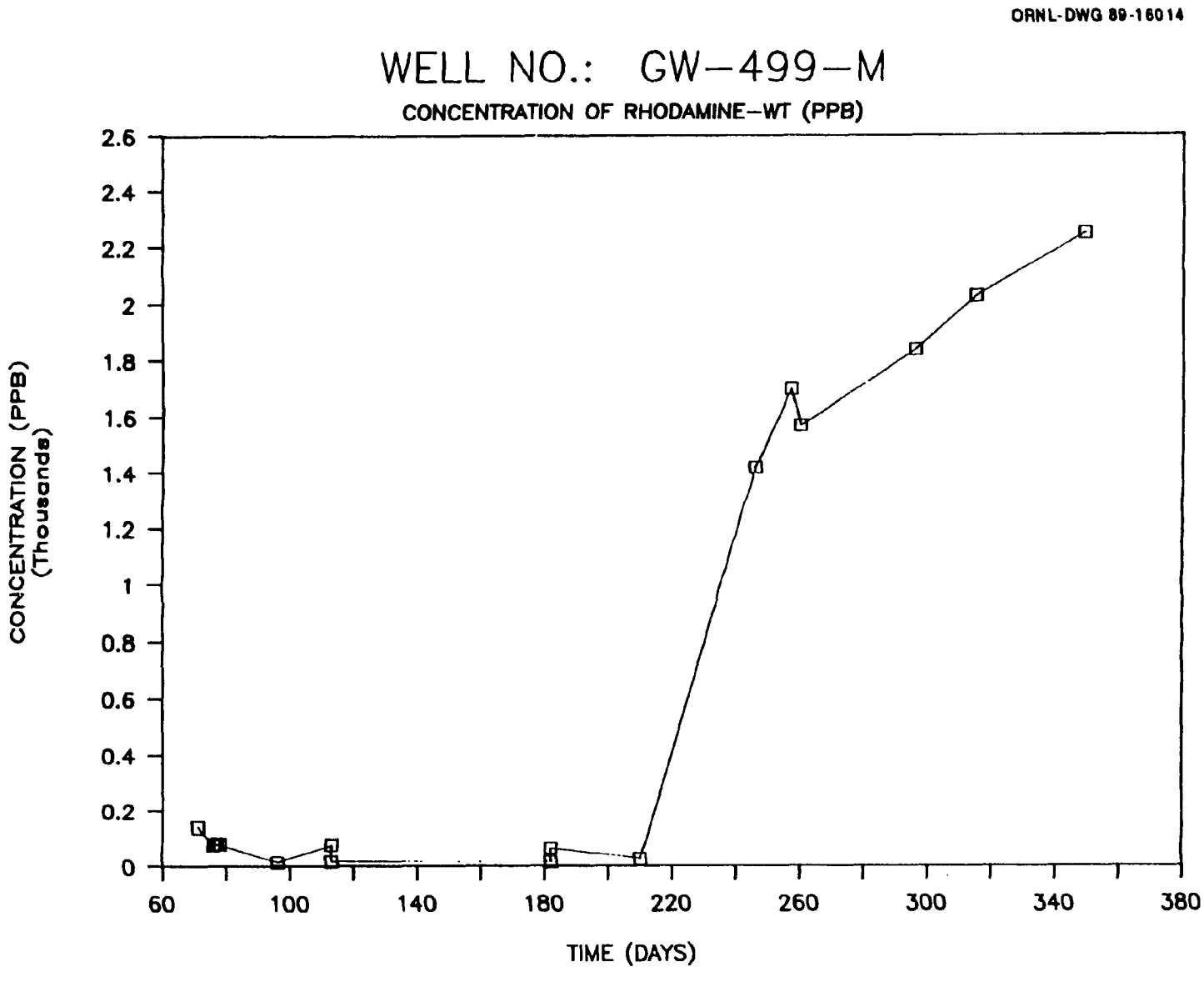

ORNL-DWG 89-16015

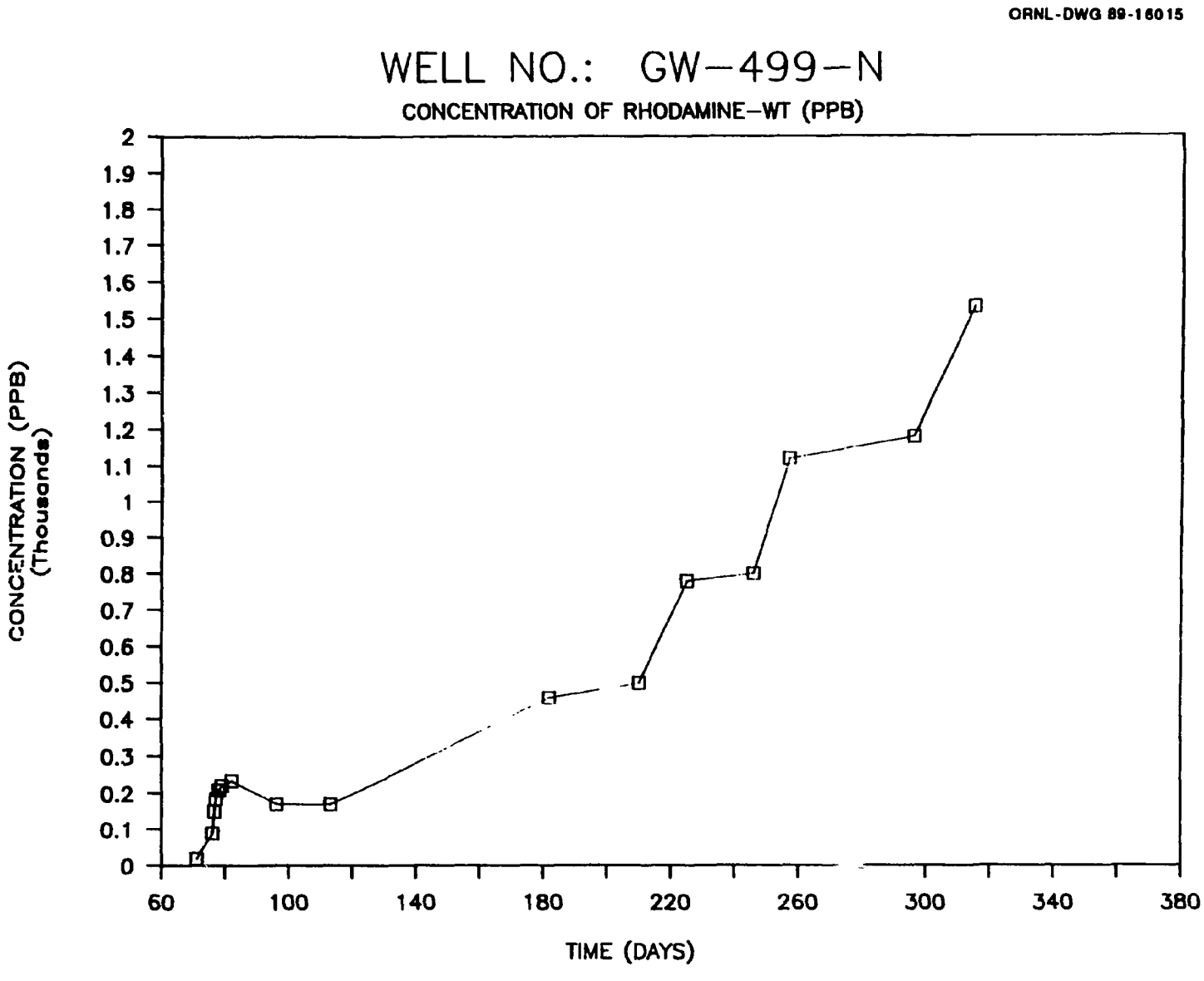

ORNL-DWG 89-16018

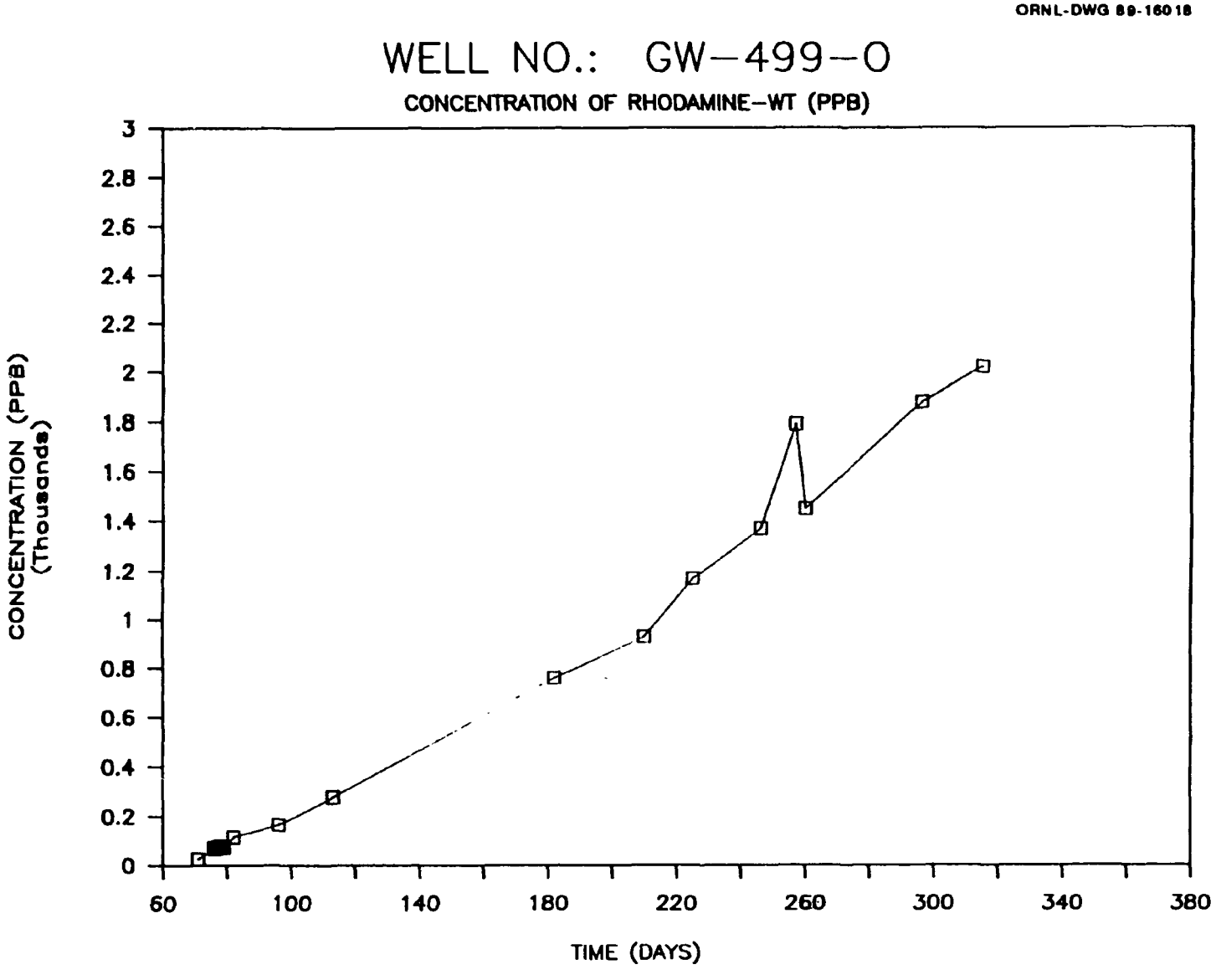

ORNL-DWG 89-16017

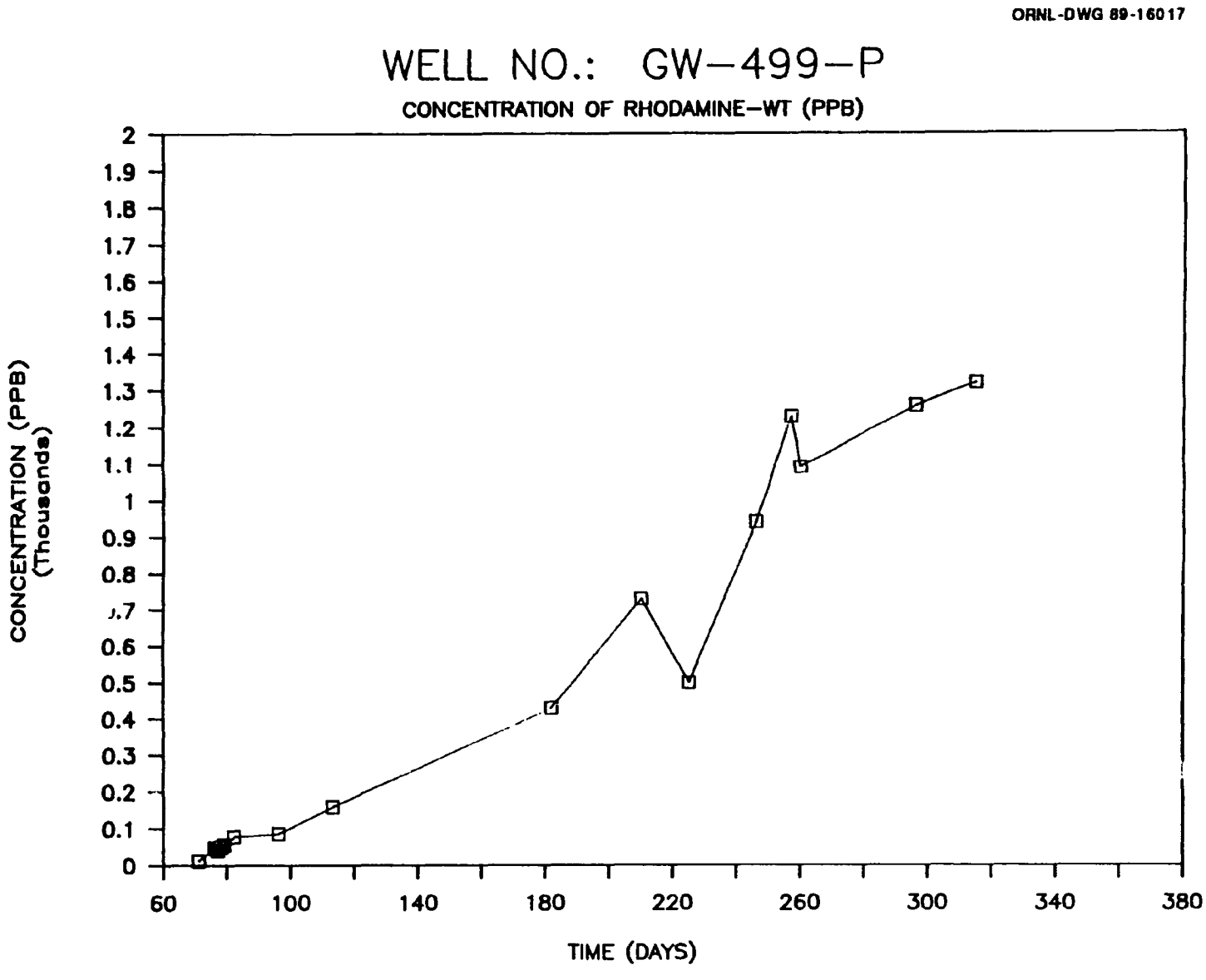

NORTHING
*10'
2985.0
2990.0
2995.0
3000.0
B40
B50
CR2
B40
CR3

MODEL VALIDAT

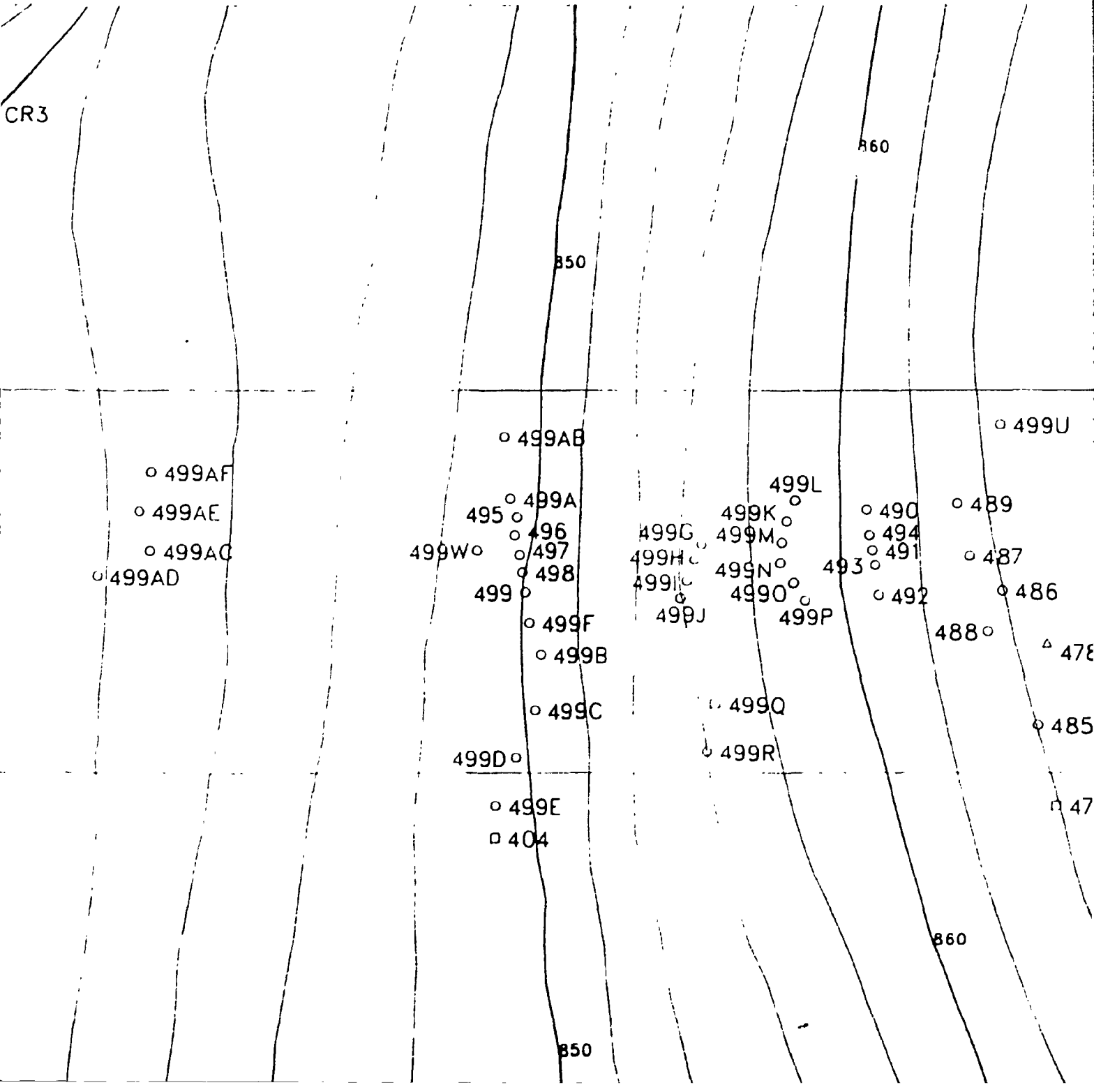

ATION SITE LOCATION MAP

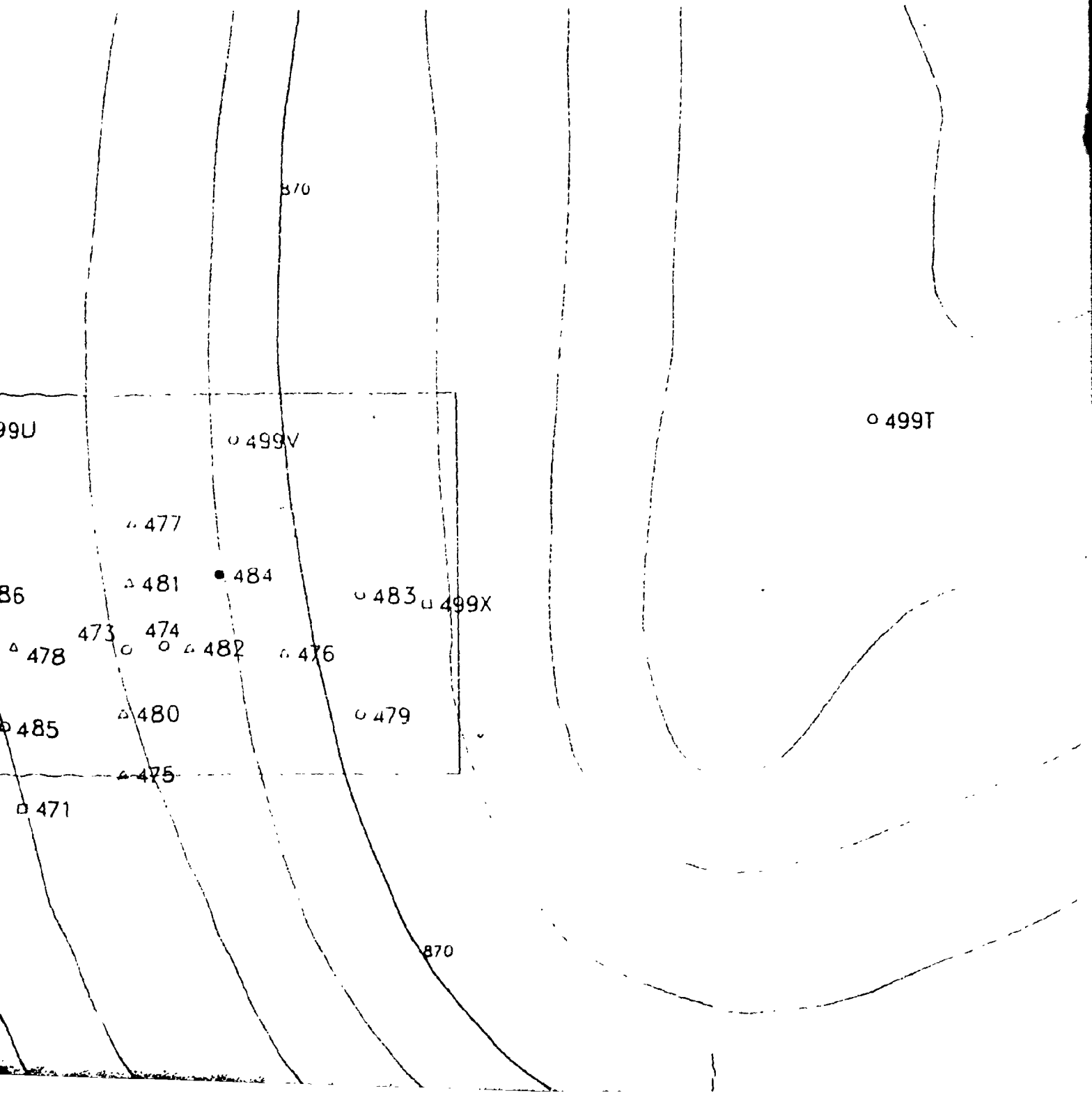

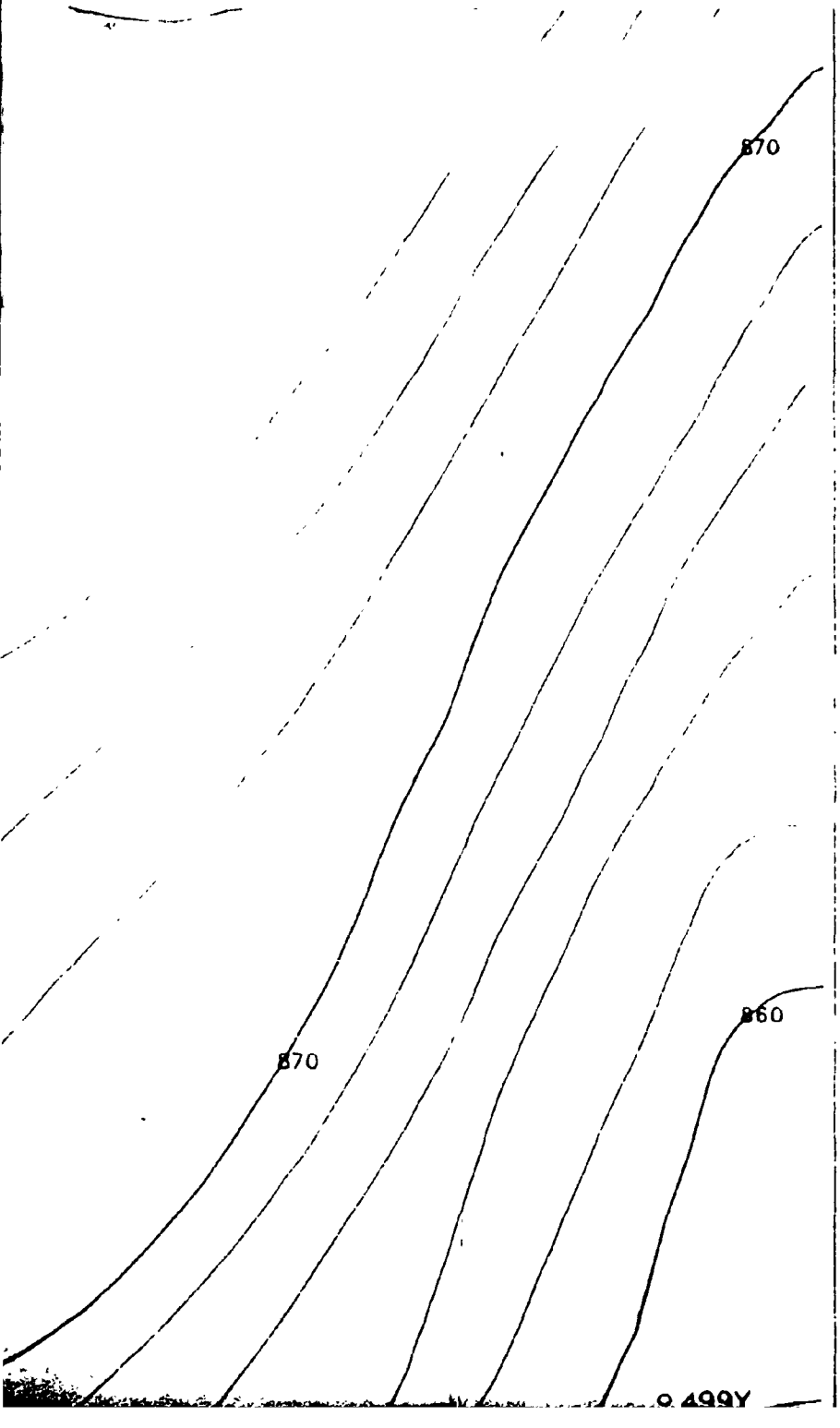
870
870
860
0.499Y

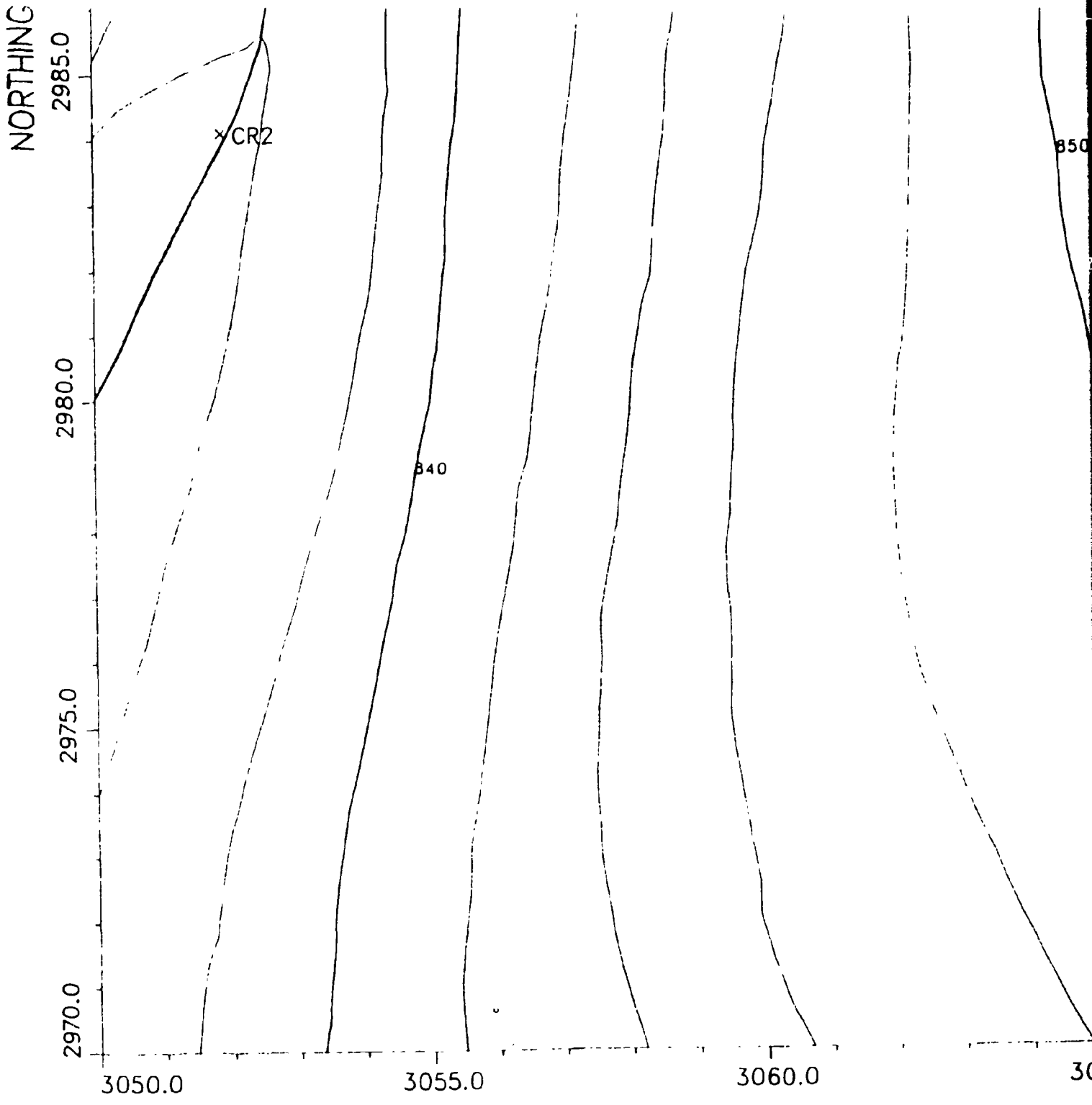
NORTHING
2985.0
2980.0
2975.0
2970.0
CR2
840
850
3050.0
3055.0
3060.0
30

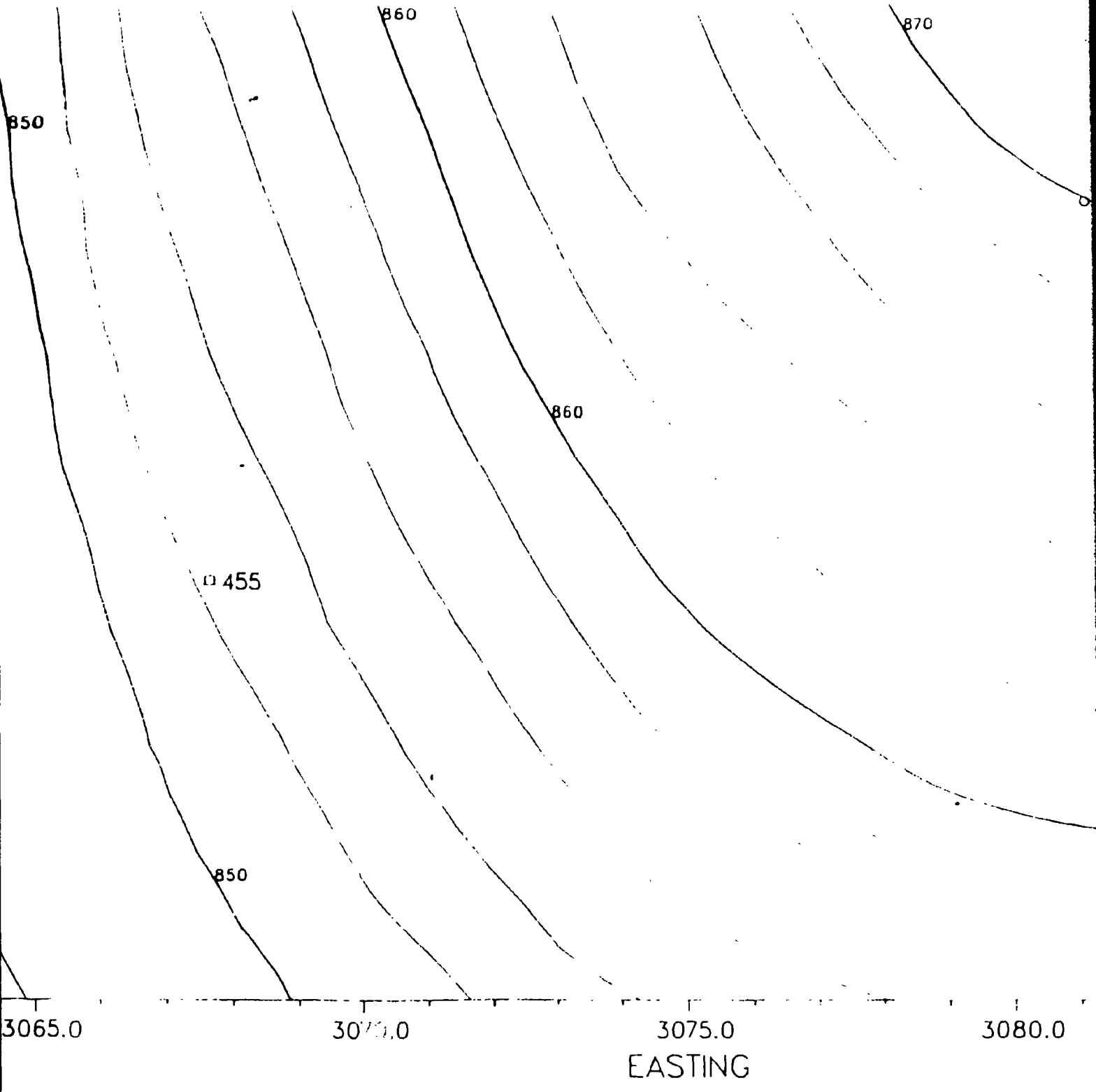
860
870
850
860
455
850
3065.0
3075.0
3080.0
EASTING

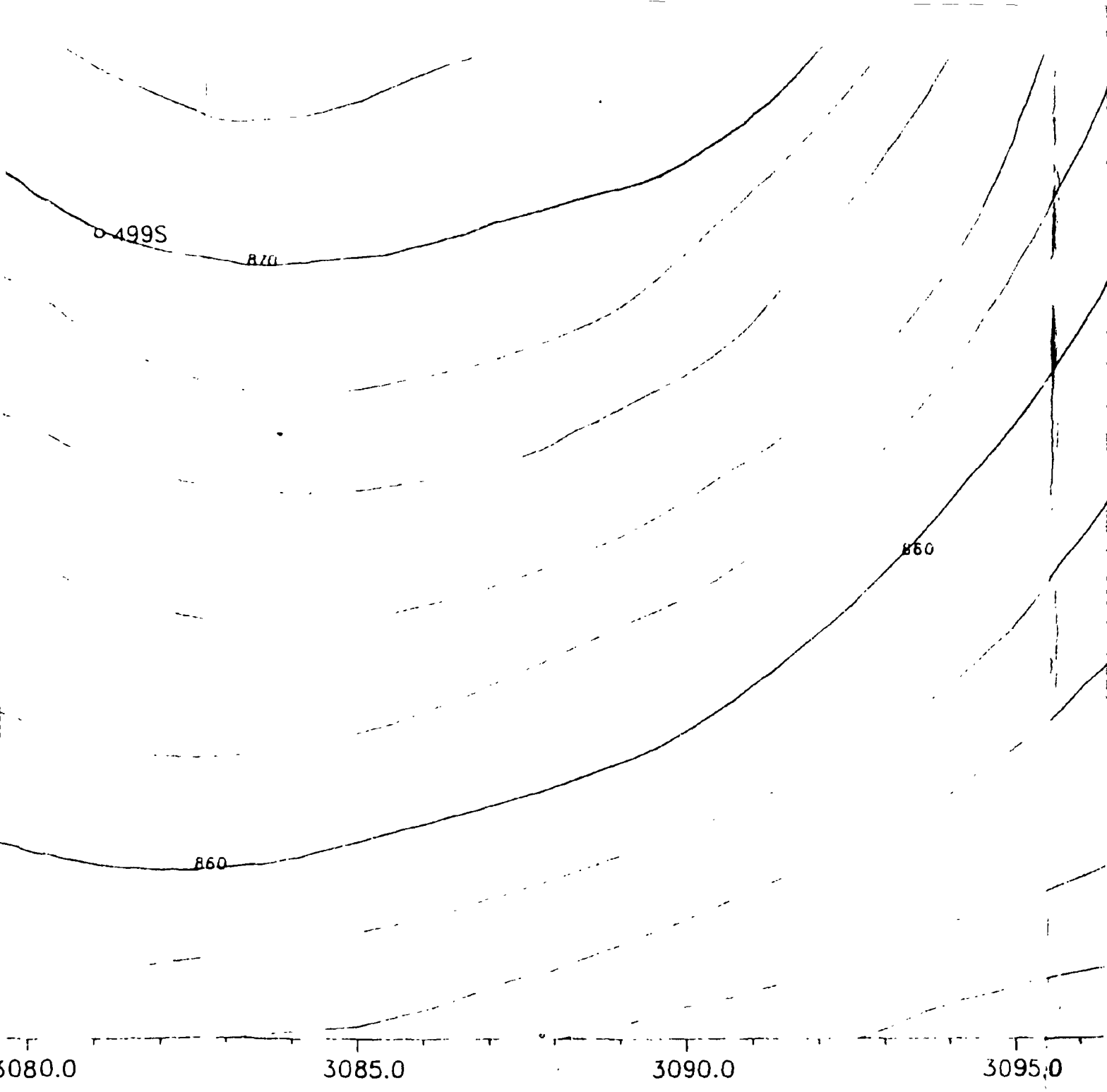
4995
870
860
860
3080.0
3085.0
3090.0
3095.0

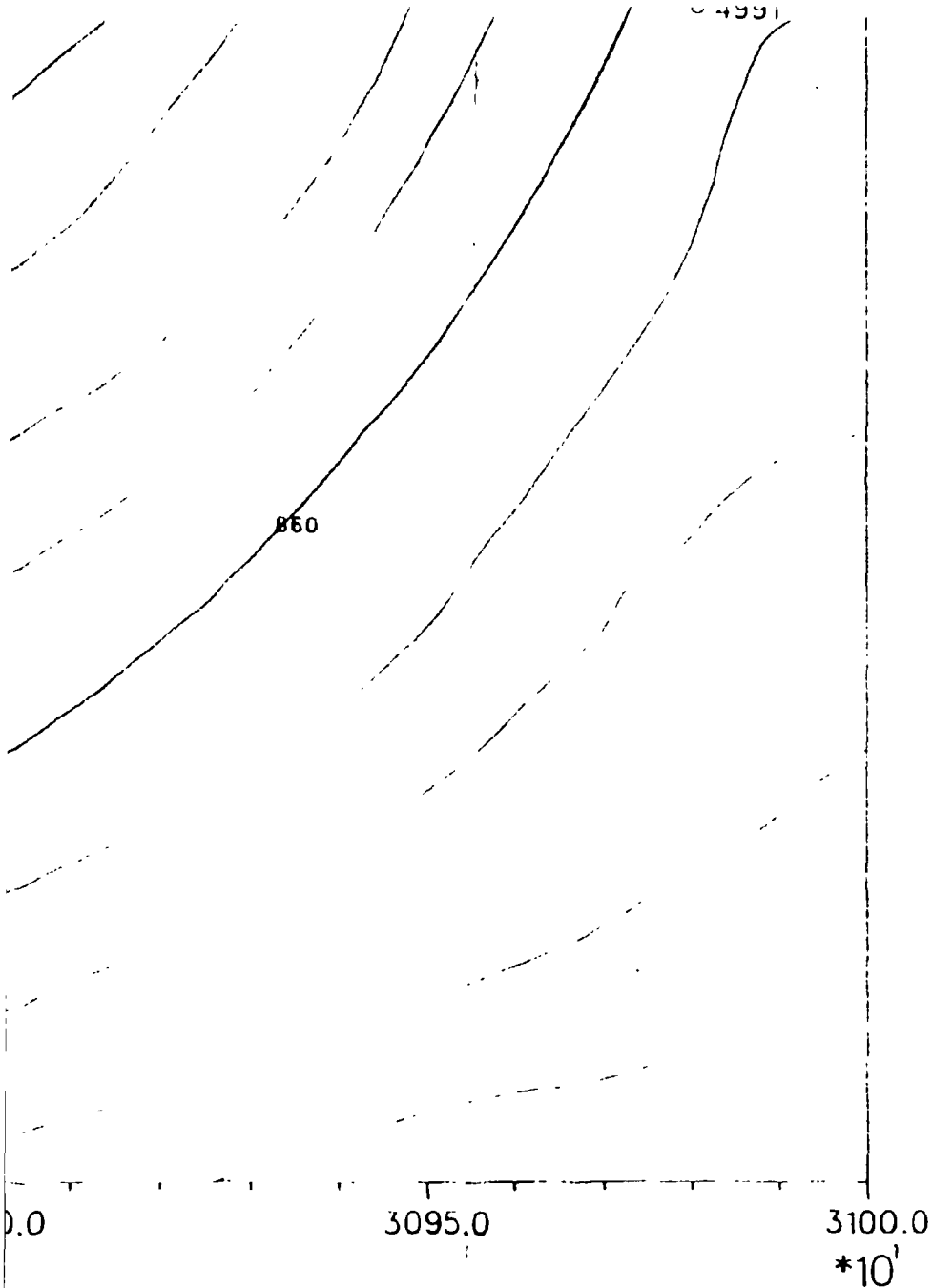

N

- CORE HOLE
- SINGLE ZONE PIEZOMETE
- MULTI-ZONE PIEZOMETE
- CREEK ELEVATION LOCA
- TRACER INJECTION WELL

1" = 20'

TOPOGRAPHIC CONTOUR INTERVAL 2'

RECTANGLE REPRESENT MODEL GRID BOUNDARY

Fig. 1

24

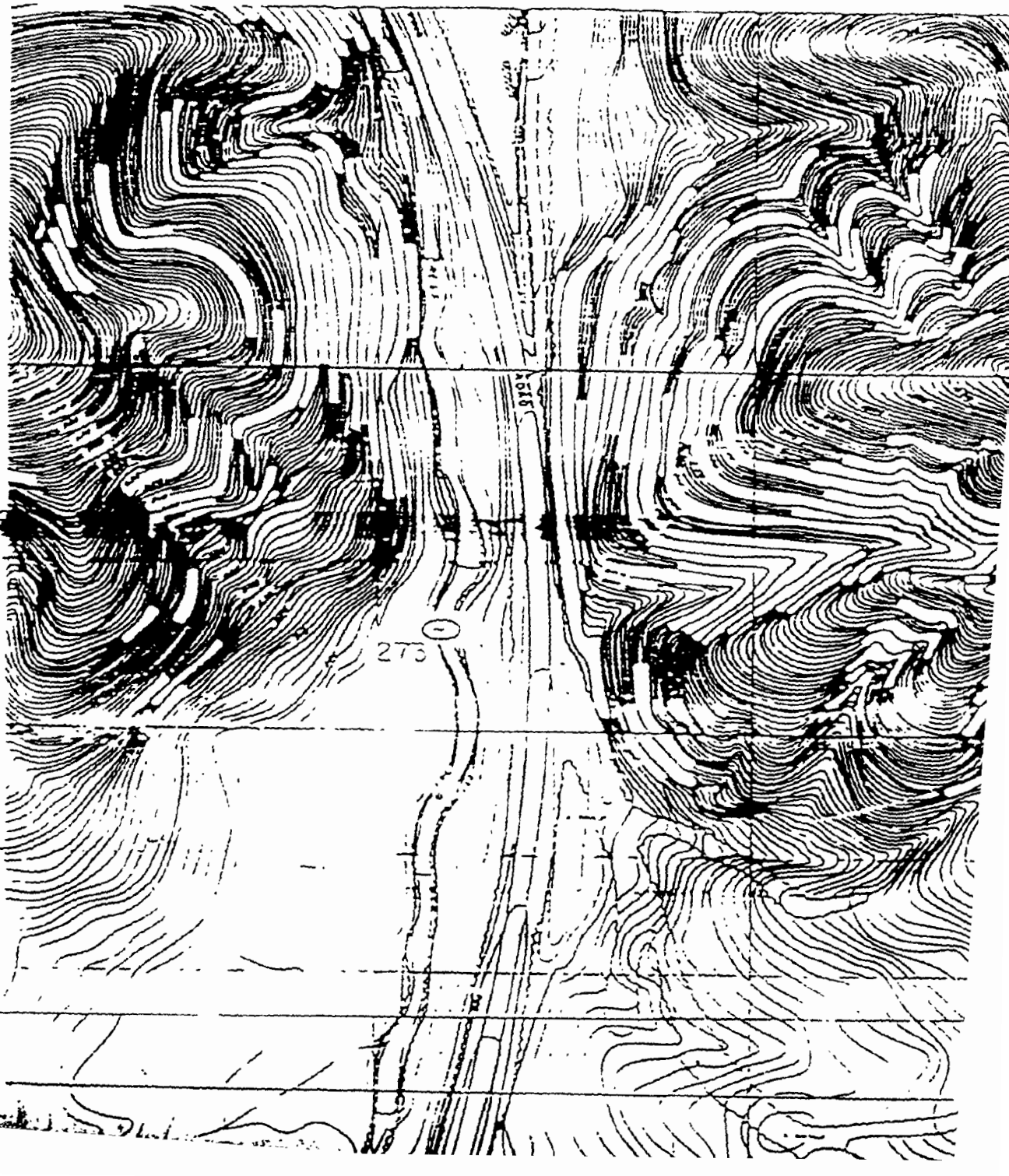

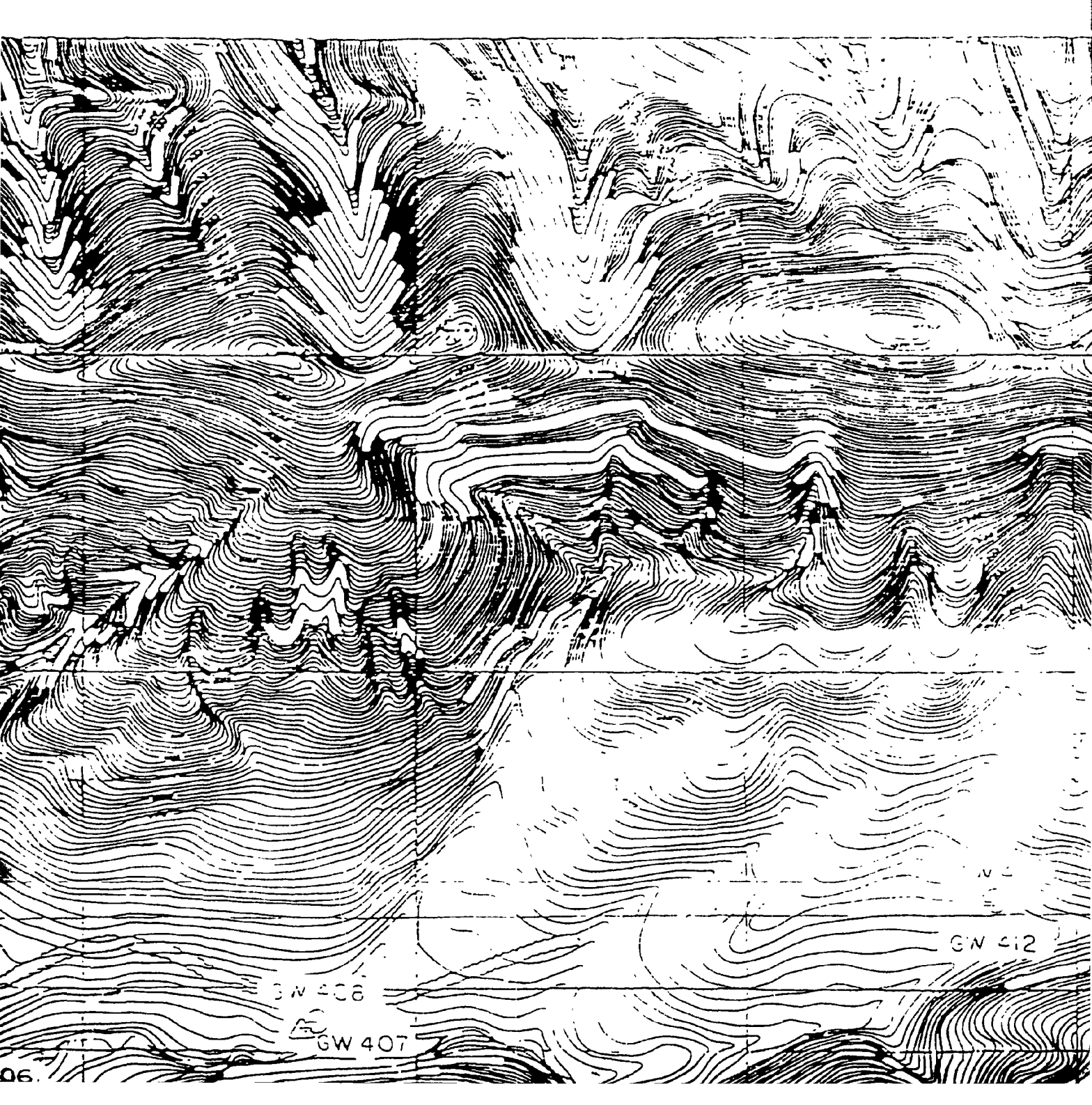
GW 412
GW 408
GW 407

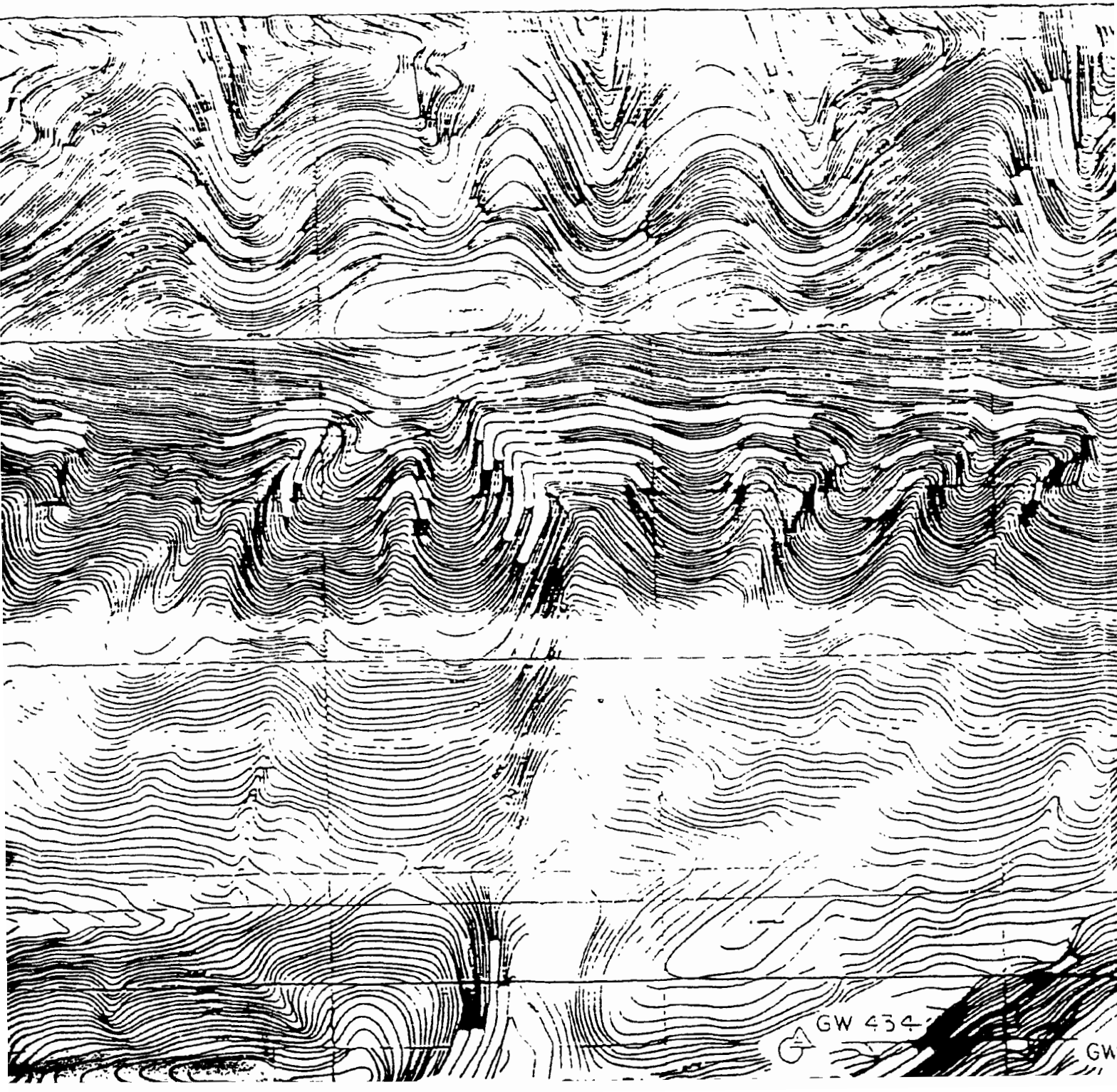
GW 434
GW

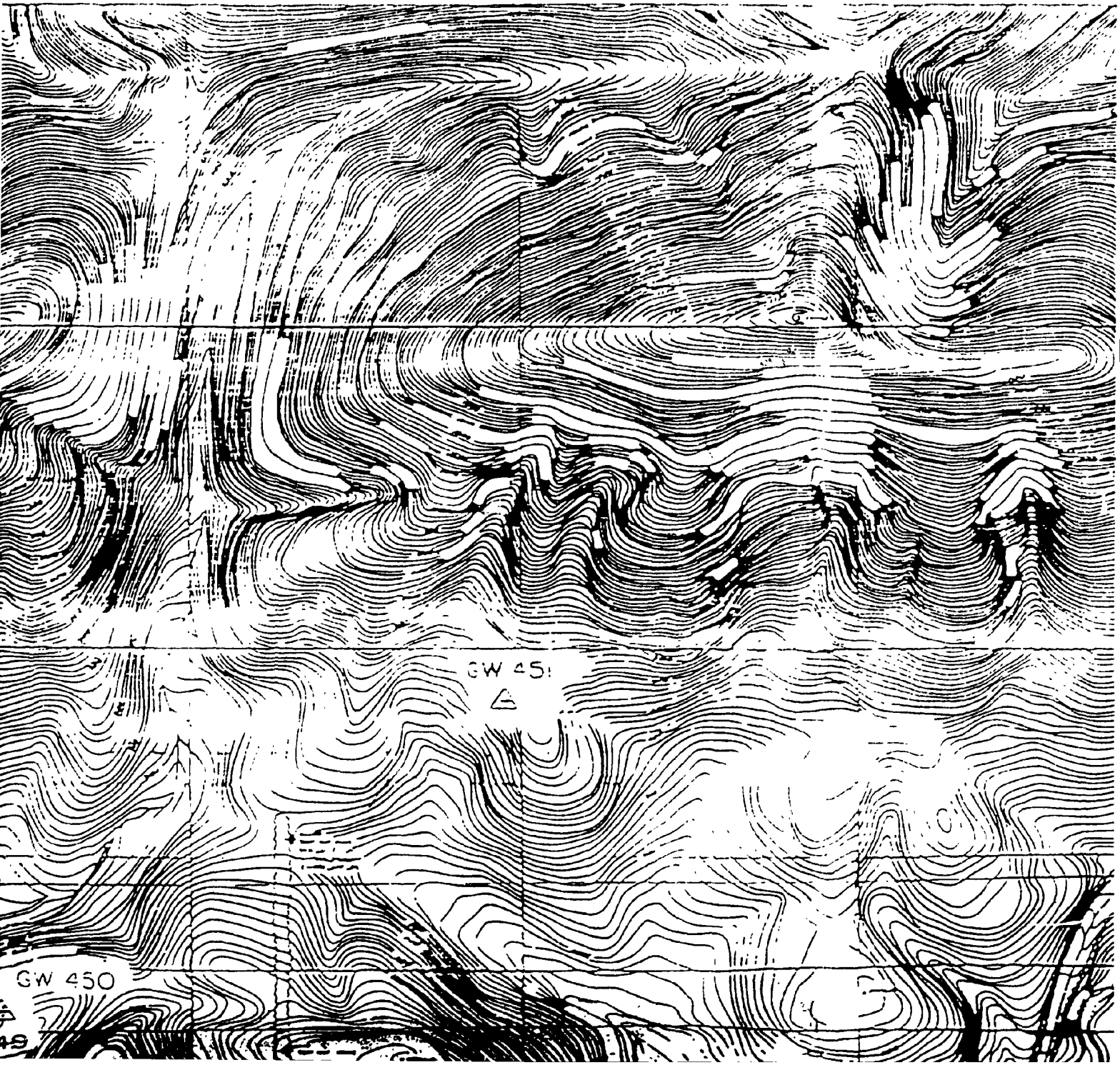
GW 451
GW 450

SURVEY DATA

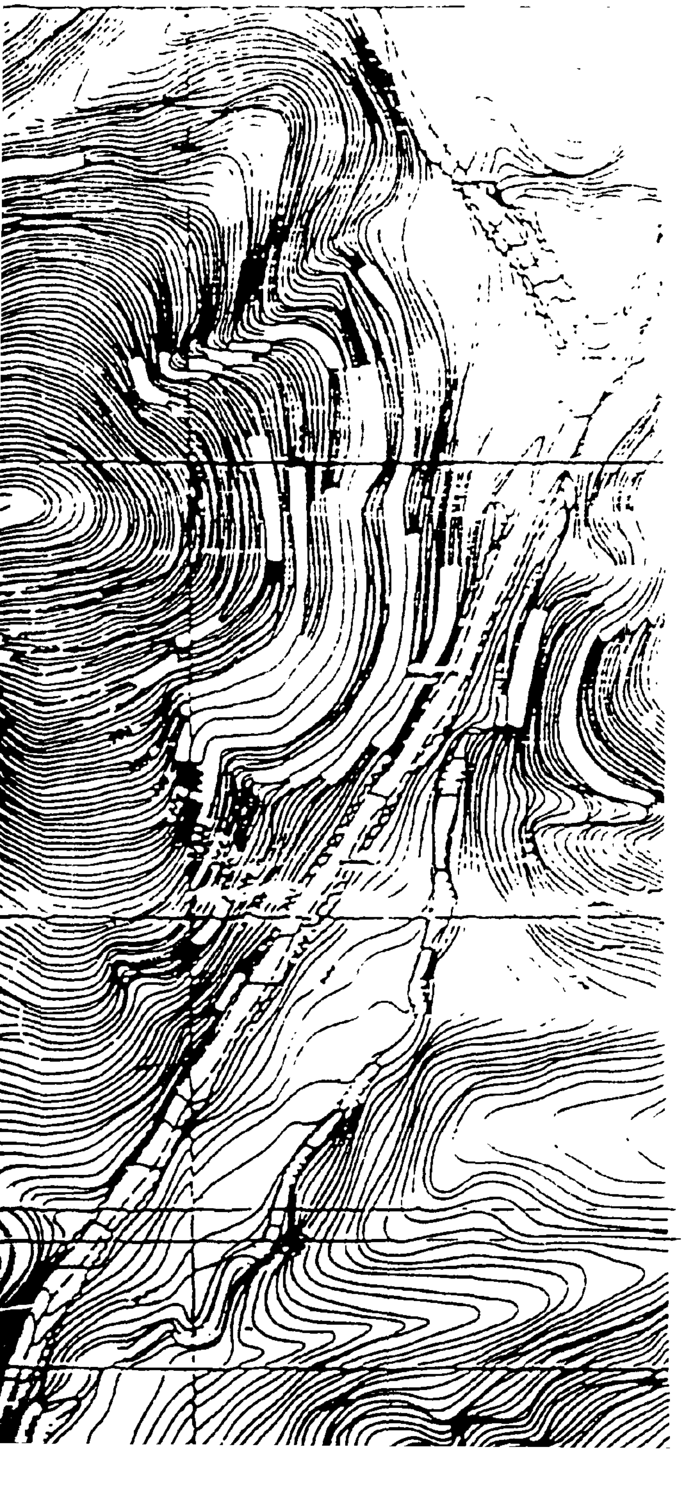

WELL NO.	AS BUILT COORDINATES NORTHING	AS BUILT COORDINATES EASTING	ELEVATION GROUND	ELEVATION TOP OF CASING
[illegible]	[illegible]	[illegible]	[illegible]	
G-137	28,772.00	32794.00	332.[illegible]	
G-138	[illegible] 00	[illegible]	[illegible]	
G-[illegible]	[illegible]	[illegible]	338.[illegible]	[illegible]
G-[illegible]01	29458.[illegible]	[illegible]	[illegible]	[illegible]
[illegible]	[illegible]	[illegible]	[illegible]	[illegible]
[illegible]	[illegible]	[illegible]	[illegible]	
[illegible]	[illegible]	[illegible]	[illegible]	
[illegible]	30327 [illegible]	[illegible]	[illegible]	316.[illegible]
[illegible]	[illegible]	[illegible]	[illegible]	316.90
[illegible]	[illegible]	[illegible]	[illegible]	[illegible]
G-[illegible]08	[illegible]	[illegible] 72	332.[illegible]	[illegible] 80
[illegible]	[illegible]	[illegible]	[illegible]	377.98
[illegible]	30283.22	[illegible]	[illegible]	372.00
[illegible]	[illegible]	[illegible]	[illegible]	[illegible]
[illegible]	[illegible]	[illegible] 36	364.00	36[illegible] 17
[illegible]	[illegible]	[illegible]	[illegible]	397.70
[illegible]	[illegible]	[illegible]	[illegible]	[illegible]
[illegible]	[illegible]	[illegible]	[illegible]	[illegible]
[illegible]	[illegible]	[illegible]	[illegible]	[illegible]
G-[illegible]	29758	29855 [illegible]	367 [illegible]	369.50
[illegible]	[illegible]	[illegible]	[illegible]	[illegible]
[illegible]	[illegible]	[illegible]	[illegible]	[illegible]
G-420	[illegible] 57	29439.30	335.07	337.[illegible]
G-42[illegible]	28850.04	28845.[illegible]	408.32	410.00
G-422	28849.5[illegible]	28855.72	407.[illegible]	409.[illegible]
G-[illegible]	28762.24	[illegible]	[illegible]	316.58
[illegible]	28773.[illegible]	[illegible]	[illegible]	316.5[illegible]
G-425	[illegible]	[illegible]	[illegible]	34[illegible]
G-426	[illegible]	[illegible]	[illegible]	34[illegible]
G-427	[illegible]	[illegible]	315.[illegible]	318.16
G-428	29672.78	[illegible] 90	315.77	318.[illegible]
G-429	[illegible]	[illegible]	335.[illegible]	337.[illegible]
G-430	[illegible]	[illegible]	[illegible]	337.24
G-[illegible]	[illegible]	[illegible]	[illegible]	[illegible] 09
[illegible]	[illegible]	[illegible]	[illegible]	[illegible]
[illegible]	30390 [illegible]	[illegible]	[illegible]	[illegible]
G-[illegible]	30397 [illegible]	[illegible]	[illegible]	37[illegible]
G-[illegible]35	30252 [illegible]	31298 [illegible]	[illegible]	[illegible]
[illegible]	30256 [illegible]	[illegible]	[illegible] 22	[illegible]
[illegible] 37	[illegible] 52	[illegible]	391.39	393.25
[illegible]	[illegible]	[illegible]	[illegible]	393.[illegible]
[illegible]	[illegible]	[illegible]	[illegible] .28	37[illegible] 26
[illegible]	[illegible]	[illegible]	[illegible]	37[illegible]
[illegible]	[illegible]	[illegible]	[illegible]	[illegible]
G-[illegible]	[illegible]	[illegible]	337.2[illegible]	34[illegible].33
~~[illegible]~~	~~28[illegible].56~~	~~[illegible]~~	~~327.7[illegible]~~	
[illegible]	ABANDONED			
[illegible]	29250.20	31805.[illegible]	[illegible]	342.20
[illegible]	ABANDONED			
[illegible]	29893.72	[illegible]	[illegible]	375.15
G-[illegible]8	29885.05	31738.3[illegible]	372.23	374.08
G-[illegible]9	30432.63	31713.87	934.2[illegible]	936.58
G-[illegible]50	30430.[illegible]	31726.0[illegible]	933.8[illegible]	935.8[illegible]

...ELL NO.	AS BUILT COORDINATES N	E	ELEVATIONS TOP OF CASING	TOP OF STEEL CASING	TOP OF PVC CASING	MEASURE POINT
...	...5.47	...35.31		850.34	858.53	856.87
G...137	28712.00	32700.00	832.88	836.11		
G...138	27759.00	32825.00	836.73	842.03		
G...430	29997.96	29...30	838.77	839.78		8...54
G...431	29438.48	28709.57	834.30	835.27	835.97	836.24	837....
...	29866.60	29902.17	830.96	831.48		831.56	83...
...	29520.54	29...73	833....	837....		839.22	83...
...	29837.16	29...21	832....	832....			
...	30327.56	30253.46	815.75	816.49		815.31	
...	30370....	30...17	815.30	816.90		815.94	
...	30...05	30229.76	832.17	834.45		834.22	
G...428	30...2.78	30...37.92	832....	834.80		834.50	
...	30...89.30	30...16....	837....	837.98		837.74	
...	30293.28	30...16.36	837....	838.00		837.75	
...	...43....	30...0....	836....	836....		836.21	
...	...0...76	30...0.36	862.30	864.17		864.09	
...	...03....	30...78.22	893.22	893.70		893.15	
...	...1....	30...29....	891....	891....		891.52	
...	...01...8	30...0.8...	894....	896....		896....	
...	...01...4	30022.25	894....	896....		896.30	
G...419	29...58	29855.75	867.23	869.50		869.16	
...	29...7....	29862.24	866.98	868....		868....	
...	...7....	...21....	...80	870....		870.39	
G...420	29...7.57	29...39.30	835.07	837.42		837.17	
G...421	29850.04	29843....	808.32	810.03		809.77	
G...422	29...6.50	29855.92	807.42	809....		809.09	
G...423	29...6.24	29...1.9...	814.77	816.58		816.35	
G...424	29...7.84	29...0....	814.33	816.51		816.28	
G...425	29937.15	29867....	841.27	843....		842.98	
G...426	29...2.33	29872.19	841.47	843.02		843.22	
G...427	29...2.11	30210.33	815.96	818.16		817.79	
G...428	29...78.78	30217.90	815.97	818.42		817.84	
G...429	29...21.6...	30...71....	835....	837.42		837.16	
G...430	29...22.24	30...02.75	834.37	837.24		836.87	
G...431	30...9....	30...23.81	862.73	863.09		863.36	
G...432	30...3.73	30...27....	862.38	863.02		863.43	
G...433	30390.62	31191....	866.39	871.23		870.76	
G...434	30397.34	31195.33	866.49	871.32		871.45	
G...435	30253.45	31298.11	902.46	904.66		904.25	
G...436	30250....	31291.34	902.23	904.3		904.03	
G...437	29960.52	31457.42	891.09	893.26		892.99	
G...438	29...97.91	31...56.01	891.33	893.77		893.25	
G...439	29...82....	31...7.39	868.29	870.26		870.25	
G...440	29...60.3...	31...53.10	868.18	870.49		870.13	
G...441	29...7....	31...14.45	836.34	838.44		838.09	
G...442	29...2.06	31...0.30	837.21	840.33		839.29	
G...443	29...1.58	31886.20	837.75		840.57		
G...444	... ...	ABANDONED	...	...	...	...	
G...445	30250.20	31805.46	842.19	842.20		846.53	
G...446	...	ABANDONED	...	...	...	...	
G...447	29893.72	31744....	872....	875.15		872.25	
G...448	29885.05	31738.31	872.23	874.08		873.86	
G...449	30422.63	31773.87	934.21	936.58		935....	


GW-436
GW-455
SW-499-AA
GW-439

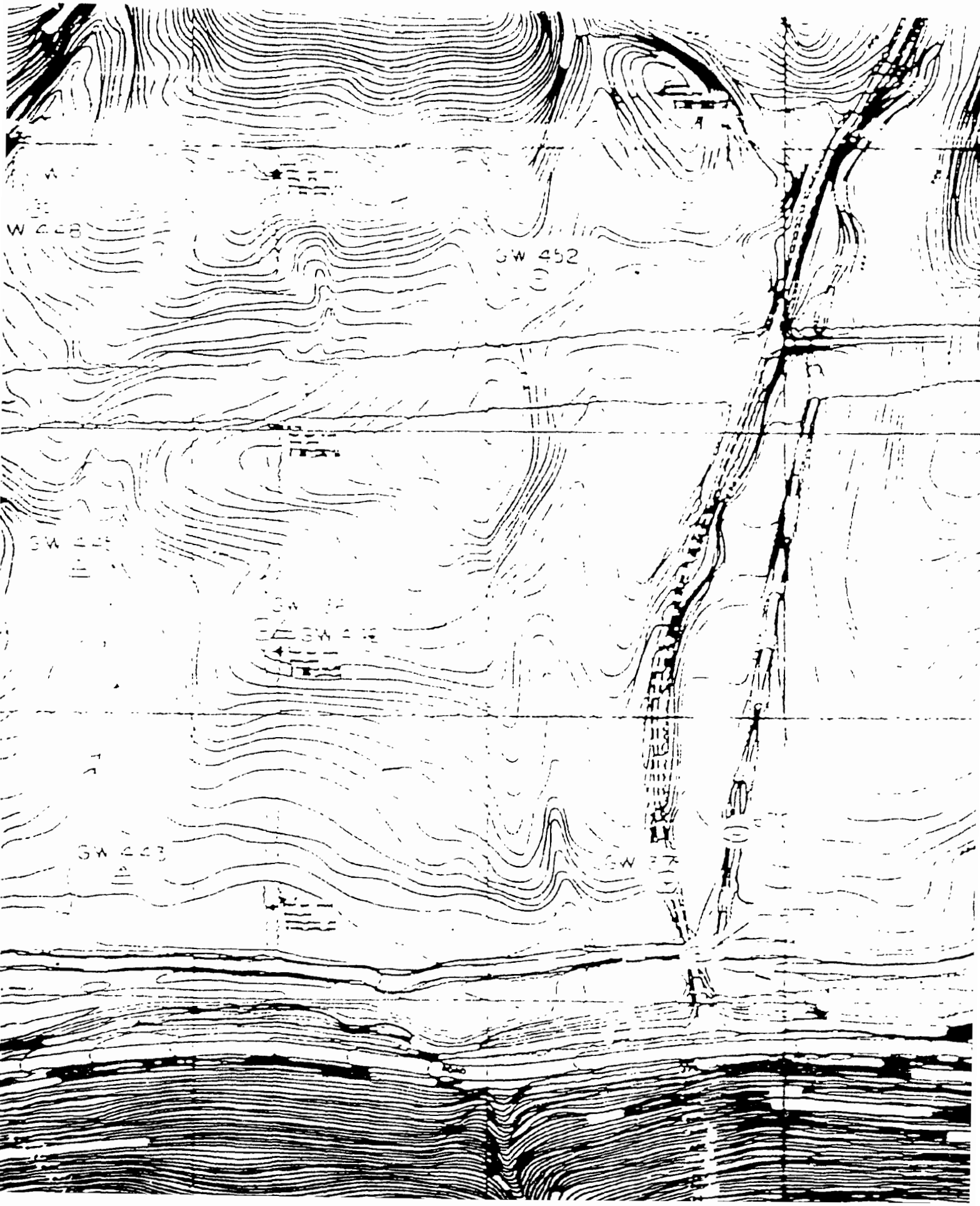
SW 452

GU-458	29581.22	30723.00	842.72	843.11		844.06
GU-459	29581.22	30726.56	842.77	843.13		845.18
GU-460	29581.91	30710.49	842.77	843.53		842.15
GU-461	29581.91	30710.49	842.77	843.53		842.15
GU-462	29581.11	30710.49	842.77	843.53		842.15
GU-463	29581.11	30710.49	842.77	843.53		842.15
GU-464	29581.11	30710.49	842.77	843.53		842.15
GU-465	29581.11	30710.49	842.77	843.53		842.15
GU-466	29581.11	30710.49	842.77	843.53		842.15
GU-467	29581.11	30710.49	842.77	843.53		842.15
GU-468	29581.11	30710.49	842.77	843.53		842.15
GU-469	29581.11	30710.49	842.77	843.53		842.15
GU-470	29581.11	30710.49	842.77	843.53		842.15
GU-471	29581.11	30710.49	842.77	843.53		842.15
GU-472	29581.11	30710.49	842.77	843.53		842.15
GU-473	29581.11	30710.49	842.77	843.53		842.15
GU-474	29581.11	30710.49	842.77	843.53		842.15
GU-475	29581.11	30710.49	842.77	843.53		842.15
GU-476	29581.11	30710.49	842.77	843.53		842.15
GU-477	29581.11	30710.49	842.77	843.53		842.15
GU-478	29581.11	30710.49	842.77	843.53		842.15
GU-479	29581.11	30710.49	842.77	843.53		842.15
GU-480	29581.11	30710.49	842.77	843.53		842.15
GU-481	29581.11	30710.49	842.77	843.53		842.15
GU-482	29581.11	30710.49	842.77	843.53		842.15
GU-483	29581.11	30710.49	842.77	843.53		842.15
GU-484	29581.11	30710.49	842.77	843.53		842.15
GU-485	29581.11	30710.49	842.77	843.53		842.15
GU-486	29581.11	30710.49	842.77	843.53		842.15
GU-487	29581.11	30710.49	842.77	843.53		842.15
GU-488	29581.11	30710.49	842.77	843.53		842.15
GU-489	29581.11	30710.49	842.77	843.53		842.15
GU-490	29581.11	30710.49	842.77	843.53		842.15
GU-491	29581.11	30710.49	842.77	843.53		842.15
GU-492	29581.11	30710.49	842.77	843.53		842.15
GU-493	29581.11	30710.49	842.77	843.53		842.15
GU-494	29581.11	30710.49	842.77	843.53		842.15
GU-495	29581.11	30710.49	842.77	843.53		842.15
GU-496	29581.11	30710.49	842.77	843.53		842.15
GU-497	29581.11	30710.49	842.77	843.53		842.15
GU-498	29581.11	30710.49	842.77	843.53		842.15
GU-499	29581.11	30710.49	842.77	843.53		842.15
GU-499A	29581.11	30710.49	842.77	843.53		842.15
GU-499B	29581.11	30710.49	842.77	843.53		842.15
GU-499C	29581.11	30710.49	842.77	843.53		842.15
GU-499D	29581.11	30710.49	842.77	843.53		842.15
GU-499E	29581.11	30710.49	842.77	843.53		842.15
GU-499F	29581.11	30710.49	842.77	843.53		842.15
GU-483	29581.11	30710.49	842.77	843.53		842.15
GU-484	29581.11	30710.49	842.77	843.53		842.15
GU-485	29581.11	30710.49	842.77	843.53		842.15
GU-486	29581.11	30710.49	842.77	843.53		842.15
GU-487	29581.11	30710.49	842.77	843.53		842.15
GU-488	29581.11	30710.49	842.77	843.53		842.15
GU-489	29581.11	30710.49	842.77	843.53		842.15
GU-490	29581.11	30710.49	842.77	843.53		842.15
GU-491	29581.11	30710.49	842.77	843.53		842.15
GU-492	29581.11	30710.49	842.77	843.53		842.15
GU-493	29581.11	30710.49	842.77	843.53		842.15
GU-494	29581.11	30710.49	842.77	843.53		842.15
GU-495	29581.11	30710.49	842.77	843.53		842.15
GU-496	29581.11	30710.49	842.77	843.53		842.15
GU-497	29581.11	30710.49	842.77	843.53		842.15
GU-498	29581.11	30710.49	842.77	843.53		842.15
GU-499	29581.11	30710.49	842.77	843.53		842.15
GU-499A	29581.11	30710.49	842.77	843.53		842.15
GU-499B	29581.11	30710.49	842.77	843.53		842.15
GU-499C	29581.11	30710.49	842.77	843.53		842.15
GU-499D	29581.11	30710.49	842.77	843.53		842.15
GU-499E	29581.11	30710.49	842.77	843.53		842.15
GU-499F	29581.11	30710.49	842.77	843.53		842.15

BUILDING
PAVED ROADS
UNPAVED ROADS
BRIDGES
CULVERTS
TRAILS
WATER
POWER POLE
TREES
TOWERS
FENCE
CEMETERY
E 30,560

D LINES REFER TO THE
ANT GRID SYSTEM

RIAL SURVEY DATE

E 29

E 30

E 30

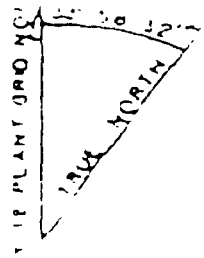

CORE HOLE

SHALLOW PIEZOMETER

BEDROCK PIEZOMETER

WEIR

CLUSTER WELLS

30,800

GW

REVISION OR ISSUE PURPOSE

6

5

REVISION APPROVALS

NOTES: 1. /STEEL CASING OR /PVC CASING REPRESENTS THE INDICATED "MEASURE POINT" LOCATED ON THE INNER CASING OF THESE WELLS

2. * INDICATES ELEVATION TAKEN AT TOP OF CONCRETE AT BOTTOM OF CASING FOR THESE WELLS

3. # INDICATES ELEVATION TAKEN AT TOP OF BLOCK

TOLERANCES UNLESS OTHERWISE SPECIFIED

FRACTIONS ±
.XX DECIMALS ±
.XXX DECIMALS ±
ANGLES
BREAK SHARP EDGES MAX
FINISH

DES C FOLDEN 8/87
DRN J PACHECO 8/87
CHK C FOLDEN 8/87
SECT CHIEF 8/18/87
DEPT'S PLANT

DRAWING APPROVALS DATE

PIEZOM

SCALE: 1" = 20'

2 0

GW-699P	29907.35	30683.35	859.37			860.87
GW-699O	29891.17	30697.93	857.54			857.86
GW-699Q	29883.59	30608.56	857.13			859.55
GW-699S	29825.00	30810.46	871.02			873.73
GW-699T	29935.25	30852.60	876.67			879.62
GW-699U	2993[illegible].75	30713.36	86[illegible].34		868.26	
GW-699V	29932.58	3075[illegible].24	869.36		871.14	
GW-699W	29915.18	30635.18	[illegible]		853.62	
GW-699X	29907.07	30783.[illegible]	872.78		873.36	
GW-699Y	[illegible]	[illegible]	[illegible]			861.55
GW-699Z	[illegible]	[illegible]	[illegible]			868.24
GW-699AA	[illegible]	[illegible]	[illegible]			854.55
GW-699AB	[illegible]	[illegible]	856.97		85[illegible].78	
GW-699AC	29915.09	30565.29	843.5[illegible]			843.88
GW-699AD	29911.03	30575.22	842.[illegible]			84[illegible].89
GW-699AE	29921.27	30581.[illegible]	843.07			844.15
GW-699AF	29927.39	30583.48	842.91			843.25
GW/HAZ-13	30640.63	32192.72	916.3[illegible]	918.23		918.61
GW/HAZ-14	30236.57	32157.15	932.47	935.09		934.95
GW/HAZ-15	29779.90	32153.06	878.43	880.00		879.09
WEIR 270	29967.56	27638.24	804.31 (CORNER OF CONC.)			
WEIR [illegible]	30358.[illegible]	27696.[illegible]	808.[illegible] (TOP OF WEIR)			
WEIR [illegible]	31142.40	2758[illegible].70	802.[illegible] (C/L OF CREEK @ BRIDGE)			
WEIR [illegible]	29799.[illegible]	3292[illegible]	[illegible].33 (TOP OF CONC.)			
WEIR [illegible]	28582.92	3295[illegible]	825.39 ([illegible] SPILLWAY)			
WEIR [illegible]	29975.18	307[illegible]	31[illegible] (TOP OF CONC.)			

C2E145178

B

Fig. 2

MARTIN MARIETTA ENERGY SYSTEMS INC

Operated for the DEPARTMENT OF ENERGY under U.S. GOVERNMENT contract DE-AC05-84OR21400

OAK RIDGE TENNESSEE • PADUCAH KENTUCKY

BEAR CREEK VALLEY

PIEZOMETER WELL LOCATION MAP

BEAR CRK VALLEY WELL LOC

M

A

DATE

SCALE 1" = 200'

A4002349

C2E145178

REV C

MODE
HYDRAUL

MODEL VALIDATION OFF-SITE
YDRAULIC HEAD DATA LOCATIONS

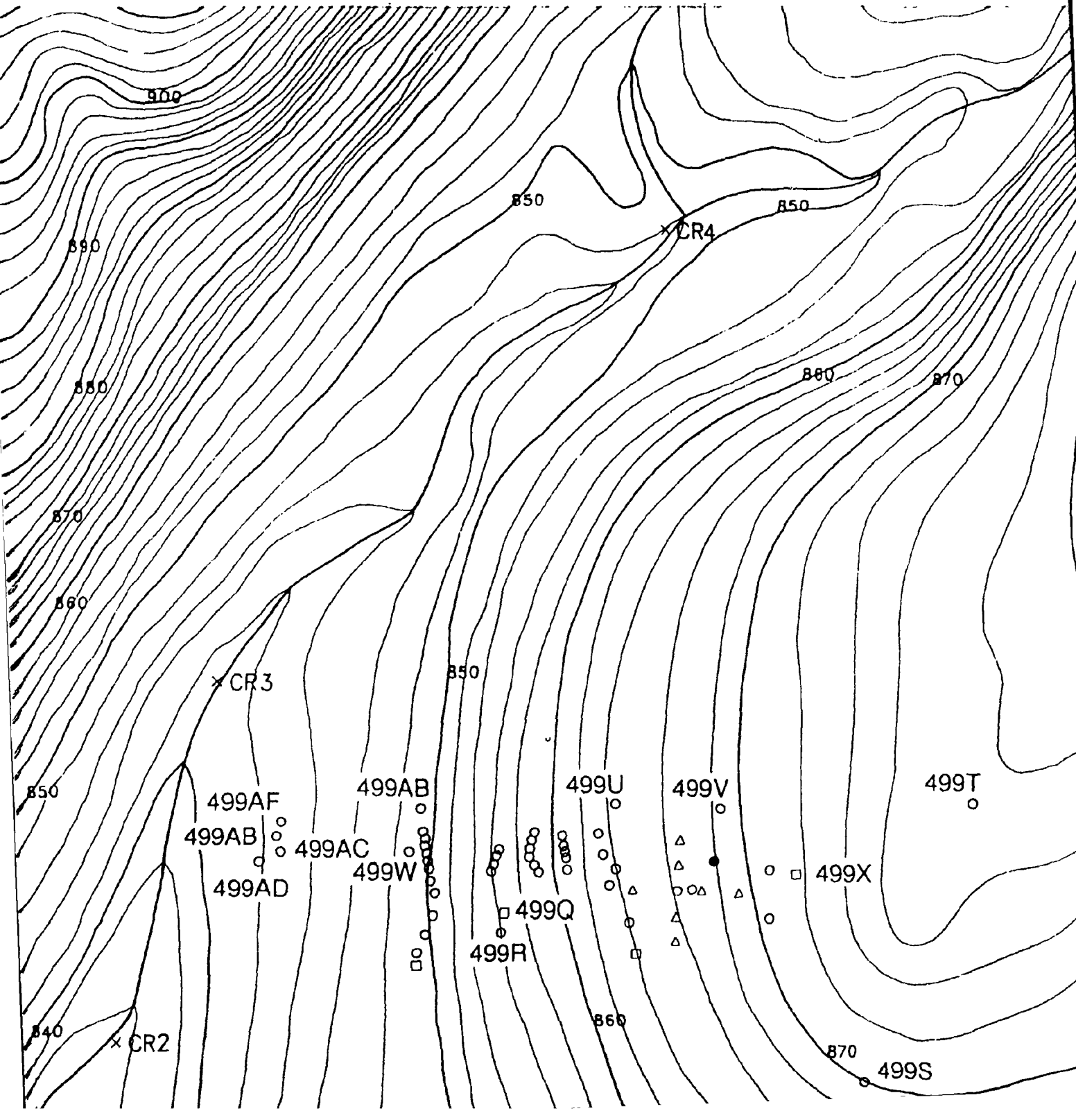

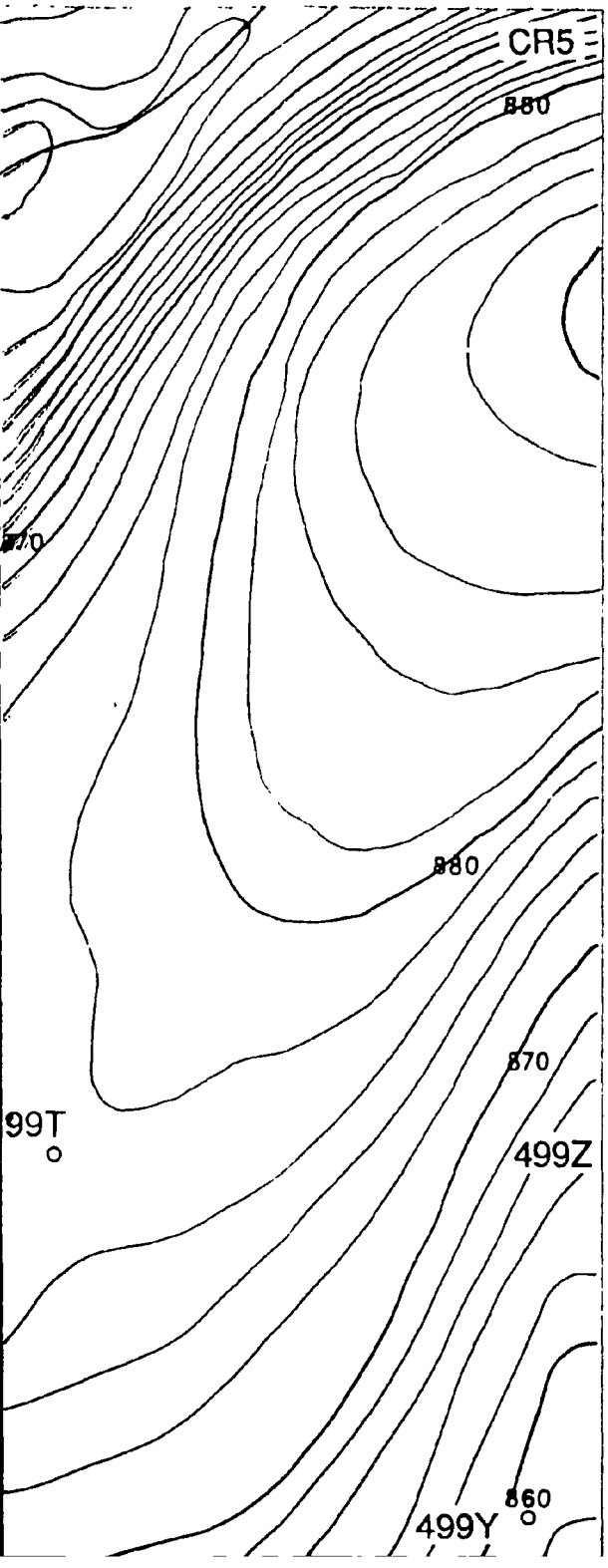

Y-12

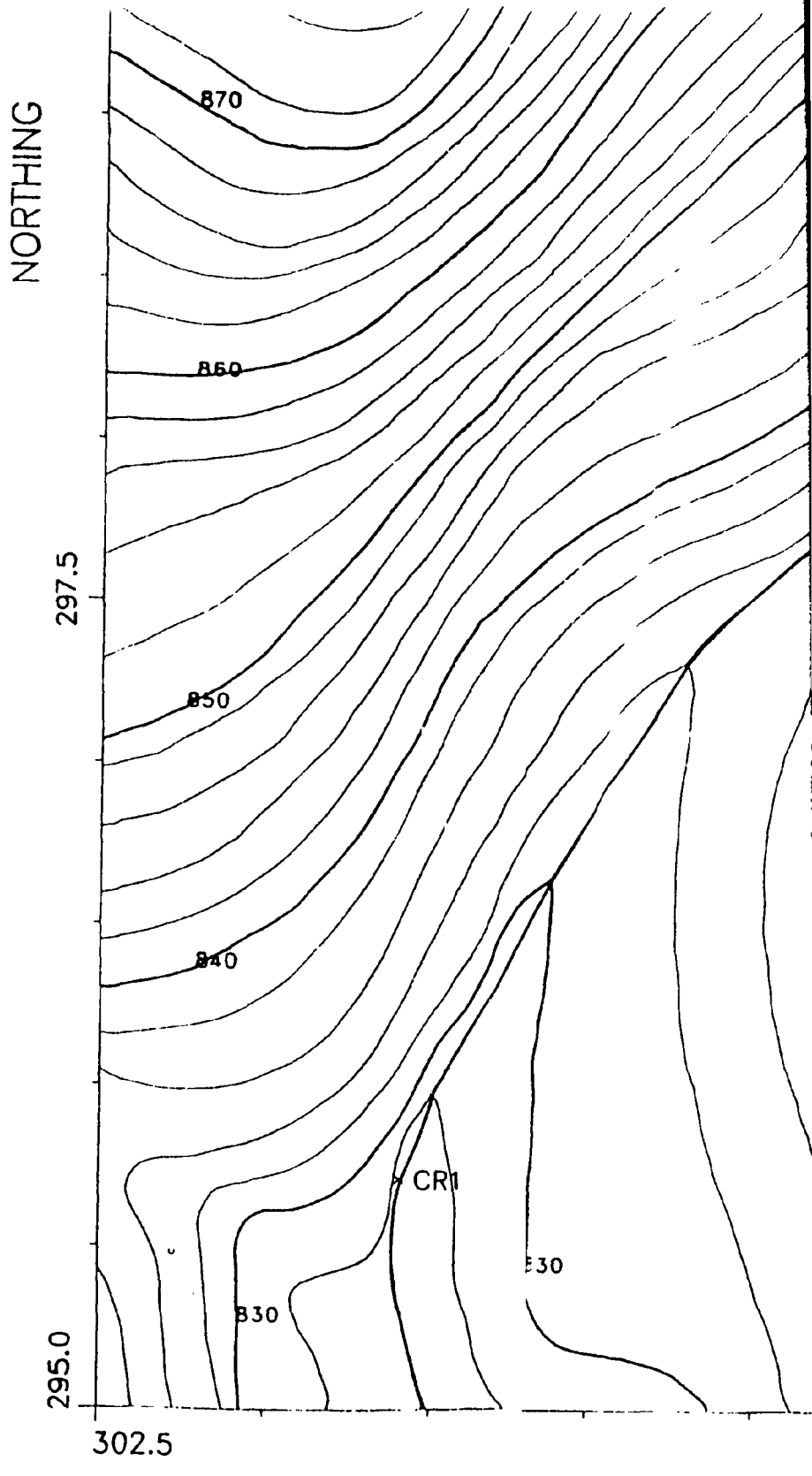
NORTHING
870
860
850
840
830
830
CR1
297.5
295.0
302.5

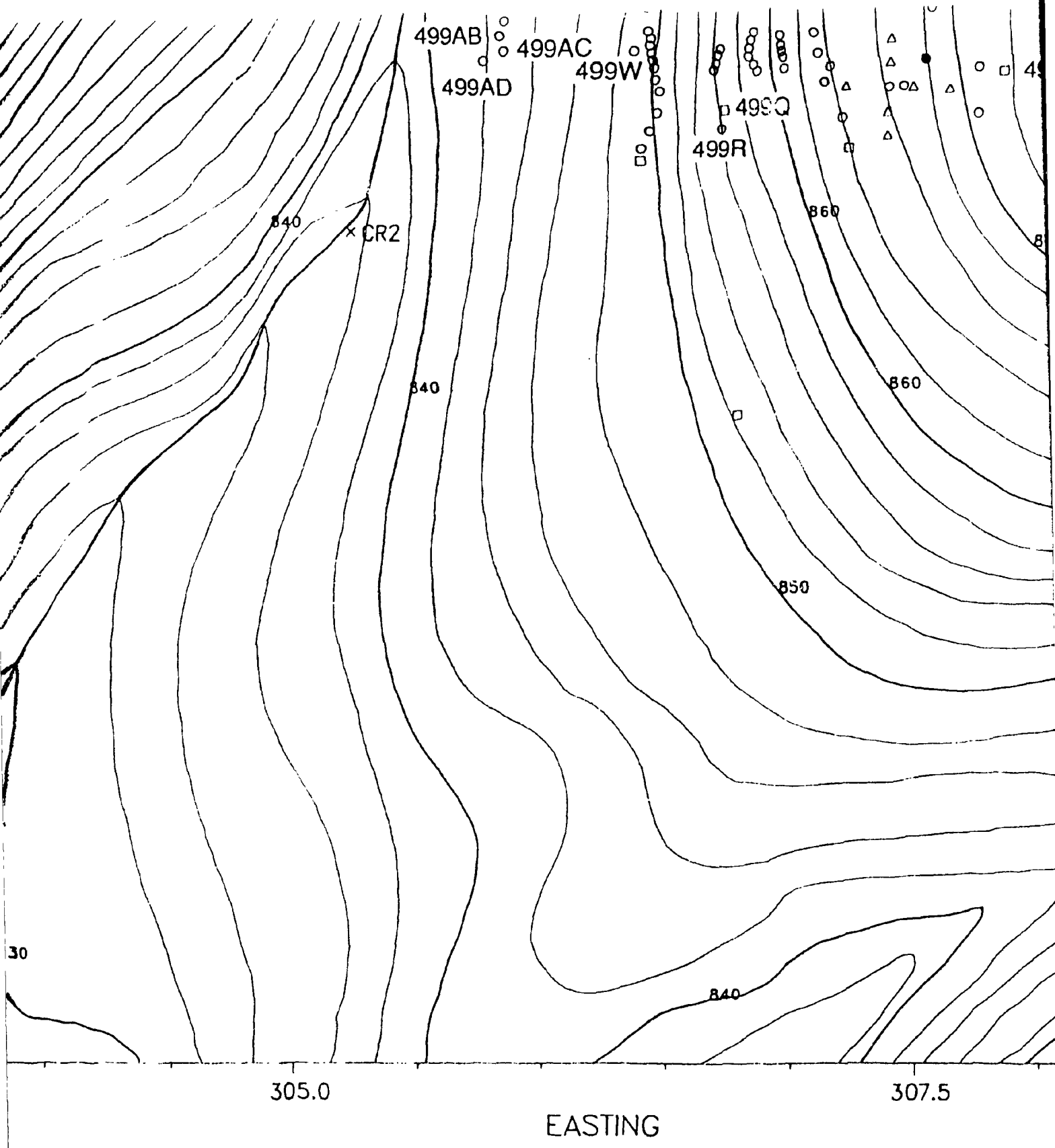
499AB
499AC
499AD
499W
499R
CR2
840
860
850
305.0
307.5
EASTING

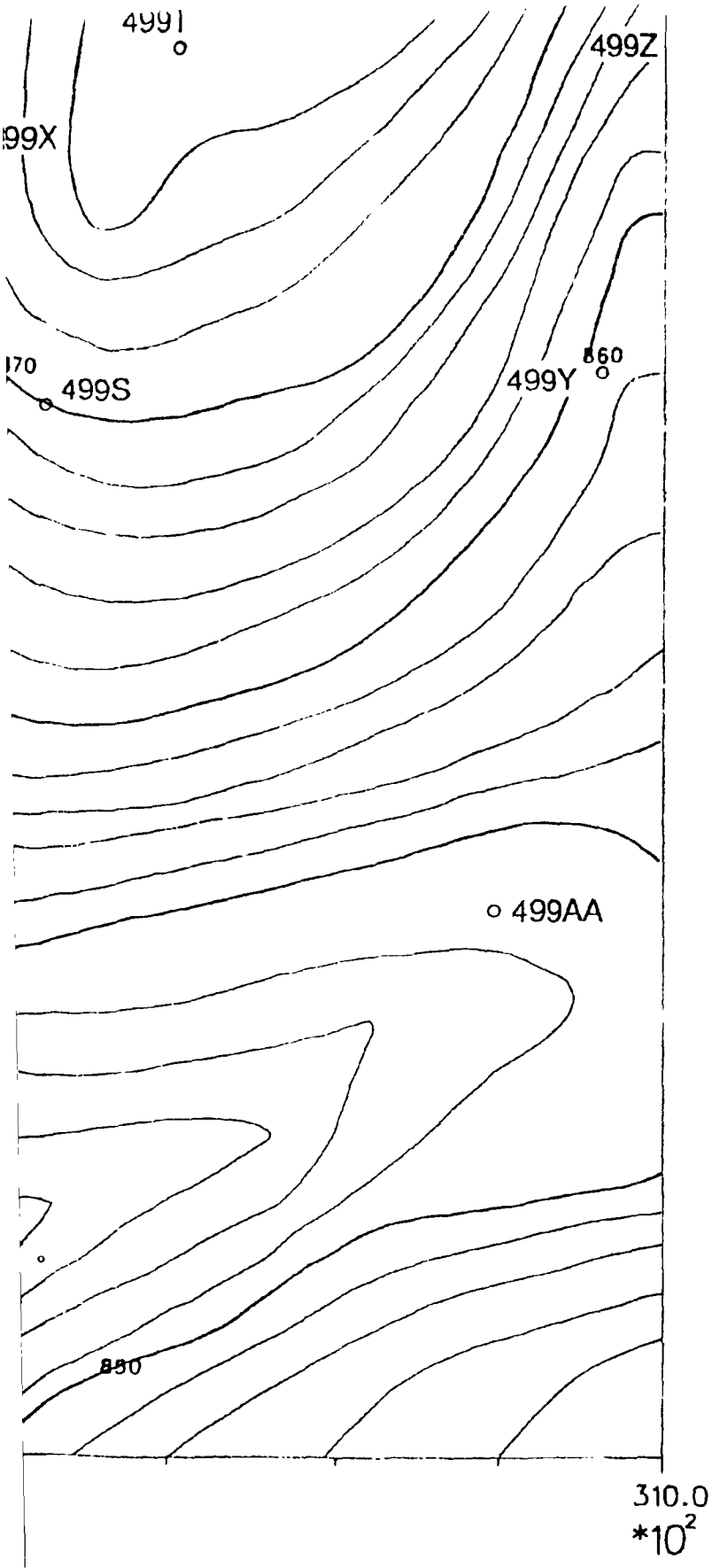

Y-12

N

- CORE HOLE
- SINGLE ZONE PIEZOMETER
- MULTI-ZONE PIEZOMETER
- CREEK ELEVATION LOCATIONS
- TRACER INJECTION WELL

1" = 50'

Fig. 3